Haploid genetic screening approach towards identifying novel regulators of immune checkpoints



Vineethkrishna Chandrasekar
St Cross College
University of Oxford

A thesis submitted for the degree of
Doctor of Philosophy
Michaelmas 2021

Declaration

I hereby declare that this dissertation is entirely my own work except for

- The batch of mutagenized HAP1 cells used for the haploid genetic screens were generated by Erica De Zan, past DPhil Student from Nijman Lab University of Oxford, UK and
- The UBE3D knockout HAP1 cell lines were generated by Frances Hundley from the Toczyski Lab, University of California San Francisco, USA
- The in vivo zebrafish studies were performed in collaboration with Dr Svanhild Nornes from Sarah De Val's lab from Ludwig Cancer Research, University of Oxford, UK

In **Chapter 2** text, I have acknowledged the work performed by others.

The data presented in **Chapter 3** presents unpublished results and figures and **Chapter 4** is being prepared as a manuscript for publication.

Word count: 25,891

(Max 50K exclusive of bibliography, appendices, diagrams)

Abstract

Priming the immune system by blockade of immune checkpoint proteins has revolutionized cancer therapy and achieved durable clinical responses. Despite the success of targeting the PD1-PDL1 axis or CTLA-4 to release the breaks on T cells, the response across cancer types and patients has not been uniform. One of the reasons is the heterogenous immune evasion mechanisms displayed by the tumour. With over forty immune checkpoint proteins identified, there remains much to understand regarding the underlying biology. Insights into the specific regulation of surface expression of immune receptors may aid in developing rational immunotherapeutic strategies. This thesis describes the use of a haploid genetic screening approach to uncover regulatory mechanisms of several immune checkpoint proteins expressed on cancer cells.

First, we investigate which endogenously expressed immune checkpoint proteins can be interrogated in the human haploid cell line HAP1 and subsequently focus on Polio Virus Receptor (PVR), B7 homolog 3 (B7H3) and Neuropilin-1 (NRP1) (Chapter 2). Chapters 2 and 3 concern the genetic screens on B7H3, PVR and NRP1, and initial validation of newly identified regulators. In Chapter 4, we report the identification of UBE3D as a novel regulator of the immune checkpoint and angiogenesis-associated protein, NRP1. Our data provide a potential mechanistic basis for a risk association between an inherited variant of *UBE3D* and age-related macular degeneration (AMD). Specifically, *UBE3D* loss of function resulted in reduced lysosomal degradation of NRP1 and increased angiogenesis in a zebra fish model.

Together, this thesis describes how haploid genetic screening can be used to improve our understanding of immune checkpoint proteins and provides a mechanistic explanation for the genetic association of *UBE3D* with age-related macular degeneration.

Acknowledgements

The undertaking of a DPhil, for me was a journey filled with excitement and perseverance to cultivate my academic curiosity. The culmination of this thesis document would not have been possible without the support of the following people along the way.

To my supervisors, Dr Sebastian Nijman, Dr Carol Leung and Prof Benoit Van Den Eynde, I thank you for taking me on as your student and encouraging me to explore the science with freedom while going out of your way time and again to provide me with the right training. Sebastian, a special thanks to you for your continued support even after moving on to your next scientific adventures. You always made sure, you were just a phone call away and provided much needed motivation and mentorship to shape my DPhil project and career decisions. Your supervision has been invaluable, and the lessons learnt will be the foundation for my academic career.

To Gurpreet, thank you for being my home every day for the past 3 years. You were a pillar of support and shared with me the excitement and the pain of the behind-the-scenes of this thesis. Thanks for being my travelling partner, Netflix partner, walking buddy, fellow foodie, best friend and for all the other shenanigans that got me through this journey. Moreover, thank you for all your support especially during the writing of this thesis. Meeting you, was one of the best things that has happened to me in Oxford, and I hope to cherish and value our relationship for the rest of my life.

To my best friend Aparna, thanks for all the transatlantic calls during the last 4 years. Every time we talk, despite our busy schedules, we always pick up where we left off. Thank you for your constant motivation, support and kindness. I look forward to your continued friendship.

To all the lab members, past and present, James, Laurine, Vinny, Erica, Ruud, Julia, Amanda, Emily, Svenja and Andrei. Thank you for creating a work environment that was brimming with fun and intellect. I am very grateful to have worked with such brilliant people. Despite the pandemic, you all made the time in and outside the lab a pleasure. Thanks Erica, for showing me the ropes in the early days in the lab. To Svanhild, thank you for your collaboration with the zebrafish experiments and your help with completing the story. To, James, Laurine and Vinny, thank you for those gentle motivational nudges when things got difficult with the project and all your support. James, a special thanks to the impromptu meet ups during thesis writing and lengthy discussions about science, travel, this DPhil and life itself. Looking forward to our continued friendship.

To my friends in Oxford, thank you for all the good times. To Ruth, Selena and Mei. You were the best housemates I could have hoped for. Thank you for all the travelling, pizza nights, motivation, and support along the way. To Peter, starting from introducing me to Kebab kid to all those coffee sessions in the old road campus, thank you for all the support and fun. To Anand and Junetha, for all the board game nights, constant support, and motivation.

To my sister, Sruthi, you have been my best friend from the very beginning and shared all my success and failures. I thank you whole heartedly for all those

phone calls in the last many years, encouraging me when life was not sailing so smoothly. I could not have done this without you.

Finally, to my parents, Uma and Chandrasekar, thanks for raising me to be independent and always follow my moral compass. Most importantly, a special thanks to you mom, for believing in me at every step and pushing me to pursue my dreams and goals. I wholly attribute all my success to you.

Table of Contents

Declaration 2

Abstract 3

Acknowledgements 5

List of tables 11

List of figures 13

List of abbreviations 16

Chapter 1: Introduction 21

1.1 Immune checkpoint blockade 21

1.2 Going beyond PD-1/PD-L1 blockade 22

1.3 Whole genome genetic screening coupled with protein abundance to dissect the tumour immune interface 25

1.4 CellSeq technology 29

1.5 CellSeq technology harnesses the power of haploid genetics 33

1.6 Research objective 34

1.7 HAP1 as a model for studying immune checkpoints 34

1.8 Specific research objectives: 37

Chapter 2: Materials and methods 39

2.1 Antibodies, Plasmids, Buffers, Kits and Reagents 39

2.2 Cell lines 46

2.3 Generation of mutagenized HAP1 (mut-HAP1) cells 47

2.4 Haploid genetic screen (CellSeq) 48

2.5 Recovery of insertion sites 51

2.6 Mutation mapping and analysis 54

2.7 Choice and prioritization of hits for validation 55

2.7.1 Pathway annotation 56

2.7.2 Visual specificity scoring 57

2.8 Cloning of sgRNA into plasmid LentiCRISPR v2 63

2.9 Knockout cell generation via transient transfection 66

2.10 Western blot sample preparation 67

2.11 Western blotting 69

2.12 Site directed mutagenesis to generate UBE3D mutants 70

2.13 Overexpression of UBE3D and NRP1 71

2.14 Immunoprecipitation 72

2.15 Lysosomal and proteasomal degradation assays 73

2.16 Zebrafish experiments 74
2.17 Morpholino injections 74
2.18 Zebrafish fluorescence analysis and confocal imaging 75
2.19 qRT PCR 76
2.20 Statistical Analysis 77
2.21 Data plotting 78

Chapter 3: CellSeq to identify regulators of B7H3 and PVR 79

3.1 Introduction 79
3.1.1 PVR 80
3.1.2 B7H3 82
3.1.3 B7H3: 'a double-edged sword' driven by glycosylation 83

3.2 Results 85
3.2.1 Identification of regulators of PVR using CellSeq 85
3.2.2 Identification of regulators of B7H3 using CellSeq 89
3.2.3 Role of sialylation biosynthesis as a potential regulator of B7H3 function 102

3.3 Discussion 104
3.3.1 FBXO11: An indirect link between the UPS and PVR expression? 105
3.3.2 Sialylation: The fine balance between B7H3 being a friend or a foe to anti-tumor immunity? 106

Chapter 4: CellSeq identifies UBE3D as a novel negative regulator of NRP1 107

4.1 Introduction 107
4.1.1 Neuropilin-1(NRP1): A multifaceted protein 107
4.1.2 NRP1 versatility: A novel immune checkpoint 110
4.1.3 Another tale of NRP1 versatility: Age related macular degeneration 112
4.1.4 UBE3D and AMD 115

4.2 Results 117
4.2.1 Identification of regulators of NRP1 using CellSeq 117
4.2.2 UBE3D is a negative regulator of NRP1 122
4.2.3 UBE3D inhibits NRP1 expression in a ubiquitin independent manner and AMD associated UBE3D sustains NRP1 expression 125
4.2.4 NRP1 interaction is stronger with UBE3D than AMD associated UBE3D V379M 129
4.2.5 UBE3D targets NRP1 towards lysosomal degradation 132
4.2.6 UBE3D loss leads to NRP1- dependent increased angiogenesis in vivo 133
4.2.7 UBE3D-NRP1 – molecular link proposed model schematic 138

4.3 Discussion 139

Chapter 5: General Discussion 144

5.1 The scope for CellSeq in immunotherapy 144
5.2 Future of functional genomics in immunotherapy 149

Chapter 6: Appendices 152

6.1 PVR screen hits (FDR < 0.05) 152
6.2 B7H3 screen hits (FDR < 0.05) 176
6.3 NRP1 screen hits (FDR < 0.05) 180

6.4 *SIRPa surface expression was not detected in HAP1 cells* *192*
6.5 *Size distribution of DNA library from PVR CellSeq screen* *193*
6.6 *UBE3D does not affect NRP1 mRNA levels* *194*
6.7 *UBE3D affects zebrafish eye development* *195*

Bibliography **196**

List of tables

Table 2.1 Primary antibodies used in this study

Table 2.2 Secondary antibodies used in this study

Table 2.3 Plasmids used in this study

Table 2.4 Buffers used in this study

Table 2.5 Commercial kits used in this study

Table 2.6 Reagents and consumables used in this study

Table 2.7 Cell lines used in this study

Table 2.8 Plasmid mix for gene trap mutagenesis

Table 2.9 List of antibodies, stimuli and staining concentration used in CellSeq

Table 2.10 List of all primers used for recovery of insertion sites

Table 2.11 LAM-PCR reaction setup for each reaction

Table 2.12 ssDNA ligation reaction setup for each reaction

Table 2.13 Illumina addition PCR master mix for each reaction

Table 2.14 sgRNA targeting sequences in this study

Table 2.15 Reaction mixture for phosphorylation and annealing of oligos

Table 2.16 Reaction mixture for LentiCRISPRV2 digestion

Table 2.17 Reaction mixture for ligation of annealed oligos to LentiCRISPR V2

Table 2.18 Primers used for site directed mutagenesis

Table 2.19 PCR conditions for site directed mutagenesis

Table 2.20 Sequencing primers used to confirm presence of mutation in UBE3D mutants

Table 2.21 Morpholino injections concentrations

Table 2.22 Primers used for qRT PCR

Table 3.1 Hits chosen for CRISPR/Cas9 validation from the B7H3 screen

Table 4.1 Examples of functions affected by NRP1 expression on immune cells.

List of figures

Figure 1.1 Schematic representing immune checkpoint axis between cancer cells and T cells.

Figure 1.2 Schematic representing CellSeq workflow

Figure 1.3 Expression of immune checkpoint proteins and their mRNA levels in HAP1 under basal conditions

Figure 1.4 Surface expression of B7H3, NRP1 and PVR in HAP1

Figure 2.1 Pipeline for CellSeq analysis

Figure 2.2 Schematic representing parameters for choice of hits for validation using B7H3 screen as an example

Figure 2.3 Size effect acts as a technical limitation resulting in recurring genes across screens.

Figure 2.4 Genes coding for transcription factors can be recurring across screens or specific to a phenotype

Figure 2.5 Conserved pathways such as chromatin modeling result in recurring genes across screens.

Figure 2.6 Genes unique to PD-L1 regulation have been reported

Figure 3.1 Schematic representing PVR structure and functions

Figure 3.2 Schematic representing hypothesis: Glycosylation of B7H3 regulates differential binding of B7H3 to its putative receptors

Figure 3.3 PVR regulatory map representing hits from pathways expected to influence PVR expression

Figure 3.4 CRISPR/Cas9 targeting of *FBXO11* leads to reduced PVR expression

Figure 3.5 B7H3 regulatory map representing the corrected mutational index of the *CD276* gene, that codes for B7H3 protein

Figure 3.6 Gene trap insertion sites for the CD276 genes across 3 different screens.

Figure 3.7 B7H3 regulator map representing hits from pathways expected to influence B7H3 expression

Figure 3.8 B7H3 regulator map representing hits from the sialylation pathway

Figure 3.9 Sialylation associated genes are putative regulators of B7H3 expression
Figure 3.10 CRISPR/Cas9 validation of select hits from the B7H3 screen

Figure 3.11 Sialylation genes *CMAS* and *SLC35A1* affect B7H3 surface and total protein expression

Figure 3.12 Biochemical vs genetic knockdown of sialic acid vary in terms of binding to B7H3 antibody clones and mobility shift in western

Figure 4.1 Schematic representing multifaceted roles of Neuropilin-1(NRP1)

Figure 4.2 Features of wet age-related macular degeneration.

Figure 4.3 Regulator map representing hits from pathways expected to influence NRP1 surface expression

Figure 4.4 UBE3D is negative regulator hit in the NRP1 screen

Figure 4.5 UBE3D is a negative regulator of NRP1 in HAP1 cells

Figure 4.6 UBE3D is a negative regulator of NRP1 in MCF7 cells

Figure 4.7 UBE3D E3 activity 'dead' mutants degrade NRP1, and AMD associated V379M sustains NRP1 expression

Figure 4.8 E1 pathway or proteasomal degradation inhibition does not rescue UBE3D driven NRP1 degradation

Figure 4.9 UBE3D interacts with overexpressed and endogenous NRP1 whereas AMD-associated V379M does not

Figure 4.10 Lysosomal degradation inhibition rescues UBE3D driven NRP1 degradation

Figure 4.11 Morpholino targeted UBE3D inhibition increases angiogenesis marker FLI1 expression

Figure 4.12 Morpholinos targeting UBE3D and NRP1 together does not increase angiogenesis marker FLI1 expression

Figure 4.13 Schematic representation of molecular link between UBE3D and NRP1

List of abbreviations

AF488	Alexa Fluor 488
Ala	Alanine
AMD	Age-Related Macular Degeneration
AML	Acute Myeloid Leukemia
ANOVA	Analysis of Variance
B7H3	B7 homolog 3
B7H3	B7 homolog 3
B7H4	B7 homolog 4
B7H5	B7 homolog 5
bp	base pair
BSA	Bovine Serum Albumin
CD226	Cluster of Differentiation 226
CD24	Cluster of Differentiation 24
CD47	Cluster of Differentiation 47
CD96	Cluster of Differentiation 96
CMAS	N-acylneuraminate cytidylyltransferase
CML	Chronic Myelogenous Leukaemia
CMTM6	CKLF Like MARVEL Transmembrane Domain Containing 6
CRISPR	Clustered Regularly Interspaced Short Palindromic Repeats
CTLA-4	Cytotoxic T-Lymphocyte-Associated protein 4
Cys	Cysteine

DepMAP	The Cancer Dependency Map
DNA	DeoxyriboNucleic Acid
DNAM-1	DNAX Accessory Molecule-1
EDTA	Ethylenediaminetetraacetic acid
EV	empty vector
FACS	Fluorescence Activated Cell Sorting
FBS	Foetal Bovine Serum
FBXO11	Fork head box 11
FGL-1	Fibrinogen-Like protein 1
FOXP3	Fork head box P3
FPKM	Fragments Per Kilobase of transcript per Million mapped reads
FU	Fluorescence Unit
Gal-3	Galectin-3
GPCRs	G-protein-coupled receptors
GPI	Glycosylphosphatidylinositol
GSK3B	glycogen kinase three beta
HA	HaemAgglutinin
hg	human genome
HLA-1	HLA class I glycoproteins
HRP	Horseradish Peroxidase
IFN-γ	Interferon gamma
INS	number of recovered insertions

IP	ImmunoPrecipitation
IRF1	Interferon Regulatory Factor 1
K	Lysine
L3MBTL3	Lethal (3)Malignant Brain Tumor-Like Protein 3
LAG-3	Lymphocyte-Activation Gene 3
LAM	Linear Amplification
LAMP-1	Lysosomal-associated membrane protein 1
LPS	Lipopolysaccharide
MED16	mediator complex subunit 16
Met	Methionine
MHCI	major histocompatibility complex, class I
MHCII	Major Histocompatibility Complex, class II
MI	Mutational Index
MICA	MHC class I polypeptide-related sequence A
MICB	MHC class I polypeptide-related sequence B
microRNA	micro Ribo Nucleic Acid
MO	Morpholio antisense oligonucleotides
MR1	major histocompatibility complex, class I-Related
mTOR	Mechanistic Target of Rapamycin
NANP	N-acetylneuraminic acid phosphatase
NANS	Neu5Ac 9-phosphate synthase
NF- ϰB	Nuclear Factor Kappa-light-chain-enhancer of activated B cells

NK	Natural Killer
NRP1	Neuropilin-1
PCR	Polymerase Chain Reaction
PD-1	Programmed cell Death protein 1
PD-L1	Programmed Death-ligand 1
PFA	Paraformaldehyde solution
PI	Propidium iodide
PVDF	polyvinylidene difluoride
PVR	Polio Virus Receptor
PVRL2	PVR and poliovirus receptor-related 2
QPCTL	glutaminyl -peptide cyclotransferase-like protein
RNF20	ring finger protein 20
RPE	retinal pigment epithelial layer
SAGA	Spt-Ada-Gcn5 acetyltransferase
SDS-PAGE	Sodium Dodecyl Sulphate–Polyacrylamide Gel Electrophoresis
SG	gingival epithelioid S-G
sgRNA	single guide RNA
shRNA	Short Hairpin Ribo Nucleic Acid
Siglec-10	sialic acid-binding Ig-like lectin 10
SIRPa	Signal-Regulatory Protein alpha
SLC35A1	Solute Carrier family 35 member A1

SPPL3	Signal Peptide Peptidase Like 3
SRP	Signal Recognition Particle
ssDNA	single stranded DNA
ST	Sialyl Transferase
SUMO	Small Ubiquiting like Modifier
T4 PNK	T4 Polynucleotide Kinase
TAMs	Tumour Associated Macrophages
TGFB1	Transforming Growth Factor Beta 1
TIGIT	T cell immunoreceptor with Ig and ITIM domains
TIM-3	T cell Immunoglobulin and Mucin domain-containing protein 3
TME	Tumour Micro Environment
TMem	memory T cells
TRAF3	TNF Receptor Associated Factor 3
Treg	Regulatory T cells
Ub	Ubiquitin
UPS	Ubiquiting Proteasome System
USP22	Ubiquitin-Specific-Peptidase 22
Val	Valine
VEGF	Vascular Endothelial Growth Factor

Chapter 1: Introduction

1.1 Immune checkpoint blockade

The interplay between the tumour and the immune system is highly complex. Ideally, the immune system should be able to elicit continuous cycles of immune-stimulatory factors that broaden the immune response against cancer. However, the tumours hijack the immune-regulatory factors in place to prevent overt immune responses and use it to evade and suppress the immune system(1). Specifically, the tumours express various proteins, known as immune checkpoints that applies break on cytotoxic T cells from recognizing and eliminating them in a specific manner(2). In back to back Nobel prize winning discoveries, James Allison's group first revealed that cytotoxic T-lymphocyte-associated protein 4 (CTLA-4) inhibits dendritic cells from alerting T cells regarding the presence of a tumour and soon after Tasuku Honjo's team unveiled a molecular break between programmed cell death protein 1 (PD-1) and programmed death-ligand 1 (PD-L1) that prevents T cells from attacking cancer cells(3-5). These two discoveries led to the targeting of PD-1, PD-L1 and CTLA-4 using immune checkpoint inhibitors to release the brakes on cytotoxic T cells to elicit anti-tumour immunity (Fig 1.1), and subsequently revolutionized cancer treatment(6). Checkpoint blockade dramatically increased overall patient survival in different cancer types(6-9),(10). Around 800 clinical trials are currently

targeting the PD-L1/PD-1 axis and a major number of trials are underway on other conventional checkpoints, such as CTLA4(11).

1.2 Going beyond PD-1/PD-L1 blockade

Despite the success of PD-1/PD-L1 immune checkpoint axis blockade, the response to therapy has not been uniform across patients and cancer types and is usually accompanied by immune related adverse events(10, 12-15). Reasons for this include the heterogenous nature of the tumour and a plethora of immune evasion mechanisms(15). Development of checkpoint blockade strategies to tackle the heterogenous immune evasion mechanisms displayed by the tumour is underway, with more than 40 different immune checkpoints and modulators having been identified (Fig 1.1,1.2)(2, 16). For example, Lymphocyte-Activation Gene 3 (LAG-3) is expressed on T cell and its sustained expression and interaction with Major Histocompatibility Complex, class II (MHCII) drives T cell exhaustion(17). Another protein, T cell immunoreceptor with Ig and ITIM domains (TIGIT) is a T cell activation inhibitory receptor(17). T cell Immunoglobulin and Mucin domain-containing protein 3 (TIM-3) is expressed on different subtypes of T cells and other immune cells and drives immune suppression. Its expression on dysfunctional T cells has been associated with poor prognosis in multiple cancers(18). Given their recently established central role in the tumour-immune interface, LAG-3, TIGIT and TIM-3 have been coined as the second generation T cell inhibitory receptors(18). Similar to PD-L1, there are 10 other B7 family members, and among them B7 homolog 3-5 (B7H3, B7H4 and B7H5) are

emerging as attractive targets and have been broadly shown to inhibit T cell activation albeit with some contrasting reports for B7H3(19-22).

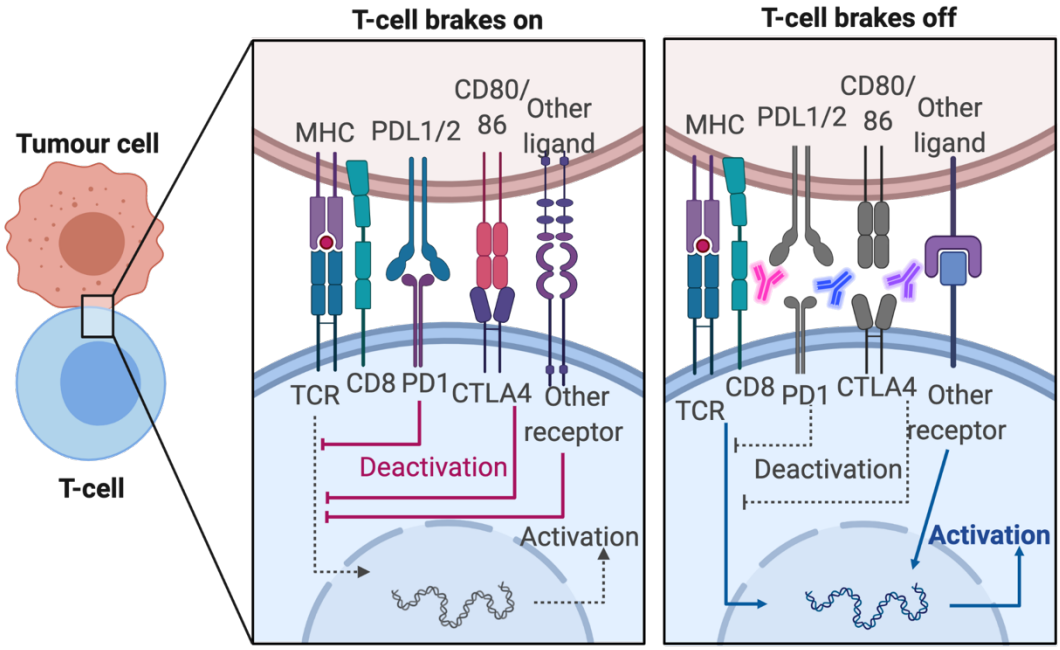


Figure 1.1 Schematic representing immune checkpoint axis between cancer cells and T cells. Antibodies against PD1 (blue), PDL1/2 (pink) and CTLA4 (purple) were used to block deactivation of T cells (Adapted from(6, 16), Created on Biorender.com

Notably, going beyond PD-L1 and PD-1 blockade, also means going beyond T cells. Other immune cells such as macrophages and Natural Killer (NK) cells can mediate tumour clearance through phagocytosis or antibody dependent phagocytosis respectively(23). Cancer cells express proteins that inhibit macrophage or NK cell mediated anti-tumour immunity. For example, the T cell inhibitory receptor TIGIT is also expressed on NK cells and inhibits NK cell

mediated tumour clearance(24). In macrophages, Cluster of Differentiation 47 (CD47) is a ‘do not eat me’ signal overexpressed on cancer cells and interacts with signal-regulatory protein alpha (SIRPα) on macrophages, and inhibits phagocytic clearance, thus acting as an innate immunity checkpoint(25). More recently, an interaction between a newly discovered ‘do not eat me signal’ CD24 expressed on cancer cells and sialic acid-binding Ig-like lectin 10 (Siglec-10) on tumour associated macrophages (TAMs) was identified as a macrophage immune checkpoint that inhibits phagocytic clearance(26, 27). Another study, reported that Neuropilin-1 (NRP1) blockade promotes memory T cells (T_{Mem}) cells responsible for durable anti-tumour immunity, thus acting as an immune memory checkpoint(27). Immunotherapeutic strategies centred around these second-generation checkpoints, B7 family members, and other immune cell checkpoints are showing encouraging results in Phase I and II clinical trials(18). However, the biology of these targets is not completely understood. For example, current LAG-3 targeting strategies focus on the LAG-3-MHCII axis driven inhibition of T cells while LAG-3 interaction with other ligands such as fibrinogen-like protein 1 (FGL-1), Galectin-3 (Gal-3) is incompletely understood(18). Another example, B7 family members such as B7H3 and B7H4 have been reported to act as a double-edged sword and drive both inhibitory and stimulatory axis on T cells(21, 22). It has been speculated that these opposing actions could be through distinct putative receptors. While there have been multiple efforts to identify the receptors of these proteins, there is still no consensus(20). Inhibitory receptors such as TIGIT have pleiotropic ligands. For example, polio virus receptor (PVR, CD155) is a ligand of TIGIT that drives an immune checkpoint axis but can also bind to

DNAX Accessory Molecule-1 (DNAM-1) and Cluster of Differentiation 96 (CD96) to activate NK cells(24, 28-30).

In summary, despite the identification of such key components of the tumour-immune interface, there remains much to be understood regarding the nature of the inhibitory receptors and their ligand interactions. In some cases, even the putative receptors of checkpoint ligand interactions have not been identified. Furthermore, understanding the mechanism of immune suppression by these checkpoints will be instrumental in identifying ideal blocking strategies. Overall, a deep dive into the complex biology underlying these promising components of the tumour immune interface will be critical to developing rational immunotherapeutic with high probability for translation(31).

1.3 Whole genome genetic screening coupled with protein abundance to dissect the tumour immune interface

Thus far the discovery of immuno-regulatory pathways relevant to tumour immunity has been preceded by years of careful mechanistic studies involving various steps such as the cloning of relevant genes and generation of knockout mice(32). However, recent technological advances in functional genomics, such as haploid genetics and Clustered Regularly Interspaced Short Palindromic Repeats (CRISPR) /Cas9 approaches that can link genotypes in an unbiased and systematic manner to cellular phenotypes, has enabled accelerated discovery and dissection of complex biology, including the tumour immune interface(33-38)(39-50).

Previously, conventional functional genetic screens were restricted to employing mutagenized libraries generated by chemical methods, gene trapping, short hairpin Rino Nucleic Acid (shRNA) and CRISPR/Cas9 towards enriching or depleting mutants and analysing the subsequent effect of the genotype on simple readouts such as proliferation and viability(51). With the advent of CRISPR/Cas9 and haploid genetics, we have been able to overcome disadvantages such as efficiency, off-target effects and scalability, thus enabling the coupling of more complex cell libraries and phenotypes. For example, one such technological advancement involves coupling massively parallel sequencing of complex cellular libraries with phenotypic readouts such as protein abundance, protein-protein interactions and other phenotypes that can be quantified by Fluorescence Activated Cell Sorting (FACS) to establish genotype-phenotype relationships(52-60). In a paradigm shifting study, to identify novel regulators of Lipopolysaccharide (LPS) induced tumour necrosis factor alpha (TNF-α) protein abundance, Parnas et al coupled fluorescence readouts of protein abundance from FACS to massively parallel sequencing of CRISPR mutant cell libraries in a FACS based CRISPR screen to link genomic mutations to protein abundance. Hereby, they generated a genome-wide mutant library of dendritic cells using CRISPR/Cas9 and stained them for TNF-α expression using fluorescent antibodies. Following this, they visualized and sorted the cells with high or low expression of TNFα at the extreme ends of the fluorescent distribution as measured by FACS. They hypothesized that, positive regulators of TNF-α would be enriched in the low expression population and vice versa for the negative

regulators. Through this method, they discovered multiple known components of TNF-α and some novel regulators(58).

In another study, Brockmann, M. et al., employed mutagenized near haploid mammalian cells in a similar approach to link physiological protein abundance and genomic mutations in a FACS based haploid screen. The use of mutagenized haploid cells facilitated high recovery of distinct mutations enabling robust statistics (50). Using this approach, they uncovered genetic wiring maps governing protein expression of key receptor complexes and proteins such as G-protein-coupled receptors (GPCRs), Lysosomal-associated membrane protein 1 (LAMP-1) and interferon regulatory factor 1 (IRF1)(50).

Recently, these FACS based forward genetic screens have been exploited to unravel key workings of the tumour immune interface. An important discovery was made by two groups at the same time by using a FACS based haploid/CRISPR genetic screening approach, CKLF Like MARVEL Transmembrane Domain Containing 6 (CMTM6) was identified as a novel regulator of PD-L1 by Mezzadra, R. et al., on a haploid cell line HAP1 and by Burr, M. L. et al., on a pancreatic cancer cell line(49, 61). These findings, extended to many other cancer cell lines, highlighting the role of such a method in identifying key unknown immunotherapeutic targets that have relevance in different cancer models. Another study, employed a FACS based haploid screen to identify novel regulators of CD47, a ‘do not eat me’ signal overexpressed on cancer cells, that interacts with SIRPα on myeloid cells and prevents tumour cell clearance(48). This study led to the discovery of glutaminyl -peptide cyclotransferase-like protein (QPCTL), a glutaminyl cyclase as a modulator of the

CD47-SIRPα interaction. Furthermore, it was reported that QPCTL blockade can enhance cellular phagocytosis and tumour cell clearance. This study provided proof of concept that such FACS based forward genetic screens can be used to unravel regulators of protein-protein interactions, that are critical regulators of immune checkpoints. Similarly, another study used a series of iterative FACS based haploid screens to identify regulators of HLA class I glycoproteins (HLA-I), a protein involved in presenting antigens to CD8+ T cells to drive anti-tumour immunity. This study identified a unique shielding mechanism by glycosphingolipids driven by signal Peptide Peptidase Like 3 (SPPL3) protease as a modulator of surface antigen presentation by HLA-I(62). Using a FACS based CRISPR screen, another study aimed to identify novel regulators of fork head box P3 (FOXP3), a master transcription factor that stabilizes tumour promoting T regulatory cells (T_{reg}). They identified ubiquitin-specific-peptidase 22 (USP22), a member of the Spt-Ada-Gcn5 acetyltransferase (SAGA) chromatin-modifying complex as a positive regulator of FOXP3 expression and ring finger protein 20 (RNF20), an E3 ubiquitin ligase as a negative regulator of FOXP3. Furthermore, they report a reciprocal ubiquitin switch in T_{reg} cells between USP22 and RNF20 in FOXP3 regulation(63). This study set the stage for using forward genetic screens towards T_{reg} immunotherapy target discovery efforts. Using a FACS based CRISPR screen, another study set out to dissect the regulatory mechanism behind interferon gamma (IFN-γ) derived MHCII expression, a key axis that's instrumental in driving CD4+ effector function in cancer cells. They uncovered glycogen kinase three beta (GSK3B) and mediator complex subunit 16 (MED16) as regulators of this axis and thus critical to driving CD4+ T cell

driven anti-tumour immunity(64). In another study, Gu et al adapted FACS based CRISPR screens to understand how to selectively upregulate major histocompatibility complex, class I (MHCI) without inducing PD-L1 expression. They achieved this by replacing the low and high expression gating strategy, by instead selectively gating for MHCI expression and PD-L1 expression with different fluorophores followed by enrichment and deep sequencing. This study discovered TNF Receptor Associated Factor 3 (TRAF3), a suppressor of the nuclear factor kappa-light-chain-enhancer of activated B cells (NF- ϰB) pathway as a negative regulator of MHCI but not PD-L1, thus identifying TRAF3 as a promoter of anti-tumour immunity(65). This study is an ideal example for how FACS based protein abundance readouts can be modified to push the boundaries of their application in dissecting the tumour immune interface.

Collectively, FACS based CRISPR/Haploid screens have both been instrumental in discovering critical components of the tumour immune interface and have accelerated our understanding of cancer immunity.

1.4 CellSeq technology

A particular FACS based haploid screen discussed in the previous section has emerged as a compelling paradigm and was pivotal in the discovery of novel regulators of key immune checkpoints such as PD-L1 and CD47(48, 49). This approach, henceforth referred to as CellSeq, was pioneered in the lab of Thijn Brummelkamp at The Netherlands Cancer Institute and adapted by our lab. The principal features of CellSeq are: 1) It functionally links individual genes to any phenotype that can be measured by a fluorescent readout. For example, protein

abundance, post translational modifications, genetic probes etc. 2) By employing a near haploid HAP1 cell line, it facilitates gene trap mutagenesis and achieves recovery of mutants at a single cell resolution. 3) Identifies high number of distinct mutations and enables robust statistics(50).

The workflow of a conventional CellSeq screen is outlined in (Fig 1.2). First, to generate a complex library of mutants covering most of the expressed genes, HAP1 cells are mutagenized using gene traps(66, 67). Retroviral gene traps induce mutations at the site of insertion by interfering with the splicing machinery and disrupting the coding sequence(68). Notably, although insertions in the sense direction lead to inactivation of the protein coding genes, anti-sense insertions do not ordinarily lead to inactivation and are not included during downstream data analysis. Next, for measuring the abundance of phenotypes such as protein expression, the mutagenized cells are stained using the respective fluorescent antibody. To ensure that, heterozygous mutations are excluded in downstream analysis, the cells are stained with propidium iodide to restrict analysis to G1 phase cells. Following this, the stained cells are visualized by FACS and the mutated cells enriched at the extreme ends of the distribution are sorted. To identify the gene trap insertion sites, the genomic deoxyribonucleic acid (DNA) from the sorted high and low populations are isolated and processed separately. A linear amplification reaction is used to amplify the gene region proximal to the gene trap, followed by streptavidin enrichment of the amplified insertion sites. Following this, ligation of adapters and polymerase chain reaction (PCR) is then used to generate a 50 base pair, single end Illumina sequencing library.

Notably, it has been reported that the rigorously optimised protocol leads to the enrichment and mapping of millions of distinct insertion sites, thus facilitating high resolution(50, 60). The distinct insertion sites of an individual gene in each of the high and low populations are calculated and the odds ratio of the enrichment is identified. The odds ratio, hereafter to referred to as mutational index (MI) thus enables the distinction of each gene as a positive or negative regulator of the phenotype of interest. Subsequently, the output of a CellSeq experiment is a high resolution phenotype-genotype map.

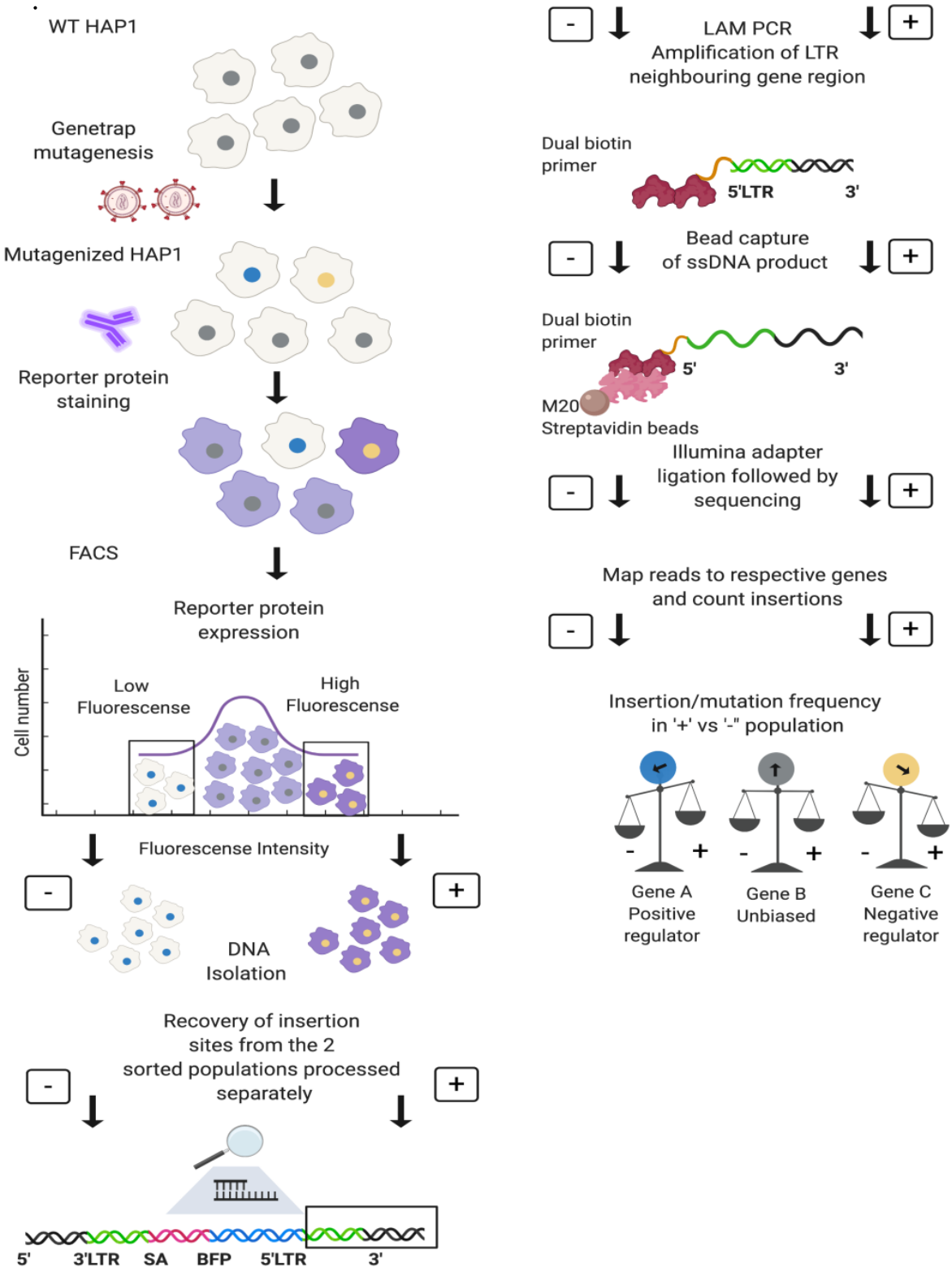


Figure 1.2 Schematic representing CellSeq workflow Adapted from(50), Created on Biorender.com

1.5 CellSeq technology harnesses the power of haploid genetics

CellSeq is centred around the use of genetrap mutagenized near haploid human cell line, HAP1(69, 70). HAP1 was generated from a patient derived chronic myelogenous leukaemia (CML) cell line, KBM-7. HAP1 contains one copy of most chromosomes instead of two, except for a 30 megabase fragment of chromosome 15 that codes for 330 genes, thus making it near haploid(70). Subsequently, it overcomes the two-allele problem, where a genetic mutation may be redundant and thus does not reflect in the organism's phenotype thus making them ideal for random insertional mutagenesis screens(71, 72). Mutagenized HAP1 cell line has since emerged as a powerful tool for systematically coupling individual genes to a phenotype of interest through forward genetic screens(50, 73-76). In a typical CellSeq experiment, the use of gene traps in haploid cells, facilitates recovery of >20 million distinct mutants and enables robust statistics and helps in identifying regulators of the phenotype of interest with a high degree of certainty. An obvious drawback of being restricted to the use of HAP1 cell in CellSeq, like any other cell line is that it represents only a limited area of biology. Therefore, it's important to evaluate the suitability of HAP1 towards the phenotype of interest. Nevertheless, by applying a combination of CRISPR/Cas9 genetic modifications and pathway stimuli, more phenotypes can be made accessible. In addition, the entire transcriptome, proteome and genome have been generated for HAP1 and thus facilitates informed choice of phenotypes. The above qualities coupled with the potential of CellSeq in identifying novel regulators of mechanisms ranging from cholesterol

metabolism to dissecting multiple layers of signalling pathways, like regulation of mechanistic target of rapamycin (mTOR) signalling, puts it forward as a state-of-the art technology in the field of uncovering genetic modifiers in human cells(50, 73, 75). Furthermore, as discussed previously CellSeq has been pivotal in identifying novel regulatory mechanisms of key immune checkpoints such as PD-L1 and CD47(48, 49).

1.6 Research objective

Therefore, the overarching goal of the thesis is to utilize such a FACS based whole haploid genetic screening approach set up in our lab to explore the underlying regulatory circuits of less understood immune checkpoints to generate comprehensive regulatory maps and functionally annotate them to identify novel immunotherapeutic targets.

1.7 HAP1 as a model for studying immune checkpoints

Using CellSeq in HAP1 cells, we set out to identify novel regulators of cell-surface proteins with a well-established role in the immune system. First, we selected a panel of forty immuno-modulators being explored at various stages of clinical trials and employed previously published transcriptome data to determine their expression in HAP1 cells(67). Of the 40 genes, 11 genes were expressed at Fragments Per Kilobase of transcript per Million mapped reads (FPKM) >1, which corresponds approximately with >1 mRNA molecule per cell (Fig 1.3).

These data indicate that 11 out of the initial 40 immune modulators are possibly expressed at detectable protein levels in HAP1.

Among the 11 putatively expressed genes, CD47, MHC class I polypeptide-related sequence A (MICA) and MHC class I polypeptide-related sequence B (MICB) have been or are currently investigated with CellSeq in other laboratories(48). Furthermore, as PVR and poliovirus receptor-related 2 (PVRL2) are highly similar we chose to focus on the former as it is gathering a lot of attention as a promising therapeutic target in the immune oncology space(77, 78). Finally, from the remaining candidates we found the biology of B7H3, PVR, NRP1 and SIRPa most interesting and hence chose them for suitability in CellSeq screening: B7H3, PVR, NRP1 and SIRPα.

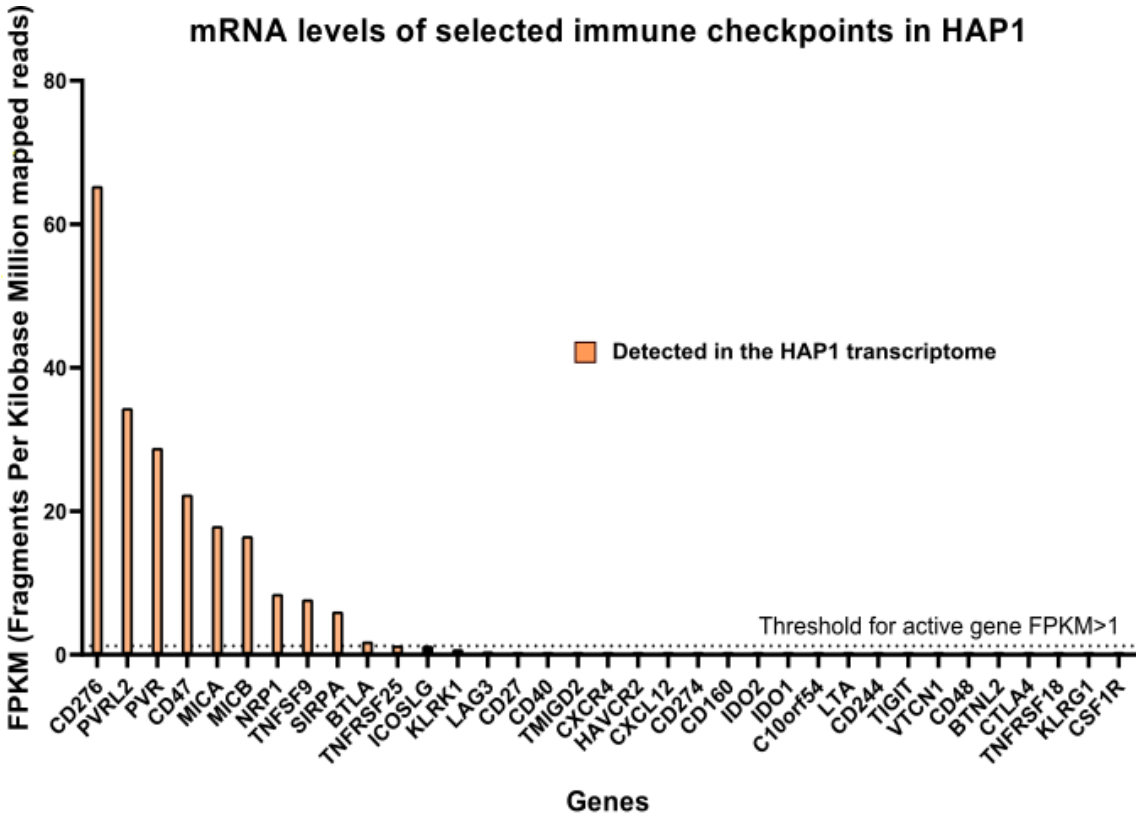


Figure 1.3 Expression of immune checkpoint proteins and their mRNA levels in HAP1 under basal conditions A) mRNA levels of immune checkpoint genes on HAP1. Threshold for choice of candidate reporters for CellSeq set at FPKM (Fragments per kilobase transcript per million reads) of > 1.

Next, we determined the cell surface expression of B7H3, PVR, NRP1 and SIRPα using fluorescently labelled antibodies directed at these individual proteins. We detected strong surface expression by FACS for B7H3, PVR and NRP1, whereas we could not detect SIRPα expression (Fig 1.4, Appendices 6.4). Importantly, the antibody signal was specific as transient transfection of single guide RNA (sgRNA) targeting these cell surface proteins along with a Cas9 expression plasmid resulted in a strong reduction of the signal (Fig 1.4). Hence, in this thesis we aim to dissect the underlying regulatory circuits of NRP1, PVR and B7H3 and identify novel regulatory mechanisms.

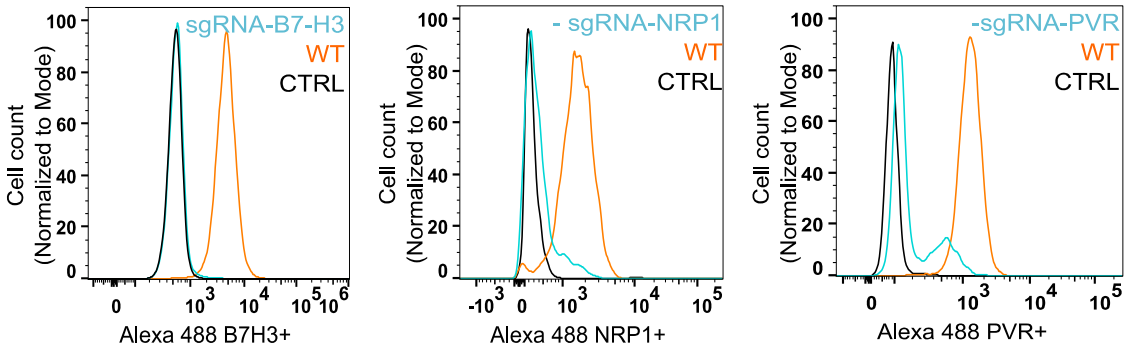


Figure 1.4 Surface expression of B7H3, NRP1 and PVR in HAP1 WT-HAP1 cells and polyclonal HAP1 cells derived by CRISPR/Cas9 sgRNA targeting (A) *B7H3*, (B) *NRP1* and (C) *PVR* were subsequently evaluated for change in their respective surface protein expression levels using flow cytometry, to determine antibody specificity.

Briefly, similar to PD-L1, B7H3 elicits a immunosuppressive effect on cytotoxic T cells(21). Another checkpoint protein, PVR engages with TIGIT on T cells and NK cells to suppress their anti-tumour effects(78). PVR has been shown to correlate with poor prognosis in Acute Myeloid Leukemia (AML)(77). OMP-31M, a drug that blocks the TIGIT-PVR axis is currently in phase 1(79). NRP1 is another protein, expressed on immune cells that has been associated with loss of effector cytotoxic T cell function by stabilizing the tumour promoting T_{reg} cell state in the tumour milieu(80, 81). These proteins will be discussed further in Chapters 3 and 4.

1.8 **Specific research objectives:**

- Evaluate the expression of immune checkpoints on HAP1 to identify candidates for CellSeq.
- Apply CellSeq to identify novel molecular regulators of immune checkpoints B7H3, PVR and NRP1.
- Validate the identified regulators from the CellSeq screen.
- Explore the underlying biology of selected regulators from the above screens using functional and mechanistic follow-up studies.

In Chapter 3, we apply CellSeq towards identifying novel regulators of B7H3 and PVR . In Chapter 4, we investigate NRP1 regulation using CellSeq and

study the novel regulator UBE3D, an age-related macular degeneration (AMD) risk associated gene as a modulator of the angiogenesis co-receptor and immune checkpoint NRP1.

Chapter 2: Materials and methods

2.1 Antibodies, Plasmids, Buffers, Kits and Reagents

Table 2.1 Primary antibodies used in this study

Protein	Catalog number	Supplier	Application
B7H3	331602	Biolegend	Flow
NRP1	354502	Biolegend	Flow
SIRPa/b	323801	Biolegend	Flow
PVR	337602	Biolegend	Flow
NRP1	3725S	Cell Signalling Technology	Western/IP
B7H3	14058S	Cell Signalling Technology	Western
B-Actin	5125S/A2066	Cell Signalling Technology/Sigma Aldrich	Western
Vinculin	13901T	Cell Signalling Technology	Western
UBE3D	ab121927	Abcam plc	Western
FLAG	A8592	Merck Life Science, UK	Western
HA	3724S	Cell Signalling Technology	IP
Ubiquitin	3936S	Cell Signalling Technology	Western

Table 2.2 Secondary antibodies used in this study

Protein	Catalog number	Supplier	Application
Goat anti-mouse IgG (H+L) Cross adsorbed secondary antibody	A-11001	Invitrogen	Flow
Alexa Fluor 488 anti-mouse IgG2a antibody, Clone RMG2a-62	407121	Biolegend	Flow
Alexa Fluor 488 anti-mouse IgG1	A-21121	Invitrogen	Flow
HRP- anti Rabbit IgG	7074S	Cell Signalling Technology	Western/IP

Veriblot secondary antibody	ab131366	Abcam	Western
HRP- anti mouse IgG	7076S	Cell Signalling Technology	Western
mAb IgG Isotype Control	3900S	Cell Signalling Technology	IP

Table 2.3 Plasmids used in this study

Plasmid	Catalogue Number	Source
pGT-en2-BFP	-	Gift from T. Brummelkamp
pGag-Pol	-	Gift from T. Brummelkamp
pAdVantage	-	Gift from T. Brummelkamp
pVSV.G	14888	Addgene
pCMV-GFP	11153	Addgene
pLentiCRISPR v2	52961	Addgene
pCDNA3.1-RFP	-	Marielle Hijmans
pCDNA3.1-UBE3D-FLAG	OHu02714D	Genscript
pCDNA3.1-NRP1-FLAG	OHu18607D	Genscript
pCDNA3.1-NRP1-HA	OHu18607C	Genscript

Table 2.4 Buffers used in this study

Buffer	Composition
PBS + 0.1% BSA solution	0.05 g BSA in 50 ml PBS
2X Binding Buffer	6M LiCl, 10 mM Tris, 1mM EDTA, pH=7.5
PBS + 0.05% Triton X-100	25 µl Triton X-100 in 50 ml PBS

iBlock	0.2% w/v I-Block and 0.1% v/v Tween-20 in 1X PBS
PBS-T	0.1% v/v Tween-20 in 1X PBS
IP Lysis buffer	TBS-0.5%NP40+PMSF
IP wash buffer	TBS-0.5%NP40

Table 2.5 Commercial kits used in this study

Kit	**Supplier/Catalogue Number**
AccuPrime Taq DNA Polymerase High Fidelity (10X Accuprime Buffer II, MgSO4, Accuprime TaqHI)	Thermo Fisher Scientific, 12346094
CircLigaseII ssDNA Ligase (CircLigase II, CircLigase II Buffer)	Cambio, CL9021K
DNeasy Blood and Tissue	Qiagen, 69506
Phusion Site-Directed Mutagenesis Kit-20 reactions	Life technologies, F541
High Sensitivity DNA Bioanalyzer kit	Agilent, 5067-4626
Plasmid Midi Kit	Qiagen, 12143
MinElute PCR Purification	Qiagen, 28004
QIAamp DNA Mini Blood	Qiagen, 51104
QIAquick Gel Extraction	Qiagen, 28704
QIAquick PCR Purification	Qiagen, 28106
QIAprep Spin Miniprep	Qiagen, 27104
QuantiTect SYBR Green PCR kit	Qiagen, 204143
SuperScript III First-Strand Synthesis kit	Thermo Fisher Scientific, 18080051
Qubit dsDNA HS assay	Life Technologies, Q32851
RNAeasy Mini	Qiagen, 74106

Table 2.6 Reagents and consumables used in this study

Reagent/consumables	Code	Supplier
10X Bulk ClearSort Sheath Fluid	AE700714	Sony
20 mL BD™ syringe with BD Luer-Lok™ tip.	302830	BD
2x Laemmli buffer	S3401-10VL	
30 mL BD Luer-Lok™ tip syringe	302832	BD
6x Laemmli buffer	J61337.AC	
Absolute EtOH	10517694	Thermo Fisher Scientific
AccuPrime™ Taq DNA Polymerase High Fidelity	12346086	Thermo Fisher Scientific
Agarose	1613101	BioRad
Bafilomycin A1	54645S	Cell Signalling Technology
BCA assay kit	23225	Thermo Fisher Scientific
BenchMark Prestained protein ladder	1078010	Invitrogen
Betaine solution	B0300-1VL	Sigma Aldrich
Bortezomib	2204S	Cell Signalling Technology
Bovine Serum Albumin	A3059-10G	Sigma Aldrich
BsmBI	R0580S	New England Biolabs
CircLigase™ II ssDNA Ligase	CL9025K	Cambio
Clarity Max Western ECL Substrate	1705062	BioRad
Distilled Water	15230147	Thermo Fisher Scientific
Distilled Water (H2O)	15230147	Thermo Fisher Scientific
DL-Dithiothreitol solution	646563	Sigma Aldrich
DMEM, high glucose, pyruvate	41966029	Thermo Fisher Scientific
dNTP Mix (10 mM)	R0191	Thermo Fisher Scientific
Dynabeads Protein A for Immunoprecipitation-1 mL	10001D	Life Technologies Ltd
Dynabeads™ M-270 Streptavidin	65305	Thermo Fisher Scientific

Ethylenediaminetetraacetic acid (EDTA) (0.5 M), pH 8	AM9260G	Thermo Fisher Scientific
Falcon 5mL Round Bottom High Clarity PP test Tube, with Snap Cap, Sterile, 25/Pack, 500/Case	352063	Corning
Falcon 5mL Round Bottom Polystyrene test Tube, with cell Strainer Snap Cap, 25/Pack, 500/Case	352235	Corning
Falcon® 175cm² Rectangular Straight Neck Cell Culture Flask with Vented Cap	353112	Corning
Fix Buffer I	557870	BD Bioscience
DMEM, high glucose, GlutaMAX	10566016	Thermo Fisher Scientific
Foetal Bovine Serum (FBS)	S-001A-BR	Antibody production service
Gel loading Dye (6X)	B7024S	New England Biolabs
Genejuice® Transfection Reagent	70967-10ML	EMD Millipore
I-Block Protein Based Blocking Reagent	T2015	Applied Biosystems
IMDM, GlutaMAX	31980030	Thermo Fisher Scientific
Lithium chloride	203637	Sigma Aldrich
Midori Green	MG 04	Nippon Genetics Europe
Millex-HA Syringe Filter Unit, 0.45 µm, mixed cellulose esters, 33 mm, ethylene oxide sterilized	SLHA033SB	Merck Millipore
MLN7243	HY-100487-5mg	Cambridge Bioscience Limited
MnCl2 0.1M	20-309	Sigma Aldrich
NEBuffer 3.1	B7203S	New England Biolabs
Alpha 2-368 Neuraminidase	P0720S	New England Biolabs
Non-stick, RNase-free Microfuge Tubes, 1.5 mL	AM12450	Thermo Fisher Scientific
NP40 cell lysis buffer	FNN0021	Thermo Fisher Scientific

NuPAGE MOPS SDS Running Buffer (20X)	NP0001	Thermo Fisher Scientific
OptiMEM	31985062	Thermo Fisher Scientific
PageRuler Plus Prestained Protein Ladder	26619	Thermo Fisher Scientific
Paraformaldehyde solution (PFA) 4% in PBS	sc-281692	Santa Cruz Biotechnology
PBS (1X)	10010023	Thermo Fisher Scientific
Penicillin-Streptomycin-Glutamine (100X)	10378016	Thermo Fisher Scientific
Perm Buffer III	558050	BD Bioscience
Phosphatase inhibitor	A32957	Thermo Fisher Scientific
Pierce™ 20X TBS Buffer	28358	Thermo Fisher Scientific
PMSF Protease Inhibitor	36978	Thermo Fisher Scientific
Propidium Iodide	P1304MP	Thermo Fisher Scientific
Protamine sulphate salt from salmon	P4380-25G	Sigma Aldrich
Protease inhibitor	11873580001	Sigma Aldrich
Protein gel (NuPage Bis-Tris 4-12%)(1.0mm) 10 well	NP0321BOX-10 gels	Thermo Fisher Scientific
Protein gel (NuPage Bis-Tris 4-12%)(1.0mm) 12 well	NP0322BOX-10 gels	Thermo Fisher Scientific
Puromycin	ant-pr	Invivogen
QIAamp DNA Mini Blood kit	51104	Qiagen
QIAquick PCR Purification Kit	28106	Qiagen
Quick-Load Purple 1 kb DNA Ladder	N0552	New England Biolabs
RIPA buffer	R0278-50ML	Sigma Aldrich
RNase A	A3832	Applichem
SH800 Setup Beads	LE-B3001	Sony
Sodium Hypochlorite	S/5040/PB17	Thermo Fisher Scientific
Stbl3 Chemically Competent Escherichia coli	C737303	Invitrogen

SuperSignal West dura Femto (ECL)	34095	Thermo Fisher Scientific
T4 DNA Ligase	M0202	New England Biolabs
T4 DNA Ligase Reaction Buffer	B0202	New England Biolabs
T4 Polynucleotide Kinase	M0201	New England Biolabs
TBE Buffer 10X	1610770	BioRad
Trans-Blot Turbo Mini/Midi PVDF Transfer Packs	170-4156/170-4157	BioRad
Trans-Blot Turbo Mini/Midi PVDF Transfer Packs	170-4156/170-4157	BioRad
Triton X-100	T8787	Sigma Aldrich
Trypsin-EDTA	25300096	Thermo Fisher Scientific
Tube Strips with Individually Attached Bubble Caps	53509-304	VWR
Tube, Thinwall, Ultra-Clear™, 38.5 mL	344058	Beckman Coulter
TurboFectin 8	TF81001	OriGene
Tween-20	WZ-88248-24	Acros Organics
Western Lightning Plus-ECL	NEL104001 EA	Perkin Elmer

2.2 Cell lines

Cell line	Mutation	Source
HAP1	-	Thijn Brummelkamp (NKI, Amsterdam)
HEK293T	-	ATCC
MCF7	-	ATCC
HAP1 UBE3D KO C4	2 bp deletion in exon 2	Toczyski Lab
HAP1 UBE3D KO C6	2 bp deletion in exon 4	Toczyski Lab
HAP1 CMAS KO	10bp deletion in exon 1	Gift from Horizon discovery
HAP1 SLC35A1 KO	2bp deletion in exon 2	Gift from Horizon discovery
HAP1 RAB7A KO	2bp deletion in exon 3	Gift from Horizon discovery
HAP1 OTUD5 KO	1bp deletion in exon 3	Gift from Horizon discovery
HAP1 YES1 KO	17bp deletion in exon 2	Gift from Horizon discovery

Table 2.7 Cell lines used in this study. Culture of HAP1 parental and mutant cells was carried out in IMDM Glutamax ™ (Thermo Fischer scientific), supplemented with 10% Foetal Bovine Serum (FBS, ELife science production) and penicillin-Streptomycin-Glutamine (Thermo Fischer Scientific). HEK293T and MCF7 cells were cultured in DMEM Glutamax ™ (Thermo Fischer scientific), supplemented with 10% Foetal Bovine Serum (FBS, ELife science production) and Penicillin-Streptomycin-Glutamine (Thermo Fischer Scientific).

2.3 Generation of mutagenized HAP1 (mut-HAP1) cells

Retroviral gene trap plasmid pGT-en2-BFP possesses an inactivated 3' LTR, a strong adenoviral (Ad40) splice-acceptor, Blue Fluorescent Protein (BFP), the SV40 polyadenylation signal and 5' LTR. Virus containing the gene trap was produced in HEK293T as described in Biomen et al(67). HEK293T cells were expanded to ~80% confluence in 6 T175 flasks. The transfection mix was prepared by combining the plasmid mix as described (Table 2.6) and 45 ul of Turbofectin 8.0 was diluted in 200 ul Opti-MEM for each transfection and incubating at room temperature for approximately 30 minutes. Simultaneously, the normal growth medium of HEK293T cells was replaced by DMEM 30% FBS 1X P/S Glut. Following this, the transfection mix was added to the HEK293T cells. 40 hours post transfection, the HEK293T supernatant was collected and passed through mixed cellulose ester 0.45 um membrane (Merck Millipore). Post filtration, the supernatant was centrifuged in Ultra-Clear tubes (Beckman Coulter) and centrifuged using an SW32Ti rotor on an Optima XPN centrifuge at 60,000 rcf at 4°C for 2 hours. Post ultra-centrifugation, the supernatant was discarded and the viral pellet resuspended in 200 ul PBS per each tube was stored overnight. The above viral supernatant collection steps were repeated twice daily for up to 3 days. For transduction, the viral supernatant concentrated from a single harvest of 3 flasks was resuspended in IMDM 1X P/S-Glut 10% FCS in the presence of 8 ug/ml protamine sulphate and added to a single flask of ~50% confluent HAP1 cells. The above transduction step was repeated for up to three consecutive days. Following transduction, the cells were expanded in IMDM P/S

Glut 10% FCS media. The efficiency of transduction was identified by the gene trap encoded BFP protein and compared to the cells that did not undergo transduction using BD LSR Fortessa X20 (BD Biosciences). Using this method, we generated batches of gene trapped mutagenized HAP1 cells and stored them in liquid nitrogen.. The mutagenized HAP1 cells used in the CellSeq screens performed in this study were generated by Erica De Zan from the Nijman lab.

Plasmid mix	**Amount**
pGag-Pol	6.02 µg
pVSV.G	1.4 µg
pAdVantage	0.84 µg
pGT-en2-BFP	6.6 µg

Table 2.8 Plasmid mix for gene trap mutagenesis

2.4 Haploid genetic screen (CellSeq)

The GT-HAP1 cells were thawed and expanded to $3x10^9$ cells. Any screen specific treatment of cells was carried out 24 hours prior to harvest. The cells were washed once with 1x PBS and then harvested using 1 mM EDTA. Harvested cells were then spun down at 1500 rpm for 5 minutes and resuspended in 1%FBS 1X PBS to be pooled together. The pooled cells were pelleted down and resuspended in reporter protein specific primary antibody dilution in 1%FBS 1XPBS for the required duration at 4°C (Table 2.9). The cells were then washed once with 1%FBS 1XPBS by centrifuging at 1500 rpm for 5 minutes, followed by incubation in the screen specific secondary antibody solution for 30 minutes at 4°C (Table 2.9). After another two washes, the cell pellet was resuspended in pre

warmed 10 ml 1:1 BD Fix Buffer I:1xPBS solution for 10 minutes at 37°C to fix the cells. Two additional washes later, the cell pellet was resuspended in 1:1 BD Perm Buffer III:1xPBS for 30 minutes on ice to permeabilize the cells. After further two washes, the cells were incubated in RNAse A (0.8 mg/ml) for 1 hour and 30 minutes and stained with Propidium iodide (PI) (10 ug/ml) for 30 minutes at room temperature to select for cells in the G1 phase. The stained GT-HAP1 cells were then resuspended in 10% FBS 1XPBS and stored at 4°C for analysis and sorting over a period of 7 days. The cells were then diluted to a concentration of a 30 million/ml in a 10 ug/ml PI 10%FBS 1XPBS solution and acquired on a Sony LE-SH800 cell sorter mounted with a 70 um chip. Alexa Fluor 488 (Alexa 488) and PI can both be excited by the 488 nm laser. However, as their peak emissions are different they are captured by different detectors (525/50 for Alexa 488 and 665/30 for PI). During acquisition, gating was performed to exclude doublets and cells in their G1 phase were characterised by their 1n DNA content. Alexa 488 stained cells in the G1 population were visualized, and sorting gates were fixed to collect approximately 10^7 cells in the 1-3% of the high-Alexa488 and low-Alexa488 extreme ends of the distribution. The sorted cells were then pooled together to be taken forward for recovery of insertion sites.

Screen	Stimuli	Primary antibody	Secondary antibody
Poliovirus receptor (PVR)	-	Anti-PVR, 15 ug/mL	Alexa Fluor 488 anti-mouse IgG1, 1 ug/mL
B7H3	-	anti-human B7H3, Clone DCN.70, 10ug/mL	Alexa Fluor 488Goat anti-mouse IgG (H+L), 1 ug/mL
Neuropilin-1 (NRP1)	IFNy 10 ng/ml	anti-human NRP1, Clone 12C2, Concn 15ug/mL	Alexa Fluor 488 anti-mouse IgG2a, Concn 1 ug/mL

Table 2.9 List of antibodies, stimuli and staining concentration used in CellSeq

From each of the high-Alexa488 and low-Alexa488 sorted cell fractions, Genomic DNA was extracted using a QIAMP DNA Blood Mini kit (Qiagen) and processed separately in all subsequent downstream steps. For DNA De-crosslinking, the cells were resuspended in a solution of 200 ul PBS, 20 ul Proteinase K (Qiagen) and 200 ul Buffer AL, following this the samples were pulse vortexed for 15s and then incubated at 56°C at 1100 rpm overnight. After the overnight incubation, 200 ul volume of 100% concentrate EtOH was added to the samples. Following this, the samples were loaded onto a QIAmp spin column and spun down at 8000 g. The samples in the column were then subject to sequential washes with 500 ul buffer AW1 and 500 ul buffer AW2 by centrifuging them at 8000 g. Following the washes, the column was dried by centrifuging at the maximum speed for 3 minutes. The genomic DNA was then eluted in a volume of 50 ul pre warmed H_2O. In case of low concentrations, another round of elution was performed with an additional 50 ul H_2O. The DNA concentration was measured using a Nanodrop 8000 Spectrophotometer (Thermo Fisher Scientific).

2.5 Recovery of insertion sites

Recovery of gene trap insertion sites was carried out as described in Biomen et al(67) and summarized in Fig 1.2. All primers used during the insertion site recovery are listed (Table 2.10). First, Linear Amplification (LAM) PCR was used to amplify the insertion sites with a dual-biotinylated primer. Reaction volumes were adjusted to obtain approximately 1 ug genomic DNA/reaction. Reaction mixture in Table 2.11 represents required amounts for 1 LAM PCR reaction. A total of 6 reactions for each of the samples from high-Alexa488 and low-Alexa488 were set up for each screen.

Primer name	**Sequence**
Dual Biotin Primer	double biotin/GGTCTCCAAATCTCGGTGGAAC
Phosphorylated ssDNA linker	phospho/ATCGTATGCCGTCTTCTGCTTGACTCA GTAGTTGTGCGATGGATTGATG/dideoxycytidine
ssDNA pre-adenylated linker	adenyl/ATCGTATGCCGTCTTCTGCTTGACTCAGTA GTTGTGCGATGGATTGATG/dideoxycytidine
P5 LTR primer	AATGATACGGCGACCACCGAGATCTGATGG TTCTCTAGCTTGCC
P7 LAM primer	CAAGCAGAAGACGGCATACGA

Table 2.10 List of all primers used for recovery of insertion sites

Reagent	Amount (µl)	Final Concentration
Dual Biotin Primer	3	15 nM
10X Accuprime buffer 2	5	
MgSO4	1	1 mM
Accuprime™ Taq DNA Polymerase	0.4	
Genomic DNA	~ 1 µg	
dH2O	Bring to 50 µl	

Table 2.11 LAM-PCR reaction setup for each reaction

PCR amplification: 94°C 5 minutes, 120 cycles of (94 °C 30 seconds, annealing temperature of 58°C for 30 seconds and an extension temperature of 68°C for 1 minute), 68°C 7 minutes and 4°C forever.

Following this, 2.5 ul of M-270 streptavidin coated beads were prepared for pull down of biotinylated single stranded DNA (ssDNA) fragments for each reaction. i.e 15 ul of M-270 streptavidin coated beads were washed in 800 ul of PBS + 0.1% BSA for each of the samples. Following the washes, the supernatant was removed using a magnetic rack. The beads were then resuspended in equal volumes of LAM-PCR product and 2x binding buffer (6M LiCl, 10 mM Tris, 1 mM EDTA, pH= 7.5) and incubated at room temperature for 2 hours. Bead captured ssDNA were precipitated using a magnet, followed by 3 washes with PBS containing 0.05% Triton X-100 (Sigma).

Following this, ligation with ssDNA linker to the 3' of the biotinylated PCR product was carried out. For each sample, for which 6 LAM PCR reactions were carried out, 3 ligation reactions were setup. 0.05% Triton X-100 wash buffer was removed using a magnetic rack and the beads were resuspended in the DNA ligation mixture (Table 2.12).

Reagent	Amount (µl)	Final Concentration
Betaine	4	1 M
dH2O	11.5	
Circligase II buffer	2	
MnCl2	0.5	2.5 mM
pre-adenylated linker	1	1.25 µM
Circligase II	1	

Table 2.12 ssDNA ligation reaction setup for each reaction

Ligation: 60°C for 2h , followed by a 20 minute room temperature incubation, frequently agitated.

Following ligation, beads with the ligated products were washed 4x with PBS + 0.05% Triton X-100. The beads were then separated from the wash buffer using a magnetic rack and taken forward for addition of Illumina adaptors P5 (LTR primer) and P7 (LAM primer). Addition of Standard Illumina adaptors (P5 and P7) for Illumina sequencing were introduced via 3 Illumina master mix reactions for each sample that underwent 6 LAM-PCR reactions (Table 2.13).

Reagent	Amount (µl)	Final Concentration
dH2O	42.4	
10X Accuprime buffer II	5	
PI primer	1	1.25 µM
PII primer	1	1.25 µM
AccuPrime™ Taq DNA Polymerase	0.6	

Table 2.13 Illumina addition PCR master mix for each reaction

The Illumina adapter addition PCR reaction condtions: 18 cycles, annealing temperature of 55°C for 30 seconds, 105 seconds of extension step at 68°C.

Following the reaction, the PCR fragments were purified using QIAquick PCR purification Kit (Qiagen) and eluted in a final volume of 30 ul. As a quality control for library preparation, overall fragment size distribution of the prepared library was measured using Agilent Bioanalyzer to ensure absence of PCR contaminants.

2.6 Mutation mapping and analysis

PCR product libraries from high-Alexa488 and low-Alexa488 populations were then sequenced as 50 bp single reads on Illumina HiSeq2500 (Illumina) with a custom sequencing primer 5'- ctagcttgccaaacctacaggtggggtctttca- 3'. Pipeline set up in collaboration with Brummelkamp group (NKI, Netherlands) by Ruud Van Stiphout in our lab and the workflow for analysis is outlined in Fig 2.1. The pipeline was used to align unique reads to human genome (hg19) using bowtie, allowing upto 1 mismatch. The aligned reads were mapped to a custom reference annotation based on Refseq genes. Genomic regions where two or more genes overlap, were removed as insertions cannot be mapped unambiguously to these regions (1). Sense insertions, reads in the same orientation of the gene were extracted and analysis was restricted to these insertions. To calculate odds ratio (Mutational Index(MI)) of a disrupted gene ending up in the low abundance or high abundance gated population, the number of recovered insertions (INS) from these two populations were used in the below formula:

$$MI_{Gene} = \left(\frac{INS_{Gene}}{\sum INS_{AllGenes} - INS_{Gene}} \right)_{HIGH} \Big/ \left(\frac{INS_{Gene}}{\sum INS_{AllGenes} - INS_{Gene}} \right)_{LOW}$$

Significance of MI for each gene was calculated using 2-sided Fisher test, FDR <0.05.

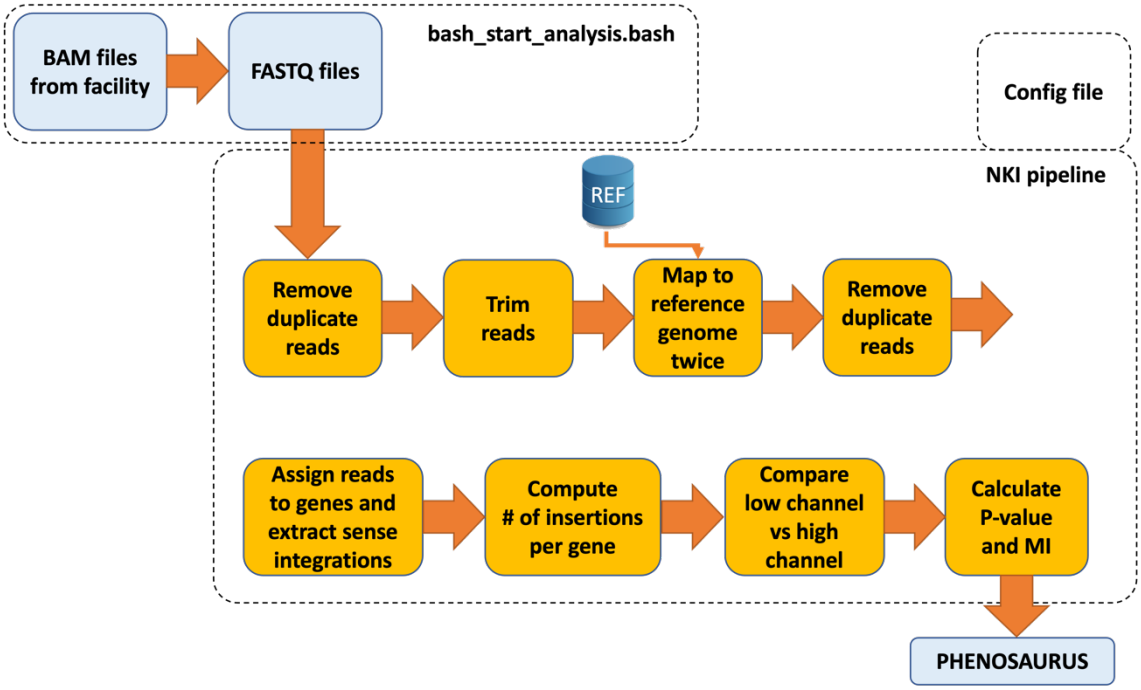


Figure 2.1 Pipeline for CellSeq analysis A flow chart representing the analysis of Illumina sequencing data followed by calculation of the odds ratio (MI score)

2.7 Choice and prioritization of hits for validation

The CellSeq technology results in an extensive dataset. Hence, it is critical to assess the dataset to enable accurate choice of significant hits for further downstream validation. The verification was done in multiple steps by ensuring, 1) Genes expected to influence the reporter expression were adequately present among the significantly scored genes. 2) The specificity of the significant genes towards the candidate reporter. In this section, various parameters that were

taken into consideration to ensure that the above 2 conditions were met are discussed (Fig 2.2):

2.7.1 *Pathway annotation*

To identify pathways expected to have an effect on the reporter expression, as a first step towards choosing genes for downstream validation, the principle that each hit can be clustered with others into specific phenotypes, and this can correlate to the reporter phenotype was employed. Functional enrichment analysis by STRING (www.string-db.org) was used to categorise hits into clusters of functions expected to affect reporter phenotype. STRING functional enrichment analysis integrates REACTOME, biological processes, KEGG, Cellular component etc. This classification enabled us in identifying expected pathways and confirming that all our screens were working as expected in sync with what is already known about the reporter protein regulation while aiding in further streamlining of the hits as described in the subsequent chapters.

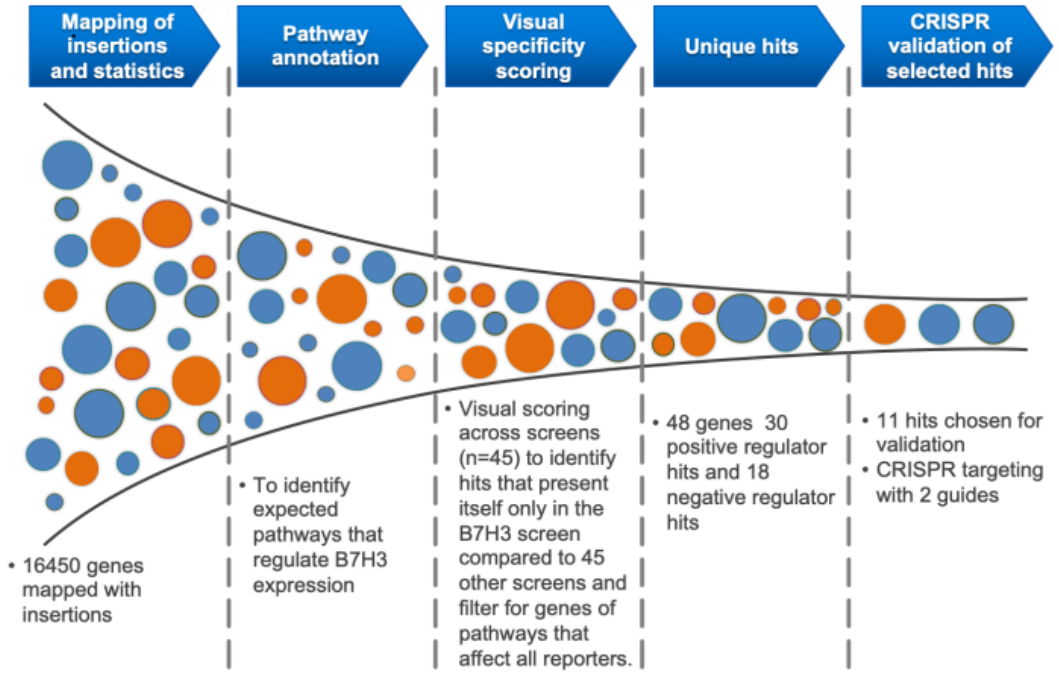


Figure 2.2 Schematic representing parameters for choice of hits for validation using B7H3 screen as an example

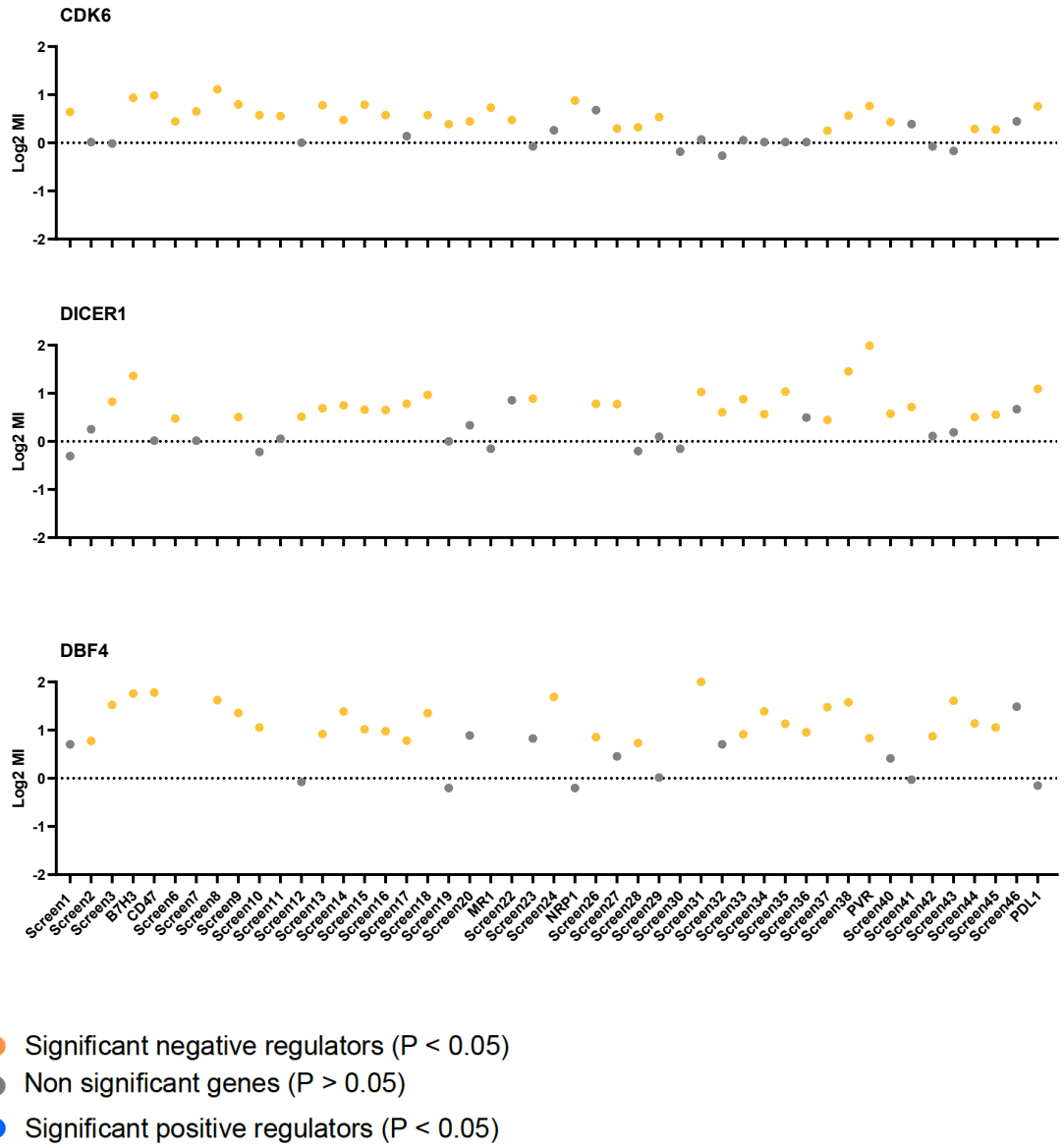
2.7.2 *Visual specificity scoring*

A substantial number of hits are recurring in multiple (n=46) screens performed using the same CellSeq approach. As previously described in published screens, there are certain processes that are enriched across all screens. To visualize each putative regulator gene and compare them across screens with other reporters performed using CellSeq to identify hits unique to the protein being evaluated in the specific screen, visual specificity scoring maps were used.

Visual specificity scoring maps use log2MI of each gene as a measure and compare them across 45 other screens to identify their specificity. For example, most genes that play a role in cell size tend to result in higher reporter protein

signals and this is not completely corrected for during sorting. Examples for these types of “false positive hits” include genes associated with cell cycle and positive regulation of cell development that affect the cell size such as DBF4, DICER1, TFDP1, CDK6 and CREBBP. Visual specificity scoring maps representing the recurrence of genes DBF4, DICER1 and CDK6 across screens (n=46) (Fig 2.3). Another example, transcriptional regulation can have a possible general effect on all proteins and in turn appear as negative or positive regulators across screens. Recurrence of genes associated with transcriptional regulation across screens has been illustrated by taking PBRM1 as an example (Fig 2.4). Another example is chromatin organization. Some key players involved in regulation of chromatin organization are NCOR1, TLK2 and KDM1A are recurring hits across all screens (Fig 2.5). Although the recurring genes constitute a substantial portion of the statistically significant genes owing to common regulatory mechanisms or technical differences, dominant regulatory pathways of the reporter protein often stand out in terms of MI score and specificity. These genes upon visual specificity scoring across all screens performed reveal a very specific profile with strong effect sizes. For example, in the PD-L1 screen CMTM6 (MI -6.39) was identified to stabilize PD-L1 expression by preventing it from STUB1(MI 4.12) mediated ubiquitin degradation on the cell surface. CMTM6 and STUB1 were highly specific hits as determined by visual specificity scoring (Fig 2.6). Hence, we listed all the unique hits that appear only in the reporter of interest screen as compared to other CellSeq screens and used it as a criterion for choice of hits and ensured that we picked true hits for downstream validation across all our screens as described in the subsequent chapters. Using a combination of the above-

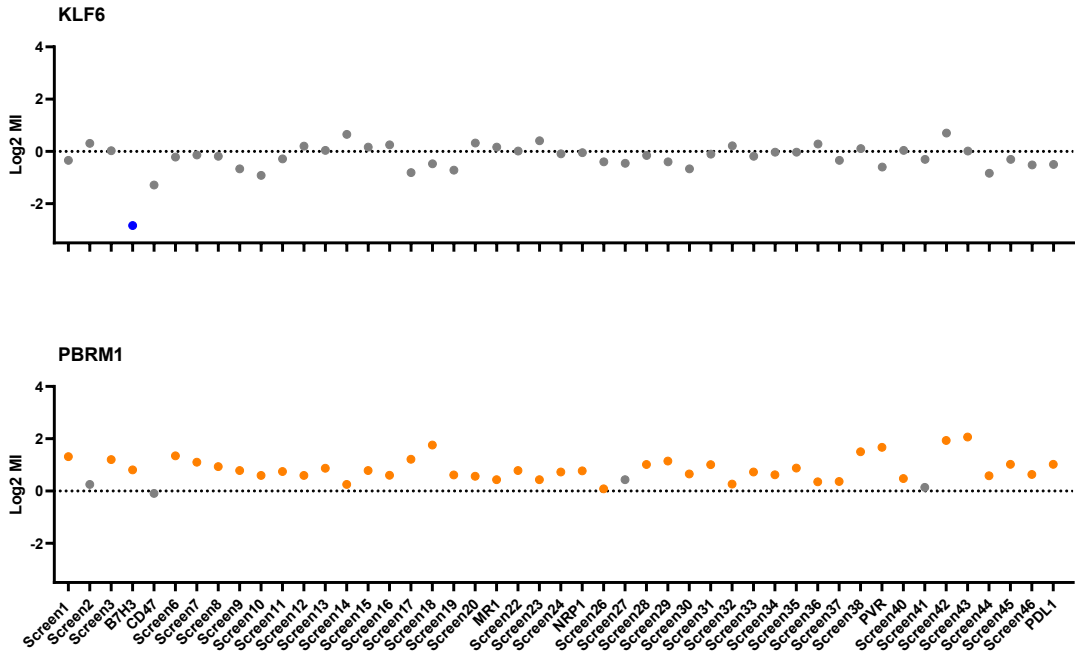
mentioned criteria under section 2.8, we selected hits based on a combination of MI score, specificity, novelty and high confidence for further biological investigation.



- Significant negative regulators (P < 0.05)
- Non significant genes (P > 0.05)
- Significant positive regulators (P < 0.05)

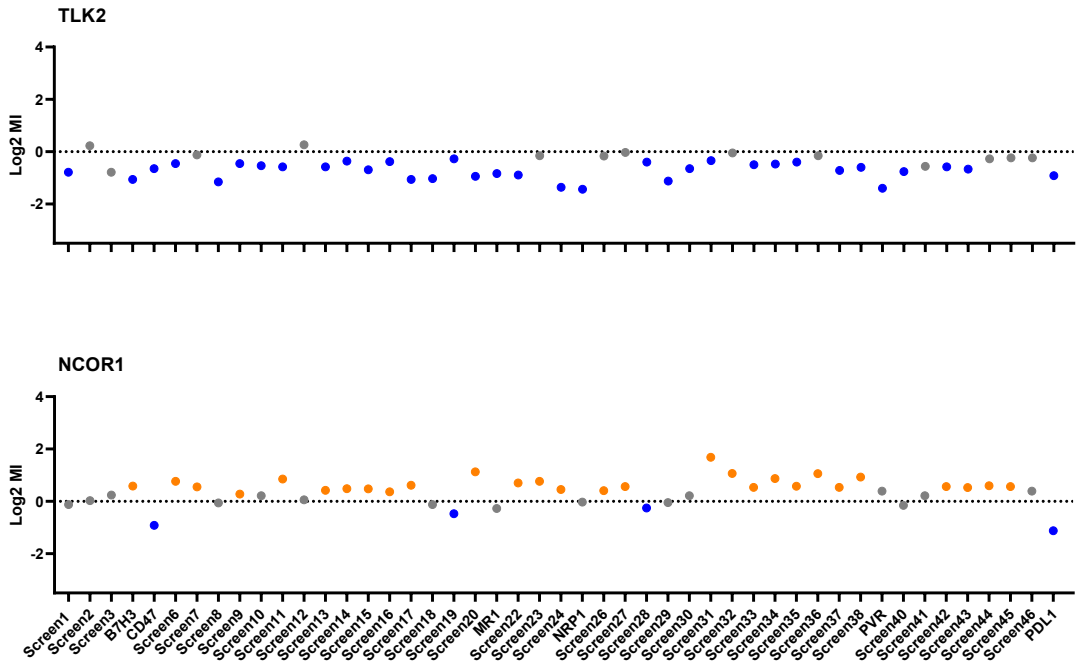
Figure 2.3 Size effect acts as a technical limitation resulting in recurring genes across screens. Visual specificity scoring maps for genes DBF4, DICER1 and CDK6 across ~50 other screens. Visual specificity scoring is performed to

determine how a gene scores across various CellSeq screens performed on different proteins to determine specificity of gene effect to phenotype.



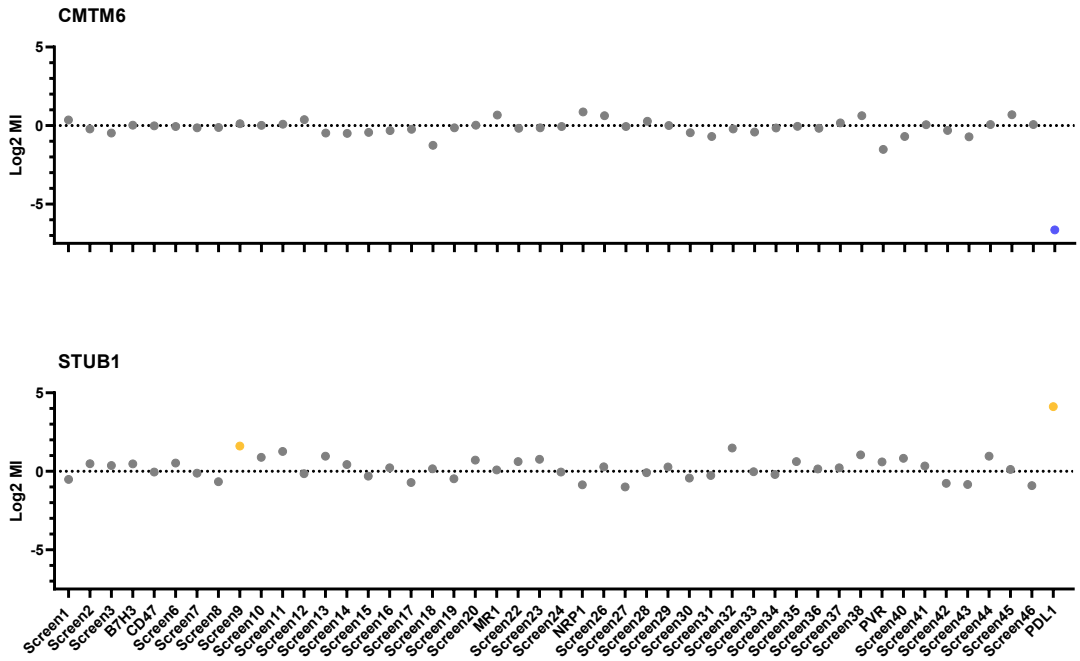
- Significant negative regulators (P < 0.05)
- Non significant genes (P > 0.05)
- Significant positive regulators (P < 0.05)

Figure 2.4 Genes coding for transcription factors can be recurring across screens or specific to a phenotype Visual specificity scoring maps for genes KLF6 and PBRM1 across ~50 other screens. Visual specificity scoring is performed to determine how a gene scores across various CellSeq screens performed on different proteins to determine specificity of gene effect to phenotype.



Significant negative regulators (P < 0.05)
Non significant genes (P > 0.05)
Significant positive regulators (P < 0.05)

Figure 2.5 Conserved pathways such as chromatin modeling result in recurring genes across screens. Visual specificity scoring maps for genes *TLK2* and *NCOR1* across ~50 other screens. Visual specificity scoring to determine how a gene scores across various CellSeq screens performed on different proteins to determine specificity of gene effect to phenotype.



Significant negative regulators (P < 0.05)
Non significant genes (P > 0.05)
Significant positive regulators (P < 0.05)

Figure 2.6 Genes unique to PD-L1 regulation have been reported Visual specificity scoring maps for genes *CMTM6* and *STUB1* across ~50 other screens. Visual specificity scoring is performed to determine how a gene scores across various CellSeq screens performed on different proteins to determine specificity of gene effect to phenotype.

2.8 Cloning of sgRNA into plasmid LentiCRISPR v2

Validation of hits was carried out by knocking out genes of interest by using the LentiCRISPR v2 plasmid encoding the S. pyogenes Cas9 and an incorporated gene-specific single guide RNA (sgRNA) sequence. The design of these plasmids to target different genes of interest was carried out using the tool TKO version 3 web tool (TKOv3, www.crispr.ccbr.utoronto.ca/public/library/TKOv3) (Table 2.14).

To insert the targeting sgRNA sequence specific to each gene of interest into the LentiCRISPR v2 plasmid, the cloning strategy was adapted from. First, the sgRNA sequence were designed to incorporate BsmBI compatible overhangs as depicted below:

Oligo 1: 5'- CACCGNNNNNNNNNNNNNNNNNNN – 3'

Oligo 2: 3'- CNNNNNNNNNNNNNNNNNNNCAAA - 5'

Following this, annealing and phosphorylation of the sgRNA and its complimentary oligo was performed by using T4 Polynucleotide Kinase (T4 PNK) in T4 DNA Ligase Reaction Buffer and incubating at 37 °C for 30 minutes, followed by 95°C for 5 minutes and bringing down the temperature to 25°C at 5 °C /minute (Table 2.15). Next, the LentiCRISPRv2 Plasmid was linearized by digestion and dephosphorylated to block re-ligation. Hereby, the LentiCRISPRv2 plasmid was digested in the presence of 100 µM fresh DL-Dithiothreitol by using restriction enzyme BsmBI and Alkaline Calf Intestinal Phosphatase (CIP) for 2 hours at 37°C (Table 2.16). The 11kb linearized plasmid was then separated based on size on a 1.2% agarose gel and subject to gel purification using

QIAquick Gel Extraction kit as per manufacturers protocol. To ligate the annealed oligos to the linearized plasmid, 1:100 dilution of the annealed oligos were mixed with 100 ng of the digested plasmid in the presence of T4 DNA ligase in T4 DNA ligase Reaction Buffer overnight at 16°C (Table 2.17). For each transformation, 4 ul of the respective ligation mixture was added to 25 ul of StblIII chemically competent Escherichia coli bacteria (Invitrogen) and incubated on ice for 30 minutes in a vial. The cells in the vial were heat shocked for 45 seconds at 42°C without agitation. The vial was then transferred to ice for 2 minutes. Following this, 250 ul of pre-warmed S.O.C high nutrient medium was added to each vial and incubated horizontally at 37°C for 1 hour at 225 rpm. Following this, as the vector has an intrinsic ampicillin resistance gene, the 25 ul of each transformation mix was spread on a pre-warmed ampicillin supplemented LB agar plate and incubated overnight at 37°C to select transformed colonies. Colonies were then picked using non-filtered tips and cultured in 3 ml LB media supplemented with 100 ug/ml ampicillin for ~20 hours. Following this, the plasmid DNA was extracted using QIAprep Spin Mini Kit as per manufacturers protocol and eluted in 50 ul H2O. The concentration of the plasmid DNA was measured using Nanodrop 8000 Spectrophotometer (Thermo Fisher Scientific). Following this, the plasmids were sent for sequence verification by sanger sequencing using primer 5'-GACTATCATATGCTTACCGT-3' and stored in -20°C.

Target gene	Sequence
CD276	TCGCACCCAGCACCACCCGC
PVR	TTGAGGGCACCAATATCCAG
NRP1	CCTGACTCAAATCCTCCAGG
FBXO11	GTTCGATGTGAAATTCACCA
SAMD1	GGTAGCGCACGACTTCCCGC
SAMD4B	CAGCCGGAACACCTTCCAGG
SPPL3	AATTGGAAGGAACAGAGCCT
KLF6	GTCGGAGGTAAACTTGGCCG
HDAC8	GAAGGTGGCCATCTCCTCCA
BTLA	TGCCTGAGAAGGCACCAAGG
HM13	TCCGCATAACGGCAGTGCCG
UBE3D (sgRNA1)	ATTACCAGAGAACCGAAAGA
UBE3D (sgRNA2)	CTACAGTTTGTTGTTGGAGA

Table 2.14 sgRNA targeting sequences in this study

Reagent	Amount
Oligo 1 (100 uM)	1 ul
Oligo 2 (100 uM)	1 ul
10X T4 ligation buffer (NEB)	1 ul
ddH2O	6.5 ul
T4 PKN (NEB)	0.5 ul
Total	10 ul

Table 2.15 Reaction mixture for phosphorylation and annealing of oligos

Reagent	Amount
lentiCRISPRv2	5 ug
BsmBI (NEB)	3ul
CIP (NEB)	3ul
10X 3.1 Buffer (NEB)	6 ul
100 mM DTT (freshly prepared from 1M DL_thiothreitol stock)	0.6 ul
ddH2O	X ul
Total	60 ul

Table 2.16 Reaction mixture for LentiCRISPRV2 digestion

Reagent	Amount
100ng BsmBI digested plasmid	X ul
diluted oligo duplex	1 ul
10X T4 ligation buffer (NEB)	1 ul
T4 DNA ligase	1 ul
ddH2O	X ul

Table 2.17 Reaction mixture for ligation of annealed oligos to LentiCRISPR V2

2.9 Knockout cell generation via transient transfection

500,000 HAP1 cells or MCF-7 were seeded per well in a 6 well plate. Cells in each well were transfected after 24 hours with 2ug of LentiCRISPRV2 vector with the incorporated sgRNA of interest in the presence of 9 ul of Turbofectin 8.0. DNA and Turbofectin mix were prepared in Opti-MEM. Turbofectin and the plasmid were prepared separately by diluting in 150 ul Opti-MEM prior to being

mixed together and incubated for 30 minutes. Following this, the mixture was added dropwise to the cells. 24 hours after transfection, the cells were selected in the presence of 2ug/ml puromycin refreshed at 24 hours and 12 hours respectively. Once, the non-transfected cells were completely dead, the selected cells were grown in IMDM 10% FBS, supplemented with PSG. The pool of cells were expanded for upto 4 days in case of HAP1 cells and 10 days in the case of MCF7 cells. Following this, the expanded pool of cells was used to evaluate surface and total expression of proteins using flow cytometry and western blotting.

2.10 **Western blot sample preparation**

For B7H3 westerns, 500,000 HAP1 or its mutant clones were seeded in 6 well plate. Following subsequent treatments, the cells were trypsinized or detached following 1x PBS wash. The PBS was aspirated completely and the cell pellet was frozen in -80°C . If the samples were being used fresh, the sample was resuspended in ice-cold RIPA buffer supplemented with protease and phosphatase inhibitors (200ul for ~ 3-5 million cells). transferred onto a pre-cooled microcentrifuge. If using frozen samples, the cells were first thawed on ice prior to adding above described RIPA buffer. Following this, the samples were vortexed every 10 minutes for 30 minutes, while retaining the samples on ice. The samples were then centrifuged at 4°C at 12,000 rpm for 20 minutes. Next, the supernatant was carefully transferred onto pre-cooled microcentrifuge tubes on ice and the pellets are discarded. The collected cell lysate was then taken forward for protein quantification. Protein quantification was performed using

Bradford or BCA assay kit. Manufacturer's instructions were strictly followed. Bovine Serum Albumin (BSA) was used as the standard. Post protein quantification, the samples were stored at -80°C or prepared to be loaded onto the gel as described in the next steps. The volume of cell lysate required for each of the samples to reach the predetermined protein concentration (Example: 20ug) across each of the wells was determined and subsequently diluted with RIPA buffer to make up 1:1 with 2x laemmli buffer sample buffer, following heat denaturation at 95°C for 20 minutes prior to be loaded onto the gel or the samples were stored at -20°C.

For NRP1 westerns, 500,000 HAP1, MCF7 or its mutant clones were seeded in 6 well plate. Following subsequent treatments, the media was thoroughly aspirated and the cells were washed 1x with ice cold PBS. Following this, the PBS was aspirated completely. Next, 1X Lamelli buffer diluted in RIPA buffer was directly added onto the cells and allowed to incubate for 5 minute at room temperature (200-250 ul/ fully confluent 6 well and 500 ul/ fully confluent 100mm dish). Following this, the cells were scraped off the dish using a plastic cell scraper, and the sample was transferred onto a microcentrifuge tube. The samples were vortexed thoroughly followed by heat denaturation at 95°C for 20 minutes. Following this, the samples were quick spinned on a table top microcentrifuge to sediment the debris, followed by loading onto the gel or were stored at -20°C .

2.11 **Western blotting**

Samples for western blotting were prepared as described above and then run-on a on a Bis-Tris Gradient Gel 4-12% in a Invitrogen Novex System with 1X MOPS buffer. Equal volume of samples was loaded onto all wells and a pre-stained protein ladder was used to indicate the molecular weight of the separated proteins. The gel was run at 90 volts for the first 30 minutes, followed by one and half hours at 110 volts. Following this, the proteins were then transferred onto a polyvinylidene difluoride (PVDF) membrane using the Trans-Blot Turbo system (Biorad). Post transfer, the membranes were blocked to prevent non-specific binding using iBlock at room temperature for 1 hour. Following blocking, the membranes were incubated with the respective primary antibodies O/N at 4ºC. Next morning, the membranes were washed three times with PBS-T. The membranes were then incubated with species-specific horseradish peroxidase (HRP)-conjugated secondary antibodies for 1 hour at room temperature under constant agitation .In the case of membranes incubated with directly HRP conjugated primary antibodies, the secondary antibody step was skipped and directly taken forward to substrate addition. After washing with PBS-T for 3 times post-secondary incubation, the membranes probed for high expression proteins were detected with high clarity substrate and the membranes probed for low expressed proteins were detected with femto substrate and the images were obtained on chemidoc, Universal Hood III machine (Bio-Rad). Images were subsequently processed and quantified using Image Lab and Image J software.

2.12 Site directed mutagenesis to generate UBE3D mutants

For generating UBE3D mutants, pcDNA3.1 encoding wildtype UBE3D with a a C-(K)-DYK tag obtained from Genscript was used as a template. The template was amplified with Primers described in Table 2.18 to generate the V379M, C356A and ΔHect mutants respectively under PCR reaction conditions in Table 2.19. The PCR products were visualized on a 1% agarose gel, with SYBR-gold and the product at the expected size of ~8.5 kb was confirmed. Following this, DPN digestion was performed for removal of parent plasmid. The digestion was followed by subsequent phosphorylation using PNK phosphorylation reaction adapted from Table 2.15 and transformation in E.Coli DH5a competent cells, using a similar approach as described in section 2.8. Plasmid was purified using QiagenMini Prep by strictly following manufacturers protocol and eluting in 50 ul of water. Post mini prep, the plasmids were sequenced with primers in Table 2.20 to confirm presence of mutation.

Name	Forward Oligo	Reverse Oligo
V379M	CCTTCGCCGTATGAATTCCTTTCAGG	TACGGCGAAGGGATGAAGGCAGATT
C356A	TCTGCAACCGCCTTGGAGCTGCTGTT	GCGGTTGCAGAGGGCAGGGTTAGCGG
ΔHECT	CCCGCTAACGATTACAAGGATGAC	GGTTAGCGGGTGGACGCTGATGTCA

Table 2.18 Primers used for site directed mutagenesis

Reagents.	Vol (ul)	Concn
5x Phusion buffer	4	1x
10 mM dNTPs	0.4	200 uM
Primer A (10uM)	1	0.5 uM
Primer B (10uM)	1	0.5 uM
Template DNA (1ug/ml stock)	1	1 ng
Phusion DNA Pol	0.2	0.02 U/Ul
Water	12.4	
Total	20	

Table 2.19 PCR conditions for site directed mutagenesis

Name	Sequencing primer
V379M	TGACATCAGCGTCCACCCGCT
C356A	GGTCCTCTACCAGCCATGCAT
ΔHECT	TAGAAGGCACAGTCGAGG

Table 2.20 Sequencing primers used to confirm presence of mutation in UBE3D mutants

2.13 Overexpression of UBE3D and NRP1

For the overexpression of plasmid pcDNA3.1 encoding NRP1, UBE3D and its mutants with a C-(K)-DYK tag or NRP1 with a haemagglutinin (HA) tag, 300,000 HEK 293Tcells/well were seeded onto 6 well plates, or 500,000 HEK293T cells in a 60 cm dish. The cell suspension was homogenized to ensure even distribution across the wells or dish and verified under the microscope. For transfection of plasmids per well in a 6 well plate, 8 uL of Gene Juice was diluted into 192 ul of Opti-MEM separately. Simultaneously, the respective plasmid was

diluted into 200uL of Opti-MEM such that total plasmid concentrations across conditions were the same. If transfecting a single plasmid/ well, up to 2 ug of total DNA was used and in the case of 2 or more, up to 4 ug of total DNA was used. The plasmid and gene juice mix were thoroughly mixed together and allowed to incubate for 15 minutes. Following this, 300 ul of each plasmid mix was dropped onto each well of a 6 well plate, ensuring homogenized distribution by rocking the plate up and down. Volumes and DNA amount was scaled up for a 60 cm dish accordingly. pcDNA3.1 RFP was used as a control and to normalize plasmid concentration. Equal amounts of CMV-GFP was transfected onto all cells to ensure uniform transfection efficiency across all wells and conditions. Following this, the cells were monitored under the microscope at 24,48 and 72 hours after transfection for GFP expression.

2.14 **Immunoprecipitation**

For endogenous NRP1 immunoprecipitation, HEK293T cells were transiently transfected with UBE3D or V379M as described in section 2.14. Control cells were transfected with equal amount of RFP. 24 hours post transfection, the cells were washed with ice cold PBS and then the PBS was thoroughly aspirated. Following this 300 ul of lysis buffer was added (TBS-0.5%NP40+PMSF) per 6 cm dish. The cells were scraped and transferred to pre-cooled microcentrifuge tubes. The samples were placed on ice and vortexed every 10 minutes for 30 minutes. The samples were then centrifuged at 14,000 g for 10 minutes at 4°C and the supernatant was transferred to fresh pre-cooled microcentrifuge tubes. 50 ul of the supernatant was kept aside as an input

sample, 50 ul of 2x sample buffer was added and boiled for 10 minutes at 95°C. The rest of the supernatant was taken forward for immunoprecipitation. 250 ul of the supernatant was diluted with 250 ul of lysis buffer and then incubated with rabbit anti-NRP1 antibody at a concentration of 1:50, overnight at 4°C. rabbit anti-IgG was used as a control. Next morning, magnetic dynabeads A (rabbit specific), were washed and added to the lysate directly and incubated for 2 hours at 4°C. Using a magnetic rack, the supernatant was removed and the beads were washed 3x times with TBS-0.5%NP40. Following the washes, 50 ul of 1X sample buffer was added to the beads and boiled for 10 minutes at 95°C. Following this, the samples were placed on a magnetic rack and the supernatant was transferred to new microcentrifuge tubes. They were subsequently run on a gen and probed with rabbit polyclonal UBE3D ab to detect UBE3D and anti-FLAG antibody to probe for overexpressed NRP1. Veriblot antibody that can specifically detect non denatured antibodies was used as a secondary antibody. For HA immunoprecipitation, UBE3D and V379M were transiently co-overexpressed with NRP1-HA (NRP1- haemagglutinin) in HEK293T cells as described in section 2.14. Control cells were transfected with equal amount of RFP. The IP was performed as described above by immunoprecipitation with an anti-HA antibody.

2.15 Lysosomal and proteasomal degradation assays

UBE3D and NRP1-FLAG were transiently co-overexpressed in HEK293T cells for 72 hours as described in 2.14. The cells were treated with a lysosomal degradation inhibitor, 100 nm of Bafilomycin A1 or E1 pathway inhibitor, 1 uM of

MLN243, or a proteasomal degradation inhibitor, 10 nm of Bortezomib 4 hours before harvest and the cell lysates were collected for western blotting.

2.16 Zebrafish experiments

All animal experiments were performed by Svanhild Nornes under a Home Office Licence according to the Animals Scientific Procedures Act 1986, UK, and approved by the local ethics committee. Tg(fli1:GFP) zebrafish (1) and tg(kdrl:HRAS-mCherry) zebrafish (2) were bred and maintained in a fish facility at 28.5∞C in systemically circulating water. Embryos were maintained at 28.5∞C in E3 medium (5 mM NaCl, 0.17 mM KCl, 0.33 mM CaCl2, 0.33 mM MgSO4, 0.1% methylene blue).

2.17 Morpholino injections

Morpholino antisense oligonucleotides (MO) (Table 2.21) were obtained from Gene Tools (82). They were dissolved in ultrapure water and 1 - 2 nl of the MO solutions at required concentrations were injected into 1- to 2-cell stage tg(fli1:GFP) zebrafish embryos. Injections were performed with a FemtoJet 4x injector (Eppendorf, 5253000033) under an Olympus SZX7 stereo microscope (Olympus) using a manual micromanipulator (WPI). Borosilicate glass wall capillaries (Drummond Scientific Company) were pulled using a model P-1000 needle puller (Sutter Instrument) to allow backfilling of the sample and injection into the zebrafish embryos.

Morpholino	Sequence	ZFIN link	Supplier
UBE3D	ATCTTAGCGTGTACCTGTTGGCTGC	https://zfin.org/ZDB-MRPHLNO-210104-1	GeneTools
NRP1a	GAATCCTGGAGTTCGGAGTGCGGAA	https://zfin.org/ZDB-MRPHLNO-050906-3#summary	GeneTools
NRP1b	TCACACAGAGCAAACACCAGTACAT	https://zfin.org/ZDB-MRPHLNO-150302-6	GeneTools

Table 2.21 Morpholino injections concentrations

2.18 Zebrafish fluorescence analysis and confocal imaging

For screening, Tg(fli1:GFP) embryos were dechorionated and anaesthetized with 0.1% tricaine (ethyl 3-aminobenzoate methanesulfonate, A5040, Sigma) and scored for strong, medium and weak expression under an Olympus MVX10 fluorescence microscope (Olympus). For imaging, embryos were dechorionated and single embryos transferred into a flat bottom 96-well plate, embedded in 0.4% TopVision low melting point agarose (R0801, Thermo) with 0.1% tricaine. Embryos with GFP reporter gene expression were imaged under a Zeiss LSM 710 confocal microscope (Carl Zeiss) at 2 dpf. Embryos were imaged using the tile scan command, combined with Z-stack collection under the Zeiss LSM 710 confocal microscope at 488 nm excitation and 509 nm emission (EGFP) respectively. Analysis of expression interpreted as qualitative not quantitative, therefore no statistical analysis was applied to the observations of reporter gene intensity and pattern.

2.19 qRT PCR

Total RNA was isolated from cells using the RNeasy plus mini kit (Qiagen), and from tissues using TRIzol reagent (ThermoFisher Scientific), according to the manufacturer's instructions. Equal amounts of RNA were used as templates for all reactions. cDNA was generated with the SuperScript III First Strand Synthesis System (ThermoFisher Scientific). QuantiTect SYBR Green PCR kit (Qiagen) was used for PCR. The primers used to amplify NRP1 and GAPDH are listed in Table 2.22.

Gene	Forward Primer	Reverse Primer
NRP1	TACGAAACACATGGTGCAGGA	CTGCAGACCAGTTGGTGCTAT
GAPDH	ACAACTTTGGTATCGTGGAAGG	GCCATCACGCCACAGTTTC

Table 2.22 Primers used for qRT PCR

Gene expression was quantified at the transcriptional level for NRP1 target gene. Cells were harvested directly from tissue culture dishes and then centrifuged at 500g to pellet cells, and lysed using 350µl RLT lysis buffer (Qiagen). Total cellular RNA was then isolated using an RNeasy mini kit (Qiagen) according to the manufacturer's instructions, incorporating on column RNase-free DNase I (Qiagen) digestion to remove genomic DNA. RNA was eluted in 30µl nuclease- free H2O. RNA concentration was determined using a NanoDrop 2000 spectrophotometer (ThermoFisher Scientific).

A total of 0.5µg RNA was used to synthesize first single-strand cDNA the using SuperScript III First-Strand Synthesis kit (Thermo Fisher).

For quantification of mRNA expression by rt-qPCR, the QuantiTect SYBR Green PCR kit (Qiagen) was used and reactions set up according to the manufacturer's instructions. Reactions were run on the StepOnePlusTM Real-Time PCR System (Applied Biosystems) at the following conditions - 95°C - 15 minutes, (94°C 15s + 60°C 30s + 72°C 30s) x 40 cycles. Gene expression at the mRNA level for each target gene assayed was quantified relative to an internal housekeeping gene control. The housekeeping genes used were either GAPDH. To determine relative mRNA expression, the mean ΔCt (difference in cycle threshold number) was calculated for each target gene relative to GAPDH. ΔCt for a given target gene in each sample was therefore calculated according to the formula ΔCt = Ct Target gene – Ct Housekeeping gene. Relative mRNA expression data are shown as 2-ΔCt.

2.20 **Statistical Analysis**

Data were represented as Mean ± SEM (Standard Error of the Mean) of multiple biological replicates. Statistical significance was assessed using one-way ANOVA (Analysis of Variance) followed by Tukey's. SIdak's or Dunnet's post hoc test for multiple comparisons.

2.21 **Data plotting**

RStudio 1.2.5033 was used to generate the CellSeq fish tail plots or regulator maps and volcano plots by using the ggplot2 package. The Rbase package was used to create Graphics of gene trap insertion sites images.

Chapter 3: CellSeq to identify regulators of B7H3 and PVR

3.1 Introduction

CellSeq can identify molecular regulators of proteins of interest with great specificity and sensitivity by coupling Fluorescence Activated Cell Sorting (FACS) derived protein abundance readouts from mutant haploid cells to massively parallel sequencing(50). CellSeq has identified key regulatory components of programmed death-ligand 1 (PD-L1) and Cluster of Differentiation 47 (CD47) at the tumour immune interface thus establishing itself as a state-of-the-art technology for studying immune checkpoint biology(48, 49).

As discussed previously in Chapter 1, we aimed to use CellSeq to further our understanding of less understood immune checkpoints. Hereby, we identified Polio Virus Receptor (PVR), B7 Homolog 3 (B7H3) and NRP1 as screening candidates (Sec 1.7, Fig 1.3-1.4) and performed back to back CellSeq screens. In this Chapter, we will describe the suitability of CellSeq to identify novel regulators of immune checkpoints using the PVR and B7H3 screen.

3.1.1 *PVR*

PVR, otherwise known as CD155 is a member of the immunoglobulin and Nectin protein families. It was first identified as the receptor for poliovirus entry over 30 years ago(83). Following this, it has been implicated in various cellular processes, such as proliferation, migration, adhesion and immune response (Fig 3.1)(84).

PVR is a membrane glycoprotein and consists of 3 Immunoglobulin-like domains in its extra cellular region (D1 - Immunoglobulin domain V, D2 - C1-like domain and D3 - C2-like domain), a transmembrane domain and a cytoplasmic domain. It has been reported that, soluble isoforms of PVR lack the transmembrane domain and are formed as a consequence of alternative splicing, thus competing for receptor binding with membrane bound PVR(83, 85).

PVR is mainly induced upon cell stress or during aberrant signalling in cells and interacts with activating receptors on immune cells, to facilitate clearance of damaged or dying cells. Dysregulation in this axis contributes towards various disease pathogenesis such as cancer and infection(78). For example, Deoxyribonucleic acid (DNA) damage, commonly found in pre-cancerous cells induces PVR expression(86, 87). Furthermore, attenuated sonic hedgehog signalling drives PVR induction in cancer cells(78, 87). PVR overexpression has been reported to drive poor cancer prognosis and overall survival in multiple cancers because of its role in various endogenous functions such as proliferation, adhesion and motility(78, 86). Simultaneously, PVR has the rare ability to bind activating and inhibiting receptors on immune cells in the tumour microenvironment to regulate anti-tumour immunity. Specifically, PVR

interacts with DNAX Accessory Molecule-1 (DNAM-1) also known as Cluster of Differentiation 226 (CD226) and drives activation of Natural Killer (NK) cells and T cells. Hence, DNAM-1 overexpressing cytotoxic T cells are being explored as a way to target the PVR-DNAM-1 axis to promote anti-tumour immunity(88). In contrast, PVR binding to T cell immunoreceptor with Ig and ITIM domains, (TIGIT) drives suppression of NK cells and T cells(24, 28). However, PVR binds with a stronger affinity to TIGIT than DNAM-1 and hence PVR mainly drives an immunosuppressive lymphocyte phenotype in the tumour microenvironment (Fig 3.1)(78). Various antibodies targeting TIGIT-PVR axis are already in different stages of clinical trials for cancers such as non-small cell lung cancer and various advanced solid tumours, and have been reviewed in detail(78, 79, 89). In addition, it has also been reported that PVR interacts with Cluster of Differentiation 96 (CD96) and drives inhibition of NK cells(90). Collectively, PVR plays a pivotal role in modulating immunity in the tumour microenvironment and hence is an attractive immunotherapeutic target.

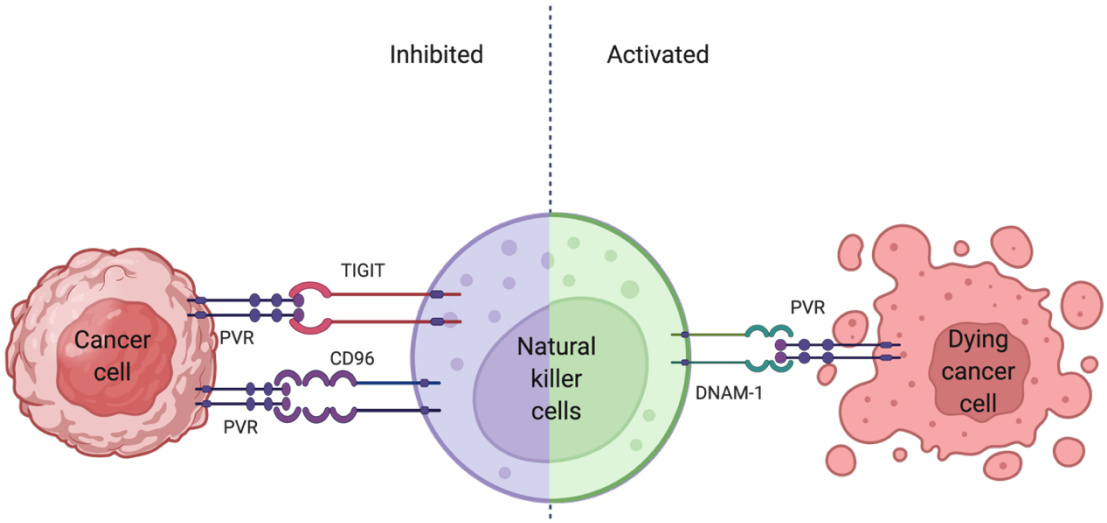


Figure 3.1 Schematic representing PVR structure and functions Adapted from(78), Created on Biorender.com

3.1.2 *B7H3*

B7H3 coded by the gene CD276, belongs to the B7 immunoglobulin superfamily and is a type I transmembrane glycoprotein. It is overexpressed in various tumours and has been implicated in regulating cancer hallmarks, such as angiogenesis, proliferation, invasion, and interactions at the tumour immune interface(91, 92).

B7H3 is a 316 amino acid long protein, containing a signalling peptide in the N-terminal, extracellular V- and C-like immunoglobulin domain (IgV-igC domains), a transmembrane domain and a cytoplasmic tail. While the mouse B7h3 has a single IgV-IgC domain, the human gene has tandem duplicate IgV-IgC domains due to an exon duplication event. However, no difference in biological functions have been reported for the two forms. The extracellular domain of B7H3, has ~25% homology to the other members of the B7 family and binds to a distinct unknown receptor(93). While most B7 family members have defined immunoregulatory roles, B7H3 has been reported as a ‘double-edged sword’ that can be a friend or foe to anti-tumour immunity(20). For example, initial studies identified B7H3 as a T cell costimulatory molecule that can induce cytotoxic T cells. In contrast, another study reported a inhibitory role for B7H3 in T cell activation(21). Contradicting roles for B7H3 have been reported. However, more recent studies have suggested that B7H3 blocks CD8+T cell and NK cell mediated tumour inhibition and thus is likely a ‘foe’ to cancer immunity(94-96).

Furthermore, clinical reports suggest B7H3 as a poor prognostic marker for multiple cancers(97-99). It has also been suggested that poor prognosis associated with B7H3 correlates with T cell suppression(100). Collectively, B7H3's role in the tumour immune interface is quite complex and not completely understood. The complexity has been linked to distinct B7H3 receptors in target cells, splicing isoforms and glycosylation or sialylation patterns on B7H3.

3.1.3 *B7H3: 'a double-edged sword' driven by glycosylation*

B7H3 has been reported to have inhibiting or stimulating roles towards lymphocyte activation(20-22). The contrasting functions have in part been hypothesised to be due to distinct putative receptors (Fig 3.2)(20). However, to date these receptors have not been identified. Additionally, glycosylation of B7H3 has also been reported to have contrasting effects on its stability. Specifically, two glycosylation pathways have been reported to affect B7H3 post translational modification. First, the addition of terminal gal residues to the surface of glycoproteins. Interestingly, it was reported that aberrant N-glycosylation leading to highly fucosylated B7H3 stabilizes its expression and drives immune suppression(101). Next, Sialylation, the process of addition of sialic acids as terminal carbohydrates to the cell surface of glycosylated proteins and lipids. In this study, it has been reported that oral cancer cells Ca9-22 have reduced levels of sialylation and highly fucosylated B7H3 (terminal gal residues). In contrast, normal cells such as gingival epithelioid S-G cells (SG) display higher sialylation levels and terminal sialic acids attached to B7H3. Interestingly, Ca9-22 cells have been reported to have a higher expression of B7H3 compared to SG cells despite

their low sialylation levels, thus suggesting that sialylation might have an inverse effect on B7H3 protein stability(102). While the relationship between sialylation and B7H3 stability has been studied, its effect on B7H3 function and putative T cell modulating receptor interactions remains unclear (Fig 3.2).

In this Chapter, we describe two haploid genetic screens (CellSeq) to identify regulators of B7H3 and PVR surface expression. We will first present the work relating to PVR, followed by B7H3.

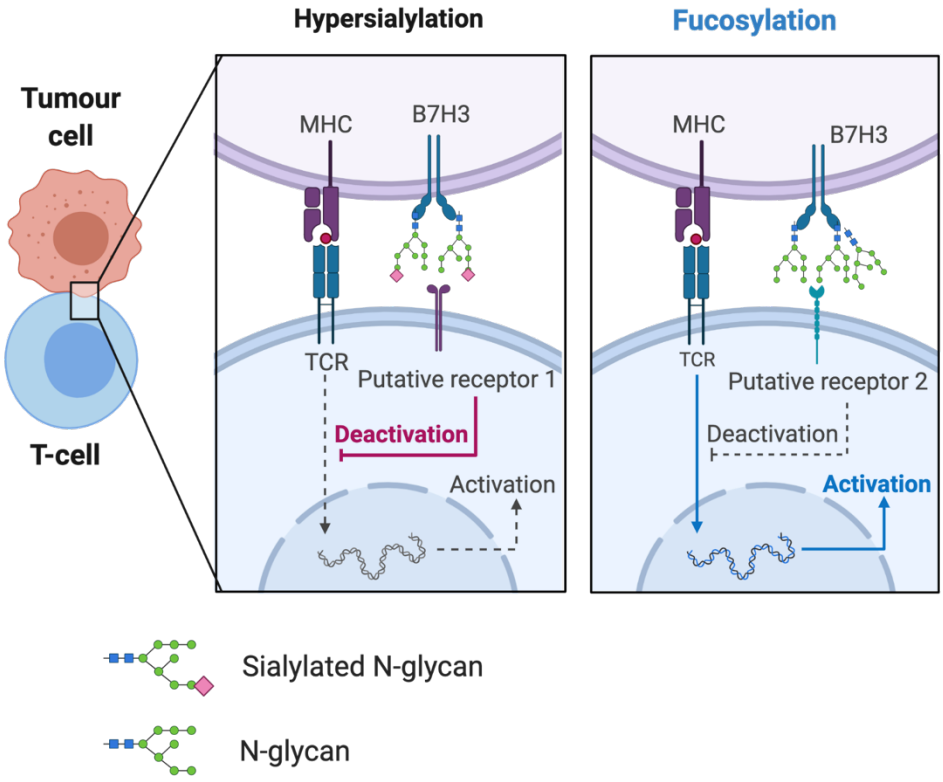


Figure 3.2 Schematic representing hypothesis: Glycosylation of B7H3 regulates differential binding of B7H3 to its putative receptors (Created on Biorender.com)

3.2 Results

3.2.1 *Identification of regulators of PVR using CellSeq*

We aimed to identify molecular regulators of surface expression of PVR. Hereby, we used a whole haploid genetic screening approach, CellSeq (Fig 1.2, Sec 2.5). Briefly, we mutagenized HAP1 cells using a gene-trap retrovirus to create a library of loss-of-function alleles covering nearly all expressed genes, as described previously and in section 2.3 Mutagenized cells were subsequently fixed and stained with antibodies specific to PVR and approximately 3 billion cells were sorted by FACS. At least 10 million cells displaying either low or high PVR specific signal were isolated and the gene trap insertion sites were amplified using Linear Amplification Mediated, Polymerase Chain Reaction (LAM)(PCR) (Sec 2.5, Fig 1.2) resulting in 2 separate DNA libraries (1x low and 1 x high) suitable for Illumina sequencing. As a quality control step, we determined the PCR product size distribution which displayed a smooth curve across sizes 200-2000bp, as expected (Appendices 6.4). Next, we sequenced the gene trap insertion sites in the high and low libraries and mapped the unique sequences onto the human genome (Sec 2.5, Fig 1.2). In so doing, we recovered ~2.5 million unique sense insertion sites covering ~16,700 genes. The odds ratio of a gene being a positive or negative regulator was calculated as a Mutational Index (MI) score (Sec 2.5, Fig 1.2) and represented on a map of putative regulators of PVR.

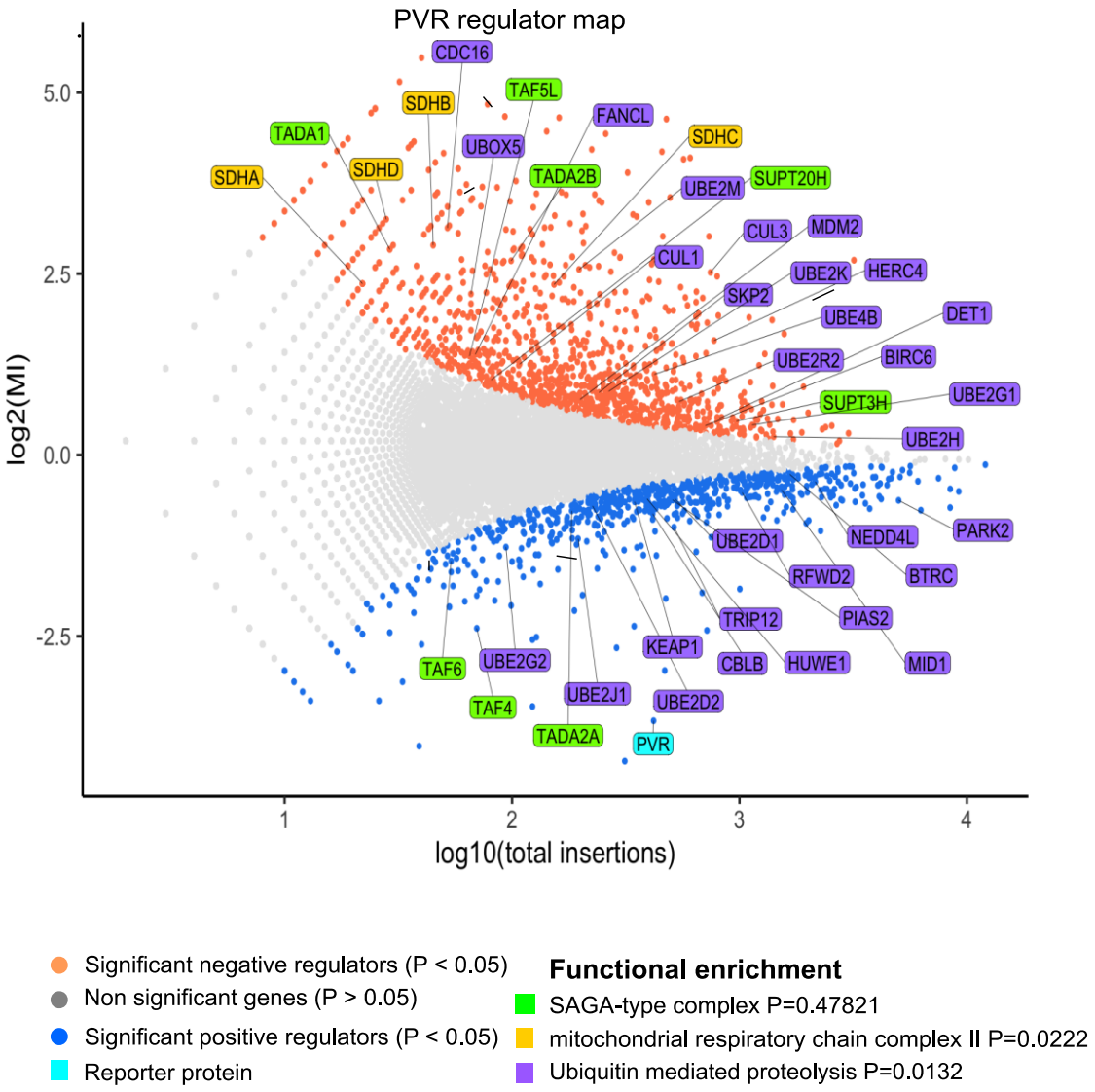


Figure 3.3 PVR regulatory map representing hits from pathways expected to influence PVR expression Fishtail plot representing the CellSeq PVR regulatory map. Each dot indicates a per gene odds ratio (Mutational Index-MI): Frequency of mutations in the PVR high expression population divided by the frequency of mutations in the PVR low expression population. It is plotted as the MI on y axis against the total number of insertions assigned to the individual gene on the x axis. Genes enriched in either population are coloured as indicated in the legend. (two-sided Fisher's exact test,

false discovery rate corrected P value ≤ 0.05. Selected pathways expected to have an effect on PVR surface expression are labelled.

Overall, the screen identified 1891 putative regulators of PVR and among these genes expected to influence surface expression of PVR were present. For example, the *PVR* gene itself scored among the strongest positive regulator hits and acted as an internal control, thus confirming the ability of the screen to detect regulators of PVR expression (Fig 3.3). Furthermore, to evaluate if 'true' regulators of PVR expression are detected, we inhibited one of the notable hits Fork head box 11 (*FBXO11*), an E3 ligase, that can target protein substrates towards proteolysis and evaluated the effect on PVR surface expression(103). Hereby, we transfected sgRNA targeting the coding region of *FBXO11* along with a CAS9 expression plasmid into HAP1 cells and evaluated surface expression of PVR using flow cytometry. As expected, targeting *FBXO11* resulted in a decrease in PVR surface expression, thus validating *FBXO11* as a 'true' regulator of PVR. In addition, there were other notable hits. For example, PVR and its soluble forms are tightly regulated by alternative splicing thus influencing surface expression of PVR(83). Interestingly, Spt-Ada-Gcn5 acetyltransferase (SAGA) complex has been reported to drive alternative splicing mechanisms and can possibly influence PVR expression(104). Genes that constitute the SAGA complex and other genes associated with the complex scored amongst the strongest hits (Fig 3,3, green). Another example, PVR and Nectin-2 are both ligands of DNAM-1, and drive lymphocyte activation and thus possibly share some regulatory mechanisms(88). Nectin-2 has been previously reported to undergo

ubiquitination mediated degradation, while PVR has not(105). Interestingly, E3 and E2 ligases such as *CUL3* and *HERC4* scored as hits along with other ubiquitin proteolysis associated genes, suggesting a positive role for the ubiquitin proteasome system in PVR regulation (Fig 3.3, purple). Lastly, the succinate dehydrogenase enzyme is essential for T cell activation(106). The genes responsible for assembly of this 4 subunit enzyme *SDHA, SDHB, SDHC and SDHD* all scored as hits (Fig 3.3, yellow)(107). The above described hits expected to influence PVR surface expression can potentially pave way to expand known biology of PVR and will be investigated during our future validation efforts.

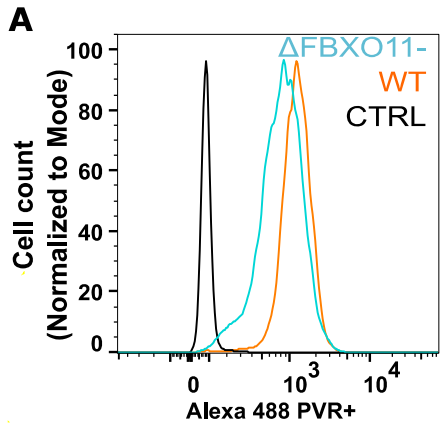


Figure 3.4 CRISPR/Cas9 targeting of *FBXO11* leads to reduced PVR expression FBXO11 gene was targeted using CRISPR/Cas9 sgRNA in HAP1 cells, following this the cells underwent 36 hours of Puromycin selection. The selected polyclonal pool of HAP1 cells were then analysed by flow cytometry 72 hours post selection, for surface PVR expression.

In conclusion, we report that our approach specifically identified known and unknown regulators of PVR surface expression, as demonstrated by PVR scoring among the strongest hits and the validation of *FBXO11* as a positive regulator of PVR surface expression. Notably, in addition to the interesting hits discussed above, we have reported several novel putative regulators of PVR expression (Appendices 6.1) that can be resourceful in enhancing understanding of PVR biology.

3.2.2 *Identification of regulators of B7H3 using CellSeq*

To identify molecular regulators of B7H3 surface expression, we used CellSeq (Fig 1.2, Sec 2.5). As an internal quality control, we investigated the effect size of *CD276*, the gene encoding B7H3. Although *CD276* scored as a positive regulator, it was not among the strongest hits (MI of -2.38) (Fig 3.5). We reasoned that, this could be possibly due to the effect of the gene traps on CD276 gene function, as a similar effect was reported for the CD274 gene coding for PD-L1, another member of the B7 family of proteins(61). Hereby, we evaluated the insertion pattern of the CD276 gene. Interestingly, we observed a B7H3 screen specific bias in insertions towards exon 1 for the high channel and upstream of exon 2 for the low channel in the *CD276* gene (Fig 3.6). It is possible that these high channel insertions are non-functional. By omitting non-functional insertions in the high channel, CD276 gene scored as the strongest hit and is represented as *VCD276* in the screen with an MI of -7.5 (Fig 3.5) and thus confirmed the specificity of the screen to detect regulators of B7H3 expression.

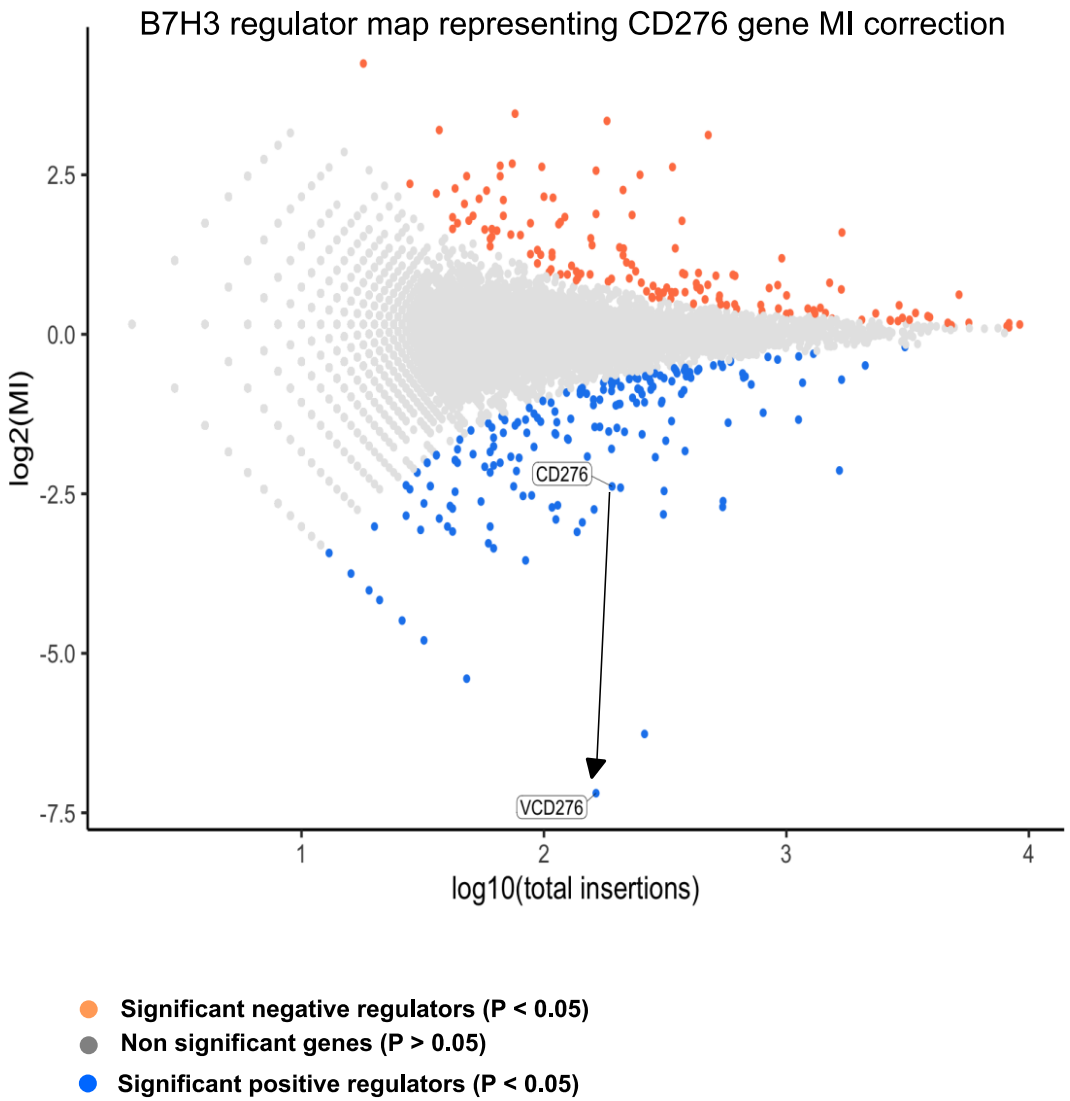


Figure 3.5 B7H3 regulatory map representing the corrected mutational index of the *CD276* gene, that codes for B7H3 protein Each dot indicates a per gene odds ratio (Mutational Index-MI): Frequency of mutations in the B7H3 high expression population divided by the frequency of mutations in the B7H3 low expression population. It is plotted as the MI on y axis against the total number of insertions assigned to the individual gene on the x axis. Genes enriched in either population are coloured as indicated in the legend. (two-sided Fisher's exact test, false discovery rate corrected P

value ≤ 0.05. CD276 gene, and its corrected mutational index after omitting non-functional insertions in the B7H3 high population are labelled.

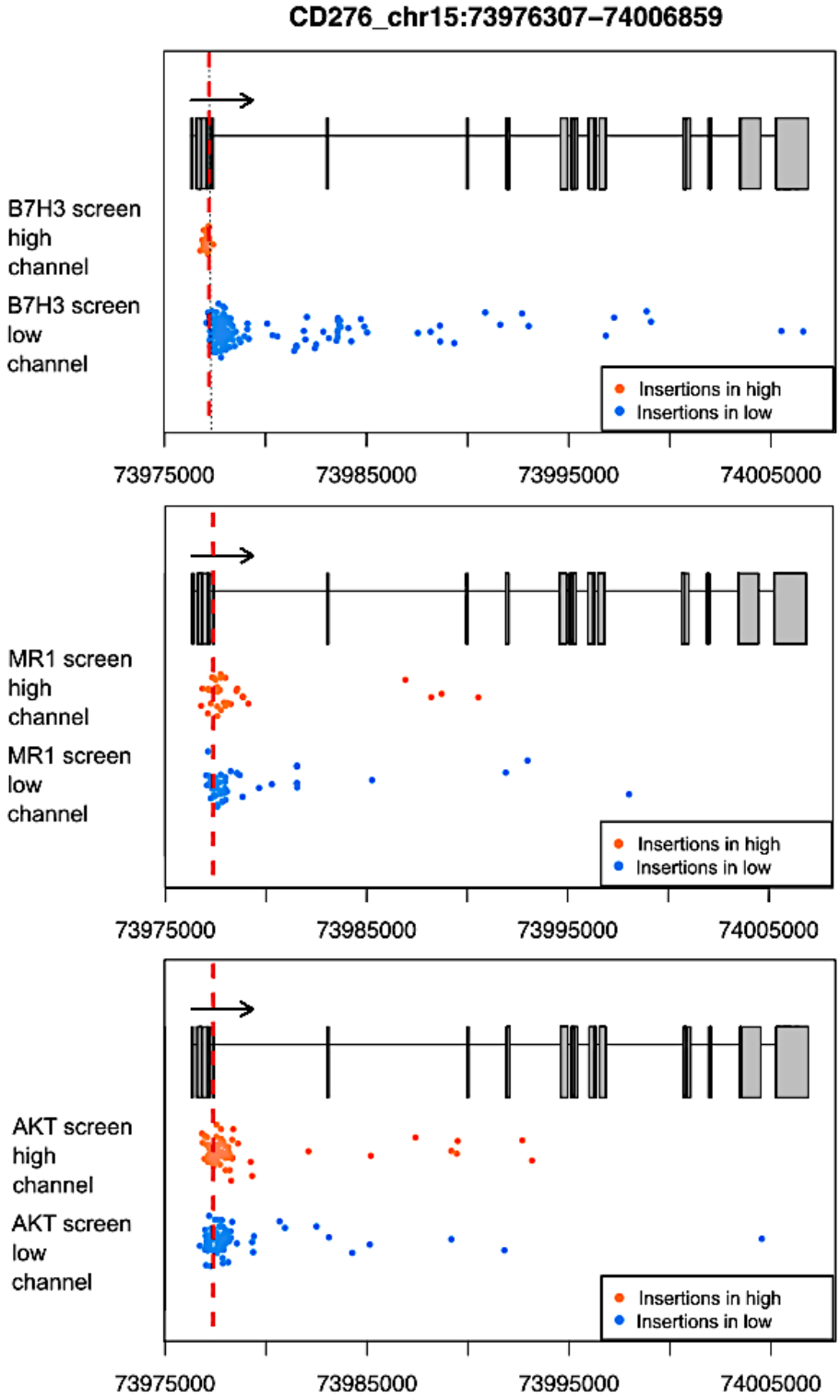


Figure 3.6 Gene trap insertion sites for the CD276 genes across 3 different screens. Analysis of gene trap insertion pattern in the CD276 gene observed in the mutagenized HAP1 cells sorted based on high and low B7H3 expression. A bias towards insertions upstream of exon 1 and exon 1 is observed for the CD276 gene in B7H3 high cells compared to B7H3 low cells. This bias appears specific compared to two other screens done on MR1 and AKT. The arrow indicates the direction of transcription, and the grey boxes indicate the exons.

Overall, the screen identified 325 hits ($P<0.05$). Among these, genes expected to modulate the surface expression of B7H3 such as genes associated with signal recognition particle (SRP) mediated targeting of proteins to the plasma membrane such as *SSR1, SSR2, SSR3, SPCS1, RPL29, RPS25* and *RPS29* scored as positive regulator hits (Fig 3.7, mustard)(108). Furthermore, known regulators of surface expression such as the retromer complex genes *VPS29, VPS35 and VPS26A* along with its interacting partner *RAB7A* (MI -3.35) presented amongst the strongest positive regulator hits (Fig 3.7, yellow). The interaction between RAB7A and retromer complex influences actin filament organization to facilitate surface expression of proteins. Consistent with this, genes coding for key players of actin filament organization that can influence surface expression such as *ARPC2, ARPC3, ARPC4, ACTR2, ACTR3* presented amongst the strong positive regulators (Fig 3.7, pink)(109). Although, some of these hits *RAB7A* and *VPS29* presented themselves as hits in a similar screen done to map molecular regulators of PD-L1, the effect size (MI) for these genes was found to be greater for the B7H3 screen compared to the PD-L1 screen(61).

This suggested a highly specific role for these pathways towards facilitating B7H3 surface expression. In addition to these pathways expected to influence B7H3 expression, few other interesting hits were detected. For example, it has been reported that B7H3 stability is regulated by both the lysosomal and the proteasomal pathways through Lysine (K) 48 and 63 linked ubiquitination respectively. However, evidence of the E3 enzyme responsible for ubiquitination of B7H3 has not been reported to the best of our knowledge. Interestingly, genes coding for UBE2L3 an E2 enzyme and CUL3 an E3 enzyme, two central players of the Ubiquiting Proteasome System (UPS) along with other associated genes scored amongst the strong negative regulators while deubiquitinating enzyme *OTUD5* scored as a strong positive regulator (Fig 3.7, blue). Furthermore, 6 protein glycosylation associated genes *ALG5, ALG8, SRD5A3, CMAS,SLC365A1* and *ST3GAL5* expected to affect protein stability scored as hits (3.7, green). Protein glycosylation is expected to stabilize surface expression of proteins(110). Intriguingly, 3 of these hits *CMAS, SLC35A1 and ST3GAL5* presented as negative regulators (Fig 3.8, green). Interestingly, these 3 genes are central players of the sialylation biosynthesis pathway. Specifically, *CMAS* codes for N-acylneuraminate cytidylyltransferase (CMAS) and is a central player in a stepwise pathway leading to addition of sialic acid to the cell surface of glycoproteins. Specifically, the biosynthesis of sialic acids is catalyzed by The bi-functional enzyme UDP-N-acetylglucosamine-2-epimerase/N-acetylmannosamine kinase to form ManNAc-6-phosphate. Next, N-acetylneuraminic acid phosphatase (NANP) and Neu5Ac 9-phosphate synthase (NANS) convert ManNAc-6-phosphate to Neu5Ac. Thereafter, Neu5Ac is then

activated to CMP-Neu5Ac by N-acylneuraminate cytidylyltransferase (CMAS). The activated CMP-Neu5Ac is then transported to the golgi by solute carrier family 35 member A1 (SLC35A1), where Sialyl Transferases (STs) such as ST3GAL5 are involved in transfer of the sialyl group Neu5Ac to terminal galactose of glycolipids or glycoproteins(111). Notably. CellSeq has mapped all of three main principal components of this three step sialic acid biosynthesis process as B7H3 surface expression modulators. We next investigated, if this pathway specifically affects B7H3. Interestingly, *CMAS* and *ST3GAL5* appeared as a negative regulator hit in only one other screen (n=46) (Fig 3.9). *SLC35A1* scored as a hit in 9 other screens (n=46) possibly owing to its broader functions (Fig 3.9). This suggested a potential specific effect of the sialylation pathway on B7H3 function compared to other proteins investigated using CellSeq. Collectively, we conclude that the above observations demonstrate the ability of CellSeq to map known and expected regulatory mechanisms of B7H3 surface expression. In addition to the notable hits discussed above, the screen identified various putative regulators of B7H3 surface expression in HAP1 cells (Appendices 6.2).

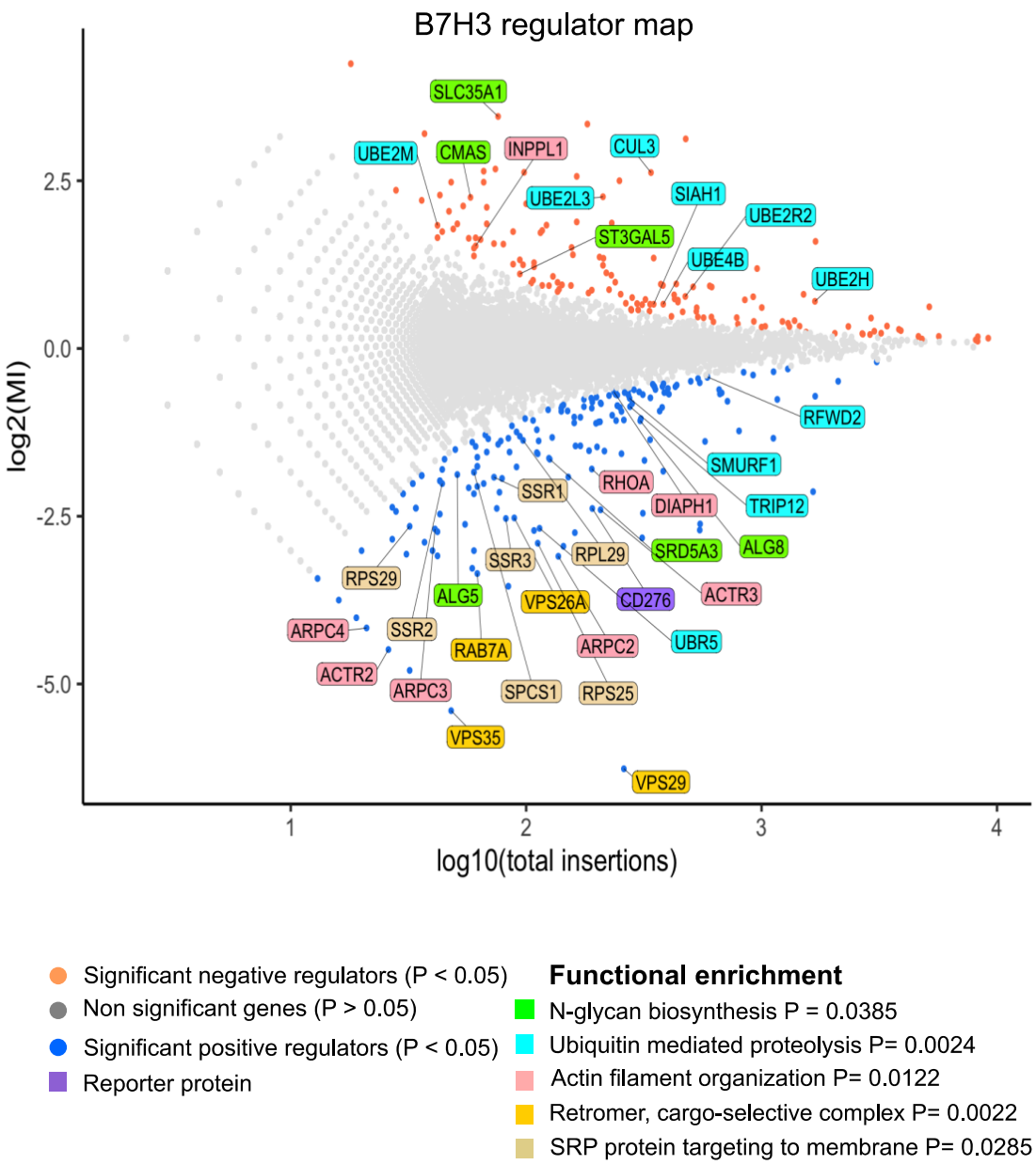


Figure 3.7 B7H3 regulator map representing hits from pathways expected to influence B7H3 expression Fishtail plot representing the CellSeq B7H3 regulatory map. Each dot indicates a per gene odds ratio (Mutational Index-MI): Frequency of mutations in the B7H3 high expression population divided by the frequency of mutations in the B7H3 low expression population. It is plotted as the MI on y axis against the total number of insertions assigned to the individual gene on the x axis. Genes enriched in either population are coloured as indicated in the legend. (two-sided

Fisher's exact test, false discovery rate corrected P value ≤ 0.05. Selected pathways expected to have an effect on B7H3 expression are labelled

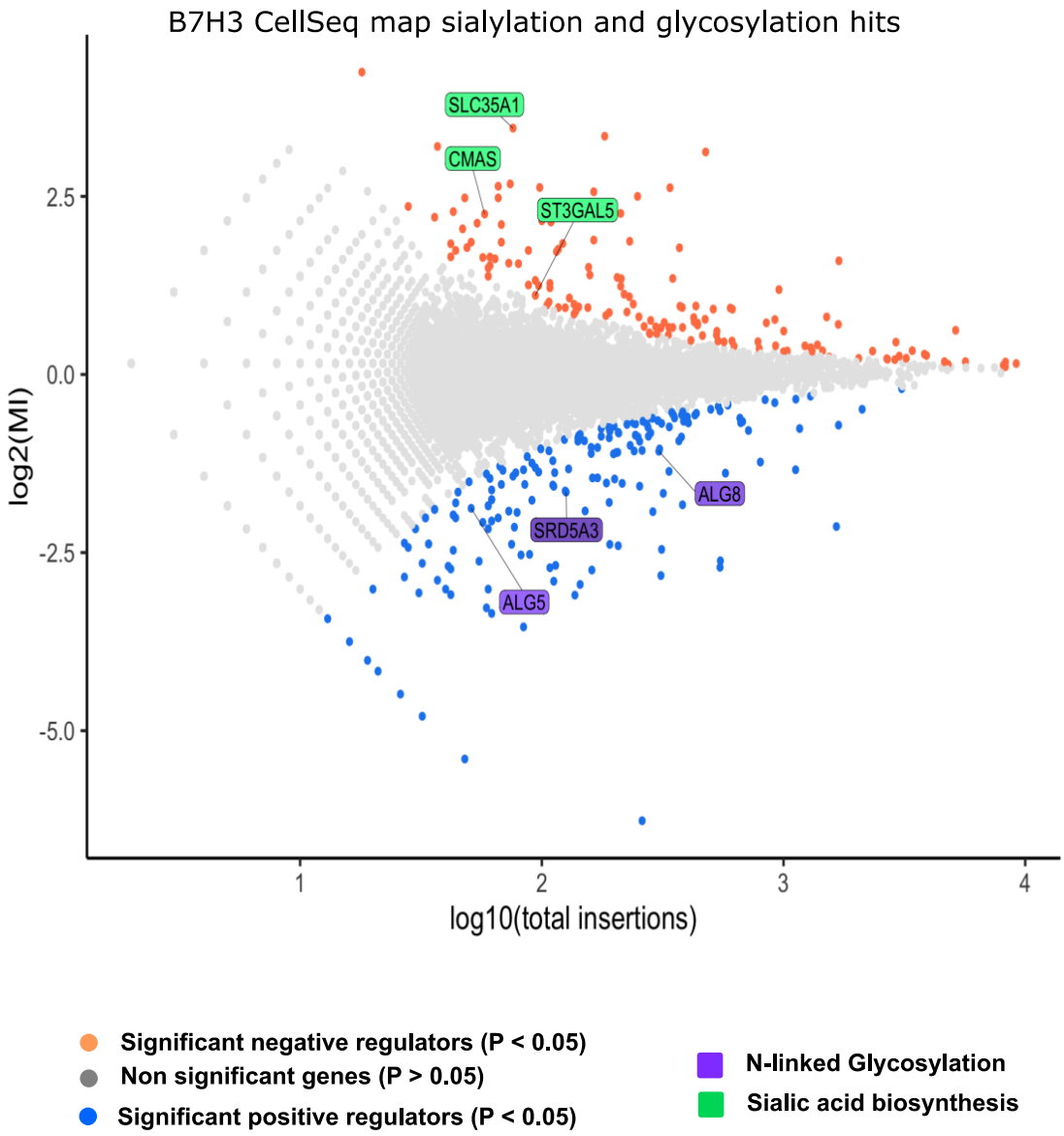
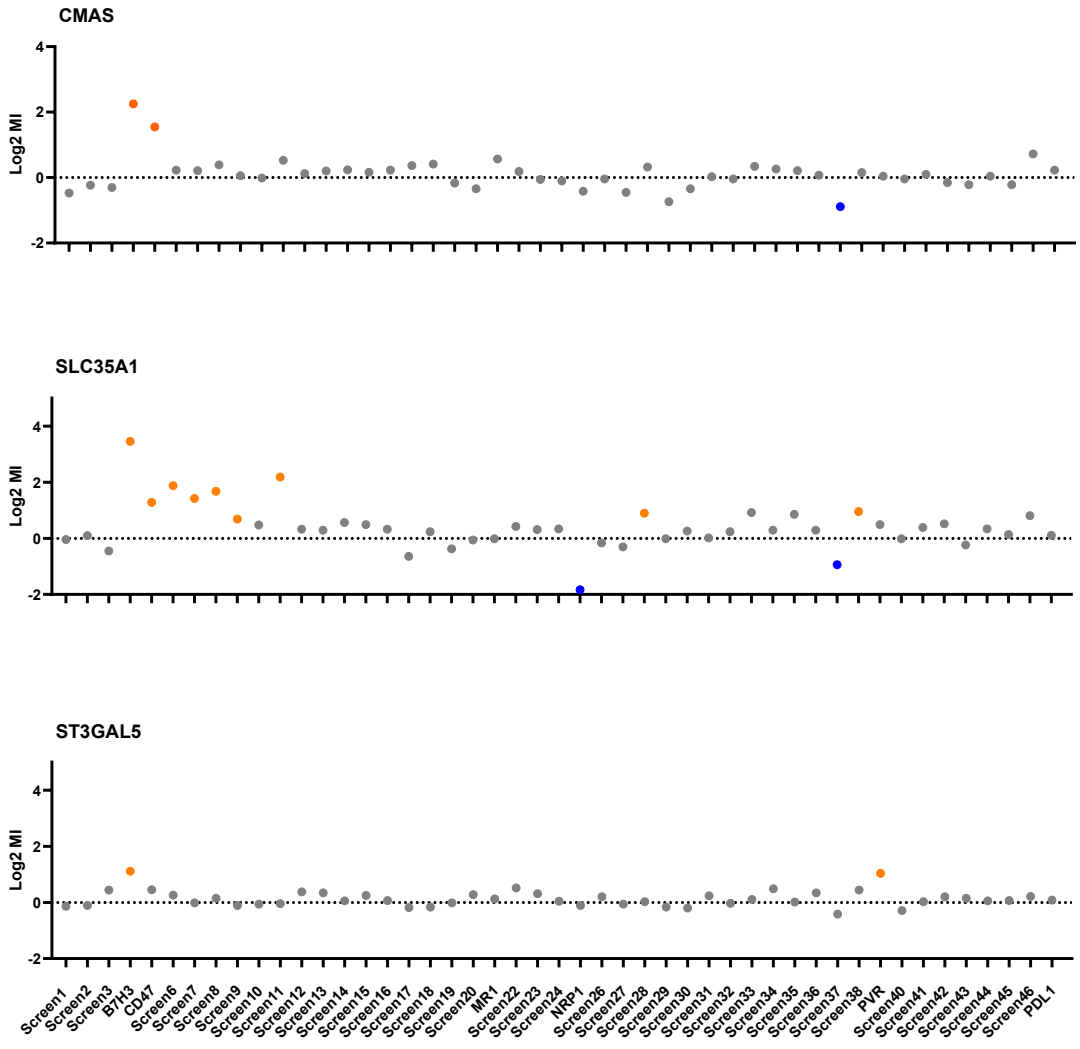


Figure 3.8 B7H3 regulator map representing hits from the sialylation pathway (a) Fishtail plot representing the CellSeq B7H3 regulatory map. Each dot indicates a per gene odds ratio (Mutational Index-MI): Frequency of mutations in the B7H3 high expression population divided by the frequency of mutations in the B7H3 low expression population. It is plotted as the MI on y axis against the total number of

insertions assigned to the individual gene on the x axis. Genes enriched in either population are coloured as indicated in the legend. (two-sided Fisher's exact test, false discovery rate corrected P value ≤ 0.05. Hits associated with the sialylation pathway have been labelled.



- Significant negative regulators (P < 0.05)
- Non significant genes (P > 0.05)
- Significant positive regulators (P < 0.05)

Figure 3.9 Sialylation associated genes are putative regulators of B7H3 expression Visual specificity scoring map for CMAS, SLC35A1 and ST3GAL5 genes

across ~50 other screens. Briefly, scoring is done to determine how a gene scores across various CellSeq screens performed on different proteins to determine specificity of gene effect to phenotype (See Sec 2.7.2).

Next, to validate some of these putative B7H3 regulators we compiled a list of 14 hits based on various parameters (Sec 2.7, Fig 2.2, Table 3.1) such as uniqueness and biology and investigated, if the inhibition of these genes will have an effect on B7H3 expression.

Hereby, we transfected sgRNA, targeting the coding region of these 14 hits with a CAS9 expression plasmid into HAP1 cells or used stable CRISPR/Cas9 HAP1 knockout cell lines and evaluated surface expression of B7H3 using flow cytometry (Fig 3.10 A-G). Interestingly, targeting *SAMD1, SPPL3* and *HDAC8* led to a reduction in B7H3 surface expression and thus confirmed them as positive regulators (Fig 3.10 D-F). Furthermore, targeting *SAMD4B* led to an increase in B7H3 surface expression and validated it as a negative regulator (Fig 3.10 G). Targeting genes such as *HM13* and *BTLA*, did not result in a shift in fluorescence intensity peak compared to empty vector control, indicating that these genes might not have been sufficiently edited and thus needs further investigation (Fig 4.10 A-B). These modest but reproducible effects on B7H3 surface expression upon inhibition of *SAMD4B, SAMD1, SPPL3 and HDAC8* validate that the screen identified 'true' regulators of B7H3 expression with great sensitivity.

POSITIVE REGULATORS				
Gene	**FCPv**	**log2MI**	**Protein name**	**Role**
SPPL3	4.35E-19	-2.74511	Signal Peptide Peptidase Like 3	- ADAM10 activation to modulate cell surface proteins.(112). -Very recently, SPPL3 implicated in lipid-based surface protein shielding. Mechanism identified using CellSeq surface protein screen(62).
CD276	1.09E-18	-2.38468	B7H3	-T cell stimulatory and inhibitory roles.
RAB7A	8.47E-09	-3.35415	Ras-related protein Rab-7a	-RAB7A interacts with retromer complex to regulate expression of proteins(109).
OTUD5	3.01E-05	-3.0911	DUBA	-OTUD5 regulates Th17 cells that have a paradoxical role in cancer(82, 113).
KLF6	0.000379	-2.88755	Kruppel Like Factor 6	-KLF6 and B7H3 have both been implicated in cancer metastasis(114, 115).
BTLA	0.003646	-0.68692	B- And T-Lymphocyte-Associated Protein	-BTLA is a tumor necrosis factor family ligand and modulates immune responses(116).
YES1	0.008475	-0.81195	Tyrosine-protein kinase Yes	-YES1 protein kinase drives drug resistance in cancer(117).
SAMD1	0.031578	-3.01307	Atherin	-Atherin has been implicated in Artherosclerosis (118).
HDAC8	0.04066	-0.74131	Histone Deacetylase 8	-HDAC8 promotes neuroblastoma growth(119).
HM13	0.043249	-1.28794	Histocompatibility Minor 13	- Implicated in EGFR driven glioblastoma progression(120).
L3MBTL3	1.29E-12	-1.56799	Lethal (3)Malignant Brain Tumor-Like Protein 3	-L3MBTL3 is an interacting protein of SAMD1as determined by BioGrid. -Small molecular inhibitor for L3MBTL3 has been identified(121).
NEGATIVE REGULATORS				
CMAS	2.97E-05	2.252098	N-acylneuraminate cytidylyltransferase	-CMAS has been implicated in: T cell modulation, breast cancer and myeloid leukemia progression(122-124).
SAMD4B	0.000917	2.28621	Sterile Alpha Motif Domain Containing 4B	-Inhibits major transcription factors such as AP-1 and p53(125).

Table 3.1 Hits chosen for CRISPR/Cas9 validation from the B7H3 screen

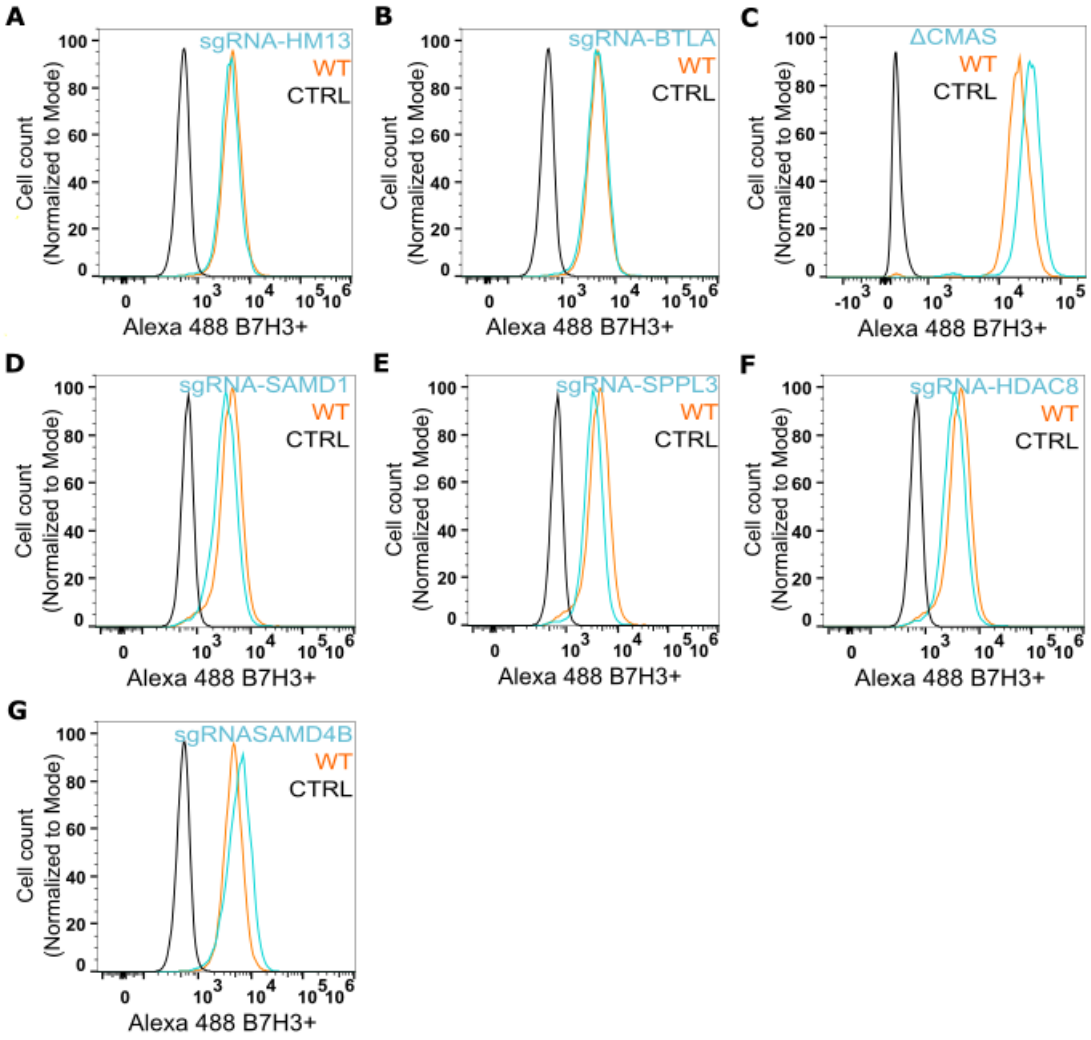


Figure 3.10 CRISPR/Cas9 validation of select hits from the B7H3 screen

Genes A) HM13, B) BTLA, D) SAMD1, E)SPPL3, F) HDAC8, G) SAMD4B were targeted using CRISPR/Cas9 sgRNA in HAP1 cells following which they underwent 36 hours of Puromycin selection. The selected polyclonal pool of HAP1 cells were then analyzed by flow cytometry 72 hours post selection, for surface B7H3 expression. C) Inhibition of CMAS gene and the subsequent effect on surface B7H3 expression was simultaneously evaluated using HAP1 CMAS gene knockout (ΔCMAS) derived by CRISPR/Cas9 editing and obtained from Horizon Discovery.

Upon inhibition of the sialylation pathway genes *CMAS and SLC35A1*, in a CMAS HAP1 knockout cell line with a 10 base pair (bp) deletion in exon 1 and

a SLC35A1 knockout HAP1 cell line with a 2bp deletion in exon 2, reassuringly lead to an increase in B7H3 and total surface expression, thus validating both genes as negative regulators of B7H3 (Fig 3.10 C, Fig 3.11 A-B). Strikingly, the B7H3 derived from CMAS and SLC35A1 knock out cells migrated more slowly in Sodium Dodecyl Sulphate–Polyacrylamide Gel Electrophoresis (SDS-PAGE), suggesting increased post translational modification of B7H3 (Fig 3.11 B).

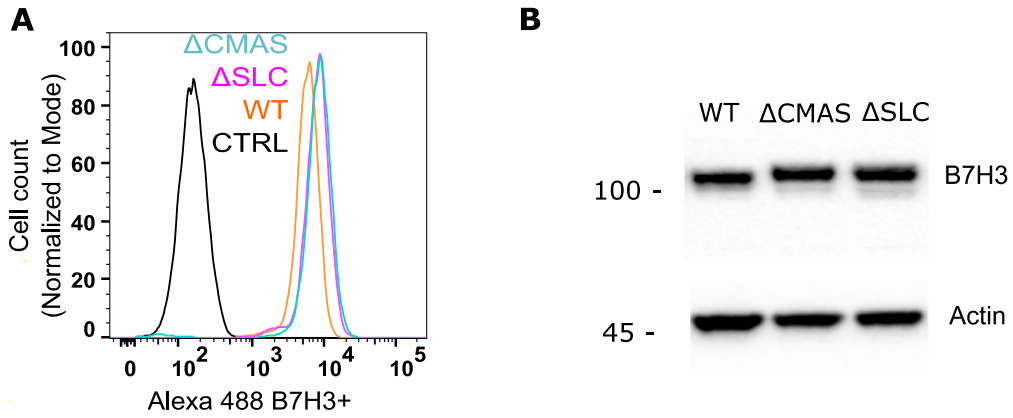


Figure 3.11 Sialylation genes *CMAS* and *SLC35A1* affect B7H3 surface and total protein expression HAP1 CMAS gene knockout and SLC35A1 gene knockout (ΔCMAS and ΔSLC) derived by CRISPR/Cas9 editing was obtained from Horizon Discovery. WT-HAP1 was used as control. A) Change in surface expression of B7H3 upon inhibition of SLC35A1 and CMAS was measured using flow cytometry and B) Using cell lysates from these clones, change in B7H3 total levels was evaluated by immunoblotting with B7H3 antibody and using actin as loading control.

Overall, we conclude that the screen retraces known biology and significantly expands our knowledge about B7H3.

3.2.3 *Role of sialylation biosynthesis as a potential regulator of B7H3 function*

We hypothesized that in the absence of CMAS (or SLC35A1) the addition of sialic acids to B7H3 would be abrogated, possibly leading to alternative glycoslylation (e.g. fucosylation) of B7H3. This change in B7H3 may in turn result in differential binding of B7H3 with its interacting partners and explain the observed change in cell-surface staining.

First, we investigated if the change in gel migration of B7H3 is because of absence of protein sialylation on B7H3 surface by using Neuraminidase, an enzyme that removes sialic acids from cell surface proteins. However, in contrast to the upward shift upon *CMAS* inactivation, we noted a downward shift of B7H3 upon neuraminidase treatment (Fig 3.12 A-B). This is consistent with a change in glycosylation rather than mere absence.

We also investigated the binding of the binding of two different B7H3 antibody clones, DCN.70 and EPNCIR122 to surface B7H3 expressed on HAP1 and CMAS knockout HAP1 cells by using the fluorescence intensity as a measure of antibody binding to B7H3. Interestingly, while there was no difference in the binding of the antibodies to both these cell lines, treatment with Neuraminidase caused differential binding of the EPNCIR122 antibody clon (Fig 3.12 C-D).

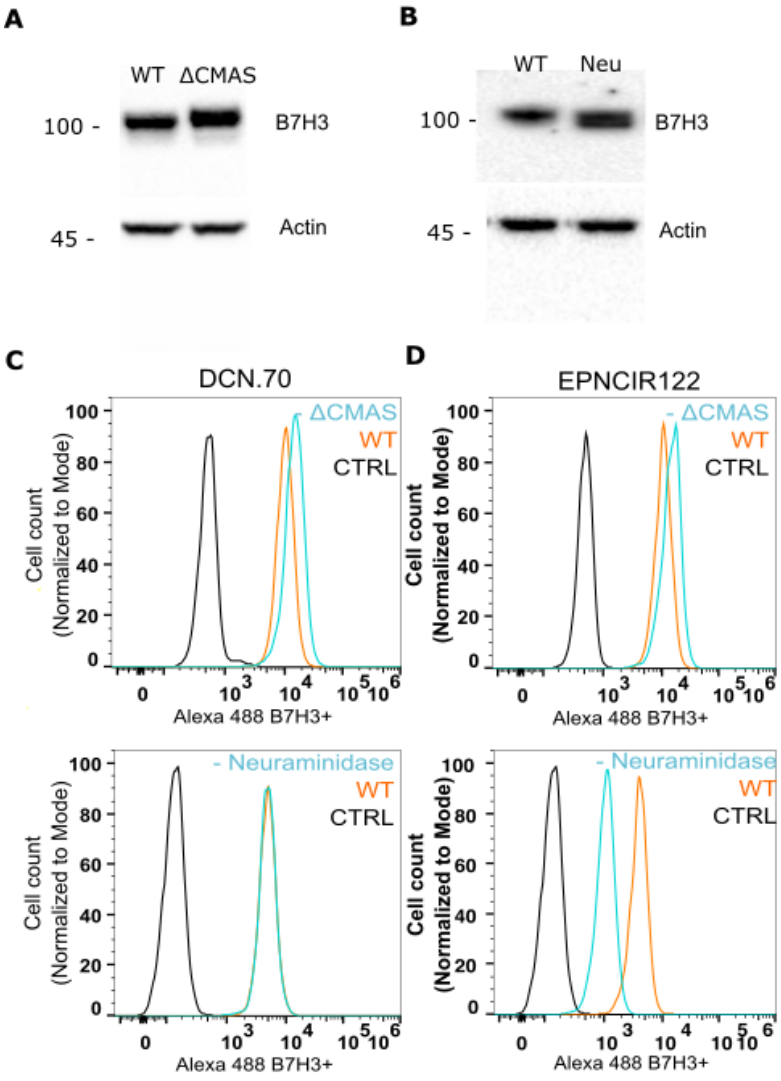


Figure 3.12 Biochemical vs genetic knockdown of sialic acid vary in terms of binding to B7H3 antibody clones and mobility shift in western A) Lysates from HAP1 CMAS gene knockout (ΔCMAS) and WT-HAP1 were probed for total B7H3 levels with actin as a loading control and B) compared to biochemical inhibition of sialic acid attachment to cell surface of HAP1 by using a Neuraminidase inhibitor and collecting the cell lysate 24 hours post treatment and probing for B7H3 levels. Shift in B7H3 molecular weight was recorded for A) and B). C) and D) Under similar conditions as described above, differential binding of described antibody clones of B7H3 to surface B7H3 on HAP1 was evaluated using flow cytometry.

Collectively, we conclude that changes to B7H3 structural properties caused by CMAS loss does not affect B7H3 differential binding, while loss of sialic acid does for certain antibody clones. Furthermore, CMAS induced B7H3 structural changes does not mimic sialic acid deficient B7H3.

3.3 Discussion

Consistent with the potential of CellSeq to delineate regulatory mechanisms of key immune checkpoints such as CD47 and PD-L1, we have demonstrated that CellSeq mapped regulators of emerging checkpoints PVR and B7H3, with exquisite specificity as confirmed by the genes coding for the protein of interest scoring as the strongest hits. The screens reiterated some known or existing biology about both the proteins and reported putative regulators that can further our understanding of their biology. Of note, while it is well established that PVR is retained in the intracellular compartments upon protein SUMO (Small Ubiquiting like Modifier) -ylation, the SUMOylation pathway members did not come up as hits. Similarly, while PVR is tightly regulated by the unfolded protein response (126) pathway, central players of UPR such as ATF6 and IRE1 did not score as hits(127, 128). Although, some of the known regulators of PVR from the literature are not detected in this screen, this could be simply due to technical limitations intrinsic to genetic screening approaches, where essential genes and genes with redundant functions do not score as hits. Furthermore, certain genes do not readily accommodate gene trap insertions and avoid detection through such haploid genetic approaches. Notwithstanding, although reported regulatory mechanisms for B7H3 surface expression are scarce, most pathways expected

to influence B7H3 surface expression scored as hits. Furthermore, the ability of CellSeq to pick up true regulators of surface expression of B7H3 and PVR was confirmed using CRISPR/Cas9. Collectively, we demonstrate that CellSeq is a state-of-art technology and has the ability to identify novel regulators of less understood immune checkpoints. Specifically, in this study, we have identified 1) *FBXO11*, a transcription factor and immune regulator gene as a positive driver of PVR expression 2) An association between sialylation associated CMAS gene, and B7H3 regulation.

3.3.1 *FBXO11: An indirect link between the UPS and PVR expression?*

A direct link between the UPS and PVR regulation has not been reported. Interestingly, for the first time our study highlights the UPS as a possible player in PVR regulation. While, E3 ligases such as CUL3 and HERC4 presented as strong negative regulator hits, the FBXO11 E3 ligase presenting and validating as a strong positive regulator hit was rather intriguing. FBXO11's ability to positively regulate PVR expression suggests an indirect role for the UPS in stabilizing PVR expression. FBXO11 has been reported to directly target key immune regulatory transcriptional repressors such as BCL6 towards proteolytic degradation(103, 129). While BCL6 has not been reported as a direct transcriptional repressor of PVR, another BCL transcription factor family member BCL9 has been reported to suppress PVR expression(130). It will be interesting to investigate, if FBXO11 broadly targets the BCL transcription factor members to regulate key immune regulatory genes such as PVR. Overall, the PVR screen

has highlighted an unexpected link between the UPS and positive regulation of PVR expression.

3.3.2 *Sialylation: The fine balance between B7H3 being a friend or a foe to anti-tumor immunity?*

While the relationship between glycosylation and B7H3 stability has been extensively studied, its effect on B7H3 function remains unclear. We hypothesize that the differential structural properties of B7H3 that we observed upon CMAS knockdown and biochemical depletion of sialic acids on cell surface B7H3 could elicit contrasting lymphocyte phenotype induction via distinct receptor interactions. Also, It is tempting to speculate, that sialylation or fucosylation levels can determine the respective putative receptors. However, we did not see any effect of the sialylation genes on different antibody clones binding to B7H3. Although we did not see a difference, it is important to note that the antibody clones binding to B7H3, necessarily does not mimic receptor ligand interactions and this needs to be investigated further. It will be interesting to first characterize the glycan signature on the B7H3 in CMAS knockdown and biochemically sialic acid depleted conditions. If the glycan structures are different, then using a co-culture system to evaluate the functional effect on T cells can be insightful. Collectively, our study highlights a distinction between sialylation defective and sialic acid deficient B7H3 and warrants further characterization of the structural and functional properties of these two forms of B7H3 and its subsequent role in anti-tumour immunity.

Chapter 4: CellSeq identifies UBE3D as a novel negative regulator of NRP1

4.1 Introduction

In Chapter 1, we identified Neuropilin-1 (NRP1) immune checkpoint protein as one of the three less understood immune checkpoint proteins that are expressed in HAP1 cells. In this Chapter, we employ CellSeq to better understand NRP1 biology. Interestingly, NRP1 and many other proteins that modulate the tumour immune interface have other pleiotropic roles. This chapter, describes a novel NRP1 regulatory mechanism revealed by CellSeq with direct implications for eye disease and paves way for future studies to understand its role in the tumour immune interface.

4.1.1 *Neuropilin-1(NRP1): A multifaceted protein*

NRP1 is a non-tyrosine kinase surface glycoprotein. It was first implicated in neuronal axonal guidance(131). Later, its fundamental role in vascular biology became more prominent with the identification of the role of NRP1 in embryonic vascular development(132-134). Over the last decade, along its well-established roles in neuronal and vascular development, NRP1 is taking its place as a central player of anti-tumour immunity(135).

NRP1 consists of a N- terminal extracellular domain, a transmembrane region, and a short intracellular domain. The extracellular domain consists of 2 CUB domains, 2 coagulation factor domains and a MAM domain. Involvement of NRP1 in neuronal guidance is mediated by Semaphorin binding to the CUB domains while NRP1 mediated vascular development is facilitated by the interaction of Vascular Endothelial Growth Factor (VEGF) to the 2 coagulation factor domains. NRP1 binds to a broad repertoire of ligands through its different domains by forming receptor complexes and drives various biological processes ranging from neuronal development to immunity. The MAM domain aids NRP1 receptor complex formation by promoting homodimerization or heterodimerization of receptors. Although, the role of NRP1 as a signalling receptor was not initially clear, it was later established that the conserved PDZ domain binding motif at the cytosolic tail of NRP1 binds Synectin and mediates various processes such as intracellular signalling and receptor internalization(136).

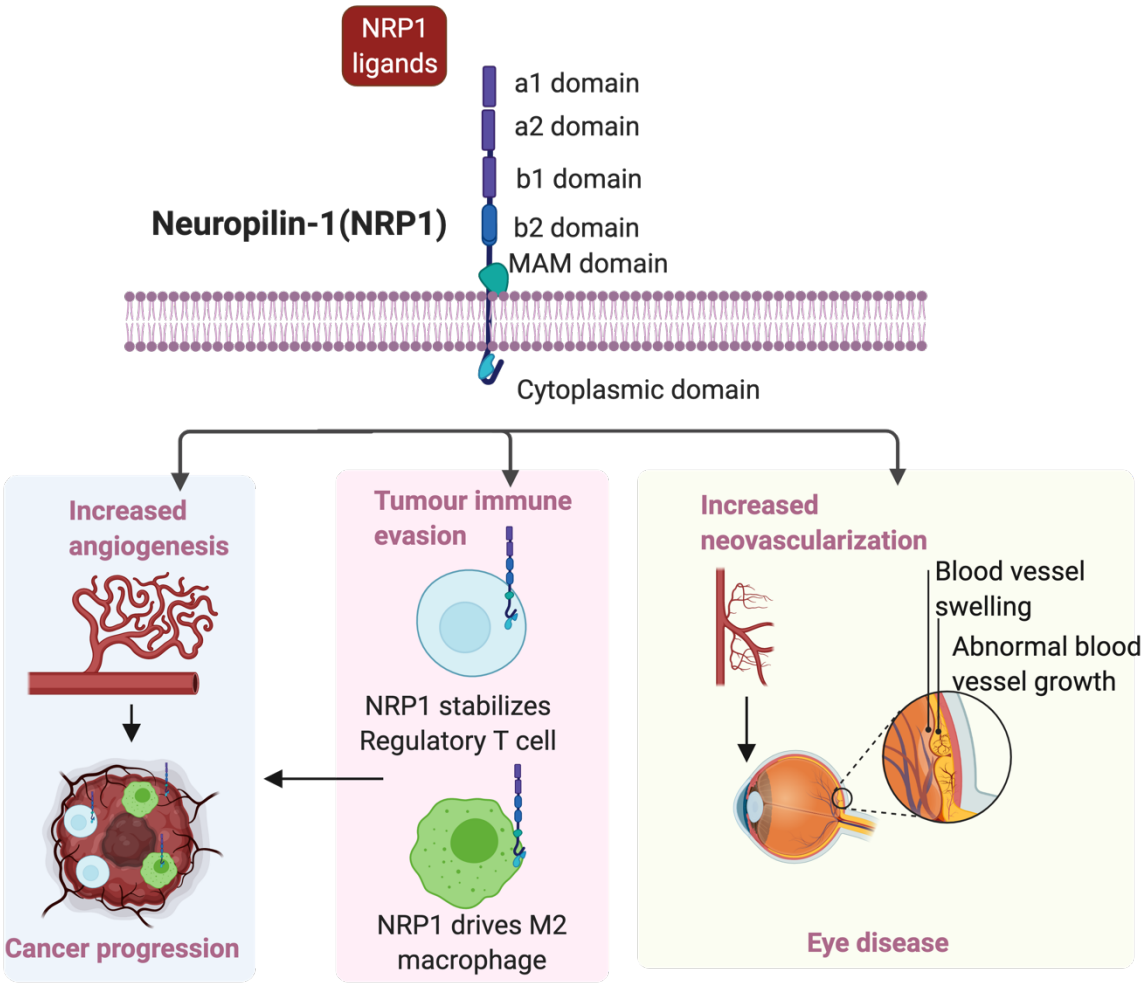


Figure 4.1 Schematic representing multifaceted roles of Neuropilin-1(NRP1)

Adapted from(134, 137, 138, 142) and created on Biorender.com

Multiple structural and splice variant isoforms of NRP1 have been reported. For example, NRP1 exists in both membrane bound and soluble form(136). Interestingly, the soluble NRP1 presenting with the extracellular domain and lacking the transmembrane domain acts as a decoy to membrane bound NRP1. For example, whereas membrane bound NRP1 acts as a coreceptor for Vascular Endothelial Growth Factor 165 (VEGF165) and drives

angiogenesis, soluble s12NRP1 acts as a decoy and inhibits VEGF165 binding to NRP1 and inhibits angiogenesis, subsequently resulting in tumour growth inhibition(139, 140). At the protein level, ADAMs 9 and 10 drive NRP1 proteolysis, leading to accumulation of a soluble form of NRP1, subsequently inhibiting VEGF signalling(141).

Overall, the ability of NRP1 to bind a broad repertoire of ligands and isoforms of NRP1 with opposing functions appear to fuel the versatile nature of NRP1 and its ability to drive various disease pathogenesis (Fig 4.1)(137, 138, 142).

4.1.2 *NRP1 versatility: A novel immune checkpoint*

Whereas NRP1 is expressed on various cell types and tissue of the nervous and vascular systems ubiquitously, the expression of NRP1 on immune cells is highly restricted to certain immune cell phenotypes. Specifically, induction of NRP1 surface expression on several immune cells drive critical immune functions (Table 4.1)(137).

Immune Cells	Function
Plasmocytoid dendritic cells	-Immune suppression in tumor infiltrating dendritic cells
Myeloid dendritic cells	-Immunological synapse formation with T cells through homophylic interaction between DC NRP1 and T cells
Macrophages and Microglia	-Vascular development -M2 macrophage polarization and immunosuppression -T regulatory cell induction -Migration to the hypoxic core through Semaphorin and Plexin signalling -Protumorigenic activities of tumor associated macrophages (TAMs) -TAM inhibition in certain cancers
T regulatory cells	-Immune suppression -Migration of T regulatory cells to the tumor microenvironment -Stabilizes T regulatory cells
CD8+ effector and memory cells	-CD8+ specific NRP1 deletion offers enhanced protection from tumor rechallenge
Tumour infiltrating CD8+ T cells	-CD8+ memory T cell differentiation inhibition and immune suppression
NKT cells	-Interaction between iNKT and macrophage cells
T foliclar helper cells	-B cell differentiation -Migration to secondary lymphoid organs

Table 4.1 Examples of functions affected by NRP1 expression on immune cells. Adapted from(137).

In the tumour microenvironment (86), NRP1 contributes to tumorigenesis by driving more than one hallmark of cancer. First, NRP1 expressed on tumour cells and stromal endothelial cells can drive increased angiogenesis and

potentiate tumour progression(140, 143). Next, NRP1 expression on immune cells can modulate the immune cells in the tumour microenvironment to promote tumour immune suppression and evasion. For example, tumour cells seize the inflammatory role of NRP1 in myeloid cells and use it to promote angiogenesis and immune suppression in the TME(144). Next, it can directly impact adaptive immunity which is responsible for specific anti-tumour immunity. Notably, NRP1 is expressed on the cell surface of one of the central immune suppressive cells in the TME, regulatory T cells (T_{reg}). NRP1 surface expression stabilizes the T regulatory cell state and promotes immune suppression and consequently tumour progression(80). Following this, very recently a study reported that there is an increased expression of NRP1 on tumour infiltrating CD8+ T cells compared to naïve CD8+ T cells. Furthermore, they show that NRP1 limits CD8+ T memory cells differentiation while having limited to no effect on effector activity and consequently the cytotoxic effect of T cells. Notably, they demonstrate that high NRP1 expression correlates with a reduced T memory CD8+ cells pool and consequently poor disease outcome. Overall, they present NRP1 as a novel immune memory checkpoint(145). Collectively, NRP1 appears to have broadly immunosuppressive and pro-tumorigenic functions.

4.1.3 *Another tale of NRP1 versatility: Age related macular degeneration*

Age related macular degeneration (AMD) is a disease caused by damage to the macula with age, the part of the eye responsible for focusing central vision. It leads to blurring of the central vision, while the peripheral vision remains intact.

It is the leading cause of vision loss in people above 50 years old. It has been reported that, AMD will affect an estimated ~288 million people by 2040(146).

There are two forms of AMD. First, Dry AMD is the most common and constitutes about 80% of the total AMD cases. It is characterized by the thinning of the macula and the increased accumulation of drusen (lipids and protein particles) that eventually leads to deterioration of the retinal pigment epithelial layer (RPE), photoreceptors and the capillaries in the eye. Subsequently, this eventually leads to central vision loss. At any stage of AMD, the disease can progress towards neovascular, or wet AMD as characterized by increased vascularization (growth of new blood vessels) leading up to the rupture and invasion of the retinal region. These new blood vessels, eventually leak or rupture leading up to fluid accumulation or haemorrhages in the retinal spaces, resulting in choroidal neovascularization, a hallmark of AMD (Fig 4.2). Subsequently, this eventually leads to central vision loss(146, 147).

A combination of factors such as genetic susceptibility, environmental factors and ageing can contribute towards AMD disease pathogenesis. Specifically, various single nucleotide variants of *HTRA1, TGFBR1, VEGF*, and *NRP1* have been reported as AMD risk factors(148, 149).

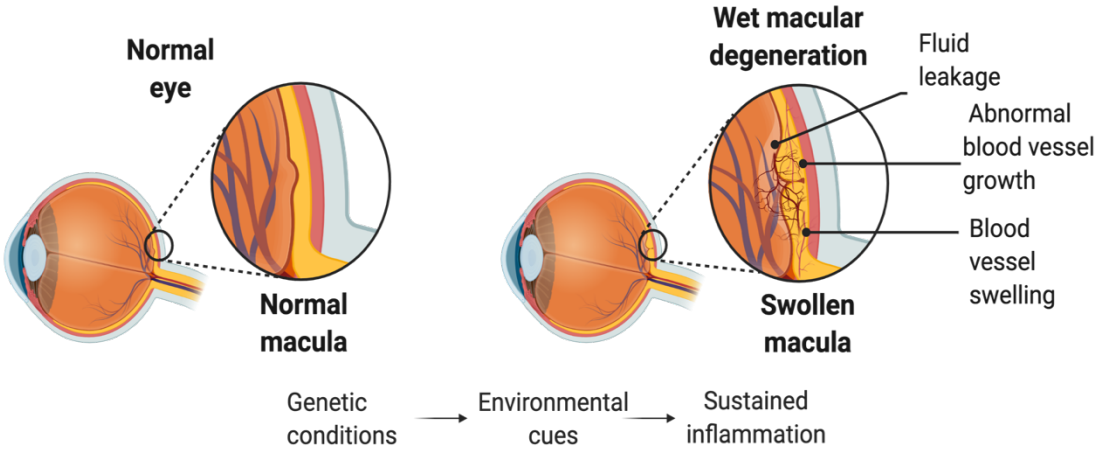


Figure 4.2 Features of wet age-related macular degeneration. Adapted from(146) and created on Biorender.com

Neovascularization is the principal driver of age related macular degeneration pathogenesis(146). Subsequently, targeting angiogenesis receptor VEGF, which is notable also an AMD risk factor is the gold standard for treatment of AMD. However, VEGF inhibition leads to systemic adverse events and ocular complications(150). Therefore, there is a need for alternative therapeutic strategies . Interestingly, NRP1 is a coreceptor of VEGFR2 and thus amplifies VEGF mediated angiogenesis signalling(132, 140). A seminal study associated NRP1 with vascularization and showed that overexpressing NRP1 in mouse embryo leads up to excessive vessel growth with leaky and haemorrhagic characteristics(151). Similarly, a zebrafish study reported defects in vessel patterning and improper arteriovenous connections, suggesting that NRP1 is

essential for angiogenesis in fish(133). Notably, NRP1 has been demonstrated to affect choroidal and retinal neovasculature in mice(152). In addition, NRP1 has also been implicated in VEGF independent modulation of angiogenesis through ABL tyrosine kinase activation. Furthermore, NRP1 acts as a coreceptor and enhances signalling through various other angiogenesis related factors such as Transforming Growth Factor Beta 1 (TGFB1) and Semaphorins(153-155).

Overall, NRP1 is an essential factor for neovascularization in eye pathologies and can thus be a promising drug target for ocular neovascular diseases(138). While its well understood that VEGF acts as a co-receptor for NRP1 and drives angiogenesis, the underlying molecular mechanism of how NRP1 contributes towards macular degeneration pathogenesis remains unclear.

4.1.4 *UBE3D and AMD*

UBE3D belongs to the E6-AP HECT E3 ligase family. Other members of the E6-AP HECT E3 ligase family such as UBE3A, UBE3B and UBE3C have been reported to facilitate substrate ubiquitination and consequently target it towards proteasomal degradation or regulate other protein fates such as lysosomal degradation, trafficking and protein-protein interactions(156, 157). However, this has not been previously demonstrated for UBE3D. While, UBE3D belongs to the E6AP family, it is structurally quite different from the other members. UBE3D is a 389 aa, ~43 kDa protein and contains a HECT like domain in its C terminus. The HECT domain of UBE3D is smaller than other members of the E6-AP family at ~5 kDa and shows a 60% homology with the HECT domain of UBE3A. The ~5 kDa HECT like domain does contain a catalytic cysteine and

suggests that UBE3D can potentially ubiquitinate target substrates. In addition, the UBE3D protein contains a E2 binding domain between 235-257 aa in the C-terminal of the protein. In vitro, this E2 binding domain has been shown to facilitate binding of UBE2C E2 enzyme and UBE3D leading to subsequent ubiquitination and 26 s proteasomal degradation of Cyclin B1. Furthermore, they demonstrate that the cysteine threonine residues in the C terminal HECT domain is essential for ubiquitination activity of UBE3D(158). However, no physiological relevance for this has been thus far demonstrated.

Interestingly, UBE3D loss has been recently implicated in neovascular AMD risk in east Asian population patients. Huang et al performed a whole exome sequencing on East- Asian neovascular AMD patients(159). They validated and identified known risk factors such as *CFH, HTRA1, B3GALTL, C2, HMCN1, CFB and SKIV2L*. In addition, they reported a novel missense SNV at the rs7739323, on *UBE3D* as a significant neovascular AMD risk factor. This is a single missense mutation of Val to Met at position 379 in the catalytic HECT domain of UBE3D (V379M). Although homozygous inactivation of UBE3D resulted in embryonic lethality in mice, heterozygous animals displayed structural changes in the retina and an abnormal electroretinography, hallmark characteristics of AMD(159). In accordance with this, the same group performed functional studies in a zebrafish model to show increased angiogenesis, melanosome transport, reduced eye size and abnormal eye morphology upon UBE3D loss(160). More recently, a pre-print from the same authors reported that UBE3D, but not the AMD-associated V379M mutant, interacts with KAP1 and regulates DNA repair, consistent with a model in which UBE3D drives AMD pathogenesis through defective DNA repair.

Collectively, these findings indicate that UBE3D deregulation can cause AMD but the mechanism whereby it would affect neovascularization has not been demonstrated.

In this chapter, using an unbiased haploid genetic screening approach (CellSeq), we identified UBE3D as a NRP1 regulator, providing a potential mechanistic basis for its association with AMD. UBE3D inactivation increased NRP1 at the cell surface whereas its overexpression reduced NRP1 levels. Surprisingly, NRP1 lysosomal degradation was also enhanced by E3 defective UBE3D mutants, indicating a ubiquitin-independent mechanism. Importantly, the AMD -associated V379M mutant did not interact with NRP1 and accordingly did not reduce its levels. The mechanistic link between UBE3D could also be demonstrated in vivo. In zebrafish, increased angiogenesis upon UBE3D inhibition could be restored by concomitant NRP1 inhibition. Together, these observations are consistent with a model in which a loss of function UBE3D V378M mutant drives pathogenic angiogenesis by reduced lysosomal NRP1 degradation.

4.2 **Results**

4.2.1 *Identification of regulators of NRP1 using CellSeq*

We aimed to map the molecular regulators of NRP1 surface expression. Hence, we performed a haploid genetic screen (CellSeq) by staining mutagenized HAP1 cells for NRP1 and enriched the extreme ends of the fluorescence distribution using FACS (Fig 1.2, Sec 2.5). As expected, upon

recovery of the insertion sites in each of the populations, we identified that NRP1 knockout cells were strongly enriched in the lower end of the fluorescence distribution. Consequently, The *NRP1* gene coding for the reporter protein itself (Fig 4.3, yellow), presented as the strongest positive regulator. This served as an internal screen quality control and confirmed the sensitivity of the screening approach.

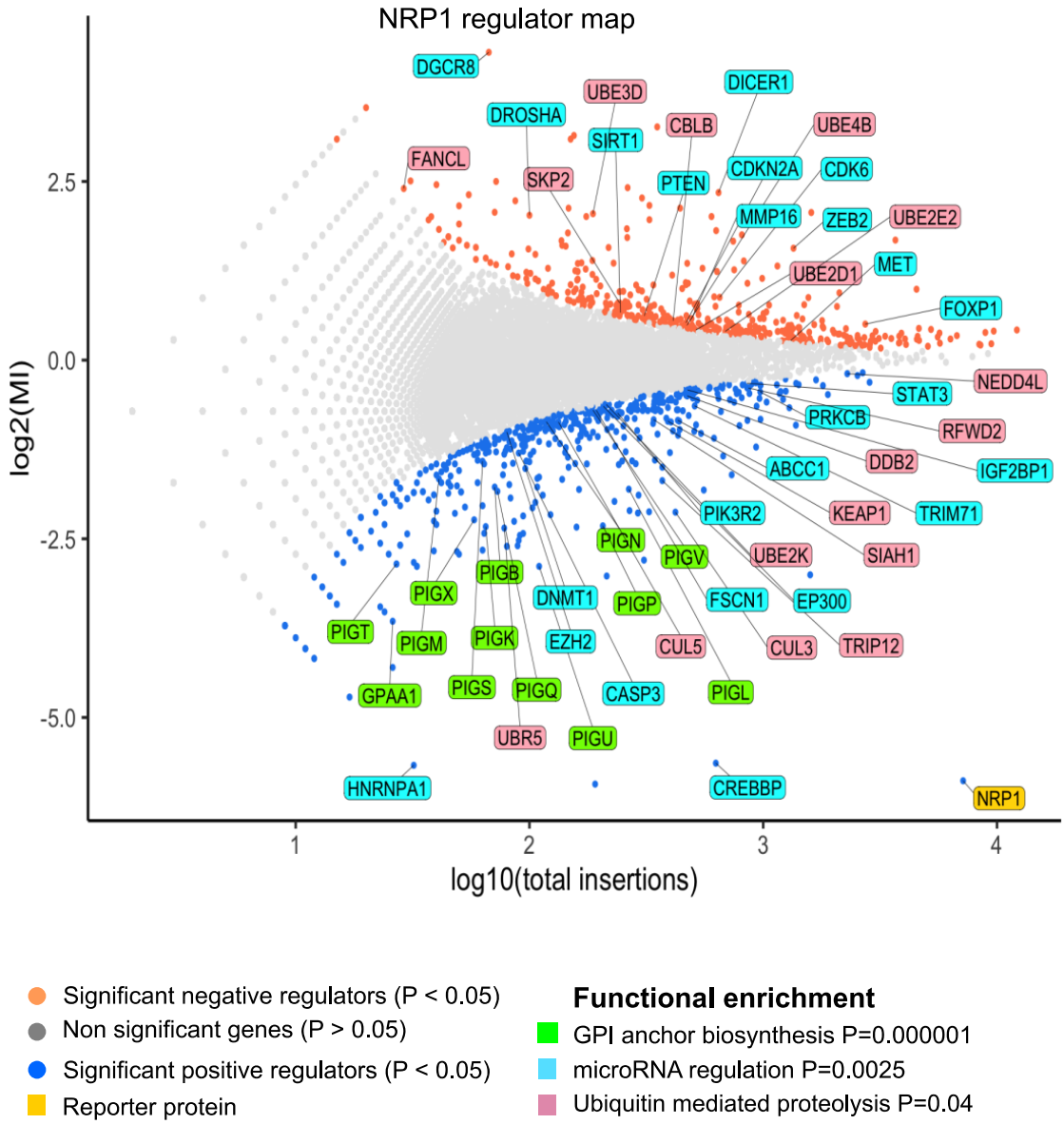


Figure 4.3 Regulator map representing hits from pathways expected to influence NRP1 surface expression Each dot indicates a per gene odds ratio (Mutational Index-MI): Frequency of mutations in the NRP1 high expression population divided by the frequency of mutations in the NRP1 low expression population. It is plotted as the MI on y axis against the total number of insertions assigned to the individual gene on the x axis. Genes enriched in either population are coloured as indicated in the legend. (two-sided Fisher's exact test, false discovery rate corrected P value ≤ 0.05. Hits from selected pathways known to have an effect on NRP1 expression are labelled.

Among the 903 hits, genes expected to drive NRP1 surface expression such as the central players of the Glycosylphosphatidylinositol (GPI) anchor biosynthesis pathway (Fig 4.3, green) presented as positive regulator hits, albeit not being the strongest(161, 162). This suggests that different forms of NRP1 could be present, consistent with what is known(136). Furthermore, various studies have reported that NRP1 is tightly regulated by micro Ribo Nucleic Acid (microRNA)(163-166). As expected, the microRNA biosynthesis pathway genes *DICER1, DGCR8* and *DROSHA1* scored among the strongest negative regulator hits along with other associated genes (Fig 4.3, blue)(167). Interestingly, it has been reported that CUL3 E3 ligase positively regulates NRP1 expression and VEGFR2 expression to drive angiogenesis(168). One of the reasons for the paradoxical role of CUL3 towards NRP1, could be that, CUL3 targets a substrate that is a putative negative regulator of NRP1. Consistent with this, *CUL3* presents as a positive regulator hit, while other genes associated with the ubiquitin mediated proteolysis presented as both potential positive and negative regulators

(Fig 4.3, pink). In addition to the notable hits discussed above, all the putative regulators of NRP1 surface expression in HAP1 cells are listed (Appendices 6.3).Together, this demonstrates that many aspects of known NRP1 regulation were captured in the screen.

Among the novel hits, *UBE3D* presented as one of the strongest negative regulators and we evaluated the individual gene trap insertion profiles in *UBE3D* (Fig 4.4 B). As expected, the insertions of sense orientation were preferentially enriched at the gene start, and regions prior to the catalytic HECT domain of UBE3D, suggesting a complete loss of activity. Furthermore, when compared across 50 other CellSeq screens, UBE3D presented as a negative regulator hit mainly in the NRP1 screen and as a weaker hit in one other screen based on acetylation (Fig 4.4 A). Although, It scored as a positive regulator hit, in quite a few screens, this observation was specific to screens performed on proteins involved in the mTOR-AKT pathways, suggesting a role for UBE3D in their regulation. Thus, we conclude that UBE3D is a strong hit and rather specific towards certain biology and a potential negative regulator of NRP1.

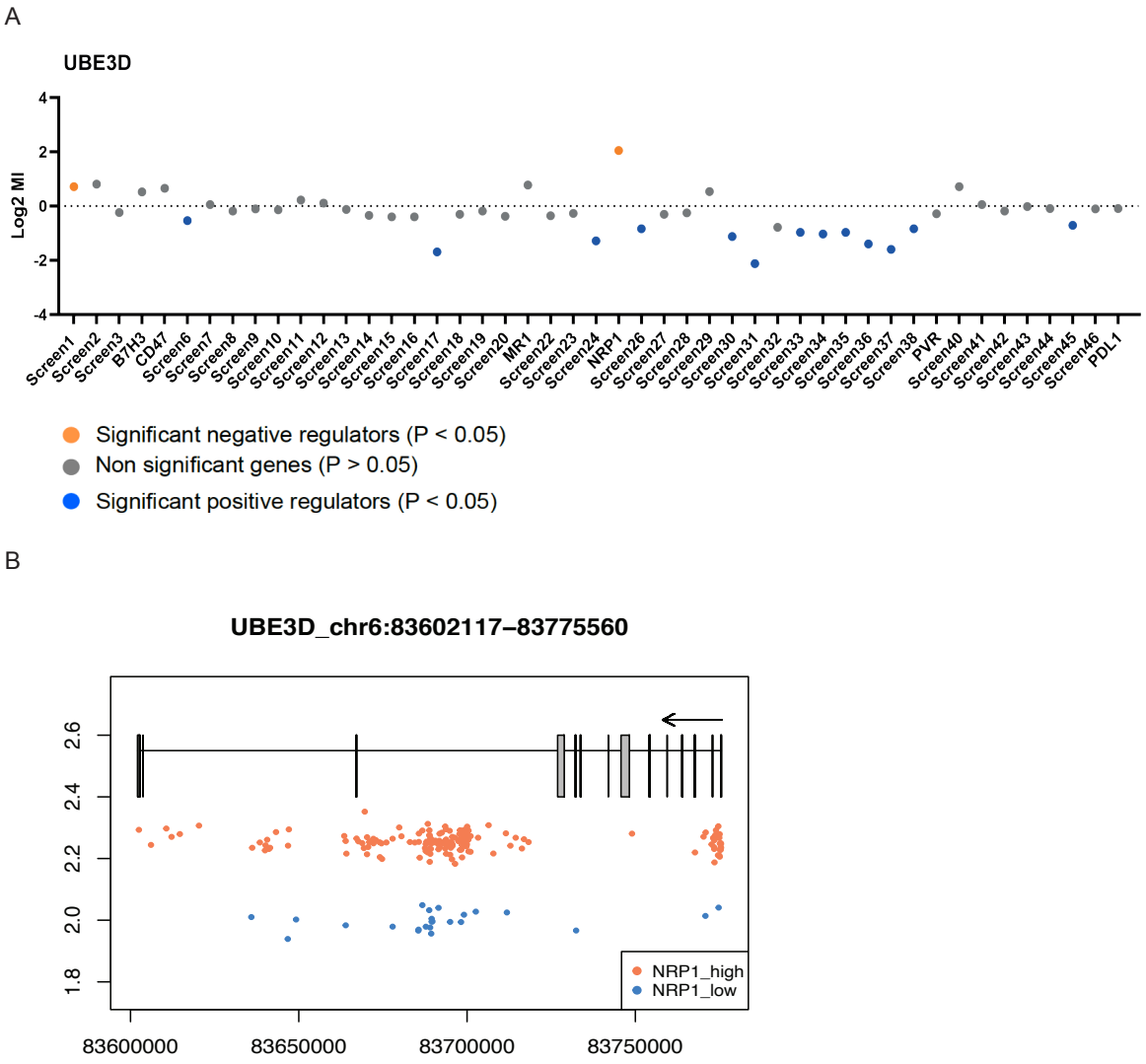


Figure 4.4 *UBE3D* is negative regulator hit in the NRP1 screen A) Visual specificity scoring map for the *UBE3D* gene across ~50 other screens. Briefly, scoring is done to determine how a gene scores across various CellSeq screens performed on different proteins to determine specificity of gene effect to phenotype (See Sec 2.7.2). B) Analysis of gene trap insertion pattern in the UBE3D gene observed in the mutagenized HAP1 cells sorted based on high and low B7H3 expression. The arrow indicates the direction of transcription, and the grey boxes indicate the exons.

4.2.2 *UBE3D is a negative regulator of NRP1*

Next, we investigated if UBE3D inhibition upregulates NRP1 expression by employing CRISPR/Cas9 edited cell lines. Hereby, we obtained 2 clones of the UBE3D knockout HAP1 cell line with single bp deletion in exon two and four bp deletion in exon two (ΔUBE3D Clone 1 and 2)(169). First, we confirmed the loss of UBE3D protein levels in these cells by western blotting (Fig 4.5 A). Reassuringly, loss of UBE3D potentiated an increase of the NRP1 surface expression and total levels as determined by flow cytometry and western blotting respectively (Fig 4.5 A,B,C). Next, to validate the effects in another cell line, we transfected 2 different sgRNA targeting different coding regions of UBE3D along with a CAS9 expression plasmid into MCF7 breast cancer cells. We first established the inhibition of UBE3D in these cells by western blotting (Fig 4.6 A). As expected, inhibition of UBE3D lead to a modest increase in total NRP1 and surface levels (Fig 4.6 A,B,C). Collectively, we conclude that UBE3D is a negative regulator of total and cell surface NRP1 expression. This indicates that the increase in NRP1 surface expression is a result of total upregulation of NRP1 protein rather than specific plasma membrane relocalization.

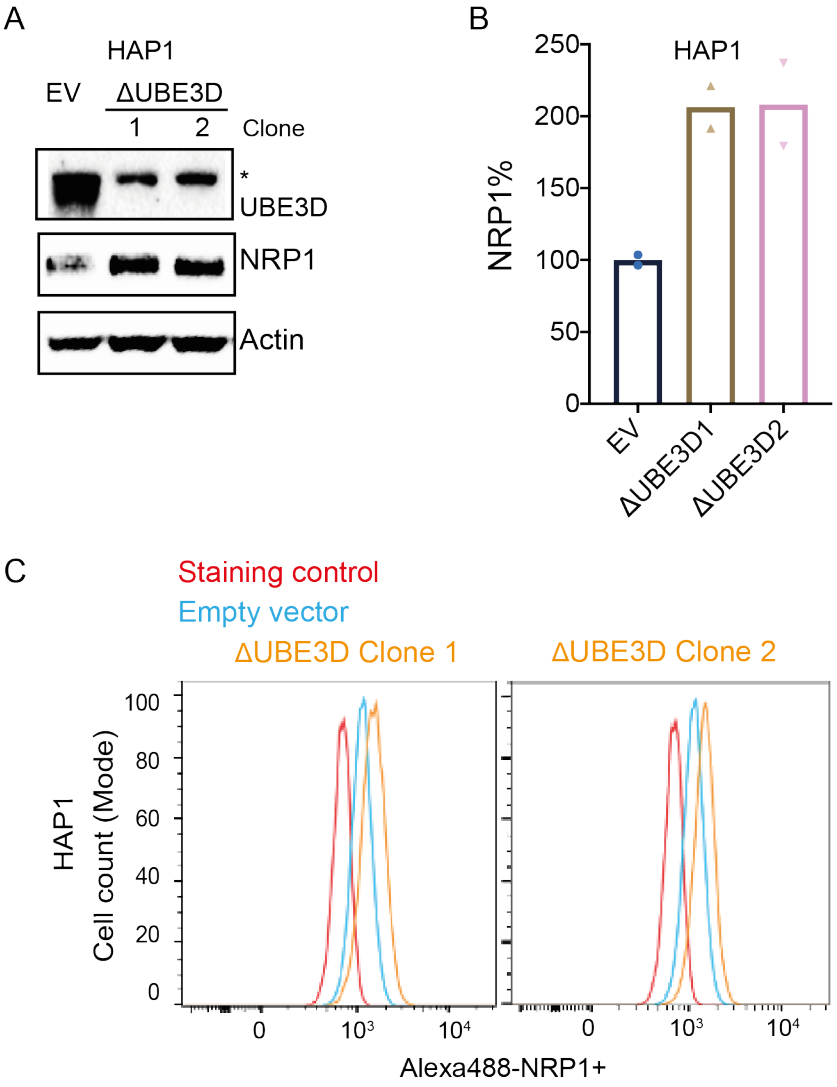


Figure 4.5 UBE3D is a negative regulator of NRP1 in HAP1 cells Two HAP1 UBE3D gene knockout (ΔUBE3D Clone 1 and 2) and an empty vector (EV) clone derived by CRISPR/Cas9 editing was obtained from Toczyski lab. A) Using cell lysates from these clones, UBE3D knockout efficiency was tested by immunoblotting with a polyclonal UBE3D antibody and B7H3 was used as loading control (B7H3 blot not shown). Subsequent effect on NRP1 was evaluated using a monoclonal NRP1 antibody and by using actin as the loading control. * - non-specific band just above UBE3D specific band.; B) NRP1 total levels were quantified using Data from n = 2 independent experiments C)

Effect of UBE3D inhibition on surface expression of NRP1 was determined by Flow Cytometry.

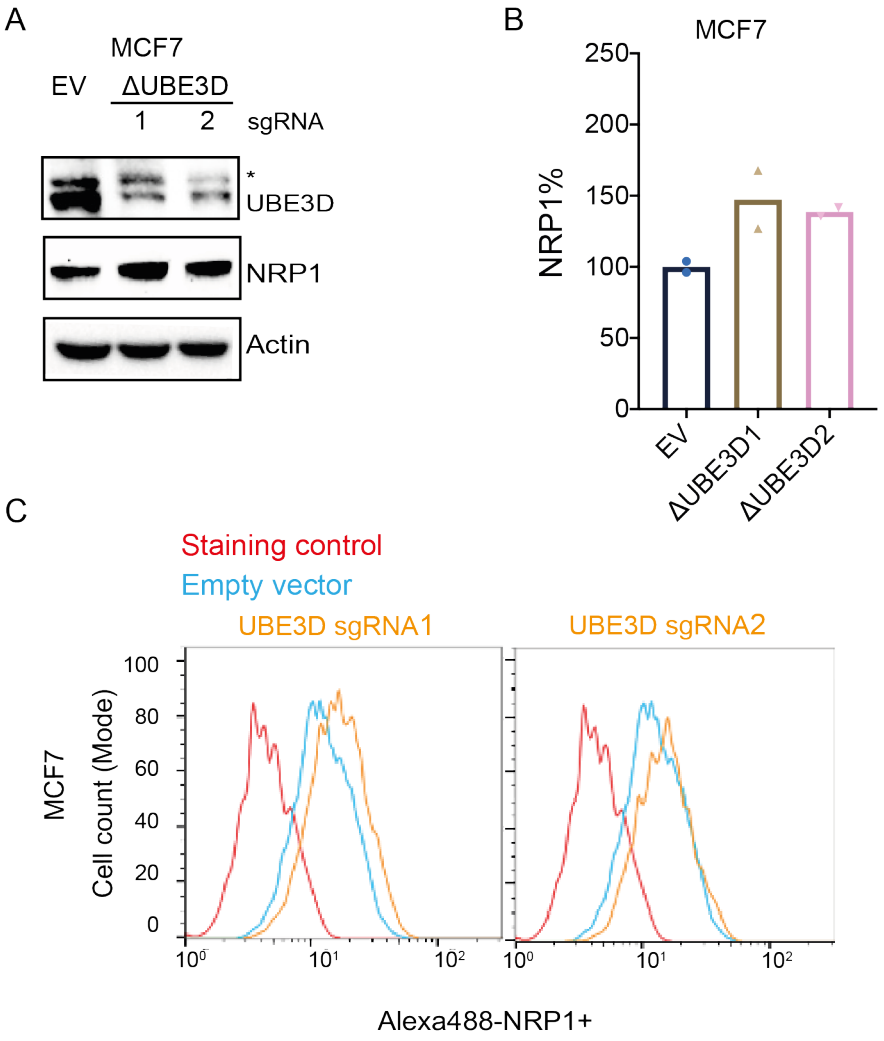


Figure 4.6 UBE3D is a negative regulator of NRP1 in MCF7 cells UBE3D gene was targeted at two different regions (ΔUBE3D sgRNA 1 and 2) using CRISPR/Cas9 and A) knockout efficiency in a polyclonal pool of MCF-7 cells was confirmed and the subsequent effect on NRP1 total protein levels was tested by immunoblotting with the respective antibodies. * - non-specific band just above UBE3D specific band. Empty pLentiCRISPR-v2 was used as control for editing efficiency (EV) and Vinculin was used as the loading control for the UBE3D blot (data not shown) B) NRP1 total levels were

quantified using Data from n = 2 independent experiments C) Effect of UBE3D inhibition on surface expression of NRP1 was determined by Flow Cytometry.

4.2.3 *UBE3D inhibits NRP1 expression in a ubiquitin independent manner and AMD associated UBE3D sustains NRP1 expression*

As UBE3D has been reported to have E3 ligase activity(158), we investigated the potential role of ubiquitination in its ability to regulate NRP1 protein levels. In addition, we hypothesized that this activity may be lost in the AMD-associated V379M mutant. Therefore, we generated three Flag-tagged UBE3D mutants.

Inactivation of HECT E3 ligases upon substitution of the conserved Cys in the HECT domain with an Ala residue has been reported(170). We reasoned that, mutating the active site Cys in the HECT domain of UBE3D can generate a catalytically inactive E3. However, it is possible that redundant neighbouring active sites can contribute towards catalytic activity of UBE3D(170). Hence, using site directed mutagenesis we generated 3 different UBE3D mutants, one in which the active site Cys is replaced by an Ala residue at position 358 (C358A), another deficient of its catalytic HECT domain (ΔHECT - catalytic dead control) and an AMD associated UBE3D mutant in which the Val at position 379 is substituted with a Methionine (V379M) (Fig 4.7 A).

To test if these UBE3D mutants regulate NRP1 protein levels, we transiently overexpressed the various UBE3D mutants or a wild type control in HEK293T cells. As endogenous NRP1 is low in HEK293T cells we co-transfected NRP1 with a FLAG tag (NRP1-FLAG)(171). UBE3D overexpression had the

opposite effect on NRP1 as its inactivation, resulting in ~40 % reduction in NRP1 levels as determined by western blotting (Fig 4.7 B,C). In contrast, the AMD mutant did not affect NRP1 supporting the notion that this is a loss of function mutation. Surprisingly, however, the catalytically inactive E3s C358A and ΔHECT, both behaved like wild type UBE3D (Fig 4.7 B,C). This suggests that the E3 activity of UBE3D is not implicated in the regulation of NRP1

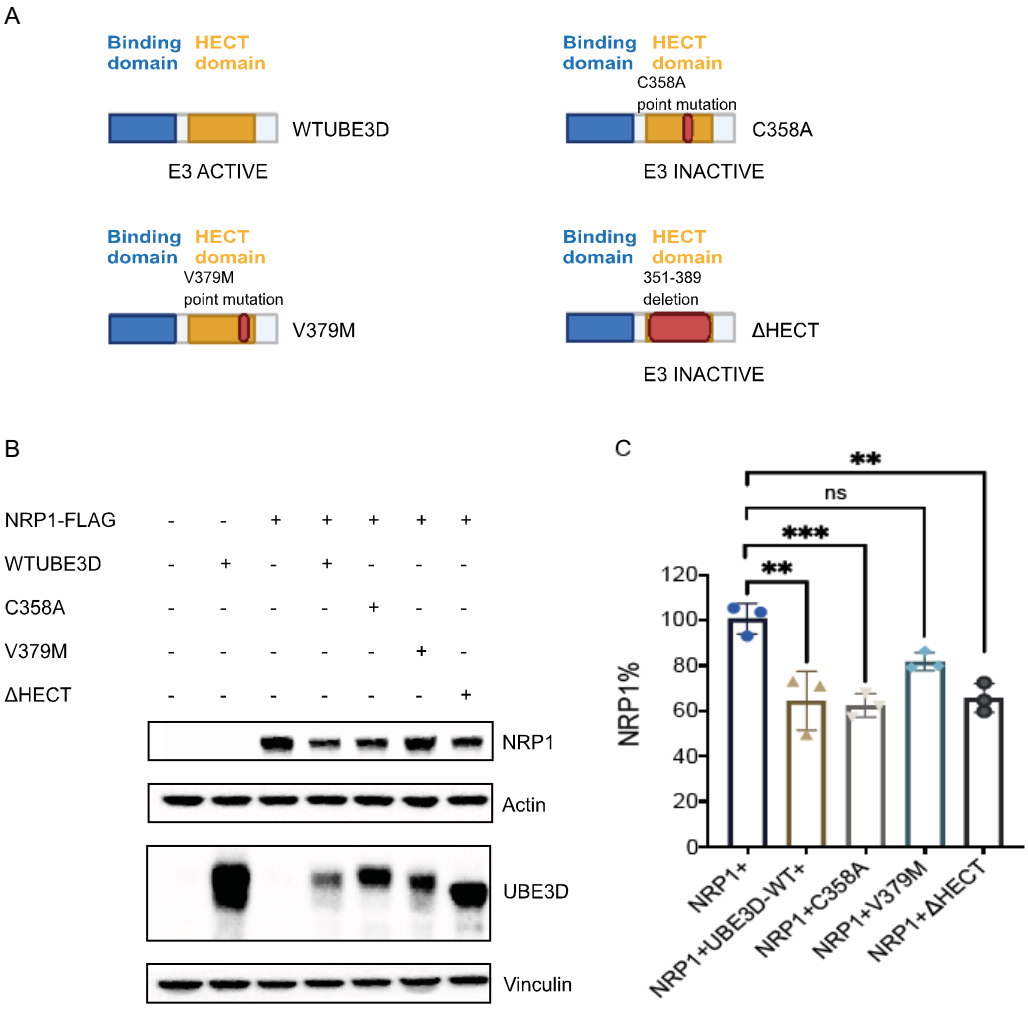


Figure 4.7 UBE3D E3 activity 'dead' mutants degrade NRP1 and AMD associated V379M sustains NRP1 expression A) Schematic representation of UBE3D and its ubiquitination inactive mutants along with AMD-associated UBE3D

derived by site directed mutagenesis B) UBE3D mutants described in (A) were transiently overexpressed along with NRP1-FLAG in HEK293T cells and cell lysates were collected at 72 hours. UBE3D levels were detected using a polyclonal anti-UBE3D antibody and NRP1 was detected using an anti-FLAG antibody. Actin was used as the loading control for NRP1 and Vinculin was used as the loading control for UBE3D. C) The change in total NRP1 levels in was quantified. Data from n = 3 independent experiments was used for quantification of NRP1 levels. Statistical analysis was performed using 1-way ANOVA followed by Tukey's post hoc test and that the amino acid change in the AMD mutant perturbs another function of UBE3D.

Next, we hypothesized that UBE3D can possibly regulate NRP1 ubiquitination by other E3 ligases. We reasoned that, blocking the first step of ubiquitination prior to E3 recruitment, the E1 enzyme and the most expected consequence post ubiquitination, proteasomal degradation can rescue ubiquitination mediated negative regulation of NRP1. Blockade of the E1 enzyme with MLN7243 for 4 hours, resulted in the depletion of ubiquitin, confirming that the drug is working(172). However, the reduction in ubiquitination did not rescue UBE3D mediated NRP1 degradation. In addition, while blockade of the proteasome for 4 hours using Bortezomib let to an accumulation of ubiquitin as expected, it did not alter the effect of UBE3D on NRP1(173). Therefore, we conclude that ubiquination mediated proteasomal degradation does not lead to UBE3D mediated negative regulation of NRP1. Notably, this is consistent with our observations that UBE3D's catalytic activity is not required for the

degradation of NRP1. Collectively, this suggests ubiquitination is not a modulator of UBE3D mediated negative regulation of NRP1.

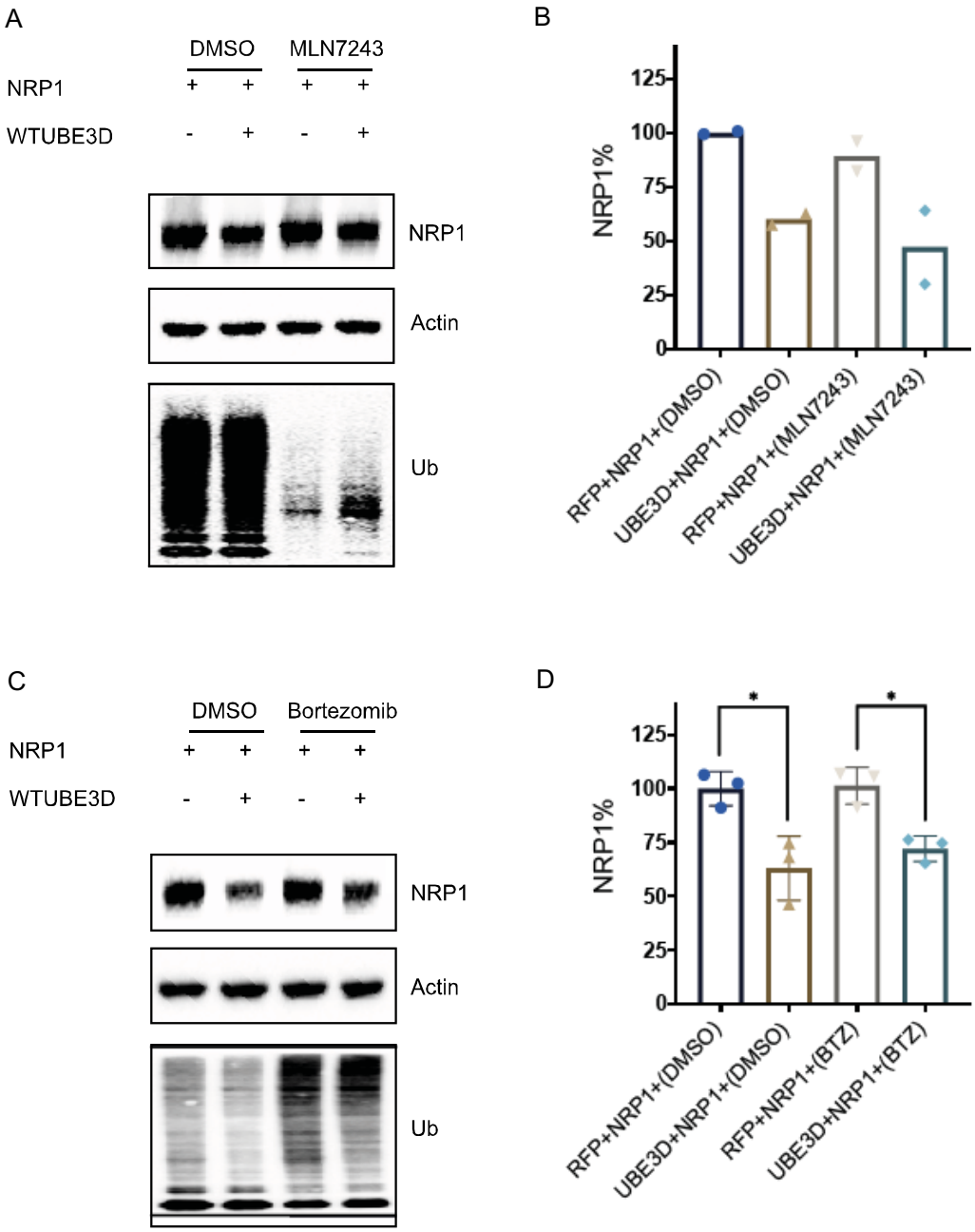


Figure 4.8 E1 pathway or proteasomal degradation inhibition does not rescue UBE3D driven NRP1 degradation UBE3D and NRP1-FLAG were transiently co-overexpressed in HEK293T cells for 72 hours and were treated with a A)

E1pathway inhibitor, 1 uM of MLN243 4 hours before harvest and cell lysates were collected. Lysates were probed for NRP1 using a FLAG antibody and Actin was used as loading control. B) Change in total NRP1 levels were quantified using Data from n = 2 independent experiments. C) and D) As described above the effect of inhibiting proteasomal degradation, using 100 nm of Bortezomib on NRP1 levels was quantified. Data from n = 3 independent experiments. Statistical analysis was performed using 1-way ANOVA followed by Sidak's post hoc test.

4.2.4 *NRP1 interaction is stronger with UBE3D than AMD associated UBE3D V379M*

We hypothesised that UBE3D ability to negatively regulate NRP1 could be dependent on the interaction between NRP1 and that this interaction is lost in AMD associated V379M. To address this, we transiently overexpressed WTUBE3D or V379M in HEK293T cells and immunoprecipitated (IP) endogenous NRP1. NRP1 levels was detected upon immunoprecipitation(Fig 4.9 A). Further, upon UBE3D overexpression, WTUBE3D was enriched along with immunoprecipitated endogenous NRP1 whereas enrichment of V379M was much lower (Fig 4.9 A). Hence, this indicated that WTUBE3D possibly interacts with NRP1 more strongly compared to V379M.

To substantiate these findings and rule out unspecific binding of the NRP1 antibody, we overexpressed NRP1 with a haemagglutinin tag at the C-terminal (NRP1-HA) along with WTUBE3D or V379M in HEK293T cells and immunoprecipitated NRP1-HA using a haemagglutinin antibody. NRP1-HA levels was detected upon immunoprecipitation, only when overexpressed,

confirming the antibody specificity (Fig 5B). Interestingly, UBE3D levels are detectable to some extent when WTUBE3D or V379M are overexpressed individually even in the absence of NRP1-HA overexpression (Fig 4.9 B), possibly due to non-specific interactions with the HA antibody. However, UBE3D is strongly enriched along with overexpressed NRP1-HA while V379M when overexpressed with NRP1-HA showed similar enrichment as its individually overexpressed counterpart (Fig 4.9 B). Together, we conclude that NRP1 interacts more strongly with WTUBE3D than V379M.

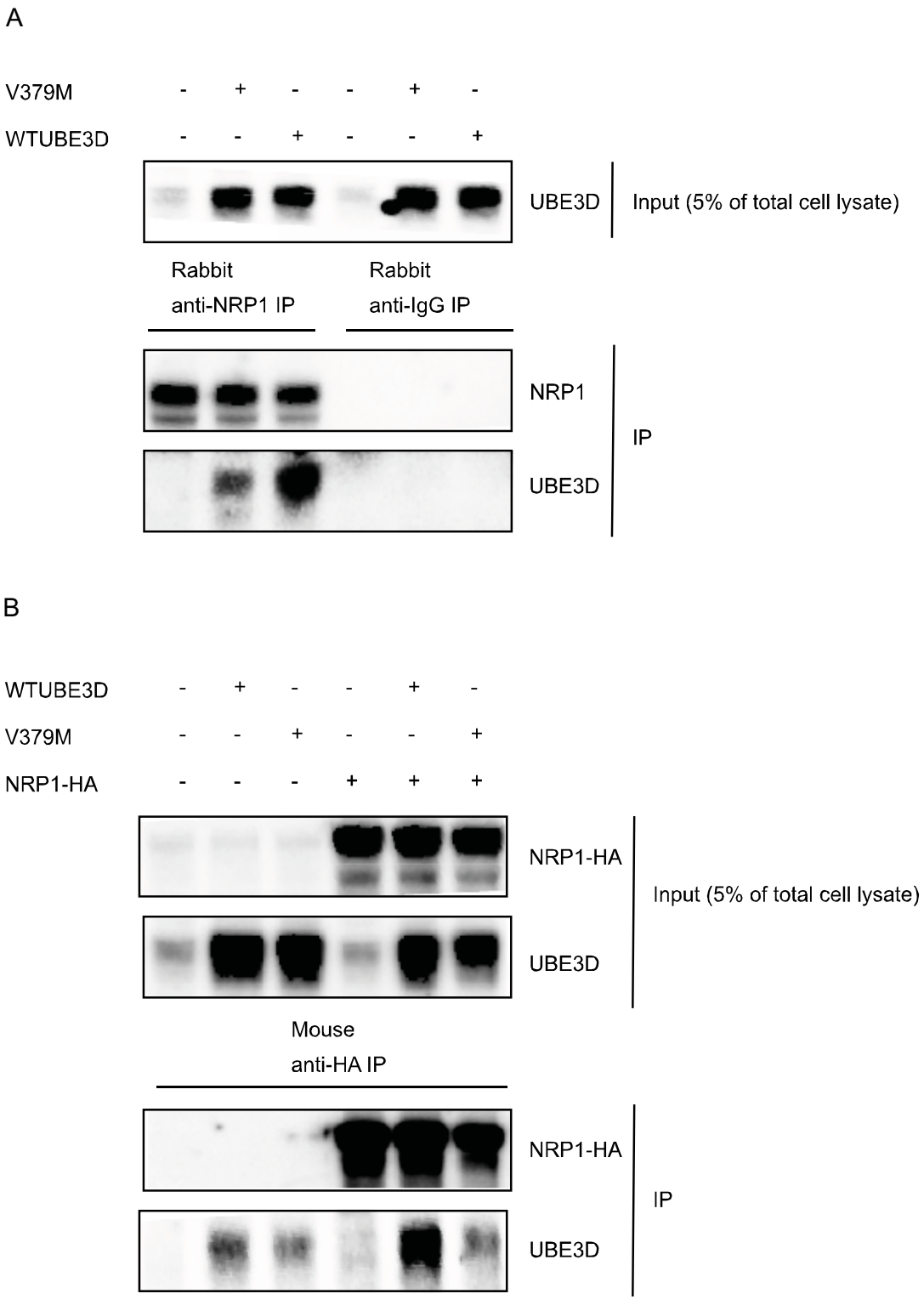


Figure 4.9 UBE3D interacts with overexpressed and endogenous NRP1 whereas AMD-associated V379M does not A) UBE3D and AMD-associated

UBE3D were transiently overexpressed in HEK293T cells and cell lysate was obtained at 24 hours. Control cells were transfected with equal amount of RFP. Supernatant was incubated with NRP1 monoclonal antibody NRP1, IgG control antibody was pulled-down using Protein A beads. Samples were boiled to detach beads and pull-down fractions were probed for UBE3D using polyclonal UBE3D antibody and NRP1 using FLAG antibody B) UBE3D and AMD-associated UBE3D were co-overexpressed with NRP1-HA (NRP1- haemagglutinin) in HEK293T cells and cell lysate was obtained at 24 hours. Control cells were transfected with equal amount of RFP. Supernatant was incubated with HA antibody to facilitate specific pull-down of overexpressed NRP1-HA by Protein A beads. Samples were then boiled to detach beads and pull-down fractions were probed for UBE3D using polyclonal UBE3D antibody and NRP1 using HA antibody.

4.2.5 *UBE3D targets NRP1 towards lysosomal degradation*

As we ruled out ubiquitin mediated proteasomal degradation, we explored other mechanisms that could be responsible for NRP1 fate. Analysis of mRNA expression of NRP1, did not show a change upon UBE3D inhibition (Appendices 6.6). Next, we investigated lysosomal degradation as an alternative mechanism for the observed changes in NRP1 levels. Treatment with Bafilomycin A1, a lysosomal degradation inhibitor, resulted in a modest increase of overexpressed NRP1 levels (4.10 A,B, compare lanes 1 and 3), indicating that lysosomal degradation contributes to the NRP1 steady state levels(174). Strikingly, the reduced NRP1 expression induced by UBE3D was nearly completely abrogated by bafilomycin (4.10 A,B, compare lanes 2 and 4). This indicates that UBE3D stimulates lysosomal degradation of NRP1.

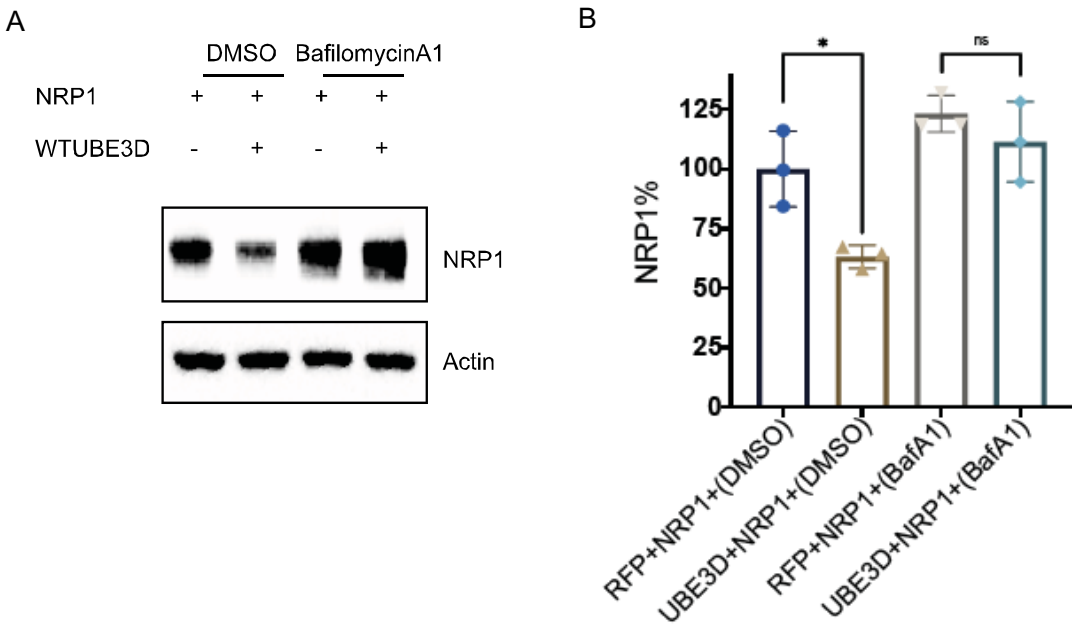


Figure 4.10 Lysosomal degradation inhibition rescues UBE3D driven NRP1 degradation A) UBE3D and NRP1-FLAG were transiently co-overexpressed in HEK293T cells for 72 hours and were treated with a lysosomal degradation inhibitor, 100 nm of Bafilomycin A1 4 hours before harvest and cell lysates were collected. Lysates were probed for NRP1 using a FLAG antibody and Actin was used as loading control. B) Change in total NRP1 levels were quantified using Data from n = 3 independent experiments. Statistical analysis was performed using 1-way ANOVA followed by Tukey's posthoc test.

4.2.6 *UBE3D loss leads to NRP1- dependent increased angiogenesis in vivo*

We hypothesized that perturbed regulation of NRP1 by UBE3D may explain the association of the UBE3D V379M mutant with AMD. In this scenario, increased NRP1 levels due to lowered lysosomal degradation would drive

neovascular AMD and inhibition of NRP1 would restore physiological angiogenesis. To test the functional relevance of the molecular link between UBE3D and NRP1 in neovascular development in the eye, we evaluated if UBE3D loss leads to NRP1 mediated increase in angiogenesis in vivo. We used a GFP-FLI1 zebrafish and targeted them with morpholinos against UBE3D (Fig 4.11 A). We reasoned that the GFP intensity corresponding to FLI1 expression can be used as a measure of angiogenesis. We categorised the GFP expression based on its intensity into strong and medium. Consistent with published experiments, nearly all of zebrafish embryo targeted with UBE3D morpholinos of 6, 8 and 10 ng respectively showed a strong GFP expression compared to only about 40 % in the control morpholino targeted embryos (control morphants) (Fig 4.11 B), and this effects was dose-dependent(160). Next, we investigated the eye size through bright field images. Interestingly, at higher concentrations, UBE3D morphants displayed a reduced eye size as reported previously (Appendices 6.7)(160).

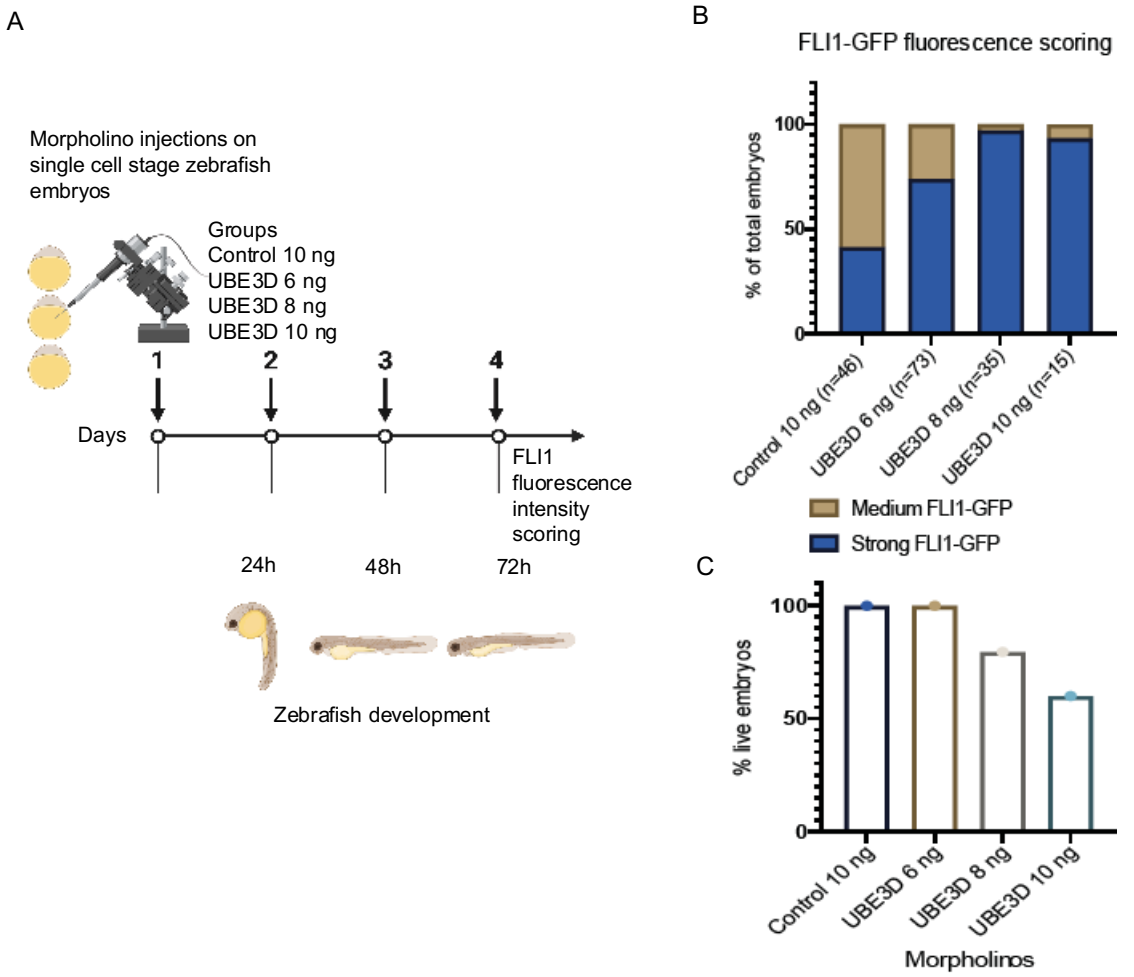


Figure 4.11 Morpholino targeted UBE3D inhibition increases angiogenesis marker FLI1 expression A) Schematic representing strategy where, Morpholino targeting UBE3D at the described concentrations were injected into 1- to 2-cell stage tg(fli1:GFP) zebrafish embryos, non-targeted Morpholino was used as control and B) scored for strong and weak expression using a florescence microscope 2 days post fertilization (dpf) C) Mortality of the embryos 2 dpf was recorded. As data was interpretated as qualitative, no statistical analysis was applied to the observations of reporter gene intensity and pattern.

Next, we sought to investigate if NRP1 is responsible for the increase in angiogenesis in UBE3D morphants by using a combination of UBE3D and NRP1 morpholinos (UBE3D-NRP1- morphants). Importantly, NRP1 inhibition alone did not result in increased GFP expression, indicating that under normal conditions it is not required for FLI1 induction and angiogenesis (Fig 4.12 A,B). However, NRP1 inhibition nearly completely supressed the UBE3D-induced FLI1-GFP expression (Fig 4.12 B-D). Thus, we conclude that the UBE3D induced increase in angiogenesis is dependent on NRP1.

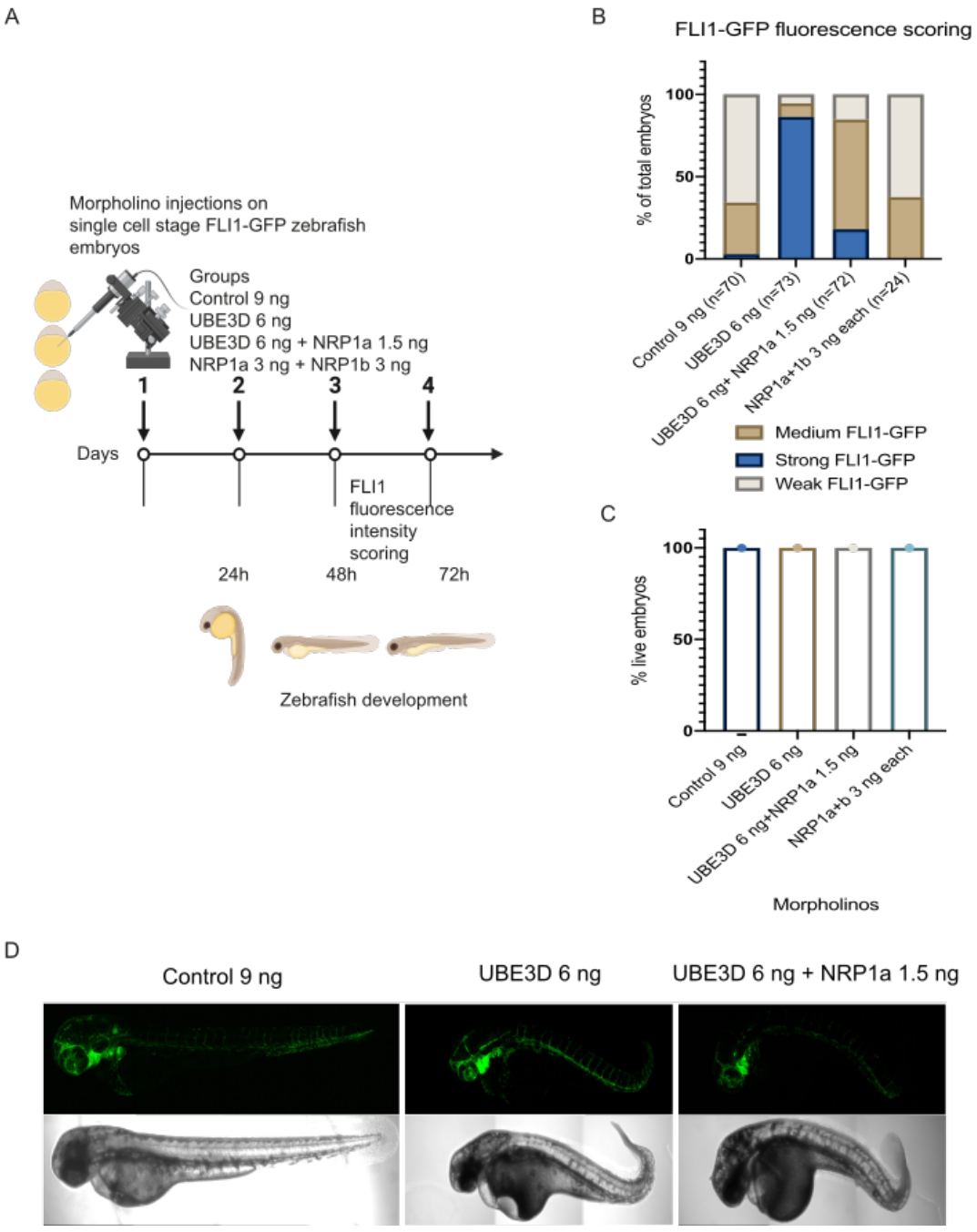


Figure 4.12 Morpholinos targeting UBE3D and NRP1 together does not increase angiogenesis marker FLI1 expression A) Schematic representing strategy where, morpholino targeting UBE3D alone or in combination with NRP1 targeting Morpholino, or NRP1 alone at the described concentrations were injected into 1- to 2-cell stage tg(fli1:GFP) zebrafish embryos and B) scored for strong, medium and

weak expression using a florescence microscope 2 days post fertilization (dpf) C) Mortality of the embryos 2 dpf was recorded. As data was interpretated as qualitative, no statistical analysis was applied to the observations of reporter gene intensity and pattern. D) FLI1 GFP expression of the embryos was imaged using a confocal microscope. Images shown are representative of n=5 independent images for each condition.

4.2.7 *UBE3D-NRP1 – molecular link proposed model schematic*

Hereby, we propose the following molecular link for UBE3D mediated negative regulation of NRP1. UBE3D interacts with NRP1 and facilitates its lysosomal degradation in a ubiquitination independent manner. AMD associated UBE3D does not interact with NRP1 and subsequently does not cause NRP1 lysosomal degradation leading to accumulation of NRP1. The accumulation of NRP1 in turn can potentiate increased angiogenesis (Fig 4.13).

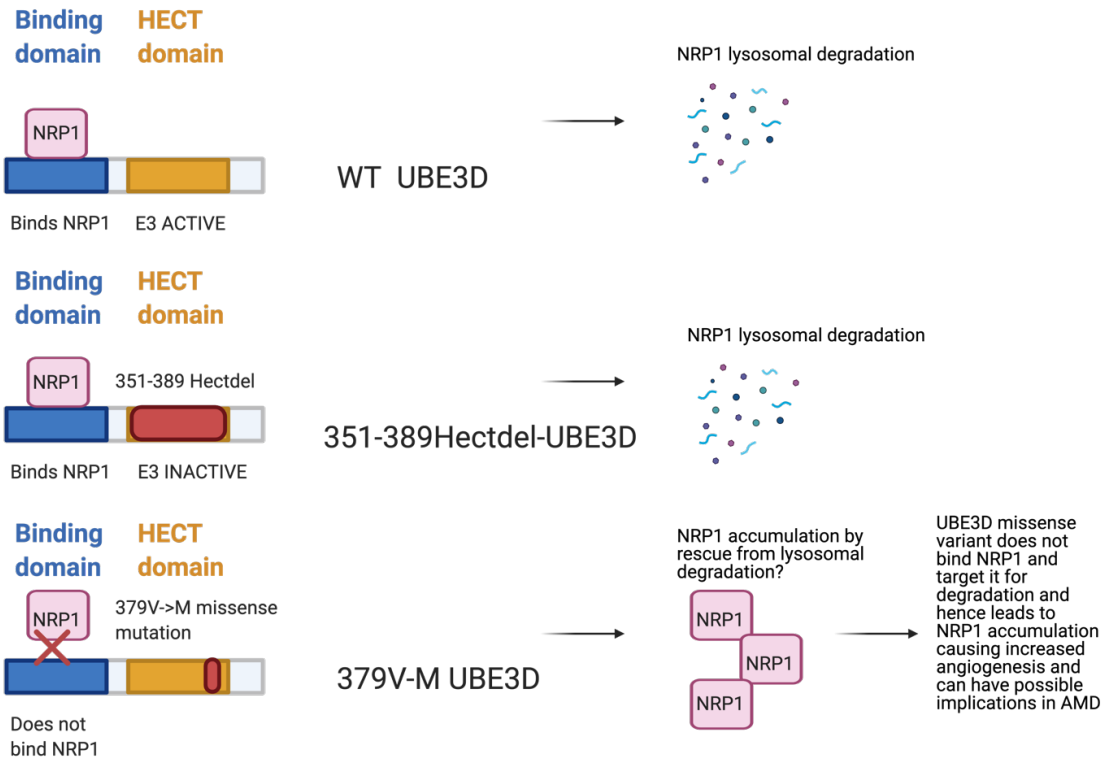


Figure 4.13 Schematic representation of molecular link between UBE3D and NRP1 V379M – AMD associated missense variant of UBE3D mimics UBE3D loss of function, results in reduced interaction with Neuropilin-1 and consequently leads to reduced lysosomal degradation and increased accumulation of NRP1. Higher NRP1 levels in turn potentiate increased angiogenesis and can thus contribute to AMD pathogenesis.

4.3 Discussion

In this chapter, we have identified UBE3D as a novel negative regulator of NRP1 and dissected the underlying molecular mechanism of how UBE3D E3 ligase drives NRP1 loss and regulates angiogenesis. While its conserved cysteine in the HECT domain, can possibly mean UBE3D targets substrates

through ubiquitination towards proteasomal degradation, CyclinB1 is the only identified candidate substrate of UBE3D(158). Here, we show that UBE3D can potentially regulate protein fate through mechanisms other that the Ubiquitin Proteasome System.

A study by Huang et al on UBE3D suggests that UBE3D E3 ligase possibly drives AMD through the UPS(159). Specifically, it has been suggested that AMD associated V379M loses its ability to ubiquitinate substrates, and hence drives an accumulation of inflammatory and angiogenesis drivers, leading up to AMD(159). In contrast, inclining towards ubiquitination independent roles reported for other HECT E3 ligases, we show that UBE3D does not require its catalytic domain, to drive NRP1 degradation(157). Furthermore, we demonstrate that, even in the absence of E1 mediated proteasomal degradation, UBE3D can still negatively regulate NRP1 protein levels. Hence, we suggest that UBE3D driven NRP1 loss is not ubiquitination dependent and involves other mechanisms.

Substrate recognition and protein-protein interactions are tightly regulated by HECT E3 ligases through their N terminal domain organization(157, 175). For example, another study from Huang et al demonstrate that UBE3D interacts with KAP1 and drives DNA repair. Also, they demonstrate that loss of ability of V379M to bind to KAP1, impairs DNA repair and can hence drive AMD pathogenesis. Similarly, we report an interaction between UBE3D and NRP1, and this interaction is lost in AMD associated V379M. However, we see that while V379M loses its ability to interact with NRP1 and cannot drive NRP1 loss, it is unclear why ΔHECT, which hosts the Valine at position 379 drives NRP1 loss. This

suggests that there could be a possible conformational switch when the Valine at position 379 is replaced with a Methionine. As discussed previously, intra and inter molecular interactions are critical for autoregulation of HECT E3 ligase. E6AP reaches an active state upon trimer formation(175). Another HECT E3 ligase, HUWE1 is maintained in a homodimer inactive state unless activated by its N terminal fragment(176). It appears that, conformational switches play a critical role in modulating HECT E3 activity. While the exact mechanism through which V379M undergoes a conformational switch leading to loss of its ability to interact with NRP1 is unclear and needs further investigation, a possible hypothesis is that UBE3D dimerizes and reaches an inactive state. This needs further investigation. In a separate experiment, we also demonstrate that UBE3D drives NRP1 loss through lysosomal degradation. Hence, it is possible that the loss of interaction between AMD associated V379M and NRP1 and not loss of ubiquitination of NRP1, can lead to increased accumulation of NRP1. Notably, we suggest an alternate mechanism in contrast to the central dogma that UBE3D drives AMD pathogenesis in a ubiquitin dependent manner and put forward the possibility that other mechanisms unique to HECT E3 ligases such as protein-protein interactions and trafficking possibly play a more important role.

UBE3D loss phenocopies overexpression of V379M in terms of NRP1 accumulation. Interestingly, we demonstrate that UBE3D loss in a zebrafish model, drives increased angiogenesis in a NRP1 dependent manner. Hence, we show a strong association of the molecular link between NRP1 and UBE3D in neovascular AMD.

VEGF inhibition is the gold standard treatment for wet AMD. However, it has been reported to cause adverse systemic side effects and ocular events(150). Therefore, there is a need for alternative therapeutic strategies. We hypothesize that, targeted inhibition of increased NRP1 expression caused by the UBE3D V379M variant, can be an effective and more specific therapeutic strategy against wet AMD. Laser induced choroidal neovascularization mouse models (CNV) are routinely used to evaluate therapeutics for age related macular degeneration (AMD). In this model, Fluorescein angiography (FA) can be performed to compare control and treated eyes to evaluate effect on the laser induced aberrant blood vessel growth and subsequent leakage. In addition, other readouts such as Immunohistochemical Staining (IHC) for angiogenesis markers such as isolectin and FLI1 can be performed on mouse choroidal flat mounts(152). To test suitability of NRP1 inhibitors as a selective therapeutic strategy for patients with UBE3D V379M variants, UBE3D heterozygous knockout, CNV mouse models can be employed. First, using FA, the effect of NRP1 and VEGF inhibition on blood vessel leakage can be evaluated. We expect that, NRP1 inhibition can prove to be more efficacious or show similar efficacy to VEGF inhibition with reduced side effects in a UBE3D dependent manner. IHC on angiogenesis markers can be used to further validate the above expected results. Overall, NRP1 inhibition can prove to be a specific and effective therapeutic strategy for select AMD patients with the V379M AMD associated UBE3D variant. The above-described experiments can greatly facilitate evaluation of pre-clinical efficacy for such a strategy.

Altogether, this study provides the foundation for the molecular link between UBE3D and NRP1 as regulators of angiogenesis with possible implications in AMD pathogenesis and paves way for future studies to explore the role of this molecular link in the tumour immune interface.

Chapter 5: General Discussion

The tremendous complexity of the tumour immune interface necessitates going beyond conventional reductionist approaches. Current functional genomics tools facilitate the delineation of complex regulatory circuits in a systematic manner and can aid in unravelling cryptic tumour immune interactions that have escaped us so far.

5.1 The scope for CellSeq in immunotherapy

CellSeq has been instrumental in the target discovery efforts at the tumour immune interface and has shed light on the biology of key immune checkpoint proteins such as Cluster of Differentiation 47 (CD47) and Programmed Death Ligand 1 (PD-L1) and this is just the beginning. Principal components of CellSeq such as fluorescence readouts and the resourceful HAP1 cell line can aid in the study of the biology of the less understood immune checkpoint proteins reported in this study and beyond.

In this study, by using HAP1 as the cell line model, we have taken advantage of the already available transcriptomic and proteomic data and highlighted 8 immune checkpoint proteins that are expressed on HAP1 under basal conditions and can thus be screened for novel regulatory mechanisms using CellSeq. By building regulatory maps for B7 Homolog 3 (B7H3), Polio Virus Receptor (PVR) and Neuropilin-1 (NRP1), we have contributed towards the efforts of a few select academic groups and companies by adding on to the

growing library of high resolution regulatory maps of these checkpoint proteins expressed on HAP1 (Sec 3.2.1-2. 4.2.1).. Furthermore, since the inception of the project, novel tumour immune checkpoints have been discovered using other methods. For example, Cluster of Differentiation (CD24)-Siglec-10 has been reported as a 'do not eat me' macrophage checkpoint axis and Cluster of Differentiation 58 (CD58) loss was associated with progressive immune evasion and their biology remains unclear(26, 27, 42). Interestingly, both these proteins are expressed on HAP1 under basal conditions and can be studied further using CellSeq. In addition, a large compendium of gene expression signatures in response to a combination of Clustered Regularly Interspaced Short Palindromic Repeats (CRISPR)/Cas9 knockouts and pathway stimuli have been reported for HAP1(177). Therefore, HAP1 as a model is not restricted only to studying the checkpoint proteins expressed under basal conditions and can be extended to dissecting the regulatory mechanism of checkpoint proteins that are inducible. For example, although PD-L1 is not expressed on HAP1 cell surface under basal conditions, Mezzadra et al reported inducing the surface expression of PD-L1 by Interferon-γ (IFN-γ) and successfully employed CellSeq to map its molecular regulators(49). Similarly, by using information on stimuli driven and gene knockout signatures of HAP1, it is possible to identify inducible screening candidates. Similarly, such an approach can also be used to study drug induced expression of checkpoint proteins such as PD-L1 and CD47 to shed light on novel immunotherapy associated resistance mechanisms. Notably, CellSeq has also been instrumental in identifying new biology of proteins that are normally not expressed on HAP1. For instance, antigen presentation protein major

histocompatibility complex, class I-Related (MR1) surface expression is critical for effective anti-tumour immunity(178). It is not expressed in the transcript or protein level in HAP1. In a recent study, MR1 was overexpressed in HAP1 cells using lentiviral particles encoding MR1 cDNA. CellSeq was then employed to map molecular regulators of MR1 surface expression and identified P5-ATPase ATP13A1 as a modulator of MR1 surface expression(179). Similarly, such an approach can be used to induce surface expression of second generation immune checkpoints such as T cell Immunoglobulin and Mucin domain-containing protein 3 (TIM-3), Lymphocyte-Activation Gene 3 (LAG-3) and T cell Immunoreceptor with Ig and ITIM domains (TIGIT) on HAP1 cells to facilitate the use of CellSeq to further understand their biology.

Of note, HAP1 has been used to discover novel biology for a plethora of phenotypes such as key signalling pathway molecules, tumour immune interface proteins, genetic disorders and viral entry mechanisms(50, 73-76). Notably, Immune checkpoint proteins often have pleiotropic roles in human health and disease(180-183). Consequently, the use of a pleiotropic cell line, such as HAP1 and the unbiased nature of such a forward genetic screening approach to dissect immune checkpoint biology can pave way to surprising findings that make way for identifying therapeutic opportunities with direct implications to the tumour immune interface but also for other human diseases with scarce therapeutic opportunities. For example, we have mapped the molecular regulators of the immune checkpoint and angiogenesis driving Vascular Endothelian Growth Factor Receptor (VEGFR)-co receptor NRP1 and identify Age related Macular

Degeneration (AMD) risk associated *UBE3D* gene as a negative regulator (Chapter 4).

Overall, such FACS based protein abundance CellSeq screens have now paved the way for a library of such protein abundance maps for these key immune checkpoints and has lot of future potential and will continue contributing towards rational targeting of the tumour immune interface and beyond. Published regulator maps generated by CellSeq for various proteins involved in key signalling pathways and tumour immunity can be accessed through (https://phenosaurus.nki.nl/).

Fluorescence readouts are one of the principal components employed by CellSeq and thus making various phenotypes that can be quantified by fluorescence more accessible to study(50). This allows CellSeq to extend its applications to phenotypes more complex than protein abundance. For example, in an attempt to use CellSeq to dissect the regulatory mechanism of CD47 using anti-CD47 fluorescent antibodies, Logtenberg et al reported that the QPCTL enzyme specifically modulates binding of anti-CD47 antibodies at the SIRPα binding site. This eventually led to the discovery that glutaminyl -peptide cyclotransferase-like protein (QPCTL) enzyme governs the binding of recombinant SIRPα protein to CD47 and does not affect total levels of CD47. Thus identifying, a modulator of the CD47- SIRPα protein-protein interaction(48). Similarly, it's possible that in our study, N-acylneuraminate cytidylyltransferase (CMAS) modulates B7H3 surface interactions by regulating post translational modifications (Chapter 3). The ability of CellSeq to probe into protein-protein interactions can be utilized to answer some long standing questions at the tumour

immune interface. Specifically, B7H3, B7H4 and other B7 family members have various antagonists targeting their putative T cell inhibitory axis, thus moving quickly through clinical trials albeit with incomplete understanding regarding putative receptor interactions(20). For decades, putative receptor identification efforts for these proteins have not been fruitful except few reports that did not stand the test of time(21). Furthermore, we hypothesize that CellSeq's ability to detect protein-protein interactions as fluorescence readouts can be exploited to deorphanize receptors of such key immune checkpoints. Specifically, the de-orphanization of the receptor for the B7 family members on T cells is limited by the challenges associated with the transient nature of the ligand-receptor interactions and limited compatibility with most proteomic technologies(184, 185). CellSeq can be used to take a bottom-up approach. We hypothesize that CellSeq can couple genomic mutations to receptor-ligand interaction abundance as measured by flow cytometry and thus map the regulators of the interaction. Specifically, we could use a HAP1 mutant library, representing gene knockouts across the genome and stain this library of cells with fluorescent recombinant checkpoint proteins of interest such as B7H3, B7H4 and B7H5. We reason that, the fluorescent signal will be specific to the putative receptor of the checkpoint protein. A challenge is of course screening for the ideal binding stimuli or genotype to facilitate recombinant protein binding if HAP1 does not express the receptor under basal conditions. We can then quantify this interaction on a flow cytometer and sort the cells at the extreme ends of the distribution using flow cytometry. In the process, separating the mutations in the cells that led to the high and low expression of the putative receptor. We expect that, the gene that

codes for the putative receptor, should be enriched strongly in the low expression population relative to all the other genes and hence leading to novel T cell inhibitory receptor identification. Such a technology, will not only be instrumental in identifying novel immune checkpoint inhibitory receptors, it can use genetics to extend to orphan receptor discovery associated with various human diseases.

Overall, the growing compendium of high resolution maps of immune checkpoints being generated by CellSeq, will better inform target validation and give raise to novel biology and at times layers of regulatory mechanisms and applications relevant to the tumour immunology interface and beyond, which otherwise can go undetected.

5.2 Future of functional genomics in immunotherapy

With recent advances in CRISPR and genetic sequencing, CRISPR screens with readouts ranging from survival to more complex phenotypes such as localization and protein abundance are now being routinely performed(186). Specifically, single cell sequencing through the transcriptomic profiling of one cell at a time has facilitated unprecedented clarity on the level of cancer and immune cell heterogeneity in tumour microenvironment(126, 187-190). The drastic increase in such unbiased high throughput experiments and sequencing modalities has resulted in the accumulation of a wealth of information. Databases such as The Cancer Dependency Map (DepMAP) and The Human Cell Atlas have leveraged the data from across various genetic screens and have made it more accessible. For example, DepMAP facilitates characterization of cancer cells based on their sensitivity towards small molecule and genetic perturbations.

Identification of essential gene patterns across cell types has enabled discovery of several key cancer drivers(191-193). Alongside, Single cell transcriptomics, is being used to drive world-wide collaborative efforts towards an ambitious goal of creating comprehensive maps of ~37 trillion human cells and are making rapid progress with some data made available to the public already(194-196). Collectively, information from these databases can be used to inform better design and choice of perturbant, genotype and conditions required to delineate specific biology using forward genetic screens, which will in turn feedback into these databases. As these databases swell with information, the major challenge is finding efficient ways to filter through and process the information. Recent advancements in Machine Learning and Artificial Intelligence are well poised to counter these challenges(197, 198). Furthermore, coupling of modalities has given rise to some powerful technologies and enabled study of complex phenotypes. For example, Perturb-CITE-SEQ, a platform that combines CRISPR mutant libraries, with single cell sequencing and protein readouts obtained from a co culture of patient melanoma cells and tumour infiltrating lymphocytes. This platform was used to identify CD58 loss as a driver of immune evasion(42). Although, single cell sequencing is already producing molecular profiles of the tumour-immune microenvironment and is being coupled with other modalities, it thus far involved tissues disintegration and therefore failed to provide spatial context to the molecular profiles of cell types. With recent advances in imaging technologies, spatial transcriptomics is able to provide molecular profiles from tissues directly, while keeping the spatial context intact(199). Recently, Pekla et al spatially profiled colorectal tumour tissues and identified unique hubs in certain

tumours where activated T cells meet T cell-attracting cytokine producing myeloid cells(200). Such technologies are spearheading extraction of new information new information from clinical samples in unprecedented details and paving way for questions we could not ask before.

Overall, forward genetic screens have been instrumental and will continue to be a pivotal player in the functional genomics toolkit to dissect the tumour immunology interface. Functional genomics has facilitated accumulation of data at an unprecedented level. Optimistically, the amount of data these technologies are accumulating will hit the inflection point where it is able to closely represent something as complex as the biology of the tumour micro environment and aid in developing clinically efficient and rational therapeutics in the effort to use the immune system against cancer.

Chapter 6: Appendices

6.1 PVR screen hits (FDR < 0.05)

Gene	fcpv	MI	Gene	fcpv	MI
USP14	0	6.43871	RAD54L2	2.58E-54	6.20151
DLEC1	7.23E-135	17.1304	CUX1	6.70E-54	4.17912
CNOT2	8.08E-126	16.9058	PPP6R3	1.03E-53	3.54217
DDX6	2.09E-117	24.8398	MERTK	9.86E-52	3.7595
PPP2R4	1.28E-116	8.08388	ZNF578	8.45E-51	18.5632
SYT1	5.39E-108	0.604336	NOX5	1.83E-50	5.24119
ZEB2	2.13E-107	3.63553	ARID5B	1.20E-49	0.5986
ZNF793	2.59E-103	18.1754	MNT	3.29E-49	0.267766
PBRM1	1.29E-100	3.17981	PARK2	2.86E-48	0.647565
PPEF1	5.24E-96	5.51979	WNK3	2.48E-47	3.48129
UBASH3B	2.10E-95	11.7251	TULP4	9.53E-47	5.33223
CUL3	1.40E-92	5.72929	DNTT	1.08E-46	11.1885
DACH1	4.76E-88	0.589661	DLG2	3.86E-46	0.722557
SMARCC1	8.23E-88	3.7239	OIT3	1.36E-45	11.385
EPC2	4.55E-75	11.191	PARN	3.67E-45	2.35389
DYRK1A	4.56E-74	0.186813	NAA35	5.82E-45	12.066
CDH1	5.41E-73	8.08726	HERC4	6.89E-45	2.98797
PVR	3.48E-71	0.0787403	ARID2	1.18E-44	3.46888
PRMT3	5.80E-69	0.277606	REPS2	2.19E-44	3.34782
NF2	4.12E-68	14.8692	CCDC170	4.03E-44	3.98323
GIGYF2	6.82E-68	4.48583	TRPS1	2.62E-42	1.91961
BTLA	9.89E-68	4.76783	CNTNAP5	3.66E-42	4.09763
CCDC109B	1.50E-65	3.7928	DICER1	7.10E-42	3.96652
MBTPS2	2.94E-63	0.127322	PBX4	1.68E-41	6.62838
FLVCR2	3.06E-62	9.76856	SLC44A2	2.98E-41	6.60238
RPS25	4.22E-61	21.555	UVRAG	3.81E-41	0.520675
ANKRD13C	7.26E-61	4.3129	ZNF91	2.33E-40	6.91945
TSPAN16	1.68E-60	9.9672	NAA30	2.07E-39	25.1603
TEX11	2.61E-60	4.97524	FBXL20	2.38E-39	4.46342
SRD5A3	2.89E-60	0.0535306	HMCN1	2.52E-39	4.54604
TAOK1	6.71E-60	2.62666	AGPS	2.94E-39	0.534043
AKT3	4.89E-58	0.483737	NRXN1	5.43E-39	0.629364
IL1RAPL1	9.33E-58	0.705476	CDKAL1	4.71E-38	0.656406
HTR7	2.33E-57	6.48156	ADGRD1	1.72E-36	10.0207
IGSF11	2.57E-57	4.50701	SND1	2.65E-36	0.253402
EPHB1	4.70E-55	3.86344	FGD3	8.48E-36	4.35498

Gene	fcpv	MI	Gene	fcpv	MI
TRPC7	2.38E-35	8.9111	UBE2M	7.01E-25	5.8969
ALG8	3.87E-34	0.194439	TIPRL	9.34E-25	12.1639
TVP23A	8.22E-34	5.76929	SCARA5	1.04E-24	4.64611
FBXO11	1.13E-33	0.158167	KIAA1324	1.04E-24	3.93354
TFDP1	1.15E-33	22.0558	UPP2	1.43E-24	8.81261
CHMP3	1.81E-33	12.0464	FAAH2	2.75E-24	4.22747
WDPCP	2.23E-33	2.64407	VPS41	4.06E-24	2.10658
NELL1	3.42E-33	0.672608	TMEM131	4.17E-24	2.52142
SLC1A2	5.31E-33	8.52981	ROR2	4.71E-24	3.3294
MYO10	5.66E-33	0.638852	KIF4A	6.40E-24	2.60913
PAK7	6.19E-33	4.76231	PTPRM	8.95E-24	0.576503
CFAP53	2.57E-32	12.335	NEDD9	1.92E-23	0.594295
KIF3B	1.27E-31	1.93367	APBA2	3.86E-23	2.08848
RQCD1	2.77E-31	7.58204	MYO1E	4.51E-23	2.78506
ZNF385B	3.75E-31	0.618483	MYH14	6.49E-23	8.79153
PPP4R2	4.41E-31	6.07952	MAP1LC3A	1.13E-22	25.4449
CCDC39	1.75E-30	9.14917	EPHA5	1.34E-22	0.549678
ZNF611	2.40E-29	4.74109	XPO5	1.36E-22	10.6737
UBAP1	9.65E-29	3.90032	GON4L	1.44E-22	2.02894
WDR37	1.31E-28	3.30526	SLC4A8	1.57E-22	2.432
UNC13B	1.48E-28	2.57061	NFYC	1.71E-22	6.14169
TNS3	3.10E-28	0.534752	KDM2A	4.59E-22	0.455598
SPTLC2	3.10E-28	3.7841	KLF3	7.10E-22	4.25437
SNRPA	4.36E-28	6.01237	ATP9B	2.18E-21	2.07025
LYST	6.08E-28	2.00598	FOXP1	3.98E-21	0.667137
CARM1	6.62E-28	2.22826	SFTPB	4.19E-21	13.7231
SPOP	7.96E-28	2.90334	ARID1A	5.27E-21	2.70734
CELF1	1.35E-27	2.89962	CFAP74	9.46E-21	3.27568
LHFPL3	1.58E-27	4.01925	PRTN3	1.04E-20	4.72114
ZNF569	1.87E-27	6.13414	KIF9	1.73E-20	2.01131
TOX	2.86E-27	0.647695	AGO4	2.29E-20	2.83345
LAMTOR5	3.66E-27	9.8638	IL6R	2.58E-20	4.9666
LRRC1	1.43E-26	0.679862	PXMP4	2.60E-20	4.2762
SCN8A	5.39E-26	3.08606	CNBD2	2.73E-20	7.49698
CSMD3	8.06E-26	0.653219	CCPG1	3.11E-20	5.52092
ZSWIM6	1.73E-25	0.396201	FHIT	3.97E-20	0.777538
CD44	1.82E-25	6.65004	KCNK2	4.30E-20	0.608082
WAC	1.82E-25	6.65004	TBC1D14	5.53E-20	2.15321
C6orf99	2.02E-25	2.90329	ST18	7.22E-20	0.679197
PLEC	3.42E-25	3.1346	TTYH3	1.09E-19	4.16088
PCMTD2	6.42E-25	4.34593	ADGRL4	1.32E-19	8.23392

Gene	fcpv	MI	Gene	fcpv	MI
KLF16	1.36E-19	3.33696	ACTN1	9.35E-17	2.92719
MICU1	1.50E-19	1.81595	ST8SIA1	9.64E-17	6.38005
B4GALNT2	1.56E-19	8.65867	ABCA1	1.03E-16	1.74996
LRP1B	1.74E-19	0.800257	PNKD	1.23E-16	2.22165
LAMTOR2	2.38E-19	28.5894	G2E3	1.39E-16	2.91357
SSR3	2.38E-19	0.0902697	CENPP	1.41E-16	2.74712
RORA	2.90E-19	0.749485	LAMTOR4	1.43E-16	4.44374
HOMER2	3.31E-19	2.35469	ZSWIM3	1.52E-16	2.88571
HHLA2	3.91E-19	6.16554	ZNF808	1.74E-16	5.47974
ARID1B	4.15E-19	1.6218	RBM18	2.38E-16	7.31896
MAML2	4.46E-19	0.668972	CACNA2D1	2.41E-16	0.701532
ST6GALNAC1	1.62E-18	6.3715	C16orf72	2.93E-16	0.225767
THEG	2.44E-18	11.3088	ATP8A2	3.13E-16	0.760771
TLK2	2.96E-18	0.382291	ATAD3C	3.54E-16	8.48158
CD48	3.04E-18	5.5421	TRPV3	3.93E-16	4.43989
WWTR1	3.70E-18	0.634743	PTPRD	5.12E-16	0.735519
INPP5K	3.72E-18	5.2054	ACTR3	6.81E-16	0.383812
WDR72	4.30E-18	3.50591	CLPSL1	7.56E-16	7.16647
TFAP2C	5.54E-18	0.334746	CSPP1	1.70E-15	2.80591
IL34	6.90E-18	3.84259	RORC	1.71E-15	6.79004
RBMS3	8.56E-18	0.689084	ACTL8	2.65E-15	8.62882
TRPM3	9.70E-18	0.748458	ACSBG2	3.04E-15	6.71856
C1orf100	1.04E-17	3.78967	KLRB1	3.17E-15	2.37463
PAK3	1.07E-17	0.749307	SYTL5	5.20E-15	4.57439
DNAJC15	1.15E-17	4.33989	VTCN1	6.12E-15	5.60903
LAMA2	2.00E-17	0.599952	EXOC4	6.30E-15	0.662565
SLCO1A2	2.25E-17	1.6686	ANKRD45	6.59E-15	7.18822
MYBPC1	2.78E-17	1.49574	ARPC2	7.09E-15	0.261742
FRMD4A	3.38E-17	2.0301	KDM1A	9.05E-15	3.01652
PNPLA1	3.61E-17	2.79957	ABCA13	1.10E-14	0.752995
TSC1	3.89E-17	3.69479	GREM1	1.14E-14	12.9604
PLXDC2	4.28E-17	0.725961	HYPK	1.18E-14	7.10653
SDHC	4.80E-17	5.10538	LIN28B	1.30E-14	0.524987
CLIP1	5.11E-17	1.88868	MBNL1	1.60E-14	1.66875
PITPNC1	5.25E-17	1.61725	MROH8	1.81E-14	2.36965
SLTM	5.90E-17	2.43872	ADAMTSL1	1.88E-14	0.721933
CP	6.09E-17	5.57505	BCR	2.00E-14	2.93848
PARVG	6.42E-17	12.9061	SLC2A14	2.31E-14	2.88998
SNTB2	7.95E-17	2.30184	TMEFF2	2.91E-14	1.80929
CDK8	8.35E-17	6.60743	F8	3.54E-14	2.80841
SYTL2	8.98E-17	4.32718	KCND2	3.89E-14	0.63787

Gene	fcpv	MI	Gene	fcpv	MI
ADAM12	5.06E-14	0.683773	DMRT1	2.95E-12	3.30914
RPRD2	6.10E-14	2.0501	EDC4	3.34E-12	15.438
Mar-08	6.84E-14	3.19008	ARGFX	3.34E-12	15.438
SIPA1L3	7.34E-14	1.65693	AMBN	3.36E-12	6.37132
PIKFYVE	1.09E-13	4.70631	ZNF385D	3.54E-12	0.561139
NUDT2	1.09E-13	1.93156	MKRN1	3.82E-12	2.39938
CCL26	1.10E-13	4.90789	CD200R1	4.27E-12	2.30751
SSR1	1.14E-13	0.175119	CHN1	4.30E-12	0.800625
HNRNPA2B1	1.58E-13	0.17098	FBXL7	4.89E-12	0.760843
ARL15	1.61E-13	2.29623	CKS1B	4.93E-12	2.96562
COLGALT2	1.81E-13	0.673366	EYA4	4.96E-12	1.88152
FN3K	2.07E-13	1.97901	ZFHX3	5.48E-12	0.751247
TULP2	2.32E-13	2.6917	TRIP12	5.71E-12	0.501414
ANGPT1	2.35E-13	0.714576	ZNF680	5.74E-12	6.28963
PLEKHA6	2.40E-13	10.7822	KIAA1033	5.86E-12	0.402671
TADA2B	2.45E-13	6.40402	XPO6	6.11E-12	0.531528
PPTC7	2.55E-13	2.54007	UBE2L3	6.26E-12	2.98942
NAV3	2.61E-13	0.722353	ZNF141	6.90E-12	44.5982
ANKRD30A	2.75E-13	0.564308	PCDH9	7.17E-12	0.810181
MGA	2.80E-13	2.04091	LARP1B	7.17E-12	2.0828
TSPAN14	4.00E-13	3.48163	RANBP3L	8.29E-12	4.04067
GPC6	4.04E-13	0.700004	PRR16	8.36E-12	0.683858
GGNBP2	4.86E-13	0.419236	STARD3	8.47E-12	4.10113
TRAPPC9	5.73E-13	2.24398	GCH1	9.28E-12	2.65318
EPHA6	6.64E-13	0.723817	NPFFR2	9.99E-12	4.84658
L3MBTL3	7.12E-13	0.413374	RANBP17	1.20E-11	3.40355
CD38	7.30E-13	5.26047	C9orf85	1.20E-11	1.55204
UBE4B	8.47E-13	2.16197	ADGRG4	1.29E-11	0.690866
GPR158	8.54E-13	0.69444	LIPC	1.44E-11	4.12506
PPM1H	9.29E-13	1.59973	SYK	1.52E-11	5.11599
SLIT2	1.03E-12	0.793568	MAOB	2.25E-11	3.43077
NAA15	1.05E-12	11.6262	PPP6C	2.25E-11	12.3504
RANBP3	1.14E-12	2.75086	FAM222A	2.44E-11	5.2096
HGS	1.28E-12	4.15503	DGCR8	2.55E-11	6.33359
KLRG2	1.32E-12	2.34854	EMILIN2	2.56E-11	5.05579
TGIF1	1.69E-12	1.53482	CCAR1	2.75E-11	3.74264
MRLN	1.86E-12	13.2653	VPS45	2.82E-11	3.03493
DNMT3L	1.99E-12	11.4356	C19orf43	3.46E-11	6.96534
VPS29	2.26E-12	0.337397	CCDC141	3.58E-11	0.557344
TET2	2.84E-12	1.79537	NGEF	3.72E-11	2.99925
CCDC91	2.86E-12	0.748346	ADAM10	4.00E-11	1.95867

Gene	fcpv	MI	Gene	fcpv	MI
CCL28	4.10E-11	5.14607	GLYR1	6.65E-10	3.33802
ZNF329	4.61E-11	17.9156	BDNF	6.65E-10	6.09898
SCML4	4.68E-11	2.63665	ATP8B1	6.65E-10	2.59443
SP1	5.63E-11	0.481822	UBR3	7.21E-10	1.6983
ZNF718	7.10E-11	2.86903	SPON2	7.23E-10	3.20203
DPH6	7.92E-11	0.612276	ADAM18	7.25E-10	1.60517
ABCC2	8.04E-11	1.87721	APC	7.50E-10	0.399578
PHKA1	9.32E-11	1.55841	C4orf19	7.62E-10	4.02537
POU2F1	9.50E-11	2.12644	PELI2	7.88E-10	2.1295
NPSR1	9.56E-11	1.99775	FRK	8.08E-10	5.33662
FNDC3B	9.82E-11	0.385084	USP34	8.41E-10	0.595791
MAP4K3	1.08E-10	1.32204	ANO3	1.03E-09	0.671895
DENND2A	1.14E-10	2.33488	HYDIN	1.08E-09	0.578369
CDK4	1.14E-10	4.20836	ESRRG	1.08E-09	0.719704
MN1	1.17E-10	5.01899	CTTNBP2	1.08E-09	0.547928
ABLIM2	1.24E-10	2.85899	TTLL10	1.14E-09	16.3908
BCAR3	1.25E-10	2.05854	RAPGEF2	1.15E-09	3.91453
USP7	1.25E-10	2.77463	CDH9	1.40E-09	0.605712
TMEM174	1.34E-10	10.292	CLIC2	1.41E-09	1.92273
PPCDC	1.37E-10	1.92107	FGF13	1.51E-09	0.59843
NRXN2	1.46E-10	2.14664	PRKD1	1.60E-09	0.689555
MGAT4A	1.60E-10	2.61868	MPPED2	1.74E-09	0.773167
CWC27	1.64E-10	2.4202	RAD23B	1.77E-09	10.7493
GTDC1	1.85E-10	1.53854	CNTNAP2	1.79E-09	0.808849
EPC1	1.97E-10	1.39811	CCDC102B	1.80E-09	1.6912
SEC61A2	1.97E-10	3.46251	CDC25A	1.89E-09	2.06409
ATIC	2.01E-10	3.72585	GRIA3	1.92E-09	0.672806
LRRC4C	2.11E-10	0.665427	C17orf99	2.09E-09	5.62982
TMEM196	2.44E-10	10.1014	NCOA3	2.10E-09	1.41102
SLC4A1AP	2.51E-10	2.93746	GPC3	2.11E-09	0.807359
ZNF644	2.82E-10	2.02954	CRYBA4	2.33E-09	35.4496
USP8	3.46E-10	4.51982	TMEM26	2.58E-09	0.704044
ATP2C1	3.48E-10	1.5389	B4GALT6	2.59E-09	0.670157
CCBL1	3.69E-10	2.20252	GPM6A	2.65E-09	0.668571
ZNF791	4.09E-10	5.89374	ATF7IP	2.72E-09	0.664127
CCDC180	4.44E-10	5.63613	CDK6	3.06E-09	1.70154
KREMEN1	4.59E-10	1.47687	KIF3A	3.07E-09	2.72382
PHLPP1	5.41E-10	1.66494	TCF12	3.15E-09	0.742102
COX5A	5.84E-10	2.18232	ITGAV	3.31E-09	2.26179
CHIC2	5.89E-10	1.60645	PPFIA2	3.35E-09	0.679173
ZNF83	5.89E-10	1.84516	ITPR2	3.68E-09	1.30442

Gene	fcpv	MI	Gene	fcpv	MI
DNAL1	3.78E-09	1.81998	NCKAP5	1.97E-08	0.566717
ODF3L2	3.92E-09	8.33158	CREB1	2.22E-08	3.76423
CCNC	4.01E-09	12.2931	PTPN23	2.23E-08	20.0119
EIF4ENIF1	4.07E-09	4.45387	KMT2A	2.33E-08	3.28776
C6orf106	4.25E-09	1.68185	PDCD10	2.40E-08	5.82172
PRKCB	4.32E-09	0.627202	PRTFDC1	2.50E-08	1.58905
KCTD5	4.58E-09	3.78257	DEPTOR	2.57E-08	1.5483
ZFX	4.65E-09	0.58809	HDAC8	2.66E-08	2.14425
MID1	4.73E-09	0.714849	RCOR1	2.74E-08	2.10604
MAP4K4	4.93E-09	1.87139	FBXO8	2.78E-08	2.15337
LY96	5.17E-09	1.90852	ARHGEF12	2.85E-08	0.586809
GRK5	5.17E-09	2.58714	SEMA5A	2.90E-08	0.573317
LMBR1	5.51E-09	0.570159	C8orf46	2.92E-08	4.21311
ADGRE2	5.78E-09	3.54901	NAA38	3.05E-08	4.38364
METTL24	6.75E-09	0.643249	ARHGAP26	3.15E-08	2.31768
PRLR	7.03E-09	1.6898	MIPOL1	3.17E-08	1.6474
TPO	7.40E-09	15.2472	PPM1E	3.28E-08	1.69238
AGAP5	7.56E-09	12.0072	Sep-10	3.30E-08	1.9804
LTBP4	7.84E-09	1.64959	FAM46D	3.33E-08	6.48011
GFPT2	8.05E-09	2.65475	ZNF148	3.38E-08	1.91994
DCHS2	8.16E-09	0.545303	SCAP	3.42E-08	0.237057
PLAA	8.65E-09	3.85953	AFF2	3.51E-08	0.72379
PDLIM3	8.68E-09	8.95778	CASQ2	3.57E-08	2.54349
ROBO2	9.07E-09	0.753954	PCBP2	3.74E-08	9.60576
GPR1	9.68E-09	1.94747	TBC1D23	4.06E-08	1.57862
XPO7	9.74E-09	2.96786	C11orf16	4.26E-08	19.4401
ZNF322	9.95E-09	2.39837	HIPK2	4.88E-08	2.17155
PLCE1	1.03E-08	1.80607	ZNF107	4.88E-08	4.43969
PARD3	1.05E-08	1.41567	MME	4.89E-08	0.629213
NRD1	1.05E-08	2.13177	TSKS	4.89E-08	4.32011
DCP2	1.11E-08	10.0632	LBP	4.92E-08	4.72669
ADGRV1	1.21E-08	0.843644	DOCK9	4.98E-08	1.77969
FLT1	1.50E-08	0.649894	THSD7A	5.03E-08	0.7423
ARHGEF6	1.58E-08	0.628263	FRMD6	5.14E-08	0.782207
CDC16	1.58E-08	8.76719	ZMYND8	5.40E-08	0.64672
CCDC7	1.61E-08	1.81291	SLC6A3	6.22E-08	2.00384
EDARADD	1.66E-08	2.15752	ZNF529	6.51E-08	2.37251
MBTPS1	1.70E-08	0.291254	NRG1	7.05E-08	0.53926
MBIP	1.72E-08	0.334664	BORCS5	7.20E-08	1.69408
TMEM116	1.82E-08	1.97452	C3	7.24E-08	3.15347
IQSEC1	1.92E-08	1.90077	HIBADH	7.42E-08	0.735648

Gene	fcpv	MI	Gene	fcpv	MI
OTUD7A	7.56E-08	2.43472	HMBOX1	4.16E-07	1.23045
SMYD3	7.81E-08	1.78566	COX10	4.23E-07	2.08159
TMEM163	7.95E-08	2.15723	ZNF568	4.30E-07	8.6909
ABLIM3	8.18E-08	18.8684	CDC14A	4.33E-07	1.72185
SLIT3	8.18E-08	0.799913	BAP1	4.90E-07	0.0618095
GRM8	8.18E-08	0.650183	ANKRD24	4.98E-07	2.95981
FAM193A	8.58E-08	2.50785	BRPF3	5.18E-07	1.6117
DEPDC5	8.81E-08	2.09659	RFWD2	5.20E-07	0.697114
RAD51B	9.14E-08	1.84678	THRB	5.30E-07	0.6346
SAV1	1.07E-07	2.33762	ST8SIA6	5.47E-07	2.23815
WDR7	1.08E-07	1.83741	FOXM1	5.60E-07	2.57303
PSMD4	1.10E-07	5.83209	KCTD16	5.60E-07	0.674558
SFMBT1	1.12E-07	0.44966	IMPG1	5.73E-07	0.438068
DOCK3	1.18E-07	1.27888	KNG1	5.81E-07	5.19793
ABCC8	1.19E-07	2.70977	ADAM29	5.82E-07	12.5789
UBE2R2	1.38E-07	1.66629	ALDH3A1	7.62E-07	2.22181
SETBP1	1.47E-07	1.44664	SMS	7.80E-07	3.43067
GNAT3	1.54E-07	0.731403	ZNF75A	8.55E-07	3.2189
DDHD1	1.62E-07	2.07277	STK39	8.96E-07	0.6497
EFHC2	1.64E-07	1.40745	CSMD1	8.97E-07	0.849212
CCNY	1.70E-07	1.63792	ZNF814	9.29E-07	2.76863
NEDD4L	1.70E-07	0.774348	NXPH1	9.39E-07	0.635829
CPLX1	1.83E-07	3.88809	RUNX1T1	9.51E-07	0.707864
ACACA	1.83E-07	0.738404	SDHB	9.66E-07	7.433
MAPK15	1.83E-07	3.88809	RBL1	9.83E-07	1.57587
FRAS1	1.84E-07	2.15264	IQGAP1	1.01E-06	0.479089
CBFA2T3	1.90E-07	5.71773	UBOX5	1.02E-06	4.66215
CDA	1.99E-07	1.99071	PHIP	1.06E-06	0.466843
SLC12A3	2.34E-07	8.91961	HCRTR2	1.07E-06	0.708279
TSC2	2.43E-07	3.69057	GANAB	1.13E-06	0.311851
MORF4L1	2.44E-07	0.64572	C12orf65	1.13E-06	1.8774
RERE	2.62E-07	1.39738	DROSHA	1.13E-06	3.14478
WHSC1	3.25E-07	1.7971	UCHL5	1.13E-06	0.333506
TANC2	3.29E-07	0.884339	MAP2K6	1.14E-06	0.518278
VAC14	3.29E-07	4.06597	LGALS9	1.15E-06	16.5812
MAN2A1	3.42E-07	0.64887	NLGN4X	1.16E-06	0.424705
ZNF84	3.44E-07	3.09868	CBLB	1.17E-06	0.569637
DEFB123	3.81E-07	2.92245	DCAF7	1.18E-06	0.248578
TAF4	3.93E-07	0.190577	TOM1L2	1.37E-06	2.3059
ARHGAP6	3.96E-07	0.638098	ERICH6B	1.42E-06	3.96879
PCCB	4.12E-07	2.12381	MUC22	1.43E-06	8.23347

Gene	fcpv	MI	Gene	fcpv	MI
FUBP3	1.43E-06	2.34733	CACNA1H	3.93E-06	3.93094
GCLC	1.44E-06	0.634242	PDE1B	4.34E-06	2.93513
UNC5B	1.46E-06	2.09192	C9orf84	4.34E-06	5.46358
TMEM218	1.46E-06	1.86787	PTH2R	4.34E-06	4.24745
TTYH1	1.48E-06	3.07578	MGAT4C	4.34E-06	0.813214
C11orf70	1.48E-06	3.07578	DDRGK1	4.69E-06	2.40149
TMEM62	1.49E-06	1.94299	UBE2J1	4.77E-06	0.449208
ASAP2	1.50E-06	1.5652	CMTM4	4.77E-06	1.53829
SCD5	1.54E-06	1.91998	TBC1D32	4.87E-06	0.582411
ZNF462	1.68E-06	1.43026	SLC16A10	4.90E-06	2.14012
PARVB	1.69E-06	1.49171	LIMCH1	4.96E-06	0.7454
TNR	1.74E-06	0.63586	MYOF	4.96E-06	2.04415
GBE1	1.76E-06	1.95083	LRRC28	5.01E-06	0.715055
LGSN	1.79E-06	0.614655	PTK2	5.01E-06	0.551649
ASXL1	1.88E-06	0.53255	RAP1GAP2	5.05E-06	1.66283
ATRX	1.89E-06	0.542136	TTBK2	5.11E-06	1.91753
PVRL2	1.93E-06	1.5133	ZNF366	5.16E-06	0.636267
FARP2	2.03E-06	2.65878	ADAMTS6	5.21E-06	2.02538
TIAM2	2.03E-06	1.82096	TRAT1	5.51E-06	1.63897
INPP4A	2.15E-06	1.92431	ASXL2	5.58E-06	2.07649
AKAP6	2.16E-06	0.659934	MYH15	5.80E-06	1.43419
PPFIBP2	2.21E-06	0.762984	POU6F2	6.12E-06	0.865177
PTPN2	2.24E-06	1.85474	SUV420H1	6.29E-06	3.37619
CMIP	2.31E-06	1.93962	TRPM8	6.36E-06	2.30831
CHRNA7	2.33E-06	2.3484	NEO1	6.44E-06	0.611065
SNCAIP	2.38E-06	0.656383	SHISA5	6.66E-06	1.5005
VCL	2.62E-06	0.709096	NUBPL	6.86E-06	0.673323
SLC30A7	2.68E-06	2.28714	MEAF6	7.35E-06	4.47887
RPGRIP1L	2.71E-06	0.717189	FBXO47	7.35E-06	4.47887
FCHSD2	2.80E-06	1.58892	TIGD7	7.35E-06	3.23177
MSI2	3.00E-06	1.33552	EDA	7.48E-06	1.86642
SCAF8	3.11E-06	2.10659	KIAA1211	7.56E-06	2.49988
KIFAP3	3.17E-06	0.62277	CHFR	8.00E-06	27.4447
DSCAML1	3.32E-06	0.511532	TBX18	8.00E-06	27.4447
FXYD5	3.36E-06	1.97641	TMEM202	8.00E-06	27.4447
C16orf45	3.49E-06	1.84138	PDCD1LG2	8.29E-06	0.598153
NCOA2	3.57E-06	0.750516	AGK	8.38E-06	0.614814
SPINK5	3.73E-06	11.4353	SH3KBP1	8.49E-06	0.738108
DNAH12	3.82E-06	2.73184	KCTD13	9.76E-06	1.76899
GGA3	3.93E-06	2.49043	DENND6A	9.97E-06	1.784
UQCC2	3.93E-06	2.49043	TMEM105	9.97E-06	1.784

Gene	fcpv	MI	Gene	fcpv	MI
TAF3	1.01E-05	0.450447	TYW1	2.04E-05	1.55279
ZBTB20	1.02E-05	0.910982	ERCC6	2.07E-05	0.508968
GALNTL6	1.05E-05	0.74239	MYO1F	2.08E-05	4.80286
GABRB3	1.11E-05	1.57314	COLEC11	2.08E-05	2.31046
ISPD	1.12E-05	1.43439	DEFB108B	2.10E-05	1.95648
ADAMTS5	1.12E-05	0.621335	UFL1	2.22E-05	2.20545
PNLIPRP3	1.12E-05	5.57474	TPK1	2.39E-05	0.726373
LAMC1	1.12E-05	1.75937	TXNRD1	2.41E-05	1.55166
KHDRBS3	1.19E-05	0.585212	EFNA5	2.43E-05	0.818248
PKD1L1	1.19E-05	2.24629	TCF4	2.44E-05	0.803809
ZC3HAV1	1.20E-05	0.59893	SGCD	2.45E-05	0.760307
SDHAF3	1.26E-05	1.58866	UBE2K	2.45E-05	1.8387
PCGF6	1.27E-05	2.33287	GDPD1	2.51E-05	1.95244
DPPA2	1.29E-05	4.91722	MBD3	2.51E-05	0.581483
SLC12A6	1.31E-05	1.99067	SNX21	2.55E-05	3.08261
OLFM3	1.33E-05	0.614484	COMMD3	2.55E-05	0.385164
BRIP1	1.43E-05	1.75057	ELAVL2	2.59E-05	1.61955
RHOJ	1.43E-05	0.344415	TTN	2.59E-05	0.633607
SUPT3H	1.43E-05	1.38072	DPYS	2.70E-05	1.84116
ESR1	1.44E-05	1.54289	HS6ST3	2.73E-05	0.802908
INO80C	1.46E-05	0.675395	RELN	2.77E-05	0.752899
DET1	1.49E-05	1.42012	NECAB2	2.83E-05	0.510592
TBX22	1.51E-05	26.3011	ORAI1	2.84E-05	1.92812
BCL9	1.51E-05	0.694948	DNAH11	2.85E-05	0.749923
TRAM2	1.58E-05	0.38504	CNTN3	2.85E-05	0.590767
COMMD8	1.58E-05	0.38504	ERC2	3.00E-05	0.840425
LCP1	1.58E-05	3.71652	LRRTM4	3.05E-05	1.32964
ZCCHC14	1.59E-05	2.1288	CDH12	3.06E-05	0.789542
MICALCL	1.59E-05	0.693602	ELOVL2	3.09E-05	0.618501
CREBBP	1.63E-05	0.524336	EFCAB13	3.13E-05	5.28885
CYP27A1	1.67E-05	3.88805	UQCC1	3.17E-05	2.11841
SFI1	1.69E-05	2.24477	CELF2	3.23E-05	0.756085
KPNA3	1.69E-05	2.99082	CTNNBL1	3.29E-05	3.00181
LSM14A	1.73E-05	1.88991	FN1	3.36E-05	0.612391
PPM1L	1.75E-05	1.76652	S100Z	3.37E-05	4.6885
PLD5	1.79E-05	0.736982	HPCAL1	3.38E-05	1.81247
MET	1.79E-05	0.758891	EGFL6	3.39E-05	1.82084
PAXIP1	1.83E-05	0.298295	C2CD3	3.42E-05	1.73353
PBXIP1	1.87E-05	5.4318	PRRC2C	3.61E-05	0.260791
FOXP2	1.97E-05	0.660695	CSNK2A1	3.63E-05	0.430106
NINJ2	2.02E-05	1.38499	RAI1	3.68E-05	1.5198

Gene	fcpv	MI	Gene	fcpv	MI
RBBP7	3.71E-05	0.362561	ARAP2	5.99E-05	0.612225
UBE2G1	3.71E-05	1.331	KIAA1324L	6.18E-05	3.25007
PYM1	3.83E-05	0.56028	SNX30	6.24E-05	2.12662
REST	3.85E-05	1.78234	KCNQ5	6.38E-05	2.06579
ANXA4	3.97E-05	1.75414	FMN2	6.79E-05	0.774344
MAP1B	4.01E-05	0.811843	ZBTB10	6.79E-05	0.299926
IRAK2	4.05E-05	3.73557	MYCBP2	6.88E-05	0.55643
MTO1	4.05E-05	2.54849	DNAH8	7.02E-05	0.565882
PDGFD	4.05E-05	0.593422	EGLN3	7.06E-05	0.642453
MEI4	4.33E-05	3.83903	RYR2	7.06E-05	1.24006
SERBP1	4.33E-05	3.83903	FLT3LG	7.07E-05	2.10967
SLC9A8	4.51E-05	1.42427	SETDB1	7.14E-05	1.80685
SH3RF2	4.58E-05	2.24138	OVOL2	7.30E-05	3.87044
MATR3	4.64E-05	1.53926	GABRB1	7.30E-05	1.65901
CST8	4.66E-05	3.9584	SDHD	7.43E-05	9.5294
SLC35A3	4.76E-05	1.59971	ARL8B	8.12E-05	1.57894
TLR4	4.87E-05	6.09884	ZNF260	8.15E-05	2.40439
DPH5	4.94E-05	0.434089	JAZF1	8.24E-05	0.726633
PIAS2	5.04E-05	0.649342	MSRA	8.25E-05	0.755466
THRA	5.07E-05	1.71995	TMEM47	8.35E-05	0.487517
NBEA	5.08E-05	0.708145	EHMT1	8.35E-05	1.93644
TULP3	5.13E-05	1.92007	CNBP	8.35E-05	1.93644
PIK3R4	5.16E-05	0.27601	CHI3L2	8.48E-05	5.39094
MRPS6	5.25E-05	0.367037	MREG	8.54E-05	2.04734
KCNAB1	5.26E-05	0.517784	FLCN	8.63E-05	4.7012
CLTCL1	5.27E-05	1.44938	NASP	8.65E-05	4.45979
NADK	5.42E-05	1.55576	SOGA3	9.25E-05	0.620461
GMEB2	5.45E-05	2.24044	THAP6	9.36E-05	0.652331
UBE2D1	5.49E-05	0.654359	DHX29	9.40E-05	0.361094
SHTN1	5.50E-05	0.731758	TMED10	9.53E-05	2.08996
MKX	5.64E-05	0.745133	NARS2	9.65E-05	0.784982
ING3	5.64E-05	2.28712	IZUMO2	9.76E-05	12.5788
CNOT10	5.64E-05	0.246631	CDH7	0.00010239	0.544167
NDUFB3	5.68E-05	2.98316	PTBP1	0.0001033	0.114348
C15orf41	5.69E-05	0.624063	CHODL	0.00010512	1.41486
ANK2	5.76E-05	1.54358	ABCC1	0.00010806	1.51233
GCNT1	5.86E-05	1.94555	ADSS	0.00010937	3.04945
PARP14	5.86E-05	1.94555	SKP2	0.00011093	1.81988
TSHZ3	5.86E-05	0.445238	LATS1	0.00011141	1.75852
SALL3	5.86E-05	0.445238	GFY	0.0001139	2.37507
BCOR	5.92E-05	0.80011	EXTL1	0.00011426	2.34289

Gene	fcpv	MI	Gene	fcpv	MI
MAPRE2	0.00011508	0.673735	ATXN2L	0.00015896	0.163354
PGR	0.00011565	3.78247	SLC26A7	0.00016066	0.756218
EPHA3	0.00011605	0.796188	MTHFD1L	0.00016343	2.19181
TTC8	0.00011651	0.719038	C12orf76	0.00016449	1.6471
KLF5	0.00011791	0.697194	IL1B	0.00016738	7.43293
ZMIZ1	0.00011791	0.580336	CECR2	0.00016959	1.37424
PPP3CA	0.00011855	0.78784	WDR88	0.00017067	1.97524
MAPK14	0.00011927	0.467324	ERP44	0.00017372	2.65466
UHRF1	0.00012035	1.66339	MAPRE3	0.00017372	2.65466
SV2C	0.00012276	2.6955	ZBTB14	0.00018246	2.55392
SEL1L2	0.00012414	3.29608	ZNF566	0.00018371	1.98336
KIRREL	0.0001257	1.94889	MRPS9	0.00018623	0.457383
SEMA3A	0.00012618	0.643672	VPS28	0.00018652	2.45527
ZBTB7C	0.00012679	3.90708	ICA1L	0.0001917	1.52479
LANCL3	0.00012702	1.65948	KLHL14	0.00019376	1.46827
LDB2	0.00012859	0.834738	PPP5C	0.00019975	2.21087
ZFP91	0.00013184	1.84833	BANK1	0.000202	0.528941
SLC1A7	0.00013386	9.14821	DACH2	0.000204	0.818627
MOV10L1	0.00013665	0.571718	TIMM8B	0.00020724	0.233893
EIF2AK4	0.00013762	1.60399	WRB	0.00020724	0.233893
C15orf65	0.00013845	4.34543	ZZZ3	0.00020724	0.233893
PYROXD2	0.00014013	4.57413	SNED1	0.00021047	3.0695
NFIA	0.00014079	0.77146	LRRC7	0.00021459	0.463855
SLC9A3R1	0.00014105	3.12969	VPS54	0.00021996	1.70018
ZSCAN18	0.00014111	4.86001	TASP1	0.00022607	0.69842
CNOT3	0.00014146	5.22757	ALDH1A2	0.00022704	1.30078
NKD2	0.00014146	5.22757	LAMTOR3	0.00023148	4.71707
RNF135	0.00014157	1.65184	RSRC1	0.00023836	0.553966
CRY1	0.00014349	1.75422	KCNK9	0.00023893	8.76703
SETD1B	0.00014359	1.58951	ABI1	0.00024739	1.44076
SEC14L1	0.00014375	1.44799	CAMKMT	0.00024964	0.801794
XPNPEP3	0.0001454	1.77254	RAPGEF1	0.00025284	1.55445
HYAL1	0.00014878	1.74208	AHRR	0.00025734	0.710542
STAG2	0.00014954	0.629326	LEPR	0.00025769	1.75036
KCTD9	0.00015035	2.06643	DPF2	0.00026114	2.46577
RAP1A	0.00015177	1.6742	FAM135B	0.00026277	0.494205
TACC1	0.00015208	0.795421	NPRL3	0.00028679	1.52073
ITGBL1	0.00015231	1.8096	TADA1	0.00029566	7.14704
HMBS	0.00015552	2.49501	HKR1	0.00029566	7.14704
ANKRD33B	0.00015712	0.571718	PPARG	0.00030113	0.606941
ZNRF1	0.00015735	1.49188	EYA2	0.00030463	2.07134

Gene	fcpv	MI	Gene	fcpv	MI
CUL1	0.00031546	2.38511	SGF29	0.00041516	2.58356
EML2	0.00032901	1.43992	DCLK2	0.0004248	0.720317
NHLRC2	0.00032953	0.425475	FAM83F	0.0004248	8.38585
SECISBP2L	0.00033038	0.711825	DLG5	0.00042556	0.505026
HSD17B12	0.00033168	0.474643	ABHD6	0.00043028	2.35244
LEKR1	0.00033404	0.581302	ST3GAL3	0.00043163	0.837287
EYA3	0.00033453	0.638299	SS18	0.0004347	1.97699
PCDHB3	0.00033463	11.4352	BMF	0.00044899	0.795501
MBTD1	0.00033513	2.71591	POLN	0.0004798	1.55098
ZNF878	0.00033579	20.5834	EIF4E2	0.00048291	2.66826
PCDHB2	0.00033579	20.5834	ASH2L	0.00049454	1.73968
ATP8A1	0.00033918	0.832547	TEN1	0.00049782	1.27007
C10orf99	0.00034764	3.35437	ITGA6	0.00049996	1.80711
MTRF1	0.00034845	1.97356	CCDC22	0.00050008	0.317632
C1orf43	0.00035945	0.678904	BCL2	0.00050465	0.521415
ARMC3	0.0003602	2.00624	PKN2	0.00050626	1.65621
THSD7B	0.00037105	1.31683	NPAS2	0.00051579	1.71535
EPB41L4B	0.00037229	0.657468	FGF1	0.00052046	0.438771
POLG2	0.00037233	0.409388	PFKFB4	0.00052147	1.97165
COL21A1	0.0003738	2.16004	ZNF354B	0.00052257	3.27813
RHBDD1	0.00038149	4.57412	LOC728485	0.00052257	3.27813
MAP2	0.00038149	0.709995	TMEM30A	0.00053228	0.44468
PPP1R3B	0.00038149	4.57412	MYPN	0.00053564	1.58154
NFIX	0.00038161	1.56074	TNRC6B	0.00053667	1.22717
RMDN2	0.00038298	2.03761	CCDC129	0.00055645	0.575187
MAPK8	0.00038472	1.94223	NIPAL3	0.00056037	0.522207
BANF2	0.00038577	2.08127	SAMD1	0.00056647	0.0952906
CYP7B1	0.00038609	0.822432	AKAP13	0.000568	0.820555
BFSP2	0.00038694	3.43061	ABCC5	0.000568	1.631
STAT5B	0.00038694	1.70436	EMX2	0.0005749	5.94634
PTPN14	0.00038958	0.529059	TRDN	0.00059361	0.784762
ENAH	0.00039032	0.684659	CCDC18	0.00060052	1.69336
CPM	0.00040142	2.23132	PCNT	0.00060359	1.81187
KPTN	0.00040142	2.23132	ZSCAN1	0.00060737	10.8635
ST3GAL5	0.00040225	2.04977	MCHR2	0.00060737	10.8635
SDHAF4	0.00040483	2.65302	GPAT3	0.0006106	1.40621
LRRC40	0.00040673	0.758366	CSNK1G1	0.00061088	0.793923
REC114	0.00041304	0.575105	PCDHB5	0.00061758	19.4399
MYBL2	0.00041419	16.0093	MACROD2	0.00063438	0.852136
CENPA	0.00041419	16.0093	PXDNL	0.00063495	1.24762
PRAMEF18@chr1-	0.00041419	16.0093	SHMT2	0.00063933	2.75489

MISP	0.00064826	4.73747	CXXC1	0.0008949	3.26724
STAT6	0.00065565	1.58598	SMCHD1	0.0008949	0.65271
WDR4	0.00065946	0.381157	PTBP3	0.00090051	0.717259
FAM177A1	0.00065952	1.64205	KIF5A	0.0009226	4.06588
SKAP2	0.00066979	0.772555	STK10	0.00092811	1.76356
METTL9	0.00067209	0.718962	DNAH14	0.00093519	0.746118
EXOC2	0.00069124	0.651436	LUZP2	0.00094405	0.80261
REPS1	0.00069746	0.541636	MSLN	0.00095849	5.71763
ACAA2	0.00069811	1.63783	MTFR1	0.00097076	0.595404
PRRX2	0.00070302	1.46095	MED13	0.00097523	1.66634
KMT2E	0.00070497	1.30849	C3orf70	0.000978	2.62061
BTBD9	0.00071239	1.66726	CMTR2	0.00099212	0.28587
SNX15	0.00071578	2.15413	ABCA12	0.00099276	0.567836
CAMK2D	0.00072196	0.713876	UMAD1	0.00099276	0.567836
TRNAU1AP	0.00072624	0.323625	MAPK10	0.00101171	0.691201
IFT172	0.00073464	1.5531	ABI3BP	0.00101811	1.52477
SCN3A	0.00073766	2.17553	LOC101928436	0.001019	0.54534
YAE1D1	0.00073766	2.17553	CCM2	0.00102297	3.34263
RPS6KC1	0.00074049	0.641317	H2AFV	0.00102297	5.14587
LMO3	0.00074594	1.28922	FPGS	0.00102297	5.14587
ADRBK2	0.00074745	1.42709	ZNF606	0.00102995	3.07325
CYSLTR2	0.00075132	8.00467	GPATCH4	0.00103191	0.481458
ZDHHC15	0.00075634	2.08822	AP4S1	0.00104008	1.61844
OSGEPL1	0.0007625	1.53442	KLF12	0.00106107	1.40168
NKAIN2	0.00076292	0.699502	REEP6	0.00106625	2.72271
PLCB1	0.00076677	0.806301	IL33	0.00106625	2.72271
TMED2	0.00079284	2.68483	DYM	0.00108053	0.898562
PAIP2	0.00080978	2.10517	CDH8	0.00108053	1.64588
HUWE1	0.00082131	0.65667	DHX30	0.00108053	1.64588
AKR1C3	0.00082466	0.610634	RTN4RL1	0.00108053	1.64588
KIAA1671	0.00083731	1.39821	WFDC11	0.00109288	10.2917
CDK13	0.00083829	1.48242	CAPN9	0.00110754	0.528489
NTN4	0.00084015	0.638676	ADGRL3	0.0011176	0.798547
C11orf49	0.00084015	1.25858	SERPINB5	0.00112463	2.63511
KEAP1	0.00084015	0.638676	ZNF665	0.00112797	18.2963
ARPC1A	0.0008467	2.44481	EGFLAM	0.00112797	0.554911
FOXN3	0.00084749	0.813303	RTKN2	0.00112844	0.684473
MTM1	0.00084749	2.06812	WDR44	0.00115496	0.682824
CCDC67	0.00085279	0.559896	ARHGEF37	0.00117432	2.40538
HTR2C	0.00089145	0.751636	PRODH	0.00120555	2.05838
CASC1	0.00089355	0.594856	COX18	0.00121034	1.59722

Gene	fcpv	MI	Gene	fcpv	MI
TSSC1	0.00121553	1.96345	UBTD2	0.00161709	1.91953
E2F4	0.00123498	3.63851	UBE2G2	0.00162617	0.414301
RCE1	0.00123498	3.63851	CHTF8	0.00165304	4.95528
GRIA2	0.00123518	0.604581	RAD52	0.00165304	1.37655
PRKACB	0.00124581	0.624768	RAB8B	0.00169091	0.637142
BAHCC1	0.00124581	1.74257	NAALADL2	0.00171778	0.802667
OSMR	0.00124581	1.35024	DNAJC27	0.00171972	1.43639
SPEN	0.00126073	0.706028	NCK1	0.00173324	1.77886
RAB31	0.00128108	0.595979	NHSL1	0.00176347	0.828187
VPS8	0.00129404	1.48601	CCDC36	0.00177624	2.01364
APOBEC3F	0.00131892	2.25345	GK	0.00181129	1.76047
GPC5	0.00132338	0.814273	SDHAF2	0.00181129	2.68731
TMEM87A	0.00135452	0.677588	KCTD1	0.00182078	1.32435
LOC81691	0.00137378	1.70892	RABGAP1	0.00184066	0.784681
YLPM1	0.00137819	2.57296	SESN1	0.00184612	0.712071
SGMS2	0.00137819	1.28086	SOX5	0.00184612	0.88756
ASPSCR1	0.00139038	1.86962	CLSTN2	0.00184614	0.753216
PLEKHA5	0.00141741	0.722319	ABHD12B	0.00186617	2.59895
KCTD20	0.0014258	1.56489	PDGFC	0.00188674	0.654879
SLC25A42	0.00145138	1.95723	VPS37A	0.00192634	2.36876
TCF24	0.00145138	3.93882	FASTKD1	0.00193434	1.46301
TMEM67	0.00145138	1.95723	TAX1BP1	0.00193452	1.3087
ZNF547	0.00145138	3.93882	FAT4	0.00196839	0.542658
NID2	0.00145746	0.602536	TNPO2	0.00198072	1.39508
ABCB1	0.00146268	0.708162	TMC7	0.00198687	2.16346
DENND5B	0.0014628	1.78583	EXOC6B	0.00198687	1.28755
ANKRD52	0.00147026	6.28938	SCHIP1	0.00199283	1.63207
MED22	0.00147026	6.28938	C10orf11	0.00200106	0.594001
VPS33A	0.00150113	1.87468	ABHD17C	0.00202107	0.732267
RPS6KB1	0.00150113	0.367546	SATB1	0.00202626	0.515679
FAM134B	0.00150757	0.743873	NFASC	0.00202626	0.515679
ZFAT	0.0015466	1.33994	TRIM33	0.00203778	1.56779
IRAK3	0.00155325	3.25467	UGT2B15	0.00205076	0.627653
DHX35	0.00155325	3.25467	HSF5	0.00206028	3.65929
LRCH1	0.001562	1.72895	KCNT2	0.00206028	0.579895
COL23A1	0.00159094	1.94188	HNRNPF	0.00206028	0.579895
LNP1	0.00160846	1.70234	ADAMTS20	0.00212391	1.75345
NAT2	0.00161709	13.7222	HTRA1	0.00213963	0.523641
HAS1	0.00161709	13.7222	VTA1	0.00214469	2.70837
SLAMF7	0.00161709	13.7222	CLCN3	0.00214559	1.44577
KDM4E	0.00161709	13.7222	FANCL	0.00219517	2.61379

Gene	fcpv	MI	Gene	fcpv	MI
RNF157	0.00220371	1.26607	DIAPH2	0.00291316	0.801378
IFT122	0.0022225	1.68874	SLC17A7	0.00291505	2.18312
IRF8	0.00222966	0.603685	PPIG	0.00291728	0.471681
SSH2	0.00225035	1.45433	HPSE2	0.00293156	0.587833
RAB11FIP4	0.00226323	1.80196	KDM4B	0.00294736	0.584248
NFYB	0.00226817	3.81176	CACNA1A	0.00294931	2.02115
ZEB1	0.00227177	1.83331	MDM2	0.00295757	1.70104
CYP3A43	0.00227648	1.30443	MARK1	0.00298191	1.60987
ADRM1	0.00228131	7.24231	C10orf91	0.00299934	3.02219
PITPNB	0.0023461	0.52938	MRPS27	0.00303036	0.624909
WDR76	0.00235721	1.4174	BIRC6	0.00305187	1.32141
SSR2	0.00235745	0.28587	ACTR2	0.00307219	0.350044
NEB	0.00236057	0.691859	DYSF	0.00311443	1.65319
REEP1	0.00236557	1.71533	RYR3	0.00312097	0.591718
FIGN	0.00237333	0.759028	FAM13C	0.00313232	0.706352
LCLAT1	0.00237378	0.845125	CATIP	0.00316132	2.32943
SYNE2	0.00242004	0.771742	SMPD3	0.00316202	1.81843
E2F3	0.00246569	1.82253	PCDHA1	0.00317428	12.5787
TLN2	0.00246959	1.89205	MS4A1	0.00317428	12.5787
ZNF69	0.002484	6.0035	NANOG	0.00317428	12.5787
ZNF544	0.002484	6.0035	SLC51B	0.00320839	1.52476
SLC18A2	0.00249116	4.00234	ZNF675	0.00321646	2.4243
PACSIN2	0.00249615	1.74624	GADL1	0.00322268	0.727936
KIAA0922	0.00253605	1.54248	TRAPPC13	0.00323608	1.71533
GSPT1	0.002575	0.504109	FMO4	0.00325074	2.85883
OTUD6B	0.00259923	0.330339	GLDC	0.00327657	2.0012
LRGUK	0.00260231	0.520785	DPEP2	0.00334189	1.72295
C3orf84	0.00260399	5.26021	TMEM135	0.00334609	0.743806
LOC100506127	0.00260654	1.44006	CTNNA3	0.00338161	0.891966
MOCS2	0.0026369	0.663604	STARD13	0.00338655	0.730338
BTRC	0.00264799	0.830244	TEX2	0.00341397	0.747071
NIM1K	0.00265054	2.32792	PEX5	0.00342093	1.92116
UBR7	0.00265371	0.22132	LRRC16A	0.00343714	0.784808
WNK1	0.00269222	0.552349	TOX3	0.00346299	0.646557
E2F2	0.00279652	1.4795	BFAR	0.0034636	1.42947
PPP1R1C	0.00279652	0.654182	ALPK1	0.00358444	0.800375
KAT6A	0.00279897	0.486302	LY75	0.0036298	0.497745
FER	0.00280426	0.681488	PAX3	0.0036298	0.703335
GLMN	0.00282423	2.05838	NTNG1	0.0036298	0.497745
SLC23A2	0.002901	1.81516	COMMD7	0.00363789	0.588544
ANKH	0.002901	1.81516	TAF5L	0.00370863	2.57295

Gene	fcpv	MI	Gene	fcpv	MI
AHNAK	0.00371726	1.53695	ARHGEF28	0.00462936	0.635251
XRN2	0.00373142	0.182958	RSU1	0.00468682	0.639557
C10orf107	0.00373552	0.707649	SLC25A13	0.0047062	0.733139
CATSPER2	0.00377465	16.0093	MRPS36	0.00472349	2.78736
CHP1	0.0037785	1.748	ANO1	0.00474933	0.613377
GFPT1	0.00381682	0.734131	C3orf67	0.0048037	0.716089
DCLK1	0.00382612	0.778396	ATCAY	0.00481353	2.21084
TNN	0.00383811	0.477652	GUCA1A	0.00481897	0.629926
DIP2C	0.00384768	0.703964	HOXC4	0.00497695	2.09104
FANCC	0.00394252	1.71533	ERBB2IP	0.0050333	1.38939
UPK1B	0.00394371	6.86113	ZNF385A	0.0050333	2.66824
CPNE4	0.00396467	1.39771	CDK14	0.00504397	0.736727
PLEKHB2	0.00397657	1.42206	ARFGEF2	0.00507654	1.57509
KIAA1328	0.00398711	0.79606	CCDC79	0.00512688	3.07873
ATRNL1	0.00402952	1.79968	TEAD1	0.00517079	0.83903
C6orf10	0.00406627	0.678145	UBE2D2	0.00519048	0.614511
MAP7D2	0.00406627	0.678145	ARHGAP15	0.005199	0.720363
PITX2	0.00406777	2.75793	MED1	0.00522077	2.443
ADGRB3	0.00406893	0.789587	HNRNPD	0.00522717	1.73214
ZNF827	0.00410848	0.809766	CLPSL2	0.00524554	1.91419
CHSY3	0.00411651	0.326709	RALGAPA1	0.00528918	1.39408
PIGN	0.00411885	0.545015	FGFR2	0.0053556	0.727309
SLC25A32	0.00413868	2.00817	CNIH3	0.00541791	0.536729
MCF2L2	0.00413868	2.00817	TNFRSF19	0.00544104	0.766639
ARHGAP31	0.00416357	1.31601	RAB30	0.00556131	0.692707
USH2A	0.00417018	0.795078	CCDC178	0.00559663	0.779282
SFXN4	0.00417787	1.66214	TBCD	0.00561374	1.94922
DEPDC1	0.00418319	0.629237	CNGA1	0.00561374	1.94922
TSHZ2	0.00419738	1.6391	ART1	0.00579578	9.14816
RUFY3	0.00420756	1.33226	PCDHB6	0.00579578	9.14816
CHMP5	0.00423582	5.0315	PDZD8	0.00581762	0.686066
NLRP12	0.00423582	5.0315	NDC1	0.00582771	0.51259
TGFBR1	0.00426923	0.36494	ATP10B	0.00587463	0.641938
GMEB1	0.00426997	1.97521	CPQ	0.00589108	0.719067
CLUAP1	0.00430422	1.7891	AHCY	0.00589508	1.7607
SLC24A4	0.00432733	2.64818	PTPRG	0.00597446	1.14368
ABCB4	0.00432733	2.28707	KIAA0825	0.00597446	0.714132
ZNF852	0.00438417	2.50488	CCDC62	0.00597953	1.58513
SNX7	0.00442225	0.711648	SSBP2	0.00598668	0.708847
SORBS2	0.00443398	1.48127	ELAVL1	0.00598705	2.24472
CNST	0.00462936	0.635251	SVIL	0.00604215	0.678757

Gene	fcpv	MI	Gene	fcpv	MI
HN1	0.00607093	0.589881	MAP7	0.00746473	0.801945
PCDHGA1	0.00615334	3.71645	MAP2K5	0.00750868	0.828956
ST5	0.00615334	1.21375	GRID1	0.00762194	1.5753
WNT5A	0.00615334	0.442636	TADA2A	0.00762194	0.585906
ABCD1	0.00615334	2.3865	GAB1	0.00763773	1.47029
SUCLG1	0.00615334	2.58799	EYS	0.00769474	0.8939
MKL1	0.00616743	1.3122	CSRP2BP	0.00783757	0.302687
PIGL	0.0061857	1.45545	MAML1	0.00792078	1.73319
RNF214	0.0061857	1.50702	AFF4	0.00793391	1.80002
SUFU	0.0061963	1.67134	SERPINF1	0.00793391	0.664518
SPA17	0.00621336	11.4351	OSBPL11	0.00793391	1.80002
HNRNPLL	0.00627529	0.714648	UMPS	0.00806268	2.74447
ERF	0.00628964	0.61872	SDK2	0.0083362	0.636862
CXorf65	0.00648616	3.22267	GLRB	0.0083362	0.688186
CYB5R2	0.00653764	2.85882	SLAMF1	0.00838256	2.62339
THBS4	0.00657291	1.54176	KCNH8	0.00838816	0.728354
PLA2G6	0.00657738	1.45145	ASPM	0.00844055	1.50615
ZNF432	0.00659315	1.79418	TDO2	0.00851628	0.603244
HECTD1	0.00664387	1.63955	SLC9A1	0.00853345	2.33678
RNF20	0.00676194	6.47995	RYR1	0.0085377	0.812135
VWC2L	0.00676194	6.47995	SHOX2	0.00853776	0.702936
DHX36	0.00676194	6.47995	MFHAS1	0.00855326	1.40747
AGGF1	0.00682145	2.20539	CHST12	0.00863664	1.61137
ST6GALNAC2	0.00684153	2.71588	COLEC12	0.00866221	1.82527
PLLP	0.00685484	1.45955	CIC	0.00871016	1.33794
ZNF177	0.00693541	4.80279	PRKG2	0.00871016	2.39597
EIF2AK3	0.00704802	0.657011	CHD7	0.00878054	0.652442
PRH1	0.00704802	1.3515	NR1H4	0.00902565	0.7301
TJP2	0.00711327	1.46036	CASC3	0.00902565	0.266814
VCPIP1	0.00712569	0.438333	ATL1	0.00905839	0.828697
CASP3	0.00712569	0.438333	LRRIQ4	0.00942445	0.671551
UNC5D	0.0071344	0.45376	ACSL4	0.00947529	1.82967
CPEB3	0.00724027	1.30341	TRAF3	0.00949343	0.718369
VPS36	0.00736034	3.31622	LOC389895	0.00949623	0.372297
SH3BGRL	0.00736421	0.766896	GATAD2B	0.00959888	0.71297
ANO7	0.00738157	1.62788	AMZ1	0.0096004	3.57351
RRAS2	0.0073929	0.602755	ME3	0.00974835	3.11871
SALL1	0.0073929	0.598118	SPOCK3	0.00979746	0.773968
RNF10	0.00739534	1.87346	TOE1	0.00983591	2.00119
ARHGAP18	0.00739534	0.62509	BRD7	0.00995771	2.28706
ZNF804B	0.00744588	0.804338	SLC37A3	0.00998976	1.5394

Gene	fcpv	MI	Gene	fcpv	MI
RWDD2B	0.01006935	1.46674	ATXN7	0.0118993	1.33188
ETV4	0.01022042	2.33904	SMARCA4	0.01193091	1.41223
CDKN2A	0.01035564	1.35573	C1orf27	0.01196613	1.95605
ZFPM2	0.0104564	0.566183	KCNMA1	0.01199851	0.571734
ASIC5	0.0104564	0.692363	ARHGAP39	0.01209643	1.52124
SPATS1	0.0104564	0.566183	FLI1	0.0121201	0.351841
FAF1	0.01047274	1.494	SLC39A12	0.01213266	2.34151
ADNP	0.01050015	0.659936	ZCRB1	0.01213266	2.34151
TBC1D22A	0.01053654	0.699341	SRSF5	0.01213449	0.127055
PSD3	0.01072392	0.791419	VIPR2	0.01213449	0.127055
TAF6	0.01076769	0.362568	CA1	0.01216916	10.2916
MYLIP	0.01077319	0.411653	FAM9C	0.01216916	10.2916
SNTG1	0.01078147	0.879036	ZNF81	0.01225546	0.760176
TYMS	0.01080667	4.19291	TGFBR2	0.01234392	0.66373
NTN5	0.01080667	4.19291	UBE2V2	0.01235451	1.74541
PROCA1	0.01080667	1.55617	DEFB124	0.01240046	13.7222
RSF1	0.01080667	1.25277	EBF2	0.01240046	0.482404
FAM186A	0.01083414	0.735342	ZNF423	0.01242069	0.726473
ZNF138	0.01087126	1.67389	GRXCR1	0.01243321	2.95411
ANKHD1	0.01087126	1.67389	FBXO46	0.01243321	1.36036
LIPH	0.01087126	1.97801	ITGB2	0.01243321	2.95411
AGL	0.010882	1.57392	C1GALT1	0.01248118	2.0445
HS3ST2	0.01114761	3.20187	FAM73B	0.01270114	3.30351
VAV1	0.01120749	1.82033	DPCD	0.01274022	0.582521
SUN3	0.01121554	1.40495	ILK	0.01277976	0.453448
FKBP1A	0.01122684	2.07266	TXLNA	0.01290605	1.79379
OFD1	0.01135302	0.760193	UBE2H	0.01298534	1.18989
KREMEN2	0.01149174	2.24132	ATP8B4	0.01309676	0.780093
SMARCAL1	0.01151504	1.66631	ENOX1	0.01314132	0.809246
FUT3	0.01154925	5.14584	GNAQ	0.01316756	1.32802
ZFP3	0.01154925	5.14584	STK31	0.01323826	1.87867
SDHA	0.01154925	5.14584	FAM208A	0.01333791	0.538104
ZNF442	0.01154925	6.09877	HOOK3	0.01338579	1.65731
USP6	0.01154925	5.14584	MYO1A	0.01341117	0.276014
ZNF540	0.01154925	6.09877	PDLIM5	0.01355793	0.813691
CTNNA2	0.01154925	0.753321	RAB27B	0.01358007	0.519761
CACNB2	0.01155712	0.80793	YAP1	0.01358007	0.73564
TMEM248	0.01164288	1.65351	COL24A1	0.01361258	0.703661
DDA1	0.01166563	2.66823	SGCA	0.01396413	0.103954
ITGA2	0.01177518	0.668086	ZNF704	0.01400943	2.08991
SYN3	0.0118993	1.56486	TCERG1	0.0140127	2.57294

Gene	fcpv	MI	Gene	fcpv	MI
TSHZ1	0.01404301	0.698775	CPA2	0.01754646	1.28277
ZNF410	0.01409716	1.72501	PIK3AP1	0.01762079	1.75929
MPHOSPH9	0.01409716	1.41347	SERF2	0.01794519	1.24098
RMND1	0.01409716	1.9471	ADHFE1	0.01802775	4.34538
SKAP1	0.01411375	0.661276	EPB41L2	0.01811146	0.77706
HIVEP3	0.01411791	0.536444	ITPK1	0.01811146	1.77365
MTMR3	0.01424077	0.838007	ARF1	0.01822623	0.30493
RAB12	0.01426338	0.716997	MRE11A	0.01822623	0.30493
FAM53B	0.01432766	1.25735	PIK3CB	0.01825255	2.85881
SNX3	0.01447311	0.765438	GNA15	0.01834606	1.71531
SUMO2	0.01447311	0.238227	PUM3	0.01836302	0.390458
EPB41L5	0.01467505	0.633428	SORBS1	0.01837253	0.492575
CTTN	0.01506134	0.336319	RABGAP1L	0.01847938	1.37485
LRFN5	0.0153953	0.810341	FAM216A	0.01852013	1.40086
DNAH17	0.01540502	1.67958	CDH19	0.01852013	0.583403
ADGRG7	0.01543949	0.61784	ARIH1	0.01870692	0.651138
FRY	0.01543949	0.812739	SUPT20H	0.01873034	2.05047
OXCT1	0.01554856	0.663488	USP3	0.01876834	1.29204
MLLT3	0.01557009	0.543847	GDAP2	0.01881709	0.487384
RELL1	0.01564396	1.8248	ERCC4	0.01887765	4.85996
PCDH7	0.01566656	0.773148	PVRL4	0.01887765	4.85996
MAST4	0.01567185	0.798764	ITIH2	0.01887765	4.85996
CAPZB	0.01580262	2.81483	ATG2B	0.01892407	0.708618
ZNF710	0.01612131	0.577395	FAM234A	0.01910435	1.58667
ANKUB1	0.01612131	0.39889	ZFP36L1	0.01910954	0.720129
ADGRG6	0.01618414	0.694036	OPRM1	0.01923275	3.17645
LUZP1	0.01662238	1.71531	POLDIP3	0.01932466	0.513736
A2ML1	0.01662914	3.08751	COL16A1	0.01933302	0.473164
MED27	0.01682377	2.48885	FOXF1	0.01934714	0.359381
PLA2G16	0.0168458	1.24524	DIDO1	0.01936769	0.614973
TIMD4	0.01687956	1.30452	MEFV	0.01937478	5.71759
ING5	0.01691205	4.00232	NOXRED1	0.01937478	5.71759
RALGPS1	0.01703165	1.22393	IL1RAPL2	0.01939809	1.55471
STAU2	0.01703602	0.834715	ACSS3	0.01947288	0.735072
TMEM88B	0.01704259	8.00462	DST	0.01947288	0.893176
ROPN1B	0.01704259	8.00462	AHDC1	0.01957454	2.69545
CLEC6A	0.0170965	1.67842	PPIA	0.01957454	2.69545
ZC4H2	0.0170965	0.461404	NAP1L1	0.01967243	2.41411
TMEM126B	0.01713326	1.85144	VASH1	0.01967243	2.41411
EXPH5	0.01748993	1.63363	VAMP2	0.01967243	2.41411
POU1F1	0.01749464	0.5266	SEMA3F	0.01967243	2.41411

Gene	fcpv	MI	Gene	fcpv	MI
TCF25	0.01967243	2.34423	HHLA1	0.0220226	12.5787
ZNF10	0.01967243	2.41411	ZNF516	0.02204035	0.804895
ARPC4	0.01977614	0.134529	SCN7A	0.02206375	2.04202
MED23	0.01980978	0.285872	NCALD	0.02227594	1.23239
MUC4	0.01981472	1.68719	SLC38A11	0.02229918	0.793023
SNX8	0.01985347	2.11765	SLC26A8	0.02234054	2.72687
MYH7B	0.01985758	1.30264	TYW1B	0.02247138	1.52473
CHD6	0.01986031	1.92767	ASS1	0.0226876	1.39121
MPRIP	0.02012303	1.61349	TEX29	0.0226876	0.68063
PDE11A	0.02019839	0.83901	ZNF823	0.0226876	2.2326
SLC7A2	0.02019839	1.84081	MEGF9	0.0226876	1.15964
CLN3	0.02019839	1.84081	PHKB	0.0227421	0.869984
FNBP1	0.02021665	1.62416	TFAP4	0.02284064	0.705415
PNPLA8	0.02028638	0.747936	RBM4	0.02284064	2.34724
PDZD2	0.02046435	1.21352	KCNS3	0.02284064	2.34724
DDR2	0.02058412	0.59896	JARID2	0.02286263	0.802361
ZBTB2	0.0205871	2.02024	KIF18B	0.0230487	2.42159
NRP2	0.02061435	2.14984	ZRSR2	0.0230487	2.42159
C9orf92	0.02061435	2.14984	TECTA	0.02315808	2.11113
ITGB5	0.02065395	0.668816	FAM155A	0.02315922	0.531475
CITED1	0.02072729	0.381162	IRF2BP2	0.02315922	0.531475
HDGF	0.02076945	1.28803	ZFP42	0.02320979	9.1481
MED12	0.02084105	2.91079	RERGL	0.02320979	9.1481
GUCY1A3	0.02084105	1.49206	APOC4	0.02320979	9.1481
SPOPL	0.02116635	1.76295	TSG101	0.02320979	9.1481
FAM198B	0.02117449	0.832934	VEZT	0.02320979	1.63123
U2AF1L4	0.02117449	0.274438	BAZ1B	0.0232149	1.26905
DPM1	0.02117449	0.180551	PNP	0.02322204	0.508213
GPS2	0.02117449	0.180551	ZNF414	0.02331787	1.88529
OSBPL8	0.02117449	1.42736	ANKDD1B	0.02344284	3.59392
CTNNA1	0.02117449	0.821888	VSTM4	0.02344284	3.59392
PHF6	0.02117449	0.565165	THAP4	0.02344284	1.37094
PPARGC1B	0.02126331	1.97519	TTI1	0.02344284	3.59392
NOSIP	0.02160183	1.90589	DFNB59	0.02357158	0.638213
SLC16A1	0.02164003	1.68624	AR	0.02385521	0.775211
LRIT3	0.02166928	1.87657	SEMA3D	0.0240264	0.713297
FOXK1	0.02166928	1.82421	CXCL12	0.02419763	0.11435
CDKN2C	0.02192525	0.646305	ASRGL1	0.02420579	1.39603
KIAA1549L	0.02197239	0.727649	SEL1L3	0.024245	0.776249
LHFPL5	0.0220226	12.5787	NCKAP1	0.02428726	0.521291
STAC	0.0220226	1.65178	SCAF4	0.02468026	1.71531

Gene	fcpv	MI	Gene	fcpv	MI
TMEM170A	0.0249456	1.79327	ARID5A	0.02804242	3.04939
HELZ	0.02524014	1.49454	NKX2-4	0.02812299	7.43286
CA5B	0.02535839	0.761045	TRIM2	0.02843345	0.896432
LRBA	0.02550196	0.893224	UQCR10	0.02904908	2.00118
FANCB	0.02566027	2.1831	HSBP1	0.02911882	0.478183
SLC35B4	0.02569192	0.664445	TENM3	0.0291947	0.881829
NEGR1	0.02569192	0.85723	OLFML1	0.02932859	0.539068
KDM5A	0.02569192	0.664445	DBF4	0.02939091	1.78179
MYRFL	0.02580933	2.76352	THEM4	0.02939091	1.78179
MELK	0.02585143	1.35719	KRIT1	0.0294538	1.95507
ZFHX4	0.0258598	0.74367	BMP7	0.02951875	0.732982
DNAAF2	0.0258598	0.589791	RICTOR	0.02951875	0.470846
HEG1	0.02592427	1.55688	PDE1A	0.02960015	0.619825
FAM13A	0.02616746	0.821127	TECPR2	0.02960015	1.46292
ARNT2	0.02624065	0.571737	DGKB	0.02960015	1.18879
FAM81A	0.0262582	1.56333	PAN3	0.02977013	0.590179
DOK6	0.02628111	1.27538	ZNF573	0.02977512	1.82966
ETV1	0.02635542	0.705033	RYBP	0.02978039	0.51641
CLIP2	0.02635542	0.705033	ZNF732	0.02983346	4.57407
ZSWIM5	0.02643266	0.684707	LBH	0.02988298	0.452629
CHTOP	0.0265846	0.369952	FOXE1	0.02989292	2.80683
CHD9	0.02670906	0.837829	TG	0.03009867	0.691394
PITPNM3	0.02678703	1.98212	HHAT	0.03016894	0.668965
PHF7	0.02688001	1.35487	SAFB2	0.03017331	0.564501
PTPRE	0.02700617	0.663689	RSBN1L	0.03030459	1.35677
MARK3	0.02700617	1.53834	AHCYL2	0.03041708	1.23914
SNX2	0.02711442	1.33993	PI4K2B	0.03049251	1.41664
DPY30	0.02718798	2.61377	DNAJC5G	0.03070215	0.285873
ZNF804A	0.02719773	0.72299	GLIS1	0.03070215	0.285873
REXO1	0.02742295	1.94054	HGF	0.03070215	0.285873
FANCA	0.02742295	1.79698	MTDH	0.03089212	0.675682
CACNA1D	0.02751994	0.595558	MSI1	0.03107451	1.61135
KCNH5	0.02757234	0.883822	FAM227B	0.03107451	0.71466
LRRC42	0.02761277	0.540833	CAD	0.03142095	2.6389
RBM27	0.02761277	0.540833	EPB41L4A	0.03142095	2.6389
TMEM45B	0.02780492	4.11667	ABCG1	0.03148896	0.152466
CRISPLD1	0.02791366	0.774697	POT1	0.03172401	2.35432
APELA	0.0279653	0.739059	XRCC3	0.03174775	3.28762
YTHDF2	0.02796797	0.584165	SNRNP70	0.03174775	3.28762
EIF4B	0.02802522	1.32525	MXI1	0.03206586	0.696591
PGBD1	0.02804242	3.04939	GAD1	0.03206586	0.259884

Gene	fcpv	MI	Gene	fcpv	MI
MAST2	0.03226998	0.794932	PTPN12	0.03625571	1.49158
OBFC1	0.03233967	1.83567	PLA2G4A	0.0363251	0.824279
KLF7	0.03241532	0.812999	CPSF2	0.03653985	2.28705
PPP4R4	0.03241874	0.744363	ZNF681	0.03653985	2.28705
TMEM200A	0.03250364	0.722182	FUT9	0.03677217	0.686077
PLPPR1	0.03250364	2.43952	CAPRIN2	0.03678057	0.546881
ICAM1	0.03250364	2.43952	CPNE5	0.03694398	1.69243
PSMD9	0.03250364	1.64747	ARHGAP24	0.03702577	0.812502
PAGR1	0.03254624	0.571738	ARRDC3	0.0372597	1.28205
JOSD1	0.03267916	1.49634	CLEC2A	0.03737446	0.673104
NOS1AP	0.03268624	1.73913	FSTL5	0.03760001	1.18276
PPP4R3A	0.03268624	1.73913	SLC30A5	0.03765197	0.496228
TMEM150C	0.03268624	1.47342	IL5RA	0.03765197	0.496228
NRF1	0.03268624	0.190582	EIF3K	0.03770902	2.35852
STRAP	0.03268624	0.228698	STIP1	0.03778048	2.53209
CHST15	0.03268624	0.228698	TXN2	0.03790471	0.524876
CSMD2	0.03268624	0.228698	PRPF39	0.03790471	0.524876
XRCC5	0.03268624	0.190582	LRPPRC	0.03792109	0.715394
AGR2	0.03285743	0.343047	TIMM23B	0.0380066	0.739302
NNT	0.03309787	0.763575	VPS50	0.03809848	0.643802
TPST1	0.0332903	1.52024	NPRL2	0.03825328	2.08818
CRADD	0.03348314	0.886157	RAB2A	0.03832329	1.22444
C16orf62	0.03348314	0.648265	ZNF117	0.03838058	11.4351
COL4A3	0.03390123	0.857213	NT5DC1	0.03838058	1.46242
LRRC8B	0.03403024	0.821634	SLC24A5	0.03838058	0.480263
RNH1	0.03412333	1.59759	QRFPR	0.03838058	11.4351
FAM65C	0.03414845	1.65405	GPX6	0.03838058	11.4351
FEZ2	0.03415554	1.29478	ZNF367	0.03863728	0.401766
CCDC122	0.03439459	0.435613	TSKU	0.03863728	1.39215
TMTC2	0.0346013	0.813317	CCDC6	0.03867208	1.43192
KCNIP1	0.0346208	0.548242	ZFP28	0.03886289	3.62114
SPATS2	0.0346612	1.3099	INTS12	0.03886289	3.62114
ATP8B3	0.03468751	1.944	STIM1	0.03900581	1.5623
GALK2	0.03471462	0.832102	VGLL3	0.03903648	0.667718
EFNB2	0.03486147	0.712416	RIMS2	0.03906699	0.888822
MYO5C	0.03540317	1.68294	ACOX3	0.03912414	1.74129
ZYG11A	0.03553314	2.22988	TFE3	0.03922178	0.734329
NR2C2	0.03575187	1.74016	MTHFD2	0.03982069	2.02317
AHI1	0.03584176	0.745118	FZD5	0.03982069	2.02317
ANKMY1	0.03584176	1.51158	RBM10	0.03982069	2.02317
CSRP3	0.03589166	0.669744	PTPN9	0.03985255	1.26311

Gene	fcpv	MI	Gene	fcpv	MI
RCL1	0.03994809	0.0952914	CHL1	0.04518521	0.660051
CALCR	0.04015807	0.694496	LGI2	0.04532509	0.536006
PA2G4	0.04028063	1.78503	RGS7	0.04534249	1.51111
RPH3AL	0.04053617	1.39957	USP51	0.04534249	0.421285
OSCP1	0.04080141	0.72188	PCDH18	0.04534249	0.676416
N6AMT2	0.04103656	1.46057	LDLR	0.0453771	1.5767
TNIP3	0.04103656	2.92233	FRMPD4	0.0453771	0.754679
ITM2C	0.04103656	0.763675	TMPRSS9	0.0454721	1.66956
HIP1R	0.04123737	1.93217	PSIP1	0.04574124	0.457394
IPMK	0.04129471	1.89397	ARRB1	0.04574124	1.53997
ALDH3B1	0.04129471	1.89397	NT5C3A	0.04582163	0.687625
FAM19A2	0.04171925	0.498974	NBPF20	0.04611172	0.801284
IQCK	0.04193694	0.796216	SYCP1	0.04620121	3.14468
SPN	0.04193694	0.127055	SLC25A16	0.04620121	1.29672
FCGR2B	0.04193694	0.127055	UBE2T	0.04620121	3.14468
GPR132	0.04193694	0.127055	C12orf40	0.04620121	0.693456
EIF4A1	0.04193694	0.127055	DNAJC8	0.04629118	6.86109
NAV1	0.0419761	0.766269	PKLR	0.04629118	6.86109
ANKRD17	0.04222211	1.35664	ZNF586	0.04629118	6.86109
ALDH2	0.04267253	1.31859	MRGPRX3	0.04629118	6.86109
MAX	0.0429848	3.88796	KLF1	0.04629118	6.86109
C5orf46	0.0429848	3.88796	ZNF763	0.04629118	6.86109
SACS	0.0429848	0.749957	C3AR1	0.04629118	6.86109
SLC35B3	0.04303064	0.742503	COL11A1	0.04635896	0.725545
CHAF1B	0.04327385	2.28705	C11orf73	0.04646505	0.767804
GRAP2	0.04354957	1.16779	FZD2	0.04679014	2.01261
CUX2	0.04376353	0.677912	MTHFD1	0.04679419	1.77248
RIT2	0.04387114	0.748009	NR4A3	0.04679419	4.28819
RHPN2	0.04387114	1.7886	ASB18	0.04679419	4.28819
PTGDR	0.04387114	2.55094	ZNF841	0.04679419	4.28819
CDS1	0.04387114	1.7886	TMEM117	0.04738403	0.820803
TRMT10B	0.04387114	1.7886	KLHL32	0.04772199	0.533625
CEP128	0.0438853	0.711487	RCN2	0.04773738	0.701511
PKP4	0.04392948	1.62503	CDKL5	0.04795214	1.36763
PON3	0.04392948	8.00458	FBXO31	0.04800271	1.23386
PREX2	0.04396022	1.54533	PRR5L	0.04800271	1.59732
DOT1L	0.04431236	1.4373	PCBD2	0.04816687	1.64253
SYNPO2	0.04431236	1.7153	UBAP2	0.04838494	1.48284
YTHDF3	0.04431236	0.733126	ALDH1A1	0.04844205	1.96034
PTPRB	0.0444333	0.403584	TUBA1A	0.04847748	1.84983
PBLD	0.04482582	1.27863	FAM227A	0.04851085	0.592403

Gene	fcpv	MI
PROX1	0.04864104	0.729745
FEN1	0.04875939	0.163357
SLC26A5	0.04899133	0.240735
PTMA	0.04899133	0.240735
TNIK	0.04920605	0.586399
APIP	0.04938965	0.800712
FRA10AC1	0.0495714	0.490065
RCBTB2	0.0495714	1.41262
MS4A5	0.04965464	5.33641
CEP44	0.04965464	5.33641
SBF2	0.04983925	1.11337
CHCHD2	0.04983925	0.393074
ATP11C	0.04983925	0.802465
PRELP	0.04984765	2.74445

6.2 B7H3 screen hits (FDR < 0.05)

Gene	fcpv	MI	Gene	fcpv	MI
WDR20	7.15E-144	0.227768	UBR5	1.29E-12	0.15607
USP14	6.70E-99	3.02291	L3MBTL3	1.29E-12	0.337278
CREBBP	3.08E-77	8.7161	GTF3C2	2.75E-12	0.15255
ZFX	9.81E-66	0.153234	CDK6	2.78E-12	1.90872
VPS29	4.34E-63	0.0130109	CARM1	3.72E-12	1.88784
DYRK1A	5.48E-63	0.163202	TIPRL	6.32E-12	6.16944
DACH1	9.55E-50	1.53799	AUTS2	6.32E-12	0.712742
UVRAG	4.19E-44	0.395667	RALGAPB	6.32E-12	3.69706
CUL3	3.24E-43	6.15487	RHOA	9.65E-12	0.287917
SP1	5.22E-39	0.141346	VPS35	3.79E-11	0.0237197
MBTPS2	2.71E-32	0.182319	TAOK1	1.33E-10	1.65312
ATP2C1	3.40E-32	2.28391	HSD17B12	3.23E-10	0.264988
DDX6	3.30E-31	10.1594	ADNP	4.06E-10	0.346662
KLF16	3.41E-29	5.65701	PICALM	5.53E-10	1.88973
RSF1	1.03E-26	0.426589	DPH6	5.84E-10	0.579812
PPP2R4	3.06E-25	3.43113	NAA35	1.08E-09	4.40915
MNT	3.46E-25	0.2814	CDK13	3.29E-09	1.94779
PBRM1	7.23E-24	1.74999	TRPM3	4.15E-09	1.26102
KDM2A	1.32E-23	0.382813	CREB1	4.63E-09	6.38556
UBE2L3	3.54E-21	4.79468	VPS26A	7.61E-09	0.173736
CNOT4	1.75E-20	0.263124	RQCD1	7.61E-09	4.4598
ACTR3	1.89E-20	0.188935	RAB7A	8.47E-09	0.0977911
UBE2H	2.73E-20	1.62824	MSI2	8.47E-09	1.52637
ACACA	4.82E-20	0.610832	ZNF711	1.38E-08	0.361746
PPP4R2	8.22E-20	5.91816	KDM1A	1.68E-08	0.347873
SPPL3	4.35E-19	0.149156	SCAF8	2.19E-08	2.53873
ARPC2	9.09E-19	0.116869	DICER1	2.44E-08	2.57165
CD276	1.09E-18	0.191487	SSR3	2.61E-08	0.172717
FBXO11	1.83E-18	0.129622	WAC	2.85E-08	3.57555
KIAA1033	7.21E-18	0.31463	DCAF7	4.29E-08	0.103224
EPC2	5.18E-17	3.65483	TMEM131	8.15E-08	1.94308
NARS2	1.68E-15	0.590908	TFAP2C	9.28E-08	1.91942
MECOM	1.14E-14	1.37018	TFDP1	9.97E-08	6.24362
RPRD2	3.19E-14	2.54569	ALG8	1.34E-07	0.47403
RPS25	5.76E-14	0.133774	HGS	1.84E-07	0.123869
UGP2	5.65E-13	1.70643	LRRC41	1.84E-07	2.83809
WHSC1	5.72E-13	0.389476	DYM	2.36E-07	1.21831
DHX29	6.63E-13	0.0857536	DBF4	2.47E-07	3.3833
SLC35A1	6.85E-13	10.9902	MRPS9	3.81E-07	0.365789

Gene	fcpv	MI	Gene	fcpv	MI
TLK2	4.04E-07	0.484449	SP3	4.41E-05	0.467745
CKS1B	4.06E-07	2.36113	FNDC3B	4.45E-05	0.461843
NAA30	5.51E-07	5.57465	ZBTB20	4.73E-05	1.11253
CAND1	5.71E-07	3.3064	MRPL23	8.37E-05	0.123871
ANKRD17	5.77E-07	0.524063	BCL11A	8.37E-05	1.61674
PIK3R4	7.49E-07	0.191609	ZMIZ1	8.62E-05	0.501654
PARN	7.52E-07	0.625383	MRPS27	0.00010278	0.521951
TAPT1	9.65E-07	0.365505	SSR1	0.00010564	0.264535
GMEB1	1.10E-06	2.6332	KIAA0196	0.00011151	0.222966
XPO6	1.26E-06	0.63218	ARID5B	0.00012369	1.19577
UBE2R2	1.38E-06	1.71129	NF1	0.00014107	1.32179
GPC3	1.50E-06	1.20319	VAC14	0.00014807	3.62349
SRD5A3	1.66E-06	0.318515	COMMD3	0.00017312	0.24774
MAPKAP1	2.15E-06	0.544208	TADA2A	0.00017312	0.398985
C16orf62	2.46E-06	0.321799	MBTPS1	0.00017766	0.240454
MERTK	2.92E-06	0.477759	ZZZ3	0.00017808	0.150654
WDR44	3.31E-06	1.73968	ACTR2	0.00018604	0.0445939
RANBP3	3.45E-06	2.18474	KLF9	0.00018951	1.52317
ARID4B	5.07E-06	2.13115	EDC4	0.00019265	4.3583
COMMD8	5.24E-06	0.226448	TRIP12	0.00019611	0.548353
DLG2	6.19E-06	1.129	ARPC3	0.00029248	0.154839
MPPED2	7.04E-06	1.25521	SYT1	0.00033154	1.13317
PYM1	7.30E-06	0.474935	NCOA2	0.00033263	1.2975
SRRD	1.02E-05	0.0359626	GPATCH4	0.00033462	0.384878
NASP	1.12E-05	4.30043	KLF6	0.00037878	0.135133
CSRP2BP	1.32E-05	0.162579	C1QBP	0.00041131	0.237199
C11orf30	1.62E-05	0.653824	ZNF148	0.00044857	0.566335
TRPS1	1.62E-05	1.33316	ABI1	0.00046926	0.624098
DCPS	2.06E-05	9.19801	SNTB2	0.00048975	0.544124
SUPT20H	2.35E-05	3.34479	FBRS	0.00056029	0.180785
CDKN2A	2.81E-05	1.66924	CAPRIN1	0.00056372	0.463681
SUCO	2.91E-05	0.337036	ZFR	0.00059276	2.93934
CMAS	2.97E-05	4.76375	SMARCA4	0.00059707	0.600657
NCKAP1	3.00E-05	0.261287	RAD51B	0.00076847	1.65949
OTUD5	3.01E-05	0.117351	PAK3	0.00082929	1.17128
ARID2	3.29E-05	1.64745	SAMD4B	0.00091679	4.87773
USP15	3.48E-05	1.9836	FBXL17	0.00092174	1.37551
DPH5	3.55E-05	0.294188	SFMBT1	0.00092174	0.553978
ASXL1	3.85E-05	0.468981	RAD54L2	0.00092174	0.553978
MBIP	4.04E-05	0.341002	ERF	0.0009402	1.83639
SLC35A2	4.35E-05	5.57457	PPAT	0.00098848	0.343024

Gene	Fcpv	MI	Gene	fcpv	MI
UBE4B	0.00099289	1.58072	ALG5	0.0047352	0.271913
DOCK1	0.00106236	0.491272	IGF2BP1	0.0047352	1.46062
DEAF1	0.00111104	2.42661	ANKRD11	0.0047352	0.661763
NSD1	0.00113759	0.634496	SPEN	0.00480216	1.38455
INPP4A	0.00120163	1.75207	IL1RAPL1	0.00505679	1.09325
GON4L	0.00121678	1.46709	LAMTOR2	0.00550189	4.61888
HNRNPR	0.00121678	1.69235	EXOC4	0.0055133	0.786563
TNRC6B	0.00121678	1.25916	TOX	0.00558157	1.16626
GADD45GIP1	0.00128906	0.119448	LRPPRC	0.00558157	0.673859
SEC63	0.00128906	4.12516	ARHGAP12	0.00572207	1.9169
SREBF2	0.00132437	0.634426	MLST8	0.00598728	0.343027
MRPL18	0.00132544	0.278709	CCNC	0.00600585	3.43763
SPCS1	0.00132544	0.278709	MRPS18B	0.00601533	0.371612
RPL29	0.00150022	0.387093	NAA38	0.00640374	3.12175
UGCG	0.00156478	2.95453	CDC25A	0.00640374	1.57304
TEN1	0.00200888	1.32278	C15orf41	0.00682053	1.59018
ADGRV1	0.00205171	1.13316	ARID1A	0.00692238	0.565483
RANBP1	0.00214158	0.492125	ATP5J2	0.00720927	0.192215
ZBTB14	0.00239751	3.08241	ZNF217	0.00720927	0.192215
SIAH1	0.00239751	1.57954	INPPL1	0.00723356	2.88565
CNOT6	0.00247115	2.49896	SCAP	0.00734948	0.325161
TADA2B	0.00247115	2.32542	TSC1	0.00734948	2.38911
NKRF	0.00270246	3.62346	E2F3	0.00740358	1.97956
TAF6L	0.00274748	3.13569	SSR2	0.00758967	0.247743
ADGRD1	0.00275716	0.295773	PRDM15	0.00769515	0.395586
SLC1A2	0.00275716	0.295773	COMMD2	0.00787325	0.0619365
ARPC4	0.00284339	0.0557427	LRRC1	0.00809533	1.15522
FLVCR2	0.00321617	0.431995	YES1	0.008475	0.569611
SMURF1	0.0032468	0.597879	MIB1	0.00856475	0.685384
B4GALT5	0.00336114	1.5802	TBC1D14	0.00857293	0.654877
DHX36	0.003384	18.9532	TMEM30A	0.00872636	0.617919
B3GAT3	0.00348327	2.3737	ATP5B	0.00898865	0.139357
MBNL1	0.00352285	0.760137	SEMA3E	0.00912609	1.15991
TET1	0.00358602	1.25398	KIAA0391	0.00947359	0.422285
BTLA	0.0036457	0.621177	ITM2B	0.00971364	1.92968
PTGES3	0.00365184	1.82726	CRKL	0.01009344	0.384426
LAMTOR5	0.00373301	2.10598	CDH1	0.01009344	0.547961
COMMD10	0.00390679	0.403924	ADSS	0.01021496	2.82006
RPS29	0.00417383	0.159264	CNTNAP2	0.01021496	0.871087
TASP1	0.00443042	0.702136	ZFP91	0.01035681	1.77447
TULP4	0.00469687	0.539986	EP300	0.01072113	0.524622

Gene	fcpv	MI	Gene	fcpv	MI
UBE2M	0.01095939	3.56769	INSR	0.029247	0.539811
MRPL3	0.01117478	0.254822	RAPGEF1	0.02993612	0.648144
TAF11	0.01117478	0.254822	CRAMP1	0.03029113	0.449531
GATAD2A	0.01118039	1.5957	FAM49B	0.03071413	1.47111
CNTNAP5	0.01133256	0.638687	SAMD1	0.03157797	0.123873
PHF21A	0.01170973	1.37397	YAF2	0.03261952	1.9187
FOXN3	0.0123312	0.809622	PCBP2	0.03261952	3.14199
RAB2A	0.0126929	1.38556	TTC4	0.03309554	0.0929052
MKL1	0.01293288	0.712727	ROBO1	0.03388709	1.07866
GIGYF2	0.0133118	0.675488	NCOA6	0.03479528	1.48949
SDHD	0.0133118	5.12853	PHF12	0.0350865	0.604941
SDHB	0.0147213	3.34471	THRB	0.03582973	1.3177
FAM198B	0.01536188	1.25696	MTPAP	0.03687985	0.074324
TSPEAR	0.01679817	0.522574	SYK	0.03795998	0.269102
DNAJC7	0.01725448	0.575104	NUP188	0.03795998	0.269102
PARVB	0.01725448	0.671932	CCDC22	0.03795998	0.269102
COMMD7	0.01945151	0.475662	RSU1	0.03845701	0.650306
PPP4R1	0.01971677	0.61776	FHIT	0.03845701	1.10312
SFMBT2	0.02295012	0.622557	ILF3	0.03862117	0.247745
SMARCC1	0.02359761	0.742131	MRPL40	0.03862117	0.193888
PIK3C3	0.02392584	0.286675	EFCAB6	0.03862117	0.247745
ST3GAL5	0.02407681	2.16015	TM2D2	0.03883905	0.222971
SIPA1L3	0.02414931	0.732865	SMARCA5	0.03883905	0.222971
WNK3	0.02425052	0.678126	RREB1	0.03898854	0.551547
MAML2	0.02425052	1.16975	HDAC8	0.04066018	0.598196
STRN3	0.02456097	0.634172	PAN3	0.0409725	1.80103
STK24	0.02463392	0.393473	NCOR1	0.04102516	1.49908
ATAD1	0.02563362	1.28769	ZNF793	0.04222722	0.557414
DAP3	0.02563362	0.185809	AEBP2	0.04222722	1.39369
TMEM180	0.02578911	2.60145	EIF4H	0.04236298	0.484711
GMEB2	0.02612663	1.91476	ABCC1	0.04236298	0.690864
UBE2G2	0.02612663	0.363536	TM2D3	0.04250381	0.318528
TM9SF3	0.02631211	2.02446	UIMC1	0.04250381	1.96577
PPP4R3A	0.02631352	1.84391	UBASH3B	0.04250381	0.530872
RFWD2	0.02644157	0.74529	HM13	0.04324946	0.409534
INPP5A	0.0276876	0.65287	ATRX	0.04379357	0.591341
MLLT10	0.02780567	0.782365	DIAPH1	0.04405073	0.639161
DLEC1	0.0278139	0.588624	GNAT3	0.04691413	1.18499
CDC42BPB	0.02844536	1.24729	ZNF367	0.04815677	0.380061
CCDC109B	0.02844536	0.694386	HNRNPA2B1	0.04863255	0.352057
HTR7	0.02844536	0.61507	C6orf99	0.04863255	0.64542
TRAF3IP2	0.04954013	1.48658			

6.3 NRP1 screen hits (FDR < 0.05)

Gene	fcpv	MI	Gene	fcpv	MI
NRP1	0	0.0169169	ZFAT	1.05E-22	2.40137
WDR20	1.22E-295	0.124642	VPS45	1.06E-22	4.82069
CREBBP	8.68E-220	0.0200599	CADM2	1.86E-21	1.34705
USP14	5.52E-183	3.20404	NF2	2.76E-21	5.32572
MBNL1	1.63E-108	4.18692	ADNP	4.19E-21	0.254118
MECOM	1.58E-91	1.98945	PIGL	1.06E-20	0.286056
VPS29	1.54E-67	0.0163735	TRPM3	2.70E-20	1.36079
ZEB2	5.75E-59	2.96017	GPC4	3.21E-20	0.354017
DICER1	4.66E-51	5.07841	PPP4R2	8.01E-20	3.90509
TFAP4	7.16E-51	0.143742	PICALM	1.85E-19	2.10738
ZBTB20	7.76E-49	1.33993	ARNT	2.70E-19	0.197975
MLLT10	2.27E-46	0.32881	PBRM1	8.08E-19	1.71193
CUL3	2.03E-44	0.228895	PIGU	1.68E-18	0.13537
BAZ1B	2.08E-44	0.283682	CELF1	1.68E-18	2.36236
GIGYF2	3.61E-42	3.37146	ADGRV1	2.99E-18	1.30059
EMC2	2.89E-41	9.60438	KDM2A	3.02E-18	0.469073
MED15	3.86E-39	0.123192	LRP1B	8.17E-18	1.26829
EXOC4	1.86E-38	1.92064	XPO5	4.83E-17	8.83445
ARID2	1.87E-38	4.02654	SMARCA4	6.75E-17	2.4373
SMARCC1	1.09E-37	2.49172	NARS2	1.39E-16	0.563329
ROBO1	4.57E-36	1.32553	EIF2AK4	1.57E-16	0.37927
PPP2R4	1.01E-35	3.16885	RPRD2	1.89E-16	0.407781
C11orf30	1.36E-34	0.430545	ZMYND8	1.89E-16	0.529889
WDR7	2.21E-34	3.51211	TIPRL	3.21E-16	8.52978
MBD3	4.12E-34	0.229702	SETD1B	5.82E-16	2.55778
DYRK1A	7.10E-31	0.226979	FOXP1	3.35E-15	1.41859
EPC2	2.56E-30	4.36695	CDK2AP1	4.16E-15	0.557306
ATF7IP	2.97E-30	0.394618	TLK2	1.52E-14	0.36617
HDAC9	4.24E-30	1.30759	SCAF8	2.92E-14	3.57554
MIB1	2.23E-29	2.61725	ZSWIM6	4.32E-14	0.491354
ACACA	1.21E-28	0.532035	TNS3	4.32E-14	0.630128
DOT1L	1.96E-27	0.232344	PPHLN1	3.02E-13	0.376238
TRIP12	2.17E-25	0.310768	NLGN1	4.13E-13	1.25213
CHIC2	2.95E-25	2.20977	FBXL17	5.22E-13	1.70575
PHF12	7.54E-25	0.270053	SETDB1	6.39E-13	0.223363
PIGP	8.43E-25	0.200425	DDX6	8.42E-13	3.28418
TAOK1	1.17E-24	1.83458	ILF3	1.18E-12	0.165349
TRPS1	1.18E-24	1.68215	MPDU1	1.74E-12	0.285375
SMARCE1	8.73E-23	4.4839	FHIT	2.09E-12	1.2278

Gene	fcpv	MI	Gene	fcpv	MI
L3MBTL3	2.10E-12	0.363072	SYT1	2.32E-09	1.1666
LIN28B	2.37E-12	0.501762	DGCR8	2.61E-09	19.8004
SOX5	2.66E-12	1.29867	ZC3HAV1	2.70E-09	0.487943
ARPC2	4.19E-12	0.174051	RALGAPB	3.27E-09	2.98048
WHSC1	5.79E-12	0.375777	TAF11	3.29E-09	0.15839
UBE3D	6.82E-12	4.13796	TM9SF3	3.67E-09	0.31463
IFNGR2	7.95E-12	0.186138	JAK2	6.05E-09	0.365503
SMAD4	7.97E-12	0.182754	RYR1	6.13E-09	0.683506
GRIK2	9.32E-12	1.46764	FRYL	6.52E-09	1.57119
EIF4B	1.01E-11	0.482758	CCSER1	7.05E-09	1.41205
HNRNPA1	1.57E-11	0.0196516	AP2B1	9.24E-09	2.00195
PARD3	1.58E-11	1.54197	PAK3	1.03E-08	1.22537
TAF4	2.47E-11	0.164383	TRHDE	1.08E-08	1.38805
SLIT2	2.67E-11	1.25981	KDM2B	1.25E-08	0.665826
TANC2	3.17E-11	1.17226	DLG2	1.58E-08	1.15734
CERS6	6.43E-11	2.28131	LRPPRC	1.59E-08	0.470548
TOX	9.72E-11	1.32096	NFIC	2.85E-08	0.607286
WAC	1.05E-10	4.02645	ERC2	3.14E-08	1.26102
ARID1A	1.12E-10	2.10692	ATRX	3.51E-08	0.434479
BCOR	1.21E-10	0.716285	FAM208A	4.55E-08	0.186487
CDK13	1.63E-10	2.12083	ALPK1	4.72E-08	1.47198
ARID1B	1.86E-10	1.49129	ACTR3	5.05E-08	0.420617
XPO6	2.18E-10	0.533821	THSD7A	5.15E-08	1.36723
EXT1	2.93E-10	0.411379	PAGR1	5.43E-08	0.292075
SLTM	3.72E-10	2.08081	C15orf39	6.27E-08	0.36675
R3HDM1	3.96E-10	0.50974	MAGI2	6.41E-08	1.22794
CDK6	4.23E-10	1.83922	PCDH9	7.23E-08	1.21026
KIAA1551	4.88E-10	0.238733	DDRGK1	7.42E-08	0.353717
GATAD2B	6.66E-10	0.503559	ZC3H4	8.37E-08	0.553289
SLC7A11	6.75E-10	1.5971	PIGK	1.40E-07	0.19892
B3GAT3	6.98E-10	0.220718	RANBP3	1.42E-07	2.56168
UCHL5	8.25E-10	4.36636	RAB7A	1.58E-07	0.152299
CTDNEP1	1.00E-09	0.209407	TNRC6B	1.59E-07	1.3353
MAP4K4	1.09E-09	1.84783	SEMA3E	1.62E-07	1.26679
SOX6	1.51E-09	1.35719	DPH6	1.91E-07	1.59487
PPP6R3	1.53E-09	1.70432	USP8	2.04E-07	3.43398
Sep-09	1.57E-09	0.639763	PCLO	2.05E-07	1.55824
DMD	1.65E-09	1.26153	ABCC1	2.07E-07	0.557712
CRAMP1	1.70E-09	0.26989	EXD3	2.12E-07	0.548814
TMED10	1.75E-09	0.251795	UHRF1	2.89E-07	0.472851
UBR5	1.98E-09	0.196179	DGKB	3.12E-07	1.49712

Gene	fcpv	MI	Gene	fcpv	MI
USP15	3.19E-07	2.07312	DROSHA	5.62E-06	4.07726
FOXP2	3.21E-07	1.68474	Mar-01	5.62E-06	1.24475
DACH1	3.55E-07	1.17844	AGPS	5.65E-06	1.2748
NRXN1	3.56E-07	1.23342	SLC2A13	6.11E-06	1.47345
GATAD1	4.52E-07	0.262582	MRPS18B	6.16E-06	0.243678
LRRTM4	5.10E-07	1.49935	ACLY	6.75E-06	3.04625
SIN3B	5.26E-07	0.156204	SIAH1	9.79E-06	0.560984
TM2D1	5.28E-07	0.321515	LSM12	9.91E-06	0.500563
KEAP1	5.56E-07	0.552699	SETD2	1.02E-05	0.299058
PARVB	5.68E-07	0.584287	DPY30	1.02E-05	5.65724
PMM2	6.04E-07	0.317463	PDE11A	1.05E-05	1.35959
PPFIA2	7.93E-07	1.44465	TAF3	1.05E-05	0.408512
SLC1A5	8.31E-07	0.505068	GPAA1	1.05E-05	0.0794615
VPS35	9.52E-07	0.050767	MMP24	1.11E-05	0.7398
UVRAG	1.00E-06	1.40191	TMED2	1.11E-05	0.157213
ZNF280C	1.17E-06	1.7738	PIGQ	1.25E-05	0.28023
GNG7	1.17E-06	0.689982	KLF12	1.47E-05	1.65068
MAP4K3	1.24E-06	1.26995	PHLPP1	1.49E-05	0.611855
TET2	1.34E-06	1.7293	REST	1.61E-05	1.95473
REPS1	1.63E-06	0.390151	NCOA3	1.62E-05	0.737301
MYO10	1.69E-06	0.80678	IRF2	1.76E-05	2.57029
LUZP2	1.98E-06	1.39722	MITF	1.86E-05	1.9779
TCF12	1.98E-06	1.30344	MED13L	1.87E-05	0.781257
STAG2	2.00E-06	0.541101	HNRNPF	2.06E-05	0.476268
HGS	2.08E-06	2.62851	MBNL3	2.13E-05	1.63771
TCF4	2.08E-06	1.3021	EPHA6	2.13E-05	1.2556
NEGR1	2.17E-06	1.37134	SIPA1L3	2.19E-05	0.69455
EYS	2.18E-06	1.2341	ZNF385B	2.33E-05	1.23992
KCND2	2.52E-06	1.37134	MNT	2.64E-05	0.68081
PLAA	2.52E-06	3.18472	UTRN	2.94E-05	1.18739
PRMT3	2.55E-06	0.665131	DNMT1	3.13E-05	0.349537
PIGX	2.57E-06	0.21251	NKAIN3	3.16E-05	1.31145
C15orf41	2.97E-06	1.71791	TM2D2	3.20E-05	0.135379
ITPR2	2.97E-06	1.2895	SLC35A2	3.20E-05	0.135379
NPRL3	3.31E-06	0.569367	TFAP2C	3.31E-05	0.527953
BMPR1A	3.54E-06	0.723683	PIGB	3.35E-05	0.291906
ROBO2	4.07E-06	1.28751	PRKAR1B	3.46E-05	0.471818
PPP6C	4.40E-06	4.69118	SORL1	3.57E-05	2.55493
ING3	4.55E-06	3.02087	TADA2A	4.24E-05	0.427881
ARID4B	5.24E-06	2.07151	AFF4	4.38E-05	2.4196
BRD9	5.33E-06	0.425158	TRIM71	4.99E-05	0.641091

Gene	fcpv	MI	Gene	fcpv	MI
ACTR2	5.04E-05	0.0870295	RNF146	0.00021376	4.19698
ELFN1	5.36E-05	0.617703	OTUD5	0.00021735	0.203068
GSE1	5.57E-05	0.456889	TMEM238	0.00022158	0.483377
WBSCR17	6.06E-05	0.140586	ISPD	0.00022158	1.4547
C1orf43	6.08E-05	0.617785	NELL1	0.00022306	1.16402
KDM5A	6.65E-05	0.510254	GALNTL6	0.00023159	1.32632
NAV3	6.70E-05	1.23672	RAB10	0.00023159	1.88316
PPP4R3A	6.80E-05	2.29642	FBXO8	0.00024988	1.94332
PAXIP1	7.43E-05	0.240474	CPA6	0.00025262	1.47646
CTNNA3	7.43E-05	1.18064	OSBP2	0.00027564	0.399472
FAM198B	8.29E-05	1.34017	POU6F2	0.00027665	1.14395
CCDC91	8.36E-05	1.22297	CDH2	0.00027766	1.39201
UBTF	8.70E-05	0.373376	ITSN1	0.00028867	1.35965
TM2D3	9.13E-05	0.226275	RBM27	0.00030515	0.367817
PTPRD	9.94E-05	1.20192	DENND1A	0.00034863	1.43476
STK11	0.00010735	0.328966	SFMBT2	0.00035367	0.612716
COG4	0.00010967	0.091381	SERBP1	0.00036786	0.21007
DEPDC5	0.0001108	0.523593	THAP4	0.00037401	0.631381
LOC339862	0.00011746	1.47542	RAPGEF1	0.00038319	0.568568
PTBP1	0.00012445	0.0380755	NCKAP1	0.00038957	0.3046
PRKCB	0.00013648	0.735122	PIGT	0.00039156	0.138456
ITGB5	0.00014774	0.49681	GADD45GIP1	0.00039156	0.138456
UNK	0.00014774	0.723645	LCOR	0.00041056	1.70593
RQCD1	0.00014774	2.19041	CKS1B	0.00042408	2.05291
TBCK	0.00014774	1.32091	PIBF1	0.00043396	1.36014
EPHA7	0.00014959	1.80494	RASIP1	0.00045907	0.619557
VPS50	0.00015643	1.94962	TRDN	0.00048803	1.3207
RALBP1	0.00016257	0.37567	RSF1	0.00050578	0.72337
MAZ	0.00016321	0.567452	CAMK2D	0.00051626	1.49055
HNRNPD	0.00016561	0.478178	SKI	0.00053344	0.41268
LRBA	0.00016587	1.20235	DNAJC2	0.00053783	2.93869
FCHO2	0.00017448	2.36315	MTF2	0.00054036	0.503242
MGA	0.00017977	1.55386	APCDD1L	0.00054196	0.788519
DEDD2	0.00018209	0.609171	LARP7	0.00055024	0.360546
ZNF566	0.00018445	0.445177	PIK3C3	0.00055496	4.97542
GLIS3	0.00018477	1.31505	HIRA	0.00057227	0.231077
KMT2A	0.00019264	2.37988	TASP1	0.0005949	0.678221
ATP2C1	0.00019451	1.38711	ADSS	0.0006481	2.78969
PHF20	0.00020086	0.489861	PRR12	0.0006481	0.44384
SH3BP2	0.0002023	0.689839	GTF2IRD1	0.0006481	0.510932
PPP3CA	0.00021376	1.29694	MORN3	0.00072534	0.620119

Gene	fcpv	MI	Gene	fcpv	MI
ATP1A1	0.00073412	2.19329	TSC1	0.00206949	0.454479
BNC2	0.00073844	1.29861	VWDE	0.00211997	1.76314
HNRNPL	0.00074229	0.612985	MINK1	0.00211997	0.617643
NMT1	0.00076344	0.278492	TLE2	0.00214677	0.692476
EIF3L	0.00076344	0.166147	GULP1	0.00214677	1.32524
KCTD8	0.00076344	1.64316	CHID1	0.00214677	0.555958
MTPAP	0.00076344	0.166147	TXLNG	0.00214677	2.03082
C1GALT1C1	0.00076344	0.278492	RSBN1L	0.00217011	1.58173
CENPT	0.00081752	0.732009	CTDSPL2	0.00218226	0.512613
USP22	0.0008477	0.467326	USP32	0.00229067	0.721818
TTN	0.00086619	1.5392	TMEM131	0.00234142	1.42502
TENM1	0.0008675	1.40774	CACNG8	0.00235016	0.435141
FOXM1	0.0009532	2.17588	TENM3	0.0023713	1.18992
PDGFC	0.00097013	1.68239	CRY1	0.00243266	1.86224
SLC38A11	0.00107046	1.38427	CALN1	0.00243662	0.294776
DENND1B	0.00109089	1.52771	CDK14	0.00243703	1.43337
PPM1G	0.00124437	0.413384	GPC6	0.00248112	1.21668
ATXN2	0.00124437	0.613187	ASXL3	0.00250564	1.63392
ALDH1A2	0.00125038	1.33676	INPP4A	0.00253096	0.609183
TICAM1	0.00130059	0.630934	DDX27	0.00262217	0.0609213
CDH10	0.00130059	1.39034	WDR48	0.00262217	0.0609213
CASP3	0.00131198	0.406132	PSMB10	0.0026391	0.599438
RPL29	0.00133908	0.152302	PTPRN2	0.00268541	0.594206
MRPS27	0.00139971	0.521196	RALYL	0.00278942	1.30428
PRR16	0.00139971	1.25763	LAMA2	0.00284784	1.26282
RBMS3	0.00141256	1.20131	CERS2	0.00287791	0.518942
SLC35B2	0.00141393	0.185411	MAP7	0.00290929	1.29541
IWS1	0.00141473	2.43697	EMP3	0.00295181	0.58818
UBAP1	0.00144969	1.70908	GRID2	0.00297945	1.24337
JAG2	0.00145725	0.579225	COL19A1	0.00306178	1.23491
C16orf72	0.00150501	0.522163	PLCB4	0.00306178	1.26367
MMP16	0.00165219	1.49547	MSRA	0.00306178	0.787375
B4GALT7	0.00169998	0.275124	DCBLD1	0.00320152	1.35451
MGAT4C	0.00170322	1.19823	FAT1	0.00328809	1.90552
ESRRG	0.00170433	1.2301	HIP1	0.00340474	0.637422
NSD1	0.00173629	0.666472	POLG2	0.00340474	0.365521
ANGPT1	0.00179338	1.19376	ABCA3	0.00340474	0.622237
TET1	0.00183785	0.798602	TMEFF2	0.00340522	1.41596
AIP	0.00193376	0.295371	HMBOX1	0.00345653	1.16654
CAPRIN1	0.00193376	0.57077	RFWD2	0.00351113	0.763033
VPS13A	0.00201718	1.74712	ADAMTSL1	0.00354778	1.17606

Gene	fcpv	MI	Gene	fcpv	MI
GGNBP2	0.00360445	0.649792	MIER1	0.00501966	1.43062
ZNF318	0.0036717	0.401813	IGDCC4	0.00501966	0.754287
ERF	0.00371646	0.604193	FN3K	0.00504582	0.679714
PRRG2	0.00371922	0.538356	ITGB8	0.00505768	1.71527
TSC2	0.00371922	0.270758	PPFIA3	0.00521583	0.677957
MBTPS2	0.00379881	1.72621	C16orf62	0.00523321	0.543136
SH2B1	0.00382492	0.66363	ADGRB3	0.00525768	1.32163
SREK1IP1	0.00384689	2.0786	ETNK1	0.00529371	1.72137
GLTSCR1	0.00390912	0.439977	AGO2	0.00529371	1.99239
PIK3R2	0.00393161	0.599033	POLR3B	0.00529371	0.0937248
PTPN23	0.00398946	4.46771	IFNGR1	0.00529371	0.0937248
DAZAP1	0.00403142	0.42271	MORC3	0.00529371	0.503249
VCL	0.00406997	0.763457	MEIS1	0.00531515	1.32124
LRFN5	0.00406997	1.32529	NKRF	0.00537195	0.304603
GTDC1	0.00408437	1.37301	TAF12	0.00537195	0.304603
CNTN1	0.00409618	1.23725	CSMD3	0.00537195	1.16981
CLIP2	0.00412574	0.664559	PDXK	0.00548124	0.646229
CHORDC1	0.00413834	2.80249	RCC2	0.00551652	0.472654
AP3B1	0.00420709	1.48773	C10orf95	0.00558699	0.598113
TBCD	0.00420709	0.414775	PPP1R21	0.00579791	1.93435
TRIM33	0.00420709	0.618415	TRIQK	0.00579791	1.25042
ANK2	0.00420709	1.53138	TBC1D16	0.00579791	0.78218
PDE4A	0.00420709	0.662306	ZNF592	0.00584968	0.579032
FAM13A	0.00422044	1.31795	DNAH7	0.00591285	1.71966
CIRBP	0.00426136	0.557345	C17orf89	0.00604506	0.467778
MED16	0.00428103	0.257741	USP7	0.00616567	0.542331
MYLPF	0.00428347	0.572639	MORC2	0.00632097	0.0553829
WDR82	0.00430806	0.169225	MPHOSPH8	0.00632097	0.0553829
GABRB1	0.00437833	1.69046	RAC1	0.00647757	0.304603
CNTNAP4	0.00440376	1.33702	AKAP8L	0.00652358	0.427737
SKP2	0.00442617	1.74072	EBF3	0.00653575	1.30289
OLA1	0.00446765	1.62957	C19orf45	0.00653575	0.598012
HN1L	0.00448839	0.555636	DLG3	0.00662497	0.711603
WWTR1	0.00450097	0.82583	PPP4R4	0.00662497	1.4748
YBEY	0.00451334	0.678979	CLCN3	0.00668697	1.4993
FBXO30	0.00454716	5.48308	SNX13	0.00683885	1.69447
PLCB1	0.00487255	1.2476	TANGO6	0.00690794	0.32491
PIGS	0.00487278	0.374894	NEK9	0.00690832	0.438624
KIAA0391	0.00487278	0.45413	MEF2C	0.00698955	1.3772
CALCR	0.00490175	1.67979	MRPL48	0.00717132	0.342678
CCDC18	0.00499006	1.73931	DDB2	0.00721106	0.706532

Gene	fcpv	MI	Gene	fcpv	MI
ZNRF2	0.00721177	1.16117	CDCA4	0.01066332	0.468616
ADCY9	0.00728985	0.785041	GNB1	0.01066332	0.641492
OTUB1	0.00735872	0.410857	MAGI1	0.01066332	1.38216
ZNF804A	0.0075025	1.55917	C19orf54	0.01086098	0.649501
COBLL1	0.00754356	1.36851	NTMT1	0.01086196	0.678491
RNF207	0.00767015	0.66898	COG8	0.01086196	0.516895
PCOLCE	0.007863	0.524585	DGAT1	0.01092448	0.411212
ST3GAL3	0.00812355	0.861371	ZNF292	0.01098961	1.35191
DACH2	0.00812982	1.19484	HYPK	0.01098961	3.74243
LIAS	0.00813075	0.536092	ALG8	0.01098961	0.60316
AHCY	0.00813075	0.536092	C7orf50	0.01115369	0.676455
MYO1C	0.00830513	0.679202	RBL1	0.01117888	0.715854
G2E3	0.00832553	1.82773	CBLB	0.01127471	1.46524
SNTG1	0.00832553	1.17234	PRRC2A	0.01141476	1.81419
SNRPA	0.00833343	1.94299	PUS1	0.01155796	0.453661
SGF29	0.00838095	0.378694	ANKLE1	0.01192539	0.56462
INPP5A	0.00846679	0.689759	ST18	0.01192587	1.15537
TEKT5	0.00846679	0.702205	MCC	0.01200143	1.30132
CLUH	0.00855089	0.504492	ANKRD13C	0.01205809	1.53296
KLHL1	0.00870346	1.7	THOP1	0.01216148	0.530872
EPC1	0.00892373	1.2011	RABIF	0.01220421	1.85745
CDKN2A	0.00920058	1.43768	STK26	0.01234155	1.48929
CNTN6	0.00922809	1.3305	PA2G4	0.0125249	0.527365
CUX1	0.00925943	0.710706	DPM3	0.0125249	0.20307
AKT1S1	0.00931471	0.672717	MUM1	0.0125249	0.727847
HMCN1	0.00938676	1.73912	ALX1	0.0125249	1.64966
CDK8	0.00944983	2.11058	TNPO2	0.01253476	0.722706
IFT57	0.00955368	2.32091	SAV1	0.01258326	1.6396
ZCCHC6	0.00970776	1.7227	PALM3	0.01259704	0.456901
FEM1A	0.00983507	0.49562	SRSF6	0.01263351	0.0761518
ADGRL2	0.00997631	1.52621	DYNC1I1	0.01270442	1.29555
GLG1	0.01009726	0.64863	CDH6	0.01270442	1.40536
PIGM	0.01016312	0.315885	DCBLD2	0.01275014	2.19855
NDUFS3	0.01044048	0.27922	DIAPH3	0.01278292	1.53987
SLC35A1	0.01044048	0.27922	ZNF384	0.01286214	0.482763
FILIP1	0.01049356	1.39207	NRTN	0.01286214	0.162456
NUP210	0.01051888	0.614629	CACNA1F	0.01286214	0.0609213
TIPARP	0.01057894	2.34556	ALKBH8	0.01286214	1.93216
POLRMT	0.01057894	0.101535	ATAD1	0.01286214	1.31461
IRF1	0.01057894	0.101535	SEC16A	0.01286214	0.0609213
ZFHX4	0.01057894	1.46938	GLI3	0.01303158	1.31169

Gene	fcpv	MI	Gene	fcpv	MI
ARIH2	0.01306784	0.65398	UBE4B	0.01710191	1.40172
RSRC1	0.01308499	1.62466	CUL5	0.01714655	0.548278
HS3ST4	0.01315377	0.190378	FGD4	0.01725627	1.75158
HNRNPA2B1	0.01315377	0.406136	PER3	0.01727663	0.690409
PLD6	0.01326431	0.690644	USP25	0.01727663	1.41137
SGMS2	0.01340493	1.29791	MCF2L	0.01755198	0.758757
ALAS1	0.01372012	0.261089	ATF7IP2	0.01759163	0.514669
GATC	0.01372012	0.261089	CHCHD2	0.01768715	0.338448
MYT1	0.01398267	0.720197	EMC1	0.01792066	5.68613
ZNF84	0.01404494	0.477805	NADK	0.01792066	0.714856
FREM2	0.01428842	1.32703	FHOD1	0.01818188	0.595805
MRPS25	0.01445072	0.140587	GAK	0.01818188	2.98524
PMAIP1	0.01445072	2.15772	ZNF410	0.01822215	0.578737
GPBP1	0.014537	0.596368	SGMS1	0.01822215	1.5197
HIRIP3	0.01472298	0.571591	SETD5	0.01822215	1.6781
UNC13A	0.01472782	0.552338	RBM18	0.01843128	2.02354
TRAT1	0.01476402	1.5107	ETV1	0.01849168	1.50675
BCL7C	0.01497913	0.789073	DDAH1	0.01849168	1.28423
PTEN	0.01513432	1.53697	SNX16	0.01849168	1.28423
LARS2	0.01522363	0.538566	FIGN	0.01849868	1.29379
ADGRL3	0.01525639	1.22273	SOHLH2	0.01865134	1.35778
GUCD1	0.01532438	0.52217	LMF1	0.01870833	0.516271
AGFG1	0.01532438	2.47502	HMOX2	0.01870833	0.731572
DLG5	0.01557443	0.615107	MRPL3	0.01870833	0.276913
ADAM18	0.01570949	1.34546	SNX4	0.01870833	0.516271
GSPT1	0.01589486	0.535356	MRPL12	0.01870833	0.276913
PGAM5	0.01589486	0.535356	CNOT10	0.01870833	0.276913
MRPS9	0.01597424	0.51782	HN1	0.01873279	0.6025
VAV3	0.01625952	1.82773	ZNF708	0.01885783	0.406136
MACROD2	0.01627926	1.15408	TMEM132C	0.01885783	0.406136
MAU2	0.01627926	0.243684	PRKCZ	0.01885783	0.406136
EPHA3	0.01640499	1.21094	FAM168A	0.01886595	0.723215
AFF1	0.01640803	1.21594	SNCAIP	0.01892111	1.31101
MTA1	0.01641806	0.570639	FAM195A	0.01903199	0.59535
ABHD17C	0.01647204	0.763003	WNK2	0.01914314	0.511293
PARN	0.01647204	1.26262	AKAP6	0.01918987	1.2947
ERBB4	0.01647204	1.30557	SLC1A2	0.01956341	2.20485
MEPCE	0.01665138	0.400335	MRPL15	0.01964391	0.110766
ABCA2	0.01665138	0.400335	NDUFV1	0.01964391	0.110766
UBE2E2	0.01692497	1.32242	DENND5A	0.0200469	0.787127
MYO19	0.01700434	0.602644	LRRC8B	0.02014889	1.25461

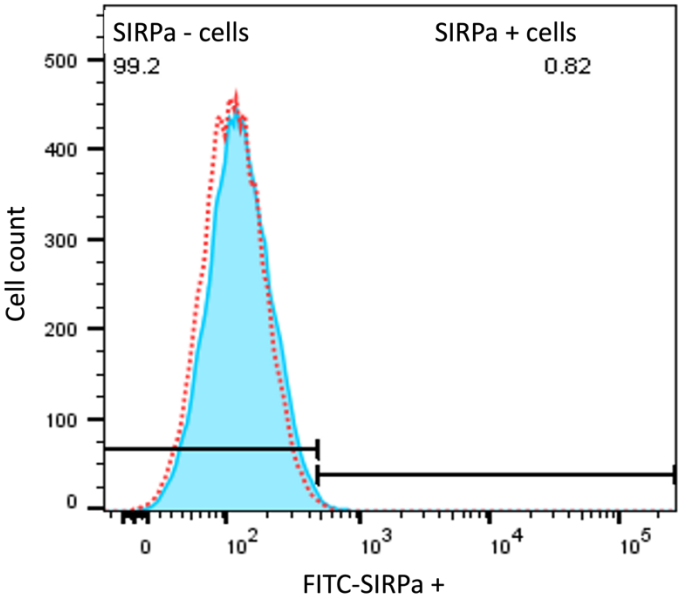
Gene	fcpv	MI	Gene	fcpv	MI
CDC42EP1	0.02046261	0.741948	BAZ2A	0.02479254	0.632852
ZDHHC8	0.02067055	0.432856	KMT2E	0.02487012	0.803613
FSCN1	0.02070765	0.61554	KCTD17	0.02528883	0.0676904
SGCZ	0.02073482	1.25178	COA5	0.02528883	0.0676904
DPYD	0.02073482	1.35829	TXNRD2	0.02540688	0.708935
CADPS2	0.02103495	1.45242	HNRNPM	0.02542847	3.04616
RBFOX1	0.02108076	0.445759	RAD23B	0.02542847	2.57752
MYOM2	0.02108076	0.445759	SCAMP5	0.02550514	0.369876
PPM1H	0.02120758	1.27199	RIMS1	0.02563138	1.39322
SPATA2L	0.02121371	0.365524	SSBP3	0.02568809	0.62747
RAB3A	0.02121371	0.507668	NOVA1	0.02588782	1.38703
ZNF268	0.02121371	0.328035	LINGO3	0.02608182	0.464155
DPP10	0.02123075	1.15107	CHCHD3	0.02621774	0.473825
FAM184A	0.02141236	1.798	UFC1	0.02633734	0.609196
MRPL18	0.02141236	0.348118	ZNF121	0.02633734	0.522172
SPINT2	0.02141236	0.348118	CORIN	0.02633734	1.5429
ZNF28	0.02151252	0.17406	FBN1	0.02640744	1.45196
CNEP1R1	0.02151252	0.17406	PPM1L	0.02650527	1.59927
BTBD10	0.02181331	1.53413	PIGV	0.02653443	0.615745
INSR	0.02241516	0.650846	FAM133B	0.02656363	3.19846
GAPDHS	0.02247711	0.523699	SLC25A40	0.02660692	1.50235
TMEM161B	0.02247711	1.77234	SUFU	0.02665675	1.63866
ZNF445	0.02267393	0.437377	RALGAPA1	0.02666645	1.42159
UNC13C	0.02285762	1.27832	MET	0.02698038	1.20885
NFIB	0.02289404	1.18962	DEAF1	0.02715163	0.586063
ITGB4	0.02289404	0.609195	EFNA5	0.02729869	1.1556
NXN	0.02296319	0.797568	C3orf38	0.02752933	1.92925
HNRNPLL	0.02296319	1.37181	PLOD2	0.02752933	1.53874
PDCD10	0.02336741	2.52397	ATXN7	0.02752933	1.31601
KLC1	0.02354117	0.748782	PVRL2	0.0277312	0.760888
LZTR1	0.02354117	0.577551	SCAP	0.0277312	2.69078
SIRT1	0.02367051	1.58583	HPD	0.0277312	0.705765
WBSCR16	0.02370567	0.304604	PIGN	0.02787066	0.550245
ASB3	0.02393167	0.724771	PRR25	0.02787066	0.553817
SPIN1	0.02399771	0.470748	CCNC	0.02793649	4.02091
SLC39A11	0.0240349	0.646273	TSPEAR	0.02818954	0.494977
RERE	0.0240349	1.20909	ZNF114	0.02843077	0.740742
GLA	0.02406561	2.24455	UBAP2	0.02843077	0.615965
ZNF263	0.02422093	0.42809	UQCRC2	0.02847763	0.250851
FAF2	0.024452	0.256509	SAMD1	0.02847763	0.250851
ERBB2IP	0.02462463	1.4823	KAZALD1	0.02847763	0.77416

Gene	fcpv	MI	Gene	fcpv	MI
IER2	0.02890132	0.708872	CCNJL	0.03540851	0.399136
DNAAF2	0.02904715	1.7008	DST	0.03542352	1.1314
RBPMS	0.02911498	1.20022	NDUFS2	0.03567502	0.649424
STAT3	0.02955867	0.799018	LHFP	0.03567502	1.28563
EYA4	0.02960612	1.40414	ZNF398	0.03567502	0.767891
SRGAP1	0.02968215	1.2533	PPP1R9A	0.03583802	1.27549
VAV2	0.03017952	0.739721	SLC2A4RG	0.03583802	0.533051
CAD	0.03017952	0.361012	TUBA1C	0.03602246	0.809635
PPP6R1	0.03017952	0.513641	FANCL	0.03604192	5.27997
FIBP	0.030403	0.448888	EIF5B	0.03622472	0.18745
GRIN2B	0.03080701	0.228454	CEBPZ	0.03622472	0.18745
SIGMAR1	0.03090169	0.584163	C22orf24	0.03622523	0.547248
RAP1A	0.03137435	1.54782	DDX10	0.03622727	1.77962
SNAP23	0.03142491	1.98566	UBXN7	0.03645467	0.609197
MYADM	0.03192367	0.481696	OR5AC2	0.03645467	0.121843
ATP8A1	0.03192367	1.15593	CSNK1G2	0.03651454	0.560072
TMCO6	0.0321222	0.424598	ARID3A	0.03651454	0.560072
SEC14L1	0.0321222	0.764959	PET117	0.03676571	0.344335
RADIL	0.0321222	0.424598	MRPL23	0.03691711	0.27076
KLF3	0.0321222	1.7308	EIF3K	0.03691711	0.365525
ISL2	0.0326368	0.704972	TAF13	0.03691711	0.27076
SCCPDH	0.03275079	0.549279	PLXDC2	0.03698405	1.12333
ZNF382	0.03285993	0.439982	OGDH	0.03706212	0.217576
PAWR	0.03285993	1.36874	DCP1A	0.03706212	0.418829
SPNS1	0.03317653	0.288573	NUP155	0.03706212	0.217576
SPATA5	0.03317653	0.288573	MRPS5	0.03706212	0.217576
PRKRIR	0.03332811	1.86579	ASH2L	0.03706212	1.54999
SLC35F1	0.03350478	1.39462	ATP6V1A	0.03706212	3.30725
SLC25A36	0.03393262	1.79479	CYB5R4	0.03706212	3.30725
KDM5C	0.03393262	0.412688	COL4A6	0.03728988	1.40794
EP300	0.03400151	0.639353	BTG4	0.03731318	11.5753
KLHL15	0.03405042	0.691866	REEP3	0.0373484	1.91174
ELOVL6	0.03405042	0.78685	C19orf48	0.03793313	0.582713
RAB26	0.03419894	0.685339	UBE2K	0.03815833	0.650596
YLPM1	0.03419894	2.26771	C12orf29	0.03820562	3.55384
AMOT	0.03436914	1.70587	IPMK	0.03839233	2.65846
VPS37B	0.03447638	0.832673	AMBN	0.03855463	3.89907
DMXL1	0.03453704	1.28446	SLC8B1	0.03855463	0.523915
CPNE7	0.03477123	0.562338	UQCRC1	0.03875521	0.152303
FOLR2	0.03491973	8.52914	LARP1B	0.03875521	1.45578
DEFB123	0.03536386	2.10463	BCKDHB	0.03885123	1.52312

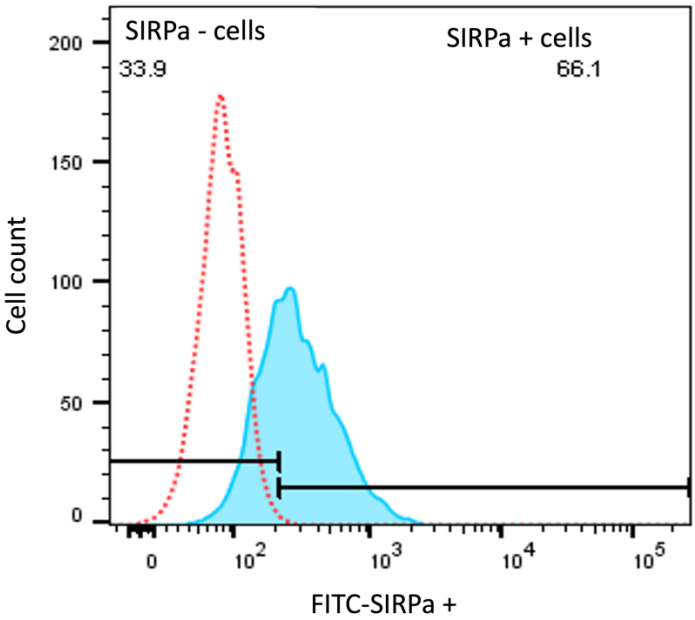
Gene	fcpv	MI	Gene	fcpv	MI
MOGS	0.0389275	0.406138	MLIP	0.04327001	1.48274
ZNF628	0.03934487	0.435147	BICC1	0.04327001	1.48274
C9orf135	0.03936281	1.25961	SLC7A5	0.04327001	0.702912
HSD17B12	0.03936281	0.530231	INTU	0.04344714	1.36743
WDR45	0.03938793	0.696218	SPOP	0.04344714	1.36743
KCNK2	0.03950827	1.18143	EML6	0.04408682	1.24642
RBM10	0.03999786	0.500901	GIN1	0.04435193	1.53635
EFR3A	0.03999973	1.46352	ATP5G2	0.04441816	0.719949
UBE2D1	0.04013177	1.33961	CRYBB1	0.04470959	0.26653
WDFY3	0.04013177	1.32178	TPM4	0.04507357	0.701227
SQSTM1	0.04013177	0.745879	ZBTB4	0.04507357	0.755163
TFG	0.0401578	0.472134	RBM6	0.04566316	1.34276
PHYKPL	0.0401578	0.609198	AMMECR1	0.0458292	1.32731
GAREM	0.0401578	1.30077	CCR10	0.04626998	0.635975
EPHA5	0.0401578	1.208	SULF2	0.04636219	0.591283
FDX1	0.0401578	0.472134	CTBP1	0.04636219	0.591283
GALNT11	0.0401578	0.46102	TGFB1	0.04649414	0.630204
ASXL1	0.04037096	0.635683	COX6B2	0.04660497	0.443059
GALE	0.04041669	0.391633	ARMC5	0.04660497	0.581084
NECAB1	0.04049591	1.30878	ZNF771	0.04687553	0.569898
YDJC	0.04060833	0.671145	SEMA3D	0.04687553	1.40681
NEDD4L	0.04082861	0.876695	CIR1	0.04690756	2.97
BTLA	0.04103366	1.44461	C21orf58	0.04712376	0.600739
GPATCH8	0.04113001	0.640597	EZH2	0.04728611	0.49844
IGF2BP1	0.0412544	0.749324	RAB5C	0.0473723	1.67879
ZFHX3	0.04130711	0.885096	CHMP4B	0.04738273	0.0761518
RASAL2	0.04130711	1.30245	PPA1	0.04738273	0.0761518
VPS33A	0.04130711	1.75156	PIK3R6	0.04738273	0.0761518
CARS2	0.04155602	0.541513	INTS5	0.04738273	0.0761518
SRRM2	0.04192414	0.332296	KIF17	0.04738273	0.609199
FUT9	0.04194762	1.48597	TSEN34	0.04738273	0.0761518
RANBP10	0.04216813	0.520361	SYDE1	0.04738273	0.456904
FAM172A	0.04228246	1.20256	POLE2	0.04738273	0.0761518
WAPL	0.04228246	0.355372	ZNF638	0.04760802	0.591542
HTR7	0.0423377	1.59664	ALDH3A1	0.04765149	0.616813
CACHD1	0.04236344	1.31351	MATK	0.04765149	0.616813
PTPRA	0.04291526	0.785299	LAMTOR4	0.04859223	0.58151
PKNOX1	0.04302916	0.616627	HMMR	0.04897099	1.41961
SIN3A	0.04302916	0.759465	YEATS2	0.04938523	0.554809
ZNF74	0.04302916	0.651003	ABHD13	0.04943073	3.13318
CWC27	0.04323823	1.55591	NECAB3	0.04945985	0.657932

Gene	fcpv	MI
ELAVL3	0.04953402	0.304605
ERAL1	0.04953402	0.304605
MBNL2	0.04978929	1.27082
CHD3	0.04978929	0.779564

6.4 **SIRPa surface expression was not detected in HAP1 cells** Surface expression of SIRPa protein levels was determined using flow cytometry, THP-1 monocytic cells were used as control to determine antibody specificity.



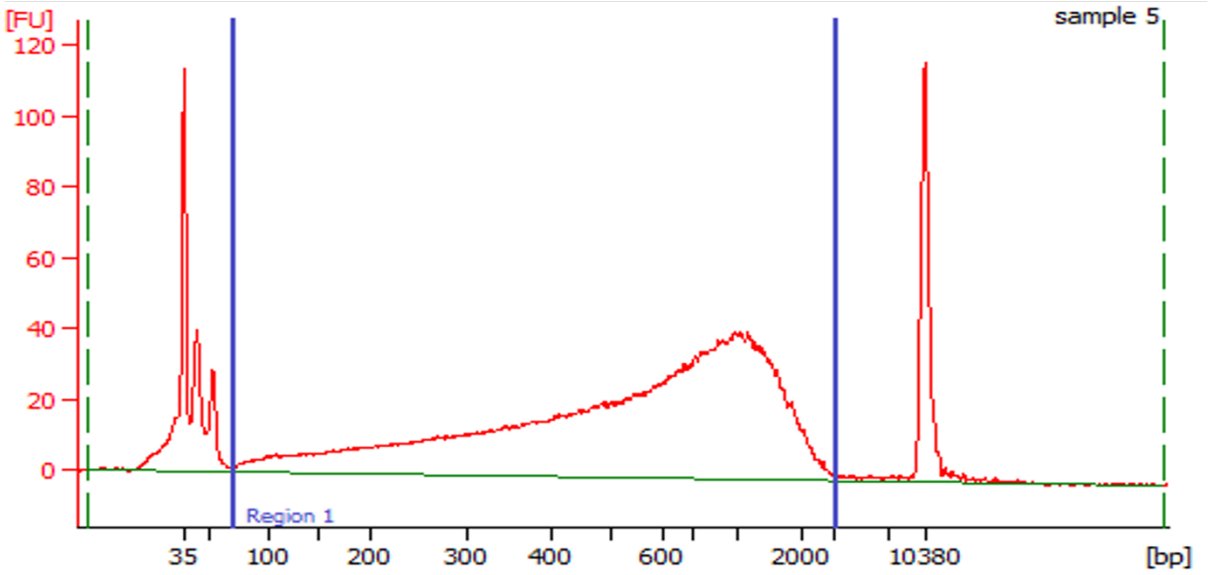
HAP1 cells



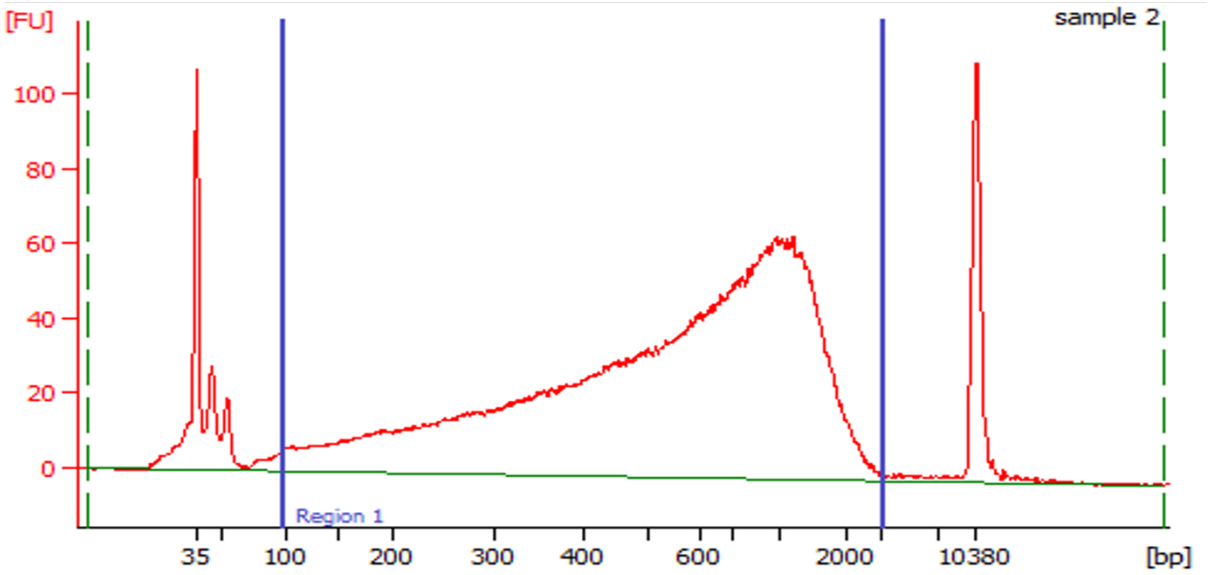
THP-1 cells

6.5 **Size distribution of DNA library from PVR CellSeq screen** (bp – base pairs, FU- Fluorescence unit)

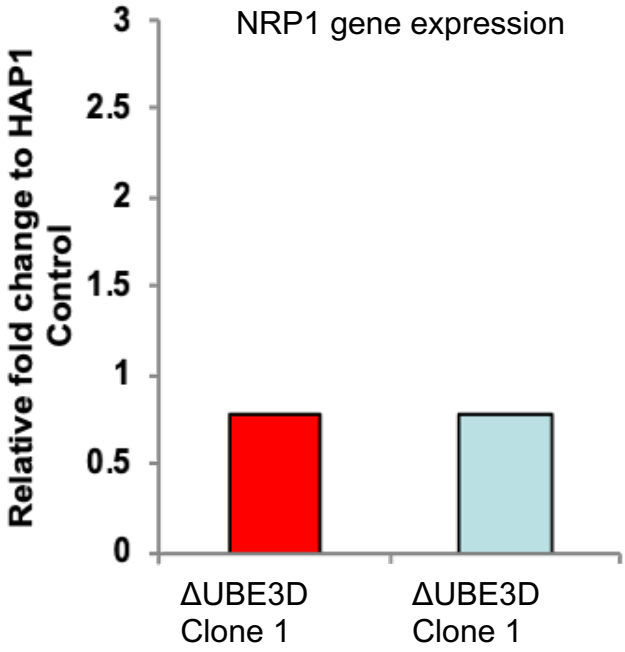
DNA from low PVR expression sorted population



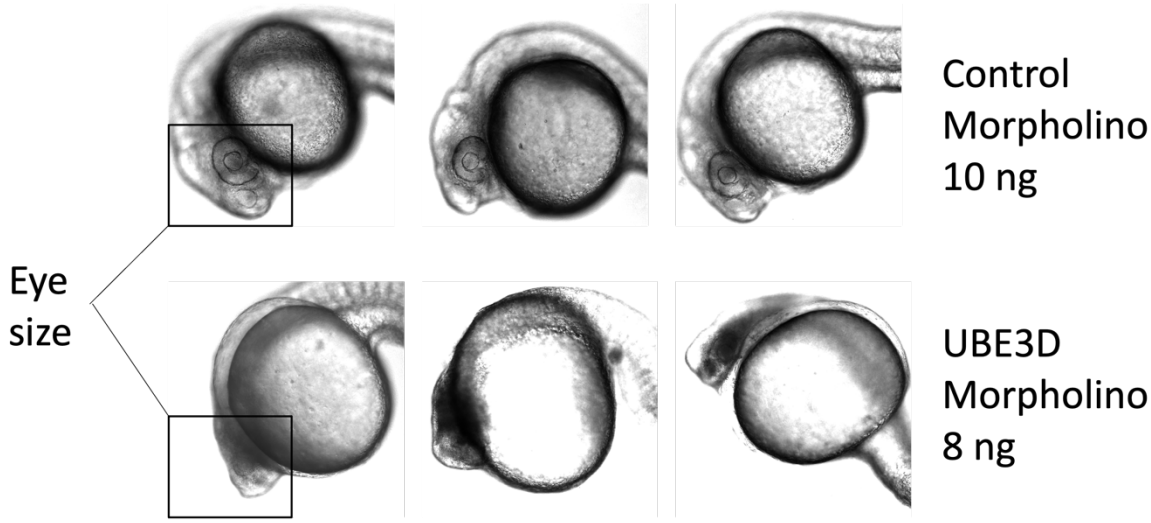
DNA from high PVR expression sorted population



6.6 UBE3D does not affect NRP1 mRNA levels (qRT PCR mRNA levels of NRP1)



6.7 **UBE3D affects zebrafish eye development** 6 ng Morpholino targeting UBE3D and were injected into 1- to 2-cell stage tg(fli1:GFP) zebrafish embryos, 10ng non-targeted Morpholino was used as control and eye size was captured using Zeiss LSM 710 confocal



Bibliography

1. Chen DS, Mellman I. Oncology meets immunology: the cancer-immunity cycle. Immunity. 2013;39(1):1-10.

2. Wellenstein MD, de Visser KE. Cancer-Cell-Intrinsic Mechanisms Shaping the Tumor Immune Landscape. Immunity. 2018;48(3):399-416.

3. Leach DR, Krummel MF, Allison JP. Enhancement of antitumor immunity by CTLA-4 blockade. Science. 1996;271(5256):1734-6.

4. Iwai Y, Ishida M, Tanaka Y, Okazaki T, Honjo T, Minato N. Involvement of PD-L1 on tumor cells in the escape from host immune system and tumor immunotherapy by PD-L1 blockade. Proc Natl Acad Sci U S A. 2002;99(19):12293-7.

5. Huang PW, Chang JW. Immune checkpoint inhibitors win the 2018 Nobel Prize. Biomed J. 2019;42(5):299-306.

6. Pardoll DM. The blockade of immune checkpoints in cancer immunotherapy. Nat Rev Cancer. 2012;12(4):252-64.

7. Krummel MF, Allison JP. CTLA-4 engagement inhibits IL-2 accumulation and cell cycle progression upon activation of resting T cells. J Exp Med. 1996;183(6):2533-40.

8. Parry RV, Chemnitz JM, Frauwirth KA, Lanfranco AR, Braunstein I, Kobayashi SV, et al. CTLA-4 and PD-1 receptors inhibit T-cell activation by distinct mechanisms. Mol Cell Biol. 2005;25(21):9543-53.

9. Keir ME, Francisco LM, Sharpe AH. PD-1 and its ligands in T-cell immunity. Curr Opin Immunol. 2007;19(3):309-14.

10. Ascierto PA, Marincola FM. What have we learned from cancer immunotherapy in the last 3 years? J Transl Med. 2014;12:141.

11. Chae YK, Arya A, Iams W, Cruz MR, Chandra S, Choi J, et al. Current landscape and future of dual anti-CTLA4 and PD-1/PD-L1 blockade immunotherapy in cancer; lessons learned from clinical trials with melanoma and non-small cell lung cancer (NSCLC). J Immunother Cancer. 2018;6(1):39.

12. Pennock GK, Waterfield W, Wolchok JD. Patient responses to ipilimumab, a novel immunopotentiator for metastatic melanoma: how different are these from conventional treatment responses? Am J Clin Oncol. 2012;35(6):606-11.

13. Shih K, Arkenau HT, Infante JR. Clinical impact of checkpoint inhibitors as novel cancer therapies. Drugs. 2014;74(17):1993-2013.

14. Wolchok JD, Hoos A, O'Day S, Weber JS, Hamid O, Lebbe C, et al. Guidelines for the evaluation of immune therapy activity in solid tumors: immune-related response criteria. Clin Cancer Res. 2009;15(23):7412-20.

15. Zaretsky JM, Garcia-Diaz A, Shin DS, Escuin-Ordinas H, Hugo W, Hu-Lieskovan S, et al. Mutations Associated with Acquired Resistance to PD-1 Blockade in Melanoma. N Engl J Med. 2016;375(9):819-29.

16. Marin-Acevedo JA, Kimbrough EO, Lou Y. Next generation of immune checkpoint inhibitors and beyond. J Hematol Oncol. 2021;14(1):45.

17. Das M, Zhu C, Kuchroo VK. Tim-3 and its role in regulating anti-tumor immunity. Immunol Rev. 2017;276(1):97-111.

18. Andrews LP, Yano H, Vignali DAA. Inhibitory receptors and ligands beyond PD-1, PD-L1 and CTLA-4: breakthroughs or backups. Nat Immunol. 2019;20(11):1425-34.

19. Ni L, Dong C. New B7 Family Checkpoints in Human Cancers. Mol Cancer Ther. 2017;16(7):1203-11.

20. Hofmeyer KA, Ray A, Zang X. The contrasting role of B7-H3. Proc Natl Acad Sci U S A. 2008;105(30):10277-8.

21. Leitner J, Klauser C, Pickl WF, Stockl J, Majdic O, Bardet AF, et al. B7-H3 is a potent inhibitor of human T-cell activation: No evidence for B7-H3 and TREML2 interaction. Eur J Immunol. 2009;39(7):1754-64.

22. Yan R, Yang S, Gu A, Zhan F, He C, Qin C, et al. Murine b7-h3 is a co-stimulatory molecule for T cell activation. Monoclon Antib Immunodiagn Immunother. 2013;32(6):395-8.

23. Liu X, Hogg GD, DeNardo DG. Rethinking immune checkpoint blockade: 'Beyond the T cell'. J Immunother Cancer. 2021;9(1).

24. Yu X, Harden K, Gonzalez LC, Francesco M, Chiang E, Irving B, et al. The surface protein TIGIT suppresses T cell activation by promoting the generation of mature immunoregulatory dendritic cells. Nat Immunol. 2009;10(1):48-57.

25. Jalil AR, Andrechak JC, Discher DE. Macrophage checkpoint blockade: results from initial clinical trials, binding analyses, and CD47-SIRPalpha structure-function. Antib Ther. 2020;3(2):80-94.

26. Bradley CA. CD24 - a novel 'don't eat me' signal. Nat Rev Drug Discov. 2019;18(10):747.

27. Barkal AA, Brewer RE, Markovic M, Kowarsky M, Barkal SA, Zaro BW, et al. CD24 signalling through macrophage Siglec-10 is a target for cancer immunotherapy. Nature. 2019;572(7769):392-6.

28. Stanietsky N, Simic H, Arapovic J, Toporik A, Levy O, Novik A, et al. The interaction of TIGIT with PVR and PVRL2 inhibits human NK cell cytotoxicity. Proc Natl Acad Sci U S A. 2009;106(42):17858-63.

29. Tahara-Hanaoka S, Shibuya K, Onoda Y, Zhang H, Yamazaki S, Miyamoto A, et al. Functional characterization of DNAM-1 (CD226) interaction with its ligands PVR (CD155) and nectin-2 (PRR-2/CD112). Int Immunol. 2004;16(4):533-8.

30. Jin HS, Park Y. Hitting the complexity of the TIGIT-CD96-CD112R-CD226 axis for next-generation cancer immunotherapy. BMB Rep. 2021;54(1):2-11.

31. Shi T, Ma Y, Yu L, Jiang J, Shen S, Hou Y, et al. Cancer Immunotherapy: A Focus on the Regulation of Immune Checkpoints. Int J Mol Sci. 2018;19(5).

32. Baumeister SH, Freeman GJ, Dranoff G, Sharpe AH. Coinhibitory Pathways in Immunotherapy for Cancer. Annu Rev Immunol. 2016;34:539-73.

33. Hou J, Wang Y, Shi L, Chen Y, Xu C, Saeedi A, et al. Integrating genome-wide CRISPR immune screen with multi-omic clinical data reveals distinct classes of tumor intrinsic immune regulators. J Immunother Cancer. 2021;9(2).

34. Park JS, Helble JD, Lazarus JE, Yang G, Blondel CJ, Doench JG, et al. A FACS-Based Genome-wide CRISPR Screen Reveals a Requirement for COPI in Chlamydia trachomatis Invasion. iScience. 2019;11:71-84.

35. Condon KJ, Orozco JM, Adelmann CH, Spinelli JB, van der Helm PW, Roberts JM, et al. Genome-wide CRISPR screens reveal multitiered mechanisms through which mTORC1 senses mitochondrial dysfunction. Proc Natl Acad Sci U S A. 2021;118(4).

36. Sreevalsan S, Doring M, Paszkowski-Rogacz M, Brux M, Blanck C, Meyer M, et al. MLLT6 maintains PD-L1 expression and mediates tumor immune resistance. EMBO Rep. 2020;21(12):e50155.

37. Crowther MD, Dolton G, Legut M, Caillaud ME, Lloyd A, Attaf M, et al. Genome-wide CRISPR-Cas9 screening reveals ubiquitous T cell cancer targeting via the monomorphic MHC class I-related protein MR1. Nat Immunol. 2020;21(2):178-85.

38. Patel SJ, Sanjana NE, Kishton RJ, Eidizadeh A, Vodnala SK, Cam M, et al. Identification of essential genes for cancer immunotherapy. Nature. 2017;548(7669):537-42.

39. Han P, Dai Q, Fan L, Lin H, Zhang X, Li F, et al. Genome-Wide CRISPR Screening Identifies JAK1 Deficiency as a Mechanism of T-Cell Resistance. Front Immunol. 2019;10:251.

40. Zhang JP, Song Z, Wang HB, Lang L, Yang YZ, Xiao W, et al. A novel model of controlling PD-L1 expression in ALK(+) anaplastic large cell lymphoma revealed by CRISPR screening. Blood. 2019;134(2):171-85.

41. Shifrut E, Carnevale J, Tobin V, Roth TL, Woo JM, Bui CT, et al. Genome-wide CRISPR Screens in Primary Human T Cells Reveal Key Regulators of Immune Function. Cell. 2018;175(7):1958-71 e15.

42. Frangieh CJ, Melms JC, Thakore PI, Geiger-Schuller KR, Ho P, Luoma AM, et al. Multimodal pooled Perturb-CITE-seq screens in patient models define mechanisms of cancer immune evasion. Nat Genet. 2021;53(3):332-41.

43. Shang W, Jiang Y, Boettcher M, Ding K, Mollenauer M, Liu Z, et al. Genome-wide CRISPR screen identifies FAM49B as a key regulator of actin dynamics and T cell activation. Proc Natl Acad Sci U S A. 2018;115(17):E4051-E60.

44. Menasche BL, Crisman L, Gulbranson DR, Davis EM, Yu H, Shen J. Fluorescence Activated Cell Sorting (FACS) in Genome-Wide Genetic Screening of Membrane Trafficking. Curr Protoc Cell Biol. 2019;82(1):e68.

45. Panganiban RA, Park HR, Sun M, Shumyatcher M, Himes BE, Lu Q. Genome-wide CRISPR screen identifies suppressors of endoplasmic reticulum stress-induced apoptosis. Proc Natl Acad Sci U S A. 2019;116(27):13384-93.

46. Morita K, Hama Y, Izume T, Tamura N, Ueno T, Yamashita Y, et al. Genome-wide CRISPR screen identifies TMEM41B as a gene required for autophagosome formation. J Cell Biol. 2018;217(11):3817-28.

47. Sun N, Petiwala S, Wang R, Lu C, Hu M, Ghosh S, et al. Development of drug-inducible CRISPR-Cas9 systems for large-scale functional screening. BMC Genomics. 2019;20(1):225.

48. Logtenberg MEW, Jansen JHM, Raaben M, Toebes M, Franke K, Brandsma AM, et al. Glutaminyl cyclase is an enzymatic modifier of the CD47- SIRPalpha axis and a target for cancer immunotherapy. Nat Med. 2019;25(4):612-9.

49. Mezzadra R, Sun C, Jae LT, Gomez-Eerland R, de Vries E, Wu W, et al. Identification of CMTM6 and CMTM4 as PD-L1 protein regulators. Nature. 2017;549(7670):106-10.

50. Brockmann M, Blomen VA, Nieuwenhuis J, Stickel E, Raaben M, Bleijerveld OB, et al. Genetic wiring maps of single-cell protein states reveal an off-switch for GPCR signalling. Nature. 2017;546(7657):307-11.

51. Nijman SM. Functional genomics to uncover drug mechanism of action. Nat Chem Biol. 2015;11(12):942-8.

52. Carette JE, Guimaraes CP, Varadarajan M, Park AS, Wuethrich I, Godarova A, et al. Haploid genetic screens in human cells identify host factors used by pathogens. Science. 2009;326(5957):1231-5.

53. Cong L, Ran FA, Cox D, Lin S, Barretto R, Habib N, et al. Multiplex genome engineering using CRISPR/Cas systems. Science. 2013;339(6121):819-23.

54. Doudna JA, Charpentier E. Genome editing. The new frontier of genome engineering with CRISPR-Cas9. Science. 2014;346(6213):1258096.

55. Gilbert LA, Horlbeck MA, Adamson B, Villalta JE, Chen Y, Whitehead EH, et al. Genome-Scale CRISPR-Mediated Control of Gene Repression and Activation. Cell. 2014;159(3):647-61.

56. Leeb M, Wutz A. Derivation of haploid embryonic stem cells from mouse embryos. Nature. 2011;479(7371):131-4.

57. Mali P, Yang L, Esvelt KM, Aach J, Guell M, DiCarlo JE, et al. RNA-guided human genome engineering via Cas9. Science. 2013;339(6121):823-6.

58. Parnas O, Jovanovic M, Eisenhaure TM, Herbst RH, Dixit A, Ye CJ, et al. A Genome-wide CRISPR Screen in Primary Immune Cells to Dissect Regulatory Networks. Cell. 2015;162(3):675-86.

59. Douglas DN, Pu CH, Lewis JT, Bhat R, Anwar-Mohamed A, Logan M, et al. Oxidative Stress Attenuates Lipid Synthesis and Increases Mitochondrial Fatty Acid Oxidation in Hepatoma Cells Infected with Hepatitis C Virus. J Biol Chem. 2016;291(4):1974-90.

60. Staring J, von Castelmur E, Blomen VA, van den Hengel LG, Brockmann M, Baggen J, et al. PLA2G16 represents a switch between entry and clearance of Picornaviridae. Nature. 2017;541(7637):412-6.

61. Burr ML, Sparbier CE, Chan YC, Williamson JC, Woods K, Beavis PA, et al. CMTM6 maintains the expression of PD-L1 and regulates anti-tumour immunity. Nature. 2017;549(7670):101-5.

62. Jongsma MLM, de Waard AA, Raaben M, Zhang T, Cabukusta B, Platzer R, et al. The SPPL3-Defined Glycosphingolipid Repertoire Orchestrates HLA Class I-Mediated Immune Responses. Immunity. 2021;54(1):132-50 e9.

63. Cortez JT, Montauti E, Shifrut E, Gatchalian J, Zhang Y, Shaked O, et al. CRISPR screen in regulatory T cells reveals modulators of Foxp3. Nature. 2020;582(7812):416-20.

64. Kiritsy MC, Ankley LM, Trombley J, Huizinga GP, Lord AE, Orning P, et al. A genetic screen in macrophages identifies new regulators of IFNgamma-inducible MHCII that contribute to T cell activation. Elife. 2021;10.

65. Gu SS, Zhang W, Wang X, Jiang P, Traugh N, Li Z, et al. Therapeutically Increasing MHC-I Expression Potentiates Immune Checkpoint Blockade. Cancer Discov. 2021;11(6):1524-41.

66. Carette JE, Guimaraes CP, Wuethrich I, Blomen VA, Varadarajan M, Sun C, et al. Global gene disruption in human cells to assign genes to phenotypes by deep sequencing. Nat Biotechnol. 2011;29(6):542-6.

67. Blomen VA, Majek P, Jae LT, Bigenzahn JW, Nieuwenhuis J, Staring J, et al. Gene essentiality and synthetic lethality in haploid human cells. Science. 2015;350(6264):1092-6.

68. Uren AG, Kool J, Berns A, van Lohuizen M. Retroviral insertional mutagenesis: past, present and future. Oncogene. 2005;24(52):7656-72.

69. Carette JE, Pruszak J, Varadarajan M, Blomen VA, Gokhale S, Camargo FD, et al. Generation of iPSCs from cultured human malignant cells. Blood. 2010;115(20):4039-42.

70. Carette JE, Raaben M, Wong AC, Herbert AS, Obernosterer G, Mulherkar N, et al. Ebola virus entry requires the cholesterol transporter Niemann-Pick C1. Nature. 2011;477(7364):340-3.

71. Li Y, Shuai L. A versatile genetic tool: haploid cells. Stem Cell Res Ther. 2017;8(1):197.

72. Sun S, Zhao Y, Shuai L. The milestone of genetic screening: Mammalian haploid cells. Comput Struct Biotechnol J. 2020;18:2471-9.

73. De Zan E, van Stiphout R, Gapp BV, Blomen VA, Brummelkamp TR, Nijman SMB. Quantitative genetic screening reveals a Ragulator-FLCN feedback loop that regulates the mTORC1 pathway. Sci Signal. 2020;13(649).

74. Sarbanes SL, Blomen VA, Lam E, Heissel S, Luna JM, Brummelkamp TR, et al. E3 ubiquitin ligase Mindbomb 1 facilitates nuclear delivery of adenovirus genomes. Proc Natl Acad Sci U S A. 2021;118(1).

75. Loregger A, Raaben M, Nieuwenhuis J, Tan JME, Jae LT, van den Hengel LG, et al. Haploid genetic screens identify SPRING/C12ORF49 as a determinant of SREBP signaling and cholesterol metabolism. Nat Commun. 2020;11(1):1128.

76. Mezzadra R, de Bruijn M, Jae LT, Gomez-Eerland R, Duursma A, Scheeren FA, et al. SLFN11 can sensitize tumor cells towards IFN-gamma-mediated T cell killing. PLoS One. 2019;14(2):e0212053.

77. Stamm H, Klingler F, Grossjohann EM, Muschhammer J, Vettorazzi E, Heuser M, et al. Immune checkpoints PVR and PVRL2 are prognostic markers in AML and their blockade represents a new therapeutic option. Oncogene. 2018;37(39):5269-80.

78. Kucan Brlic P, Lenac Rovis T, Cinamon G, Tsukerman P, Mandelboim O, Jonjic S. Targeting PVR (CD155) and its receptors in anti-tumor therapy. Cell Mol Immunol. 2019;16(1):40-52.

79. Gorvel L, Olive D. Targeting the "PVR-TIGIT axis" with immune checkpoint therapies. F1000Res. 2020;9.

80. Delgoffe GM, Woo SR, Turnis ME, Gravano DM, Guy C, Overacre AE, et al. Stability and function of regulatory T cells is maintained by a neuropilin-1-semaphorin-4a axis. Nature. 2013;501(7466):252-6.

81. Sidaway P. Immunotherapy: Neuropilin-1 is required for Treg stability. Nat Rev Clin Oncol. 2017;14(8):458.

82. Rutz S, Kayagaki N, Phung QT, Eidenschenk C, Noubade R, Wang X, et al. Deubiquitinase DUBA is a post-translational brake on interleukin-17 production in T cells. Nature. 2015;518(7539):417-21.

83. Koike S, Horie H, Ise I, Okitsu A, Yoshida M, Iizuka N, et al. The poliovirus receptor protein is produced both as membrane-bound and secreted forms. EMBO J. 1990;9(10):3217-24.

84. Bowers JR, Readler JM, Sharma P, Excoffon K. Poliovirus Receptor: More than a simple viral receptor. Virus Res. 2017;242:1-6.

85. He Y, Bowman VD, Mueller S, Bator CM, Bella J, Peng X, et al. Interaction of the poliovirus receptor with poliovirus. Proc Natl Acad Sci U S A. 2000;97(1):79-84.

86. Sloan KE, Eustace BK, Stewart JK, Zehetmeier C, Torella C, Simeone M, et al. CD155/PVR plays a key role in cell motility during tumor cell invasion and migration. BMC Cancer. 2004;4:73.

87. Fionda C, Abruzzese MP, Zingoni A, Soriani A, Ricci B, Molfetta R, et al. Nitric oxide donors increase PVR/CD155 DNAM-1 ligand expression in multiple myeloma cells: role of DNA damage response activation. BMC Cancer. 2015;15:17.

88. Pende D, Bottino C, Castriconi R, Cantoni C, Marcenaro S, Rivera P, et al. PVR (CD155) and Nectin-2 (CD112) as ligands of the human DNAM-1 (CD226) activating receptor: involvement in tumor cell lysis. Mol Immunol. 2005;42(4):463-9.

89. Niu J, Maurice-Dror C, Lee DH, Kim DW, Nagrial A, Voskoboynik M, et al. First-in-human phase 1 study of the anti-TIGIT antibody vibostolimab as monotherapy or with pembrolizumab for advanced solid tumors, including non-small-cell lung cancer(). Ann Oncol. 2022;33(2):169-80.

90. Fuchs A, Cella M, Giurisato E, Shaw AS, Colonna M. Cutting edge: CD96 (tactile) promotes NK cell-target cell adhesion by interacting with the poliovirus receptor (CD155). J Immunol. 2004;172(7):3994-8.

91. Flem-Karlsen K, Fodstad O, Tan M, Nunes-Xavier CE. B7-H3 in Cancer - Beyond Immune Regulation. Trends Cancer. 2018;4(6):401-4.

92. Liu C, Zhang G, Xiang K, Kim Y, Lavoie RR, Lucien F, et al. Targeting the immune checkpoint B7-H3 for next-generation cancer immunotherapy. Cancer Immunol Immunother. 2021.

93. Vigdorovich V, Ramagopal UA, Lazar-Molnar E, Sylvestre E, Lee JS, Hofmeyer KA, et al. Structure and T cell inhibition properties of B7 family member, B7-H3. Structure. 2013;21(5):707-17.

94. Lee YH, Martin-Orozco N, Zheng P, Li J, Zhang P, Tan H, et al. Inhibition of the B7-H3 immune checkpoint limits tumor growth by enhancing cytotoxic lymphocyte function. Cell Res. 2017;27(8):1034-45.

95. Castriconi R, Dondero A, Augugliaro R, Cantoni C, Carnemolla B, Sementa AR, et al. Identification of 4Ig-B7-H3 as a neuroblastoma-associated molecule that exerts a protective role from an NK cell-mediated lysis. Proc Natl Acad Sci U S A. 2004;101(34):12640-5.

96. Yonesaka K, Haratani K, Takamura S, Sakai H, Kato R, Takegawa N, et al. B7-H3 Negatively Modulates CTL-Mediated Cancer Immunity. Clin Cancer Res. 2018;24(11):2653-64.

97. Li F, Chen H, Wang D. Silencing of CD276 suppresses lung cancer progression by regulating integrin signaling. J Thorac Dis. 2020;12(5):2137-45.

98. Aung PP, Parra ER, Barua S, Sui D, Ning J, Mino B, et al. B7-H3 Expression in Merkel Cell Carcinoma-Associated Endothelial Cells Correlates with Locally Aggressive Primary Tumor Features and Increased Vascular Density. Clin Cancer Res. 2019;25(11):3455-67.

99. Maachani UB, Tosi U, Pisapia DJ, Mukherjee S, Marnell CS, Voronina J, et al. B7-H3 as a Prognostic Biomarker and Therapeutic Target in Pediatric central nervous system Tumors. Transl Oncol. 2020;13(2):365-71.

100. Jin Y, Zhang P, Li J, Zhao J, Liu C, Yang F, et al. B7-H3 in combination with regulatory T cell is associated with tumor progression in primary human non-small cell lung cancer. Int J Clin Exp Pathol. 2015;8(11):13987-95.

101. Huang Y, Zhang HL, Li ZL, Du T, Chen YH, Wang Y, et al. FUT8-mediated aberrant N-glycosylation of B7H3 suppresses the immune response in triple-negative breast cancer. Nat Commun. 2021;12(1):2672.

102. Chen JT, Chen CH, Ku KL, Hsiao M, Chiang CP, Hsu TL, et al. Glycoprotein B7-H3 overexpression and aberrant glycosylation in oral cancer and immune response. Proc Natl Acad Sci U S A. 2015;112(42):13057-62.

103. Duan S, Cermak L, Pagan JK, Rossi M, Martinengo C, di Celle PF, et al. FBXO11 targets BCL6 for degradation and is inactivated in diffuse large B-cell lymphomas. Nature. 2012;481(7379):90-3.

104. Hirsch CL, Coban Akdemir Z, Wang L, Jayakumaran G, Trcka D, Weiss A, et al. Myc and SAGA rewire an alternative splicing network during early somatic cell reprogramming. Genes Dev. 2015;29(8):803-16.

105. Molfetta R, Milito ND, Zitti B, Lecce M, Fionda C, Cippitelli M, et al. The Ubiquitin-proteasome pathway regulates Nectin2/CD112 expression and impairs NK cell recognition and killing. Eur J Immunol. 2019;49(6):873-83.

106. Nastasi C, Willerlev-Olsen A, Dalhoff K, Ford SL, Gadsboll AO, Buus TB, et al. Publisher Correction: Inhibition of succinate dehydrogenase activity impairs human T cell activation and function. Sci Rep. 2021;11(1):8815.

107. Van Vranken JG, Na U, Winge DR, Rutter J. Protein-mediated assembly of succinate dehydrogenase and its cofactors. Crit Rev Biochem Mol Biol. 2015;50(2):168-80.

108. Luirink J, Sinning I. SRP-mediated protein targeting: structure and function revisited. Biochim Biophys Acta. 2004;1694(1-3):17-35.

109. Seaman MN. The retromer complex - endosomal protein recycling and beyond. J Cell Sci. 2012;125(Pt 20):4693-702.

110. Christiansen MN, Chik J, Lee L, Anugraham M, Abrahams JL, Packer NH. Cell surface protein glycosylation in cancer. Proteomics. 2014;14(4-5):525-46.

111. Boccuto L, Aoki K, Flanagan-Steet H, Chen CF, Fan X, Bartel F, et al. A mutation in a ganglioside biosynthetic enzyme, ST3GAL5, results in salt & pepper syndrome, a neurocutaneous disorder with altered glycolipid and glycoprotein glycosylation. Hum Mol Genet. 2014;23(2):418-33.

112. Ostalecki C, Lee JH, Dindorf J, Collenburg L, Schierer S, Simon B, et al. Multiepitope tissue analysis reveals SPPL3-mediated ADAM10 activation as a key step in the transformation of melanocytes. Sci Signal. 2017;10(470).

113. Asadzadeh Z, Mohammadi H, Safarzadeh E, Hemmatzadeh M, Mahdian-Shakib A, Jadidi-Niaragh F, et al. The paradox of Th17 cell functions in tumor immunity. Cell Immunol. 2017;322:15-25.

114. Xie C, Liu D, Chen Q, Yang C, Wang B, Wu H. Soluble B7-H3 promotes the invasion and metastasis of pancreatic carcinoma cells through the TLR4/NF-kappaB pathway. Sci Rep. 2016;6:27528.

115. Hatami R, Sieuwerts AM, Izadmehr S, Yao Z, Qiao RF, Papa L, et al. KLF6-SV1 drives breast cancer metastasis and is associated with poor survival. Sci Transl Med. 2013;5(169):169ra12.

116. Ning Z, Liu K, Xiong H. Roles of BTLA in Immunity and Immune Disorders. Front Immunol. 2021;12:654960.

117. Fan PD, Narzisi G, Jayaprakash AD, Venturini E, Robine N, Smibert P, et al. YES1 amplification is a mechanism of acquired resistance to EGFR inhibitors identified by transposon mutagenesis and clinical genomics. Proc Natl Acad Sci U S A. 2018;115(26):E6030-E8.

118. Lees AM, Deconinck AE, Campbell BD, Lees RS. Atherin: a newly identified, lesion-specific, LDL-binding protein in human atherosclerosis. Atherosclerosis. 2005;182(2):219-30.

119. Rettig I, Koeneke E, Trippel F, Mueller WC, Burhenne J, Kopp-Schneider A, et al. Selective inhibition of HDAC8 decreases neuroblastoma growth in vitro and in vivo and enhances retinoic acid-mediated differentiation. Cell Death Dis. 2015;6:e1657.

120. Wei JW, Cai JQ, Fang C, Tan YL, Huang K, Yang C, et al. Signal Peptide Peptidase, Encoded by HM13, Contributes to Tumor Progression by Affecting EGFRvIII Secretion Profiles in Glioblastoma. CNS Neurosci Ther. 2017;23(3):257-65.

121. James LI, Barsyte-Lovejoy D, Zhong N, Krichevsky L, Korboukh VK, Herold JM, et al. Discovery of a chemical probe for the L3MBTL3 methyllysine reader domain. Nat Chem Biol. 2013;9(3):184-91.

122. Kohnz RA, Roberts LS, DeTomaso D, Bideyan L, Yan P, Bandyopadhyay S, et al. Protein Sialylation Regulates a Gene Expression Signature that Promotes Breast Cancer Cell Pathogenicity. ACS Chem Biol. 2016;11(8):2131-9.

123. Lee DH, Kang SH, Choi DS, Ko M, Choi E, Ahn H, et al. Genome wide CRISPR screening reveals a role for sialylation in the tumorigenesis and chemoresistance of acute myeloid leukemia cells. Cancer Lett. 2021;510:37-47.

124. Cornelissen LAM, Blanas A, van der Horst JC, Kruijssen L, Zaal A, O'Toole T, et al. Disruption of sialic acid metabolism drives tumor growth by augmenting CD8(+) T cell apoptosis. Int J Cancer. 2019;144(9):2290-302.

125. Luo N, Li G, Li Y, Fan X, Wang Y, Ye X, et al. SAMD4B, a novel SAM-containing protein, inhibits AP-1-, p53- and p21-mediated transcriptional activity. BMB Rep. 2010;43(5):355-61.

126. Guruprasad P, Lee YG, Kim KH, Ruella M. The current landscape of single-cell transcriptomics for cancer immunotherapy. J Exp Med. 2021;218(1).

127. Zitti B, Molfetta R, Fionda C, Quatrini L, Stabile H, Lecce M, et al. Innate immune activating ligand SUMOylation affects tumor cell recognition by NK cells. Sci Rep. 2017;7(1):10445.

128. Gong J, Fang L, Liu R, Wang Y, Xing J, Chen Y, et al. UPR decreases CD226 ligand CD155 expression and sensitivity to NK cell-mediated cytotoxicity in hepatoma cells. Eur J Immunol. 2014;44(12):3758-67.

129. Basso K, Dalla-Favera R. BCL6: master regulator of the germinal center reaction and key oncogene in B cell lymphomagenesis. Adv Immunol. 2010;105:193-210.

130. Feng M, Wu Z, Zhou Y, Wei Z, Tian E, Mei S, et al. BCL9 regulates CD226 and CD96 checkpoints in CD8(+) T cells to improve PD-1 response in cancer. Signal Transduct Target Ther. 2021;6(1):313.

131. He Z, Tessier-Lavigne M. Neuropilin is a receptor for the axonal chemorepellent Semaphorin III. Cell. 1997;90(4):739-51.

132. Gelfand MV, Hagan N, Tata A, Oh WJ, Lacoste B, Kang KT, et al. Neuropilin-1 functions as a VEGFR2 co-receptor to guide developmental angiogenesis independent of ligand binding. Elife. 2014;3:e03720.

133. Martyn U, Schulte-Merker S. Zebrafish neuropilins are differentially expressed and interact with vascular endothelial growth factor during embryonic vascular development. Dev Dyn. 2004;231(1):33-42.

134. Lampropoulou A, Ruhrberg C. Neuropilin regulation of angiogenesis. Biochem Soc Trans. 2014;42(6):1623-8.

135. Chuckran CA, Liu C, Bruno TC, Workman CJ, Vignali DA. Neuropilin-1: a checkpoint target with unique implications for cancer immunology and immunotherapy. J Immunother Cancer. 2020;8(2).

136. Nakamura F, Goshima Y. Structural and functional relation of neuropilins. Adv Exp Med Biol. 2002;515:55-69.

137. Roy S, Bag AK, Singh RK, Talmadge JE, Batra SK, Datta K. Multifaceted Role of Neuropilins in the Immune System: Potential Targets for Immunotherapy. Front Immunol. 2017;8:1228.

138. Raimondi C, Brash JT, Fantin A, Ruhrberg C. NRP1 function and targeting in neurovascular development and eye disease. Prog Retin Eye Res. 2016;52:64-83.

139. Gagnon ML, Bielenberg DR, Gechtman Z, Miao HQ, Takashima S, Soker S, et al. Identification of a natural soluble neuropilin-1 that binds vascular endothelial growth factor: In vivo expression and antitumor activity. Proc Natl Acad Sci U S A. 2000;97(6):2573-8.

140. Soker S, Takashima S, Miao HQ, Neufeld G, Klagsbrun M. Neuropilin-1 is expressed by endothelial and tumor cells as an isoform-specific receptor for vascular endothelial growth factor. Cell. 1998;92(6):735-45.

141. Mehta V, Fields L, Evans IM, Yamaji M, Pellet-Many C, Jones T, et al. VEGF (Vascular Endothelial Growth Factor) Induces NRP1 (Neuropilin-1) Cleavage via ADAMs (a Disintegrin and Metalloproteinase) 9 and 10 to Generate Novel Carboxy-Terminal NRP1 Fragments That Regulate Angiogenic Signaling. Arterioscler Thromb Vasc Biol. 2018;38(8):1845-58.

142. Rizzolio S, Tamagnone L. Multifaceted role of neuropilins in cancer. Curr Med Chem. 2011;18(23):3563-75.

143. Miao HQ, Lee P, Lin H, Soker S, Klagsbrun M. Neuropilin-1 expression by tumor cells promotes tumor angiogenesis and progression. FASEB J. 2000;14(15):2532-9.

144. Casazza A, Laoui D, Wenes M, Rizzolio S, Bassani N, Mambretti M, et al. Impeding macrophage entry into hypoxic tumor areas by Sema3A/Nrp1 signaling

blockade inhibits angiogenesis and restores antitumor immunity. Cancer Cell. 2013;24(6):695-709.

145. Liu C, Somasundaram A, Manne S, Gocher AM, Szymczak-Workman AL, Vignali KM, et al. Neuropilin-1 is a T cell memory checkpoint limiting long-term antitumor immunity. Nat Immunol. 2020;21(9):1010-21.

146. Fleckenstein M, Keenan TDL, Guymer RH, Chakravarthy U, Schmitz-Valckenberg S, Klaver CC, et al. Age-related macular degeneration. Nat Rev Dis Primers. 2021;7(1):31.

147. Wong TY, Chakravarthy U, Klein R, Mitchell P, Zlateva G, Buggage R, et al. The natural history and prognosis of neovascular age-related macular degeneration: a systematic review of the literature and meta-analysis. Ophthalmology. 2008;115(1):116-26.

148. Lores-Motta L, van Asten F, Muether PS, Smailhodzic D, Groenewoud JM, Omar A, et al. A genetic variant in NRP1 is associated with worse response to ranibizumab treatment in neovascular age-related macular degeneration. Pharmacogenet Genomics. 2016;26(1):20-7.

149. Swaroop A, Chew EY, Rickman CB, Abecasis GR. Unraveling a multifactorial late-onset disease: from genetic susceptibility to disease mechanisms for age-related macular degeneration. Annu Rev Genomics Hum Genet. 2009;10:19-43.

150. Falavarjani KG, Nguyen QD. Adverse events and complications associated with intravitreal injection of anti-VEGF agents: a review of literature. Eye (Lond). 2013;27(7):787-94.

151. Kitsukawa T, Shimono A, Kawakami A, Kondoh H, Fujisawa H. Overexpression of a membrane protein, neuropilin, in chimeric mice causes anomalies in the cardiovascular system, nervous system and limbs. Development. 1995;121(12):4309-18.

152. Fernandez-Robredo P, Selvam S, Powner MB, Sim DA, Fruttiger M. Neuropilin 1 Involvement in Choroidal and Retinal Neovascularisation. PLoS One. 2017;12(1):e0169865.

153. Iragavarapu-Charyulu V, Wojcikiewicz E, Urdaneta A. Semaphorins in Angiogenesis and Autoimmune Diseases: Therapeutic Targets? Front Immunol. 2020;11:346.

154. Glinka Y, Prud'homme GJ. Neuropilin-1 is a receptor for transforming growth factor beta-1, activates its latent form, and promotes regulatory T cell activity. J Leukoc Biol. 2008;84(1):302-10.

155. Goumans MJ, Liu Z, ten Dijke P. TGF-beta signaling in vascular biology and dysfunction. Cell Res. 2009;19(1):116-27.

156. Qian H, Zhang Y, Wu B, Wu S, You S, Zhang N, et al. Structure and Function of HECT E3 Ubiquitin Ligases and their Role in Oxidative Stress. J Transl Int Med. 2020;8(2):71-9.

157. Weber J, Polo S, Maspero E. HECT E3 Ligases: A Tale With Multiple Facets. Front Physiol. 2019;10:370.

158. Kobirumaki F, Miyauchi Y, Fukami K, Tanaka H. A novel UbcH10-binding protein facilitates the ubiquitinylation of cyclin B in vitro. J Biochem. 2005;137(2):133-9.

159. Huang LZ, Li YJ, Xie XF, Zhang JJ, Cheng CY, Yamashiro K, et al. Whole-exome sequencing implicates UBE3D in age-related macular degeneration in East Asian populations. Nat Commun. 2015;6:6687.

160. Xia H, Zhang Q, Shen Y, Bai Y, Ma X, Zhang B, et al. ube3d, a New Gene Associated with Age-Related Macular Degeneration, Induces Functional Changes in Both In Vivo and In Vitro Studies. Mol Ther Nucleic Acids. 2020;20:217-30.

161. Kinoshita T. Biosynthesis and biology of mammalian GPI-anchored proteins. Open Biol. 2020;10(3):190290.

162. Roth L, Nasarre C, Dirrig-Grosch S, Aunis D, Cremel G, Hubert P, et al. Transmembrane domain interactions control biological functions of neuropilin-1. Mol Biol Cell. 2008;19(2):646-54.

163. Prud'homme GJ, Glinka Y, Lichner Z, Yousef GM. Neuropilin-1 is a receptor for extracellular miRNA and AGO2/miRNA complexes and mediates the internalization of miRNAs that modulate cell function. Oncotarget. 2016;7(42):68057-71.

164. Zhang G, Chen L, Khan AA, Li B, Gu B, Lin F, et al. miRNA-124-3p/neuropilin-1(NRP-1) axis plays an important role in mediating glioblastoma growth and angiogenesis. Int J Cancer. 2018;143(3):635-44.

165. Kim H, Ko Y, Park H, Zhang H, Jeong Y, Kim Y, et al. MicroRNA-148a/b-3p regulates angiogenesis by targeting neuropilin-1 in endothelial cells. Exp Mol Med. 2019;51(11):1-11.

166. Hang C, Yan HS, Gong C, Gao H, Mao QH, Zhu JX. MicroRNA-9 inhibits gastric cancer cell proliferation and migration by targeting neuropilin-1. Exp Ther Med. 2019;18(4):2524-30.

167. O'Brien J, Hayder H, Zayed Y, Peng C. Overview of MicroRNA Biogenesis, Mechanisms of Actions, and Circulation. Front Endocrinol (Lausanne). 2018;9:402.

168. Sakaue T, Sakakibara I, Uesugi T, Fujisaki A, Nakashiro KI, Hamakawa H, et al. Corrigendum: The CUL3-SPOP-DAXX axis is a novel regulator of VEGFR2 expression in vascular endothelial cells. Sci Rep. 2017;7:46915.

169. Hundley FV, Sanvisens Delgado N, Marin HC, Carr KL, Tian R, Toczyski DP. A comprehensive phenotypic CRISPR-Cas9 screen of the ubiquitin pathway uncovers roles of ubiquitin ligases in mitosis. Mol Cell. 2021;81(6):1319-36 e9.

170. Garcia-Barcena C, Osinalde N, Ramirez J, Mayor U. How to Inactivate Human Ubiquitin E3 Ligases by Mutation. Front Cell Dev Biol. 2020;8:39.

171. Huang X, Ye Q, Chen M, Li A, Mi W, Fang Y, et al. N-glycosylation-defective splice variants of neuropilin-1 promote metastasis by activating endosomal signals. Nat Commun. 2019;10(1):3708.

172. Hyer ML, Milhollen MA, Ciavarri J, Fleming P, Traore T, Sappal D, et al. A small-molecule inhibitor of the ubiquitin activating enzyme for cancer treatment. Nat Med. 2018;24(2):186-93.

173. Codony-Servat J, Tapia MA, Bosch M, Oliva C, Domingo-Domenech J, Mellado B, et al. Differential cellular and molecular effects of bortezomib, a proteasome inhibitor, in human breast cancer cells. Mol Cancer Ther. 2006;5(3):665-75.

174. Yoshimori T, Yamamoto A, Moriyama Y, Futai M, Tashiro Y. Bafilomycin A1, a specific inhibitor of vacuolar-type H(+)-ATPase, inhibits acidification and protein degradation in lysosomes of cultured cells. J Biol Chem. 1991;266(26):17707-12.

175. Sluimer J, Distel B. Regulating the human HECT E3 ligases. Cell Mol Life Sci. 2018;75(17):3121-41.

176. Sander B, Xu W, Eilers M, Popov N, Lorenz S. A conformational switch regulates the ubiquitin ligase HUWE1. Elife. 2017;6.

177. Gapp BV, Konopka T, Penz T, Dalal V, Burckstummer T, Bock C, et al. Parallel reverse genetic screening in mutant human cells using transcriptomics. Mol Syst Biol. 2016;12(8):879.

178. Vacchini A, Chancellor A, Spagnuolo J, Mori L, De Libero G. MR1-Restricted T Cells Are Unprecedented Cancer Fighters. Front Immunol. 2020;11:751.

179. Kulicke CA, De Zan E, Hein Z, Gonzalez-Lopez C, Ghanwat S, Veerapen N, et al. The P5-type ATPase ATP13A1 modulates major histocompatibility complex I-related protein 1 (MR1)-mediated antigen presentation. J Biol Chem. 2021:101542.

180. Wykes MN, Lewin SR. Immune checkpoint blockade in infectious diseases. Nat Rev Immunol. 2018;18(2):91-104.

181. Paluch C, Santos AM, Anzilotti C, Cornall RJ, Davis SJ. Immune Checkpoints as Therapeutic Targets in Autoimmunity. Front Immunol. 2018;9:2306.

182. Abers MS, Lionakis MS, Kontoyiannis DP. Checkpoint Inhibition and Infectious Diseases: A Good Thing? Trends Mol Med. 2019;25(12):1080-93.

183. Mocan-Hognogi DL, Tranca S, Farcas AD, Mocan-Hognogi RF, Parvu AV, Bojan AS. Immune Checkpoint Inhibitors and the Heart. Front Cardiovasc Med. 2021;8:726426.

184. Cao S, Peterson SM, Muller S, Reichelt M, McRoberts Amador C, Martinez-Martin N. A membrane protein display platform for receptor interactome discovery. Proc Natl Acad Sci U S A. 2021;118(39).

185. Cho WC. Proteomics technologies and challenges. Genomics Proteomics Bioinformatics. 2007;5(2):77-85.

186. Przybyla L, Gilbert LA. A new era in functional genomics screens. Nat Rev Genet. 2022;23(2):89-103.

187. Wu F, Fan J, He Y, Xiong A, Yu J, Li Y, et al. Single-cell profiling of tumor heterogeneity and the microenvironment in advanced non-small cell lung cancer. Nat Commun. 2021;12(1):2540.

188. Yuan X, Wang J, Huang Y, Shangguan D, Zhang P. Single-Cell Profiling to Explore Immunological Heterogeneity of Tumor Microenvironment in Breast Cancer. Front Immunol. 2021;12:643692.

189. Andreatta M, Corria-Osorio J, Muller S, Cubas R, Coukos G, Carmona SJ. Interpretation of T cell states from single-cell transcriptomics data using reference atlases. Nat Commun. 2021;12(1):2965.

190. Cheng S, Li Z, Gao R, Xing B, Gao Y, Yang Y, et al. A pan-cancer single-cell transcriptional atlas of tumor infiltrating myeloid cells. Cell. 2021;184(3):792-809 e23.

191. Meyers RM, Bryan JG, McFarland JM, Weir BA, Sizemore AE, Xu H, et al. Computational correction of copy number effect improves specificity of CRISPR-Cas9 essentiality screens in cancer cells. Nat Genet. 2017;49(12):1779-84.

192. Bayraktar EC, La K, Karpman K, Unlu G, Ozerdem C, Ritter DJ, et al. Metabolic coessentiality mapping identifies C12orf49 as a regulator of SREBP processing and cholesterol metabolism. Nat Metab. 2020;2(6):487-98.

193. Wainberg M, Kamber RA, Balsubramani A, Meyers RM, Sinnott-Armstrong N, Hornburg D, et al. A genome-wide atlas of co-essential modules assigns function to uncharacterized genes. Nat Genet. 2021;53(5):638-49.

194. Rozenblatt-Rosen O, Stubbington MJT, Regev A, Teichmann SA. The Human Cell Atlas: from vision to reality. Nature. 2017;550(7677):451-3.

195. Regev A, Teichmann SA, Lander ES, Amit I, Benoist C, Birney E, et al. The Human Cell Atlas. Elife. 2017;6.

196. Lindeboom RGH, Regev A, Teichmann SA. Towards a Human Cell Atlas: Taking Notes from the Past. Trends Genet. 2021;37(7):625-30.

197. Deep learning for genomics. Nat Genet. 2019;51(1):1.

198. Zou J, Huss M, Abid A, Mohammadi P, Torkamani A, Telenti A. A primer on deep learning in genomics. Nat Genet. 2019;51(1):12-8.

199. Rao A, Barkley D, Franca GS, Yanai I. Exploring tissue architecture using spatial transcriptomics. Nature. 2021;596(7871):211-20.

200. Pelka K, Hofree M, Chen JH, Sarkizova S, Pirl JD, Jorgji V, et al. Spatially organized multicellular immune hubs in human colorectal cancer. Cell. 2021;184(18):4734-52 e20.